Biogeochemistry of the deep microbial ecosystem in the Mallik 5L-38 Gas Hydrate Production Research Well

Vorgelegt von

Dipl.-Geologin

Raingard Maria Haberer

aus St. Ingbert

Von der Fakultät VI – Planen Bauen Umwelt

der Technischen Universität Berlin

zur Erlangung des akademischen Grades einer Doktorin der Naturwissenschaften

-Dr.rer.nat.-

genehmigte Dissertation

Promotionsausschuss:

Vorsitzender: 1. Prof. Dr. W. Dominik
Berichter: 2. Prof. Dr. B. Horsfield
Berichter: 3. Prof. Dr. V. Thiel
Berichter: 4. Dr. habil H. Wilkes

Tag der wissenschaftlichen Aussprache: 22. Juni 2007

Berlin 2007

D 83

Zwei Dinge sind zu unserer Arbeit nötig:
Unermüdliche Ausdauer und die Bereitschaft,
etwas, in das man viel Zeit und Arbeit gesteckt hat,
wieder wegzuwerfen.

Albert Einstein

Contents

Danksagung

Die vorliegende Arbeit entstand in der Sektion 4.3 “Organische Geochemie” am GeoForschungsZentrum Potsdam unter der Leitung von Herrn **Prof. Dr. Brian Horsfield**, dem ich herzlich für seine Unterstützung und viele hilfreiche Denkanstöße während der Entstehung dieser Arbeit, ihre abschließende Begutachtung und nicht zuletzt für die Sensibilisierung für alte Literatur danke. Bei Herrn **Dr. Heinz Wilkes** möchte ich mich für seine zahlreichen Hilfestellungen während der Ausarbeitung der Arbeit, insbesondere bei der Identifizierung und Interpretation der aromatischen Kohlenwasserstoffe und für seine Bereitschaft die vorliegende Arbeit zu begutachten herzlich bedanken. Herrn **Prof. Dr. Volker Thiel** danke ich herzlich für die Übernahme des Korreferates.

Herrn **Dr. Kai Mangelsdorf** danke ich ganz besonders herzlich für die Betreuung der Arbeit, seine unersetzliche Hilfe nicht nur bei der Erstellung von Tagungbeiträgen und Publikationen, seine Bereitschaft, die Arbeit auch zum x-ten Male Korrektur zu lesen und nicht zuletzt für seine Geduld.

Bei Herrn **Dr. Klaus-G. Zink** möchte ich mich für viele anregende Diskussionen und Gespräche über Biomarker, Phospholipide und “den ganzen Rest” bedanken. Herrn **Dr. Volker Dieckmann** danke ich für seinen Einsatz bei der Probennahme sowie für viele wertvolle Infomationen über Pyrolyse & CO. Desweiteren gilt mein Dank Herrn **Dr. Andreas Fuhrmann** für erhellende Einblicke in die wunderbare Welt der Macerale, Herrn **Dr. Robert Ondrak** für viele Informationen über das tertiäre Klima und die Geologie des Mackenzie Deltas und Herrn **Dr. Rolando di Primio** für seine Unterstützung in vielfältiger Art und Weise. Frau **Dr. Birgit Plessen** und Frau **Dr. Andrea Vieth** danke ich für ihre Mühen bei den Isotopenmessungen. Ebenso möchte ich mich bei dem internationalen Forschungsteam, das das Mallik 5L-38 2002 Gas Hydrate Production Research Well Program durchführte, sowie bei der **Deutschen Forschungsgemeinschaft**, die das Teilprojekt MA2470-1-3 finanzierte, bedanken.

Claudia Röhl, danke ich für ihre unermüdlichen Rat und tatkräftige Hilfe. Für unbezahlbare Hilfe, ungezählte Messungen und viel Spaß während der Arbeit im Labor danke ich dem Laborteam der Section 4.3 **Michael Gabriel**, **Kristin Günther**, **Cornelia Karger**, **Ferdinand Perssen** und **Anke Sobotta**. **Tanja Mohr** und **Inga Schindelwig** sowie **Julia Rutkowski** danke ich für ihre Mithilfe im Labor sowie bei der Datenauswertung. **Gerhard Berger**, **Hartmut Liep** und **Marina Ospald** danke ich für ihre Hilfe bei der Probenaufbereitung.Auch bei allen anderen Kolleginnen und Kollegen der Section 4.3 am GeoForschungsZentrum Potsdam möchte ich mich für eine schöne Zeit bedanken.

Mein ganz besonderer Dank gilt natürlich den beiden besten „Zimmergenossen“, die man sich nur vorstellen kann: **Dr. Jochen Naeth** und **Volkmar Neumann**.
Für viel unterhaltsame Ablenkung und vorallem für unbezahlbare seelisch-moralische und freundschaftliche Unterstützung während der langwierigen Fertigstellung dieser Arbeit danke ich **Anne**, **Bernd**, **Julia, Kerstin** und **Pete**.
Schließlich möchte ich meinen **Eltern** ganz herzlich für ihre immerwährende Unterstützung danken.

Index of figures

Index of tables

List of abbreviations

AGAR:	Angiosperm-gymnosperm aromatic ratio
ai:	Anteiso
AM:	Amount
APCI:	Atmospheric pressure chemical ionisation
BAME:	Behenic acid methyl ester
CAD:	Collisionally activated dissociation
°C:	Degree Celsius
CCU:	Cache Creek Uplift
CO:	Coal (lignite samples)
CPI:	Carbon preference index
e.g.:	For example (exempli gratia)
ELFZ:	Eskimo Lakes fault zone
ESI:	Electrospray ionization
eV:	Electron volt
FID:	Flame ionisation detector
Fig.:	Figure
GC:	Gas chromatography
GC-IR-MS:	Gas chromatography-isotope ratio-mass spectrometry
GC-MS:	Gas chromatography-mass spectrometry
HC:	Hydrocarbons
HI:	Hydrogen index (mgHC/gTOC)
HPLC:	High pressure liquid chromatography
i:	Iso
LC-ESI-MS:	Liquid chromatography-electrospray ionization-mass spectrometry
LPC:	Lysophosphatidylcholine
m/z:	Mass/charge
MB:	Microbiology (samples taken under specific contamination-controlled conditions)
mfb:	Mineral free basis
mg:	Milligram
µg:	Microgram
ml:	Millilitre

µl:	Microlitre
MPLC:	Medium pressure liquid chromatography
MSTFA:	Trimethylsilyltrifluoroacetamide
NSO:	Heterocompounds containig nitrogen, sulphur and/or oxygen
OHL:	Outer Hinge Line
OI:	Oxygen index ($mgCO_2/gTOC$)
PA:	Peak area
PE:	Phoyphatidylethanolamine
PG:	Phosphatidylglycerol
pH:	Negative logarithm of the hydrogen ion (H^+) concentration (in moles per l)
PI:	Production index
PL:	Phospholipid
RF_{PL}^{STD}:	Response factor
R_o:	Vitrinite reflectance
rpm:	Revolutions per minute
SIM:	Selected ion monitoring
Tab.:	Table
TAFZ:	Tarsiut-Amauligak fault zone
TC:	Total carbon
TCD:	Thermal conductivity detection
TFZ:	Taglu fault zone
TH:	Tununuk High
TIC:	Total inorganic carbon
TOC:	Total organic carbon
u:	Atomic mass unit
vol.-%:	Percent by volume
V-PDB:	Vienna Pee Dee Belemnite standard

List of publications and presentations

Publications

Mangelsdorf, K., Haberer, R.M., Zink, K.-G., Wilkes, H., Horsfield, B. (2003). Molecular evidence for a Deep Biosphere at the Mallik Gas Hydrate Research Well, Canada. Beihefte zum European Journal of Mineralogy 15: 125.

Haberer, R.M., Mangelsdorf, K., Zink, K.G., Wilkes, H., Horsfield, B., (2004) Molecular characterisation of the organic matter at the Mallik 5L-38 Research Well: Implications for depositional environment and the Deep Biosphere. Geochimica et Cosmochimica Acta, 68 (11, Supplement 1), 407.

Haberer, R.M., Mangelsdorf, K., Dieckmann, V., Fuhrmann, A., Wilkes, H., Horsfield, B., (2005). Characterization of the organic matter in lignites of the Kugmallit Formation (Oligocene) at the Mallik 5L-38 Gas Hydrate Production Research Well. In: S.R. Dallimore, T.S. Collett (Eds.). Scientifique Results from Mallik 2002 Gas Hydrate Production Research Well Program, Mackenzie Delta, Northwest Territories, Canada, Bulletin 585. Geological Survey of Canada, 11p.

Mangelsdorf, K., Haberer, R.M., Zink, K.G., Dieckmann, V., Wilkes, H., Horsfield, B., (2005). Molecular indicators for the occurrence of deep microbial communities at the Mallik 5L-38 Gas Hydrate Research Well. In: S.R. Dallimore, T.S. Collett (Eds.). Scientifique Results from Mallik 2002 Gas Hydrate Production Research Well Program, Mackenzie Delta, Northwest Territories, Canada, Bulletin 585. Geological Survey of Canada, 11p.

Haberer, R.M., Mangelsdorf, K., Wilkes, H., Horsfield, B., (2006) Occurrence and paleoenvironmental significance of aromatic hydrocarbon biomarkers in Oligocene sediments from the Mallik 5L-38 Gas Hydrate Research Well (Canada), Organic Geochemistry, 37, 519-538.

Oral presentations

Mangelsdorf K., Dieckmann V., Haberer R.M., Zink K.-G., Wilkes H., Horsfield B. and the Mallik Gas Hydrate Research Team. Investigation of deep microbial activity in gas hydrate bearing sediments of the Mallik Site using molecular organic geochemical indicators. Mallik Gas Hydrate Production Research Well Science Meeting, January 22-24, 2003, Whistler, Canada.

Haberer R.M., Mangelsdorf K., Wilkes H., Horsfield B. and the Mallik working group. Organic geochemical investigations of deep subsurface sediments at the Mallik 5L-38 Gas Hydrate Research Well, Mackenzie River Delta, Canada. ICDP/ODP Colloquium, March 26–28, 2003, Mainz, Germany.

Mangelsdorf K., Haberer R.M., Zink K., Wilkes H., Horsfield B. Molecular evidence for a Deep Biosphere at the Mallik Gas Hydrate Research Well, Canada. Gemeinschaftstagung DMG, GV und DGG, September 22-25, 2003, Bochum, Germany.

Haberer R.M., Mangelsdorf K., Zink K.-G., Wilkes H., Horsfield B. and the Mallik research Group. Molecular characterisation of the organic matter at the Mallik 5L-38 Gas Hydrate Research Well: Implications for depositional environment and the Deep Biosphere. Goldschmidt Conference 2004, June 5-12, 2004, Copenhagen, Denmark.

Haberer R.M., Mangelsdorf K., Zink K.-G., Wilkes H., Horsfield B. Organic matter in sediments from Mallik 5L-38 Gas Hydrate Production Research Well as indicator for paleoenvironment and paleoclimate. HGF Workshop “Climate variability and human habitat”, February 14-15, 2005, Umweltforschungszentrum Leipzig-Halle, Halle (Saale), Germany.

Poster presentations

Haberer R.M., Mangelsdorf K., Wilkes H., Horsfield B. and the Mallik working group. Bulk and molecular investigations of deep subsurface sediments at the Mallik 5L-38 Gas Hydrate Research Well, Mackenzie River Delta, Canada. 21st International Meeting on Organic Geochemistry (IMOG), September 8-12, 2003, Krakow, Poland.

Mangelsdorf K., Haberer R.M., Zink K.-G., Wilkes H., Horsfield B. and the Mallik working group. Molecular indicators for viable microbial communities of the Deep Biosphere in sediments of the Mackenzie River Delta, Northwest Territories, Canada. 21st International Meeting on Organic Geochemistry (IMOG), September 8-12, 2003, Krakow, Poland.

Haberer R.M., Mangelsdorf K., Dieckmann V., Fuhrmann A., Wilkes H., Horsfield B. and the Mallik research group. Characterisation of the organic matter in lignites of the Kugmallit formation at the Mallik 5L-38 Gas Hydrate Resarch Well, Mackenzie River Delta, Canada. Mallik 2002 Gas Hydrate Production Research Well Program - Mallik-Symposium "From Mallik to the Future", December 8-10, 2003, Chiba, Japan.

Mangelsdorf K., Haberer R.M., Zink K.-G., Dieckmann V., Wilkes H., Horsfield B. and the Mallik research group. Molecular evidence for the occurrence of a Deep Biosphere at the Mallik 5L-38 Gas Hydrate Research Well. Mallik 2002 Gas Hydrate Production Research Well Program - Mallik-Symposium "From Mallik to the Future", December 8-10, 2003, Chiba, Japan.

Haberer R.M., Mangelsdorf K., Zink K.-G., Wilkes H., Horsfield B. and the Mallik research group. Molecular examination of deep subsurface sediments at the Mallik 5L-38 Gas Hydrate Production Research Well. ICDP/IODP Colloquium, March 17-19, 2004, Bremen, Germany.

Kurzfassung

Im Winter 2001/2002 wurde im Mackenzie Delta (Northwest Territories, Kanada) die Mallik 5L-38 Gas Hydrate Production Research Well Bohrkampagne durchgeführt, deren Ziel es war, die im dortigen Permafrost vorkommenden Gashydrate hinsichtlich ihrer geologischen, geophysikalischen und geochemischen Eigenschaften zu untersuchen.

Im Rahmen der Mallik 5L-38 Gas Hydrate Production Research Well Bohrung wurden für die vorliegende Arbeit dreißig Bohrkernproben unterschiedlicher Lithologien (Tone, Sand- und Siltsteine, sowie Lignite) des oberen Oligozäns über, aus und unterhalb der Gashydrat-Zone (810-1100m Teufe) genommen. Das Ziel dieser Studie ist die Charakterisierung des organischen Materials, die Rekonstruktion der Paläoumweltbedingungen, sowie die Untersuchung mikrobieller Gemeinschaften hinsichtlich ihres Vorkommens, ihrer Besonderheiten und der Beschaffenheit ihres Lebenraumes in tiefen, terrestrischen Sedimentsschichten nahe einer Gashydrat-Zone mit Hilfe von biogeochemischer Analysenmethoden.

Die Untersuchungen der Zusammensetzung des organischen Materials (Bitumen und Kerogen) zeigen seinen terrigenen und unreifen Charakter an. Erste Hinweise auf die Herkunft des organischen Materials ergeben sich aus den Werten für die Wasserstoff- und Sauerstoffindizes (HI, OI), die bei der Rock-Eval-Pyrolyse bestimmt wurden und darauf hinweisen, daß das Kerogen dem terrigenen Typ III zugeordnet werden kann. Reifeparameter (T_{max}, Produktionsindex) indizieren die thermische Unreife des organischen Materials. Diese ersten Resultate wurden durch die Ergebnisse der Maceralanalyse zusätzlich untermauert. Auf molekularer Ebene wird die Unreife ebenfalls durch eine klare Dominanz der ungeradzahligen *n*-Alkane mit einem für unreifes Landpflanzenmaterial typischen Maximum im Bereich von *n*-C_{29} bis *n*-C_{31} bestätigt. Ein zweites Maximum (*n*-C_{23}) in der *n*-Alkanverteilung der Lignite deutet zusätzlich auf das Vorkommen der Mosspflanze *Sphagnum* und damit auf ihre Ablagerung in einem sumpfigen Milieu hin, während die Ton- und Sandlagen ein Ergebnis des mäandrierenden Flußsystems sind und zumindest teilweise ein allochthones Signal wiederspiegeln. Die Präsenz spezifischer höherer Landpflanzenmarker (Di- und Triterpenoide) unterstreichen den terrestrischen Charakter und erlauben einen detaillierteren Einblick in die Pflanzenvergesellschaftung zur Zeit der Ablagerung. So ist in den Tonen ein höherer Anteil an Angiospermbiomarker feststellbar, während das organische Material der Lignite und Sandsteine mehr Gymnospermbiomarker enthalten. Anhand der feststellbaren Variation der Paläovegetation läßt sich auch die Entwicklung der klimatischen Bedingungen während der Sedimentation sowohl im Mackenzie Delta als auch im oberen Flußlauf abschätzen.

Für die Untersuchungen der mikrobielle Biomasse werden spezifische Biomarker, wie Hopanoide, Glycerolether und Phospholipide herangezogen. Hopanoide, insbesondere Hopene und Hopane mit biogener 17β(H),21β(H)–Konfiguration, wurden in fast allen untersuchten Proben gefunden, was auf eine ausgedehnte mikrobielle Biomasse in den tiefen Sedimenten in Mallik hindeutet. Da allerdings nicht ausgeschlossen werden kann, daß sie Teil des fossilen Materials sind und über die Zeit konserviert wurden, werden Phospholipide (PLs) als sogenannte "Life Marker" für die Detektierung lebender mikrobieller Gemeinschaften genutzt. Durch ihren schnellen Abbau nach dem Zelltod sind sie dafür besonders prädestiniert, so daß der Nachweis intakter PLs in Sedimenten des tiefen Untergrundes die Präzens von lebenden Mikroorganismen bestätigen.

In den untersuchten Proben sind die Signale von indigenen PL-estern jedoch generell gering und oft nahe am Detektionslimit. Dennoch können Phosphatidylglycerole und Phosphatidylethanolamine, hauptsächlich mit C_{16} und C_{18} Fettsäuren, nachgewiesen werden. Zusätzlich wurden weitere spezifischer Komponenten in nahezu allen untersuchten Proben festgestellt, deren MS/MS-Fragmentierungsmuster daraufhin deuten, daß es sich um Lyso-Phosphatidylglycerolether handelt. Das Auffinden dieser Biomarker ist von besonderem Interesse, da Glycerolether als Bestandteil von Archeen bekannt sind. Somit deutet der Nachweis von Lyso-Phosphatidylglycerolen zusammen mit dem Nachweis von Glyceroletherlipiden auf eine Archeenvergesellschaftung (methanogen oder methanotroph) in den Sedimentschichten der Gashydrat-Zone in der Mallikbohrung hin.

Abstract

During the winter 2001/2002 the Mallik 5L-38 Gas Hydrate Production Research Well was conducted in the Mackenzie Delta (Northwest Territories, Canada) to investigate the gas hydrates, which are occurring in the permafrost there, with regard to their geological, geophysical and geochemical properties.

In the scope of the Mallik 5L-38 Gas Hydrate Production Research Well thirty core samples were collected for the current thesis from different lithologies (claystones, sandstones, siltstones, and lignites; late Oligocene) from above, within and below the gas hydrate bearing zone (810-1100m depth). The aim of this study is the characterisation of the organic matter, the reconstruction of the paleoenvironmental conditions, as well as the examination of the microbial communities with respect to their occurrence, their nature, and their habitat in deep subsurface sediments in a terrestrial setting near a gas hydrate zone by biogeochemical methods.

The investigations of the organic matter composition (bitumen and kerogen) indicate a terrestrial and immature character of the organic. First evidence for the origin of the buried organic matter is given by the hydrogen (HI) and oxygen (OI) index values obtained by Rock-Eval-pyrolyses indicating a type III kerogen. Maturity indicators such as the T_{max} values and the production index (PI), point to a thermally immature character of the organic material. These first results are supported by the maceral evaluation. On a molecular basis this is confirmed by the strong odd-over-even carbon number predominance of *n*-alkanes with a maximum in the range of *n*-C_{29} to *n*-C_{31} typical for immature land plant material. Additionally a second *n*-alkane maximum at *n*-C_{23} in the lignite samples indicates the presence of the moss plant *Sphagnum*, which suggests the formation of the organic carbon rich lignites in a swampy milieu, while the clay and sand layers are the result of a meandering river system. The occurrence of specific higher land plant markers like the di- and triterpenoids supports the terrestrial character of the sample material and provide a more detailed insight into the plant communities. Therefore, it was recognized that the clay samples reveal the highest amounts of angiosperm markers. In contrast, lignite and sand samples contain significant amounts of gymnosperm biomarkers. Considering the documented variations of the paleovegetation, the changes of the climatic conditions can be estimate during the sedimentation within the Mackenzie Delta as well as in the upper course of the river.

For the investigation of microbial biomass specific biomarkers like hopanoids, glycerol ethern and phospholipids were used. Hopanoids were found in significant amounts in almost all

sediment samples investigated indicating a widely disseminated microbial biomass. The predominant occurrence of hopenes and hopanes in their biogenic 17β(H),21β(H) configuration indicates the presence of immature microbial organic matter in deep subsurface Mallik sediments.

However, because it can not absolutely be excluded that the hopanoids are part of the buried organic material preserved over time, phospholipids (PLs) were used as target molecules for the detection of viable microbial communities in the deep subsurface strata. Their potential as "life marker" is their rapid degradation after cell death.

The indigenous PL ester signals are in general low and often near the detection limit. However, structural elucidation using the MS/MS technique shows the presence of phosphatidylglycerols and phosphatidylethanolamines with mainly C_{16} and C_{18} fatty. Additionally, a series of specific compounds is detectable in significant amounts in almost all samples investigated. Their MS/MS fragmentation patterns suggest that these compounds are lyso-phosphatidylglycerols ethers. Such biomarkers would be of specific interest, because glycerol ethers are known to occur in archaeal biomass, thus the finding of lyso-phosphatidylglycerols supported by the detection of glycerol etherlipids may point to a microbial community of archaea (e.g. methanogens or methanotrophs) in the gas hydrate bearing sediments of the Mallik site.

1 Introduction

1.1 Characteristics of gas hydrates

Naturally occurring gas hydrates are solid clathrates, composed of water molecules forming a rigid lattice of cages with most of the cages containing a molecule of natural gas (Kvenvolden, 1993; Kvenvolden, 1998). They have been recognized worldwide in oceanic sediments along continental margins and in polar continental settings (Figure 1.1), where specific conditions of pressure and temperature occur and where the supply of methane is sufficient to initiate and stabilize the clathrate structure (Figure 1.2). These factors limit their occurrence to aquatic sediments, both oceanic and lakes, where the depths are greater than ~300m, and to polar sediments of both continents and continental shelves (Kvenvolden, 1994;2002). The upper depth limit for methane hydrates is about 150m in continental polar region where the surface temperatures are below 0°C. In oceanic sediments, the methane hydrates occur where the bottom-water temperatures approach 0°C and water depths exceed about 300 m (Kvenvolden, 1993; Kvenvolden, 1998). The lower limit of methane hydrate occurrence is determined by the geothermal gradient. Therefore, the maximum lower limit is about 2000 m below the solid surface, although the lower limit is typically much less depending on local conditions (Kvenvolden, 1993; Kvenvolden, 1998).

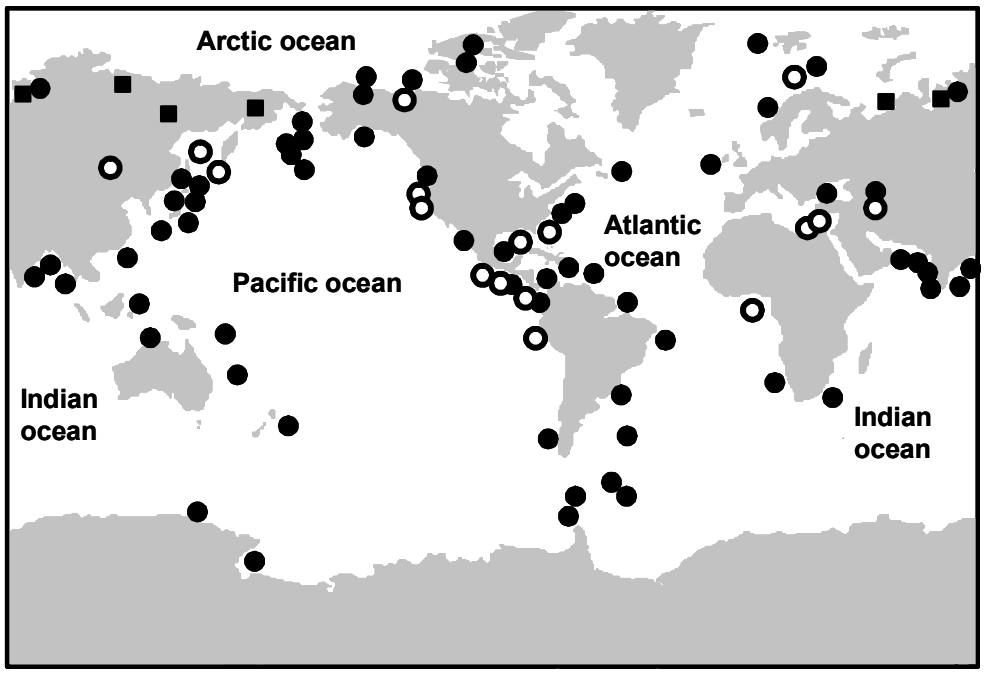

Figure 1.1: Map showing the locations of known and inferred gas hydrates in aquatic sediment and in polar continental sediment after Kvenvolden (2002). Open circles = samples of natural gas hydrates recovered. Filled circles = inferred presence of natural gas hydrates. Filled squares = regions of potential gas-hydrate occurrence in Russia.

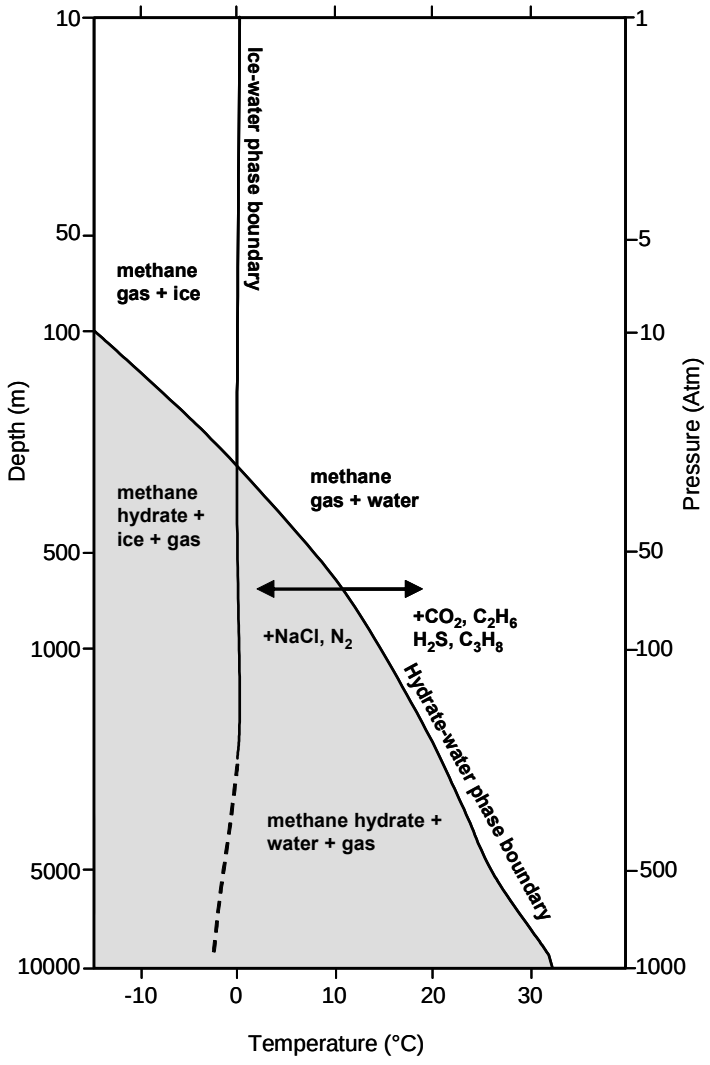

Figure 1.2: Phase diagram showing the boundary between free methane gas and methane hydrate (grey shaded) with regard to varying temperature and pressure conditions after Kvenvolden (1993).

In the sediment, gas hydrates occur as finely disseminated crystals, nodules, layers, and massive accumulations (Figure 1.3). It has been hypothesized that the evolution from smaller to larger accretions of gas hydrates represents a systematic progression in the formation of hydrates in deep-sea sediments (Kennicutt II et al., 1993). They are essential water clathrates of natural gas in which water forms a cage-like crystal structure through hydrogen bonding and crystallizes in the isometric crystallographic system rather than the hexagonal system of the normal ice. Two structures, I and II, of the cubic lattice are recognized in nature with structure I being the most common (Figure 1.4). Structure I hydrates are a 2 pentagonal dodecahedra (12 sides) and a 6 tetrakaidecahedra (14 sided) polyhedron with eight void spaces (Kennicutt II et al., 1993). In structure I, the cages are arranged in body-centred packing and are large enough to include CH_4, C_2H_6 and other gas molecules of similar molecules diameters

(0.4-0.55 nm), such as CO_2 and H_2S (Bishnoi & Natarajan, 1996; Sloan, 2003). Structure II hydrates are a pentagonal dodecahedra and an 8 hexakaidecahedra (16 sided) polyhedron with 16 small and 8 large void spaces (Kennicutt II et al., 1993). In structure II, diamond packing is present resulting in some cages being large enough (0.6-0.7 nm) to include not only CH_4 and C_2H_6 but also gas molecules as large as C_3H_8 and i-C_4H_{10} (Bishnoi & Natarajan, 1996; Sloan, 2003).

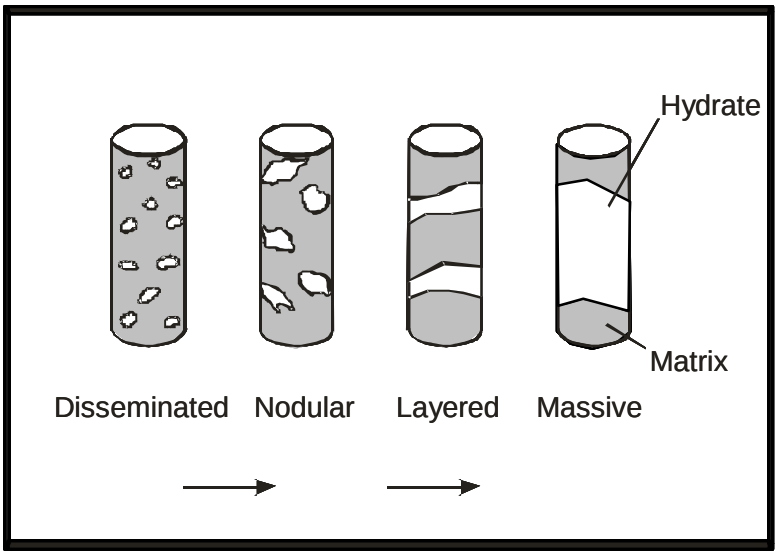

Figure 1.3: Proposed progression of hydrate formation after Kennicutt II et al. (1993).

The position of the phase boundary (Figure 1.2) is determined *inter alia* by the composition of the gas (presence of other gases than methane). However methane hydrates are the most abundant ones in nature. Due to their huge amount of methane sequestered within the clathrate structures and to the fact, that they occur in the shallow geosphere within 2000m, gas hydrates are of interest as a potential resource of natural gas. It has been assumed that 1 m³ of gas hydrates contains up to 164 m³ of methane (Kvenvolden, 1993). Although the estimated energy value of methane hydrates greatly exceeds that reservoired in proved and recoverable reserves and represents therefore an enormous hydrocarbon resource, many technological problems still remain to be solved before this potential can be realized (Kennicutt II et al., 1993).

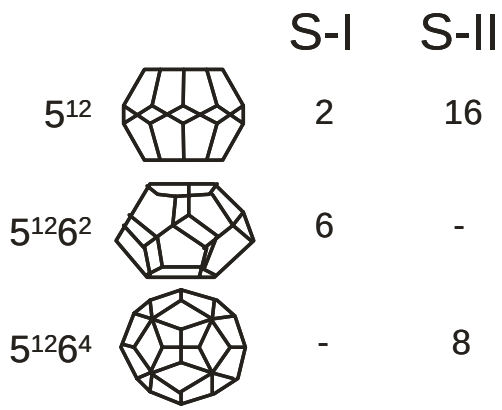

Figure 1.4: Both known natural occurring gas hydrates structures I and II are build up with different numbers of the three illustrated cage types.

Concerning gas hydrates there are also some problematic aspects. They are known to play a role as a submarine geohazard due to their potential for the catastrophic release of gases, which provoke the destabilisation of sediments resulting in mass sediment movements such as slumps (Bishnoi & Natarajan, 1996; Kennicutt II et al., 1993; Kvenvolden, 1993). Increasing water temperatures or decreasing of pressure produce the decomposition of gas hydrates, a major repository of methane, and with that the release of methane. This suggested that subtle changes in global temperature could induce a redistribution of global methane from sedimentary hydrates to atmospheric gas. Methane has been recognized as an important greenhouse gas. If the methane reaches the atmosphere its greenhouse gas properties could influence the global climate. Therefore it is suggested that the discharge of methane from gas hydrates are responsible for remarkable climate changes in the past. During the late Paleocene thermal maximum (55 Ma ago) the temperature of the deep ocean water increased by 4 to 6°C within 10,000 years. Coeval with this thermal anomaly is an extraordinary -2.5‰ excursion in the $\delta^{13}C$ of marine carbonates and organic matter deposited during the latest Paleocene (Dickens et al., 1997). They suggested that methane released from oceanic methane hydrate offers a plausible explanation, because the average carbon isotopic composition of hydrate methane (-60‰) provides the necessary carbon isotopic composition to lead to the negative carbon isotopic excursions. Katz et al. (1999) presented a scenario involving thermohaline circulation and release of CH_4 from marine gas hydrates to explain the $\delta^{13}C$ excursion during the late Paleocene thermal maximum. They supposed that similar to present day vast quantities of CH_4 greatly enriched in ^{12}C were stored in the upper few hundred meters of sediment on continental margins. During the late Paleocene a long-term global warming changed the ocean-atmosphere system, causing warm surface water to sink and intermediate to deep ocean tem-

peratures to by ~4° to 8°C. This warming converted solid gas hydrates into free gas, resulting in as increasing of pore pressure at depth and leading to sediment failure and the release of massive quantities of CH_4 into the ocean. The CH_4 react with dissolved O_2 to produce CO_2, which was enriched in ^{12}C. This adding of carbon disturbed the global carbon cycle and changed the global climate (Dickens, 2001; Dickens et al., 1997; Katz et al., 1999). Likewise Nisbet (1990) suggested that the end of the last major glaciation about 13.500 years ago is connected with the massive release of methane from gas hydrates occurring under ice and in permafrost. He assumed that may be the release of the CH_4 followed by CO_2 emission from the oceans acted together to end the ice age.

1.2 Role of gas hydrates for microbial communities in extreme environments

Gas hydrates could act as a potential carbon source for microbial ecosystems, which was already proven for marine environments (Boetius et al., 2000; Wellsbury et al., 2000). The coherence of anaerobic oxidation of methane (AOM) and sulphate reduction (SR) in marine gas hydrates has been shown by Boetius et al. (2000) and Hinrichs et al. (1999). It was indicated that certain archaea reverse the process of methanogenesis by interaction with sulphate-reducing bacteria. In the fossil record of ancient methane vent systems (Marmorito limestone, Northern Italy, Miocene), the occurrence of such a syntrophic community consisting of archaea, which are able to reverse methanogenesis, and sulphate-reducing bacteria was already proven by Thiel et al. (1999b) considering the fossil biomarker and isotopes inventories.

As sulphate is the electron acceptor, AOM is limited to zones where sulphate and methane occur coincidently. Furthermore, the AOM is influenced by many factors such as temperature, methane and sulphate supply, organic content, porosity and mineralogy of the sediment (Valentine, 2002). During the AOM, methane is oxidized while sulphate is simultaneously reduced according to the equation 1:

(1) $$CH_4 + SO_4^{2-} \rightarrow HCO_3^- + HS^- + H_2O$$

Investigations on gas hydrate bearing sediments in the Cascadian margin demonstrated that both microbial populations and their activity were increased significantly when associated with gas hydrates (Cragg et al., 1996). Within the gas hydrate zone deep microbial activity was even greater than at the sediment surface. Wellsbury et al. (2000) confirmed these obser-

vations also for deep marine sediments from the Blake Ridge. Additionally, they showed that the increase of microbial population and activity within the interval of the gas hydrate zone seems to be associated with the occurrence of free gas rather than with the solid gas hydrate itself resulting in higher microbial populations in the surrounding sediments than in the solid hydrate. The investigations of microbial communities associated with gas hydrates in the Gulf of Mexico (Lanoil et al., 2001) show that the methane dissolved in pore fluids around the hydrates drives the AOM, though hydrates themselves not harbor many microbes.

With the finding of widely disseminated microbial populations in deep marine or terrestrial sediments (Parkes et al., 1994; Parkes et al., 2000; Pedersen, 1993; Pedersen, 1997) in recent years, the assumption, accepted for a long time, that microbial processes are restricted to the upper few meters of sediments (Tissot & Welte, 1984) has been disproved. Since the discovery of the so-called "Deep Biosphere", its occurrence and nature are intriguing and important topics in the geoscientific research combining different science disciplines like geology, geochemistry and microbiology. The overall aim of these examinations is to decipher the factors controlling the occurrence of life in the deep subsurface.

Parkes et al. (1994) reported the occurrence of viable bacteria populations in sediments in more than 500 m depth at five Pacific Ocean sites. They demonstrate that even if the population at 518 mbsf ($1.1x10^7$ cells/cm^3) shows a significant 120-fold decrease from near the surface value, it remains still substantial (Figure 1.5) and they supposed that bacteria are present to even greater depths. The bacteria population profiles in the five investigated sites are remarkably similar to each other, and some deviations can be linked to specific environmental changes. In high productivity zones elevated bacteria populations are present in comparison to those in low productivity and hydrothermal heated sites (Parkes et al., 1994).

Moreover, Fredrickson and Onstott (1996) showed that the pressure has only a minor effect on deeply buried microorganisms. As microorganisms are able to live under temperature conditions up to 113°C (Blöchl et al., 1997), temperature can not be a limiting factor for microorganisms in the deep subsurface. Thus, the abundance of microbial communities in the deep subsurface depends not only on temperature or pressure (Blöchl *et al.*, 1997; Fredrickson & Onstott, 1996), but also on the presence of water, pore spaces of sediments and rocks, and the availability of nutrients and energy (Parkes et al., 2000). A common energy source for microbial organisms is the organic matter incorporated into the sediments during the progressive burial over geologic timescales.

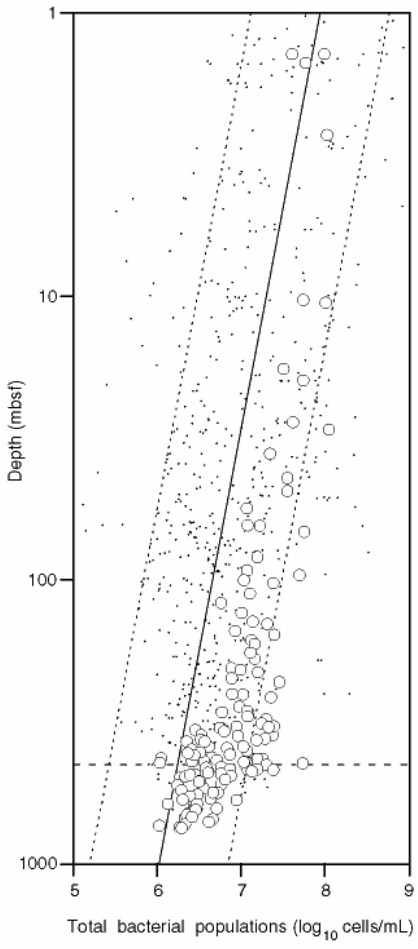

Figure 1.5: Bacterial populations in deep marine sediments after Wellsbury et al. (2000). Small dots = all sediments analyzed, open circels = populations from Sites 994,995, and 997. Note the logarithmic scale.

For the identification of microbial communities with organic geochemical methods specific biomarkers are used, mainly constituents of microbial cell membranes, such as hopanoic hydrocarbons or phospholipids. Pentacyclic triterpenes of the hopanoid family are major constituents of bacteria and it is assumed, that they act as reinforcers of the membrane (Kannenberg & Poralla, 1999; Ourisson *et al.*, 1987; Rohmer *et al.*, 1992; Rohmer *et al.*, 1984). Due to the wide range of synthesizing hopanes, they are a very abundant and widespread group of biological marker in sediments and crude oils (e.g. Rohmer et al., 1984; Rohmer et al., 1980; van Dorsselaer et al., 1977; van Dorsselaer et al., 1974). However, hopanoic hydrocarbons are not unrestricted utilisable as indicators for living microorganisms, because they can also be a part of the immature dead microbial biomass incorporated in the sediments during deposition.

Phospholipids (Figure 1.6) could be used as specific molecular markers for living microbial communities in deep subsurface sediments (Zink et al., 2003), because they are part of the cell membranes of almost all prokaryotes, only stable in intact cells and rapidly hydrolysed after cell death during early diagenetic processes (Harvey et al., 1986; White et al., 1979). Therefore, they are considered to be particularly suitable as indicator for viable microorganisms (White et al., 1979; White et al., 1997). Thus, their identification in deep sediments serves as proof of the existence of viable microbial communities in the deep subsurface (Zink et al., 2003).

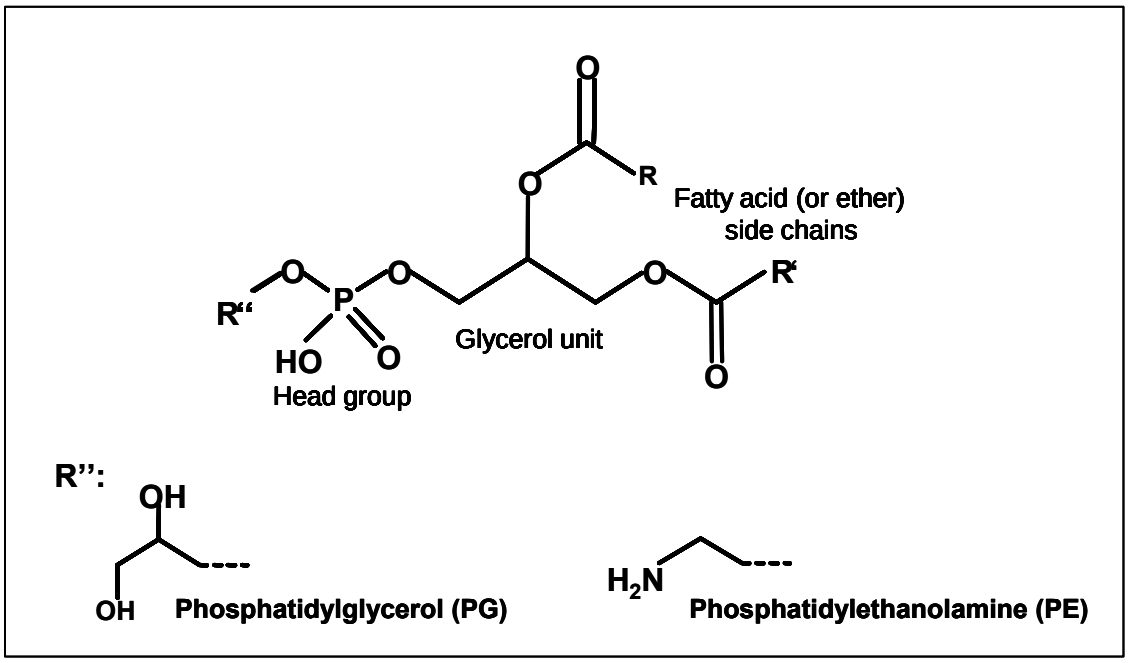

Figure 1.6: General structure of phospholipids.

1.3 Objectives of the Mallik 5L-38 Gas Hydrate production Research Well

The presented study was carried out within the scope of the JAPEX/JNOC/GSC et al. Mallik 5L-38 Gas Hydrate Production Research Well project. The well is located in the Mackenzie Delta in the northwest of Canada, where since the early Cenozoic a delta system is established. Due to the prevalent arctic conditions, permafrost occurs down to several hundreds of meters, which permits the formation of gas hydrates in the subsurface.

Contrary to marine gas hydrates, very little is known on the biogeochemistry of terrestrial gas hydrates and their usefulness as a carbon and energy source for microbial communities. Therefore, the Mallik 5L-38 Gas Hydrate Production Research Well provided an excellent

and rare opportunity to explore a microbial ecosystem in a deep terrestrial setting near a gas hydrate deposit. In the context of the Mallik 5L-38 project, the goal of this study is to examine the existence and nature of a deep microbial ecosystem at the Mallik site using organic geochemical methods.

The Mallik gas hydrate field has been the site of ongoing gas hydrate research for more than thirty years. Gas hydrate was first identified in the 1970's, through the interpretation of well logs and drill-stems test results obtains during the course of exploratory drilling of the Imperial Oil Ltd. Mallik L-38 discovery well. Studies in the 80s and the 90s expanded the known distribution of natural gas hydrate occurrences to many other wells, both onshore in the Mackenzie delta and offshore beneath the southern Beaufort Sea. In 1998, Canadian, Japanese, and American researchers undertook a major scientific and engineering research program at the Mallik L-38 research site. The JAPEX/JNOC/GSC Mallik 2L-38 research well tested many engineering technologies and their application to gas hydrate research, collected modern downhole geophysical data, and recovered the first subpermafrost gas hydrate samples. The Mallik 2002 Gas Hydrates Production Research Well Program continues the gas hydrate research at this remote Arctic location. Fieldwork was undertaken during the winter of 2001-2002. Major goals were to advance research pertaining to gas hydrate production and to assess the environmental implications of terrestrial gas hydrate deposits, including geohazard and climate-change considerations. From the outset, a multidisciplinary approach was taken in the program design. In situ geothermal and geomechanical measurements, borehole and surface geophysical surveys, and a wide variety of laboratory studies on the recovered core were designed to complete the production-test program and carefully quantify the in situ reservoir properties. After the field program, numerical modelling studies were undertaken to analyze the test data and predict possible reservoir response to long-term production and climate change. During the fieldwork and subsequent laboratory and modelling studies, nearly 300 scientist and engineers, Canadian, Japanese, Indian, Germans and American participated in the Mallik program. Insights are also given on the implications of the obtained results for the future production of natural gas from gas hydrates deposits and the assessment of the environmental conditions of terrestrial gas hydrates (Dallimore & Collett, 2005).

In the Mallik 5L-38 well gas-hydrate layers were recognized in the depth interval from 889 to 1108 m (Figure 1.7) (Dallimore et al., 2005a; Uchida et al., 2005). The gas hydrates layers occur mainly in sand and conglomerates and are absent in clay- and siltstones. The methane hydrate saturation in the intergranular pores was high, however, there was no massive gas

hydrate observed (Uchida et al., 2005). Structure I (Figure 1.4) was the only gas hydrate structure identifiable in the Mallik 5L-38 gas hydrate samples (Ripmeester et al., 2005).

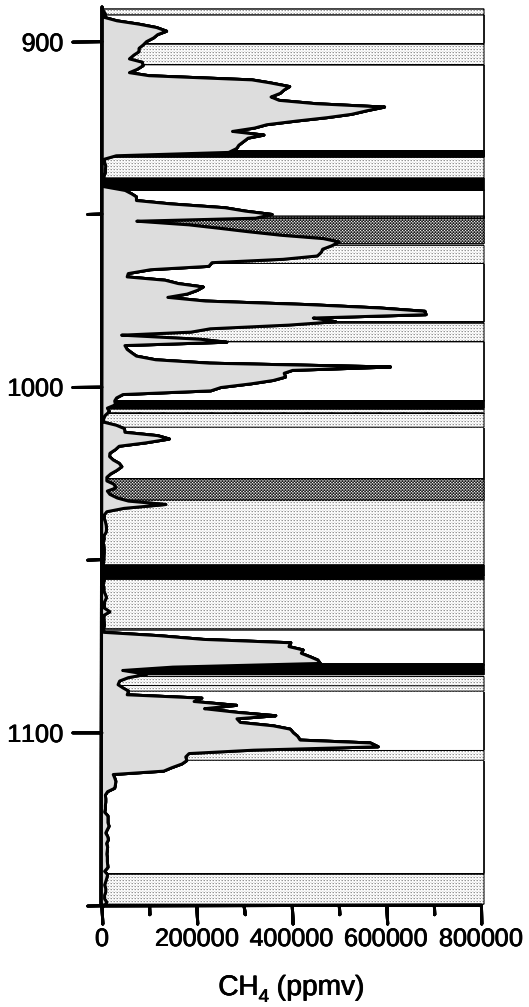

Figure 1.7: Depth profile of the methane content of the cored Mallik sediments representing gas hydrate bearing layers (data from Dallimore et al., 2005).

The main goal of this thesis was to elucidate the occurrence and nature of deep microbial ecosystems in the well and to investigate whether there is any interaction between the gas hydrates and a deep biosphere (formation or consumption of methane) as observed in surface near marine gas hydrate formations and gas seeps. For a comprehensive characterisation of a possible deep microbial community at the Mallik Site the starting point of this study was the bulk and molecular characterisation of the organic matter incorporated into the sediments, because this organic matter is considered to be an important source of carbon and energy for a possibly existing microbial ecosystem in the deep subsurface. Therefore, the composition of biomarkers occurring in a free (monomolecular) and bound (macromolecular) form in the

sediments was investigated to identify their biological origin, the depositional environment and the burial history. Thus, the geological development of the habitat for the possible existing deep microbial ecosystem was elucidated. To prove the occurrence of a "Deep Biosphere" in the Mallik area selected biomarkers were used as special indicators for microbial biomass such as hopanoids and phospholipids as so called "lifemarkers". The determination of the stable carbon isotopic signal of individual biomarkers, as molecular indicators for organisms (e.g. hopenes) was conducted to elucidate if the methane included in the gas hydrates is used as a carbon and therefore energy source for these microbial communities.

1.4 Characteristics of terrestrial organic matter

Information on the permanently alteration processes of the earth are enclosed in all types of rock. Especially sedimentary rocks give information on the palaeoenvironmental conditions concerning the sedimentary deposition, the palaeovegetation and the palaeoclimate. The organic material embedded in the sediment contains different indicators which can be used for the reconstruction of past geo-ecosystems. Thus, they contribute to the understanding of the interaction of climate and geo-biological processes. The production as well as the conservation of the organic matter are determined by the environmental condition and its changes in time. Organic-geochemical investigations assist to characterise the organic matter which differs in its amount, its origin and its composition. Sediments, enriched in organic carbon, act as archives for palaeoenvironmental conditions and are adducted for the reconstruction of palaeoclimatic conditions.

Organic matter is composed of the complex macromolecular kerogen and the bitumen. Kerogen, which is insoluble in common organic solvents, comprises typically more than 90% of the organic matter, and the bitumen or free lipid fraction, soluble in these solvents, represents usually 1-10% of the organic matter (e.g. Rullkötter, 1992; Summons, 1993). The composition of the organic material is controlled by physical, chemical and biological processes, acting from the time of sedimentation through to deep burial during subsidence. The non-soluble organic matter, the kerogen, is distinguished in three types, lacustrine, marine, and terrestrial, corresponding to different origin of the organic matter (Espitalié *et al.*, 1977; Tissot & Welte, 1984). The type I kerogen originate from algae (lacustrine or marine), type II is characteristic for marine organic matter mainly composed of phytoplankton and bacteria, with less terrestrial input and type III is representative for terrestrial organic matter (Espitalié et al., 1977). For the investigation of the soluble organic matter, the bitumen, biomolecules (biomarkers) are used, which are also called "molecular fossils". In the organic geochemistry, they act as a

tool for the characterisation of the origin of the organic material incorporated into the sediments, the climatic and environmental conditions during the deposition and the diagenetic transformation of the organic matter in the sediments since sedimentation (Peters & Moldowan, 1993). In the current study biomarkers are used to characterise the organic matter and with that to interpret the paleoenvironment and paleoclimate, and to examine the microbial biomass signal in the deep subsurface at the Mallik site.

In terrestrial sediments higher land plants are the main contributors to the organic matter. In soils almost the entire organic matter is biologically degraded. Therefore, in terrestrial settings the conservation of higher amounts of organic material is restricted on swamps and peat bogs (Killops & Killops, 1993). The peat formation on floodplains or deltaic environment is favoured by a river hinterland of low relief and therefore low energy, which reduces the sedimentary load of the river. The mire types vary according to the main plant genera assemblages such as reeds, woody species and moss plant likes *Sphagnum* (Diessel, 1992).

For the organic geochemical characterisation of terrestrial organic matter numerous specific molecular markers could be used. The bulk material of higher land plants consists of cellulose and lignin, only some parts, such as pollen, spores and leaves are enriched in lipids (Killops & Killops, 1993; Tissot & Welte, 1984). Terrestrial organic material corresponds usually to types III kerogen, which has a high oxygen and low hydrogen content, because of the high proportion of polyaromatics and oxygenated functional groups and minor amount of aliphatic chains in higher land plants (Espitalié *et al.*, 1977; Tissot & Welte, 1984).

When investigating the bitumen fraction, the first indicator for higher land plant material is certainly the *n*-alkane distribution with a preference of odd-numbered long-chain hydrocarbons in the range of *n*-C_{21} to *n*-C_{35} (Eglinton & Hamilton, 1967). This odd-numbered *n*-alkanes are either directly synthesised by plants or defunctionalization products of the early diagenesis from even-numbered fatty acids or alcohols. Some plants show a very specific *n*-alkane distribution like *Sphagnum* sp. with a characteristic *n*-alkane maximum at *n*-C_{23} (Corrigan et al., 1973; Nott et al., 2000).

In addition, many cyclic hydrocarbons are characteristic biomarkers for continental organic matter. For example, di- and triterpenoids such as pimaranes, phyllocladanes or oleananes are known biomarkers for terrestrial plant material (Peters & Moldowan, 1993). A more detailed organic geochemical characterisation of the fossil higher land plant assemblages are especially provided by aromatic terpenoids, which are often used as chemotaxonomic markers (e.g. Killops *et al.*, 1995; Otto & Simoneit, 2001; Simoneit *et al.*, 1986; Stout, 1992). The

structural similarity of sedimentary biomarkers with biomass constituents of extant plants allows inferences on the composition of ancient plant communities.

1.5 Sedimentary processes in a delta system

The conservation of the organic matter depends on the sedimentary conditions for instance a fluvial deltaic setting for the Mallik site. A delta is formed where a jet of sediment-laden water intrudes a body of standing water (Selley, 1992). Ancient delta systems host most of the world's coal reserves and a significant part of its oil and gas resources. Rapid sedimentation of organic-rich sediments in a dominantly reducing environment is conducive to the genesis of coals in peats and subsequently for the generation of oil and gas (Selley, 1992; Tissot & Welte, 1984).

River deltas are characterise by a supply of mud, silt and sand and are classified into river-dominated deltas, tide-wave deltas and wave-dominated (e.g. Reading & Collinson, 1996). River-dominate deltas typically show bird-foot morphology. The river channels branched finger-shaped into the mouth and the river build out into the basin with its sedimentary loaded distributary channels overprinting the marine influences like waves or tides. In contrast the wave or tidal-dominated deltas are strongly influenced by marine influences. Waves-dominated deltas build barrier beaches; tidal dominated delta linear sand bars (e.g. Reading & Collinson, 1996).

One of the characteristics of ancient river deltas is a thick predominantly clastic succession from offshore facies into onshore and finally fluvial facies. Additional characteristics are a sediment body of restricted lateral extent since the delta forms a depocenter around the river mouth, repetitive or cyclic successions due to repeated progradation and abandonment of the entire delta or lobes within the delta (e.g. Reading & Collinson, 1996).

Deltaic successions comprise three principal facies associations: delta plain, delta front, and prodelta (e.g. Reading & Collinson, 1996; Selley, 1992). Delta plains are widespread lowland areas comprising active and abandoned distributary channels and their associated levees. Bays, floodplains, lakes, tidal flats, marshes, and swamps are located between the river channels. These interdistributary areas of delta plain swamps support woody vegetation, which passes seaward into marshes, supporting non-woody plants such as grasses, reeds and rushes. Peat is formed in backswamps on flood plains and on flood basins between rivers channels (e.g. Diessel, 1992; Stach et al., 1982). The peatlands are separated from the river channels by levee banks. Upper delta plains are unaffected by marine processes and contain three coal producing sub-environments: back-levee swamps, abandoned channels, and flood basin

swamps. Here, swamps, marshes and lakes are widespread and channels may bifurcate downstream. Lower delta plains are affected by fluvial processes, but many are also penetrated by saline water and tidal processes.

The delta front is the zone of the interaction between fluvial and basinal processes. Here, the fluvial sedimentary input is especially affected by waves and tides. In river dominated delta systems, where basinal processes are weak, coarser sediments are deposit as distributary mouth bars. In tidal or wave dominated deltas beach ridges and tidal sandbars are formed.

The prodelta is the zone of quiet sedimentation disturbed only by gravity sliding and mass flow deposition. Prodelta and/or shelf facies records the depth salinity, physical activity and oxygenation of the basin and offshore area as well as the mode of sedimentation in the basin (e.g. Reading & Collinson, 1996; Selley, 1992). It comprises quiet water laminated or bioturbated mudstones mass flow deposits including turbitides and many types of deformational facies.

2 Study area

2.1 Geographical setting

The Mackenzie Delta (Figure 2.1) is located at the southern Beaufort Sea margin in northern Canada (Northwest Territories). Geographically, it is framed by the Yukon coastal plain and the Richardson Mountains in the west and the Anderson Plain and the Tuktoyaktuk Peninsula in the east (Dixon et al., 1992b). One of the main characteristics in this area is the occurrence of permafrost. In the Mackenzie delta permafrost extends down to about 600 m depth. The extreme temperature conditions allow the appearance of gas hydrates, another special feature of this region. In the Mackenzie delta area gas hydrates, whose formation depends on specific low temperature and high pressure conditions (see chapter 1.3), occurs in layers between 810 to 1100 m depth (Dallimore & Collett, 1999).

Since the early seventies, many exploration wells were drilled in the Beaufort Sea and the adjacent on- and offshore areas. In 1998 at the northeastern edge of the Mackenzie Delta on the Richards Island, the Mallik 2L-38 Gas Hydrate Research Well was drilled at 69°27'40.71''N and 134°39'30.37''W for scientific objectives such as the geological, geophysical, and geochemical properties of the artic gas hydrate occurrence (Dallimore et al., 1999). About 100 m from the Mallik 2L-38 well of 1998, the Mallik 5L-38 Gas Hydrate Production Research Well was drilled from January to March 2002 at 69°27'39.5''N and 134°39'38.3''W (Dallimore et al., 2005b).

2.2 Geological setting

The geological history of the Mackenzie Delta was subject to several studies during the last decades (Dallimore & Collett, 1999; Dietrich et al., 1985; Dietrich et al., 1989; Dixon, 1986; Dixon, 1996; Dixon et al., 1992a; Dixon & Dietrich, 1990; Dixon et al., 1992b; Norris, 1985a; Willumsen & Cote, 1982; Young & McNeil, 1984; Young et al., 1976). Due to different stratigraphic approaches, the use of lithostratigraphy in older studies and sequence stratigraphy in the recent ones, the stratigraphic classifications in this area are partly not unique. Therefore, in the current study a simplified overview on the geological history of the Mackenzie Delta is presented considering both stratigraphic approaches.

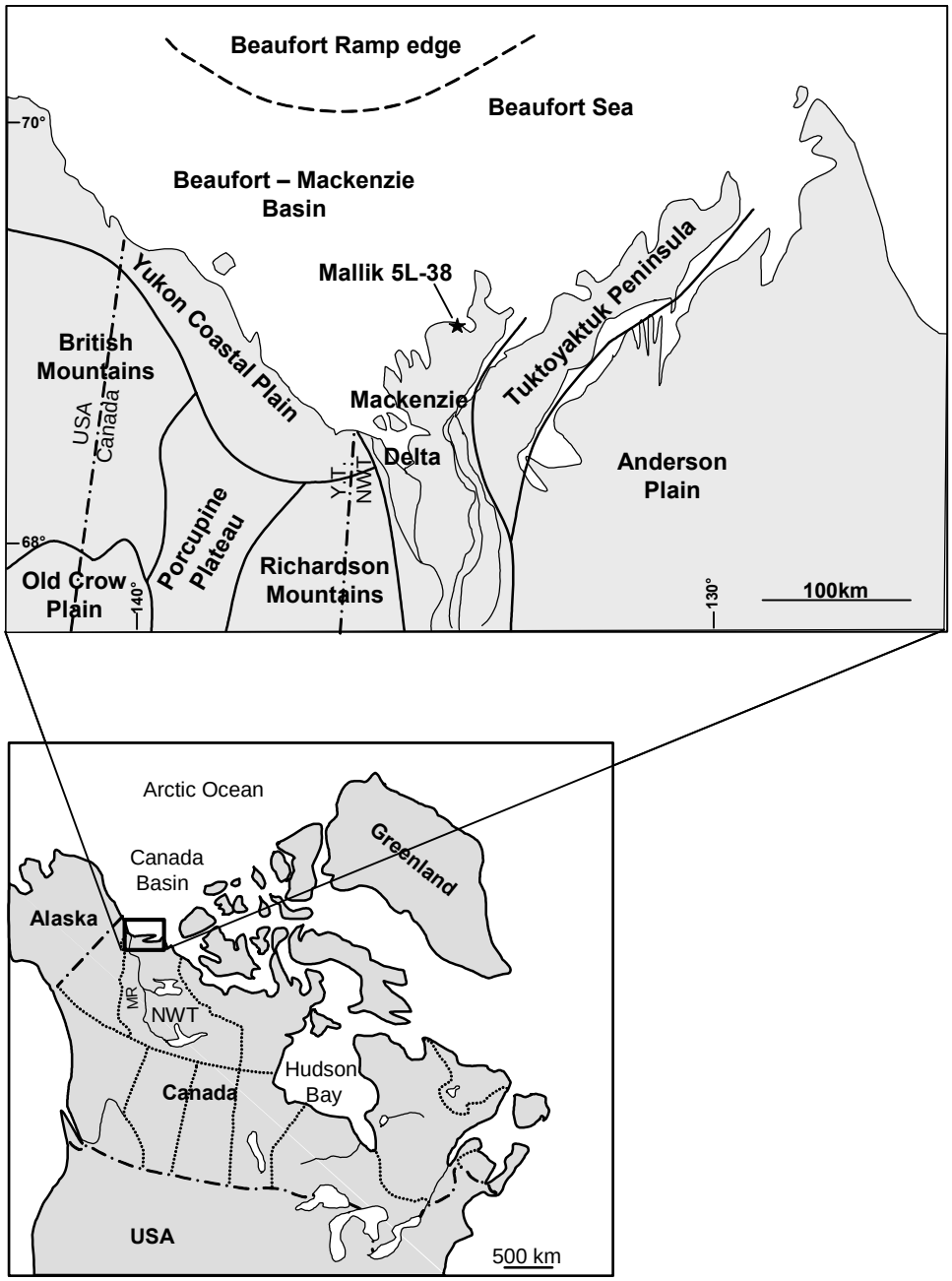

Figure 2.1: Map of the Mackenzie Delta and the drilling location of the JAPEX/JNOC/GSC et al. Mallik 5L-38 Gas Hydrate Production Research Well (MR = Mackenzie River, YT = Yukon Territories, NWT = Northwest Territories).

2.2.1 Tectonic structures at the Beaufort-Mackenzie Basin

The evolution of the Beaufort-Mackenzie basin is closely connected to the origin of the Canada basin in the Arctic Ocean and the Laramide orogenese (Cordillera). During the rising of the Cordilleran orogen vast amounts of sediments were supplied to the Beaufort-Mackenzie-basins (Dixon et al., 1992b). As a result the Beaufort-Mackenzie basin is underlain by 12 to 16 km of post-Albian sediments, which have been extensively deformed in the southern Beau-

fort Sea and the adjacent onshore area by folding and faulting processes during the Tertiary (Lane & Dietrich, 1995).

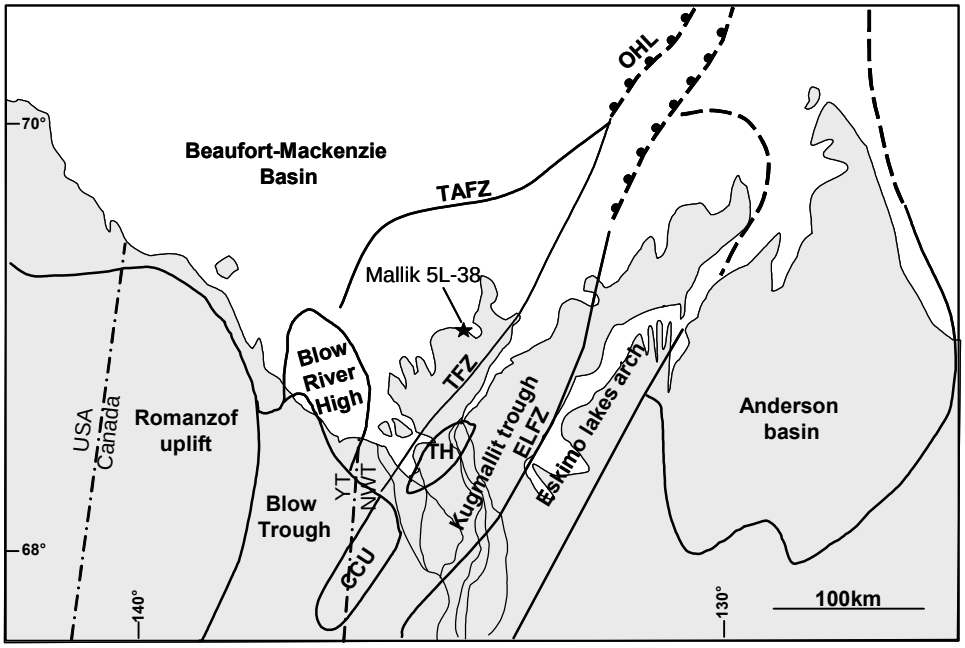

Figure 2.2: Main tectonic structures in the Beaufort-Mackenzie Delta area (CCU = Cache Creek Uplift, ELFZ = Eskimo Lakes fault zone, OHL = Outer Hinge Line, TAFZ = Tarsiut-Amauligak fault zone, TH = Tununuk High, TFZ = Taglu fault zone).

In the Beaufort foldbelt these deformation processes have provoked anticlines and thrust faults. In the Mackenzie Delta area (Figure 2.2) the tectonic processes have produced two extensional fault zones: the onshore Taglu fault zone (TFZ) and the offshore Tarsiut-Amauligak fault zone (TAFZ). Tectonically, the Mackenzie Delta is framed by the TAFZ in the northwest and the TFZ in the southeast. The northeast- to east-trending TAFZ is a zone of normal faults and faulted anticlines, and causes locally complex structural pattern and its main development occurred during the Miocene. The eastern end of the TAFZ merged with the northeast-aligned Outer Hinge Line (OHL). The TFZ consists of northeast – and east-trending normal faults which were mainly developed during the Eocene. During mid to late Tertiary the deformation within the TFZ shifted from extensional to contractional (Lane & Dietrich, 1995). The TFZ runs parallel to the Eskimo Lakes fault zone (ELFZ), a zone of northwest dipping listric normal faults in the western front of the Eskimo Lakes arch. The northern end of the TFZ fused like the TAFZ with the OHL. Between the TFZ and the ELFZ, the Kugmallit trough, a half-graben principally developed in Jurassic-early Cretaceous, is situated. This depression influenced the Tertiary deposition through differential subsidence. Below the Mackenzie Delta the northwest flank of the Kugmallit trough rises up and forms the Tununuk

High (TH) (Dixon et al., 1992b). The Cache Creek Uplift (CCU) is the elongation of the TH in southwest. The wide-ranging structural framework is build by the Romanzof uplift, the Blow River high and the Blow through in the west to southwest and the Anderson basin in the east.

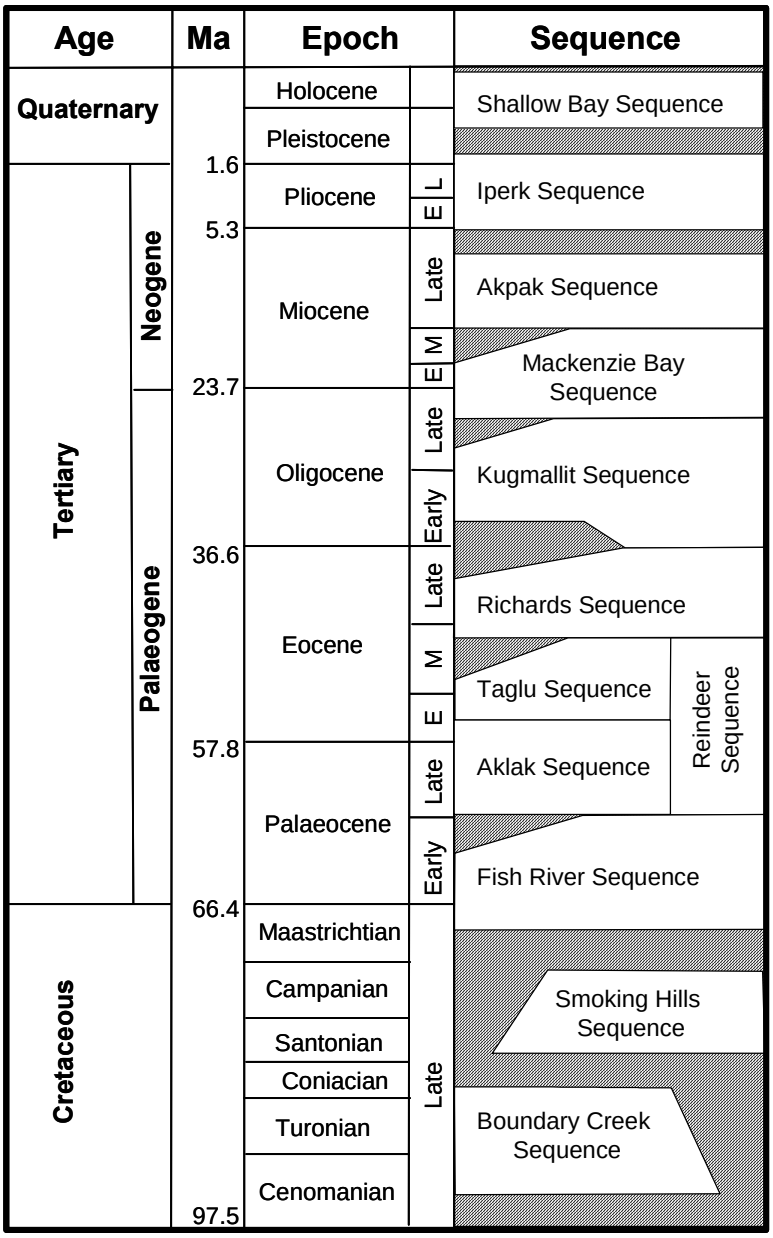

Figure 2.3: Upper cretaceous to Holocene sequence stratigraphy of the Beaufort-Mackenzie Delta area after Dixon et al. (1992a) and Medioli et al. (2005).

2.2.2 Sedimentary development of the Mackenzie Delta

The sedimentary history from the Upper Cretaceous to Holocene in the Mackenzie delta is characterized by 12 to 16 km of strata accumulated in a consecutiveness of northward prograding sequences (Figure 2.3), mainly dominated by deltaic processes (Dixon et al., 1992b). For the Paleocene to the Oligocene the dominance of wave-modified and river-dominated deltas has been suggested (Dixon et al., 1992b). The position of the delta moved through time. Analysing the paleo-drainage system of the Mackenzie River from the Eocene to the Pleistocene, Lane and Dietrich (1995) supposed that the northern Cordillera act as the source for the clastic Mackenzie-Beaufort Basin sediments and that the paleo-drainage of the Porcupine River (Figure 2.4) was responsible for the depocenter near the present Mackenzie Delta.

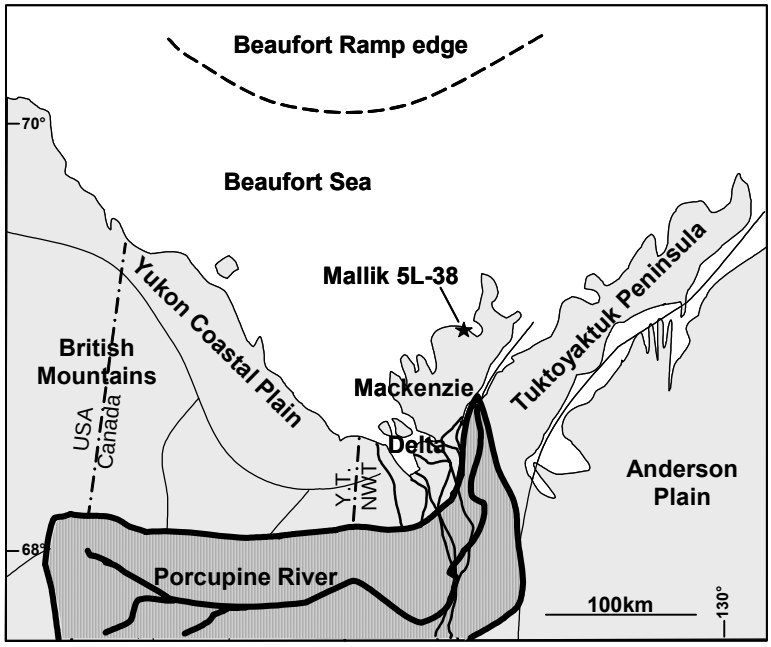

Figure 2.4: Course of the Porcupine River during the Early to Late Tertiary providing clastic sediments to the Kugmallit delta after Lane and Dietrich (1995).

In the Mallik area eight sequences are defined since the late Maastrichtian – early Paleocene (e.g. Dixon, 1986; Dixon et al., 1992b; Willumsen & Cote, 1982) reflecting the deltaic sedimentary conditions. During the late Maastrichtian – early Palaeocene, the Fish River sequence (Figure 2.5a) was deposited consisting of gravity flow deposits including conglomerates, sandstones and shales. Subsequently, during the late Paleocene – middle Eocene, widespread thick shale deposits were formed within the basin, reflecting a transgression throughout the formation of the Reindeer Sequence. After the deposition of the Aklak sequence, the lower part of the Reindeer formation (late Palaeocene-early Eocene), the deltaic depocenter shifted

from west to east, which may be related to the collision of the Cordilleran Laramide Orogen into the south-western part of the basin during the Eocene (Dixon et al., 1992b). Additionally, the Taglu fault zone (TFZ) was mainly developed during the deposition of the Taglu sequence, the upper part of the Reindeer formation, and the Richards sequence (Lane & Dietrich, 1995).

The predominantly shale-dominated Richards Sequence (late Eocene, Figure 2.5b) represents a continuation of the Reindeer Sequence. The contact between the Richards sequence and the Kugmallit sequence (early - late Oligocene, Figure 2.5c) is characterized by an unconformity due to erosion. The Kugmallit sequence is overlain by the generally shale-dominated Mackenzie Bay (late Oligocene - middle Miocene) and Akpak Sequence (late Miocene). In contrast, the following Iperk Sequence (early Pliocene – early Pleistocene, Figure 2.5d) consists of sandstones and conglomerates. And the subsequent Shallow Bay Sequence (Pleistocene – Holocene) is mostly inseparable from the Iperk Sequence.

2.2.3 Geological characteristics of the Mallik site

The sedimentary succession of the Mallik 5L-38 Gas Hydrate Production Research Well (Figure 2.6) comprises the Kugmallit, the Mackenzie Bay and the Iperk sequence. The Well has penetrated both the permafrost (0-600 m depth) and the gas hydrates zone (896-1100 m depth). From the sand-dominated Kugmallit (Oligocene) sequence only the upper part, the so-called Arnak member (Young & McNeil, 1984), has been drilled (930-1165 m, late Oligocene), whereas the lower Ivik member has not been penetrated by the Mallik well. The Arnak member is composed of sand, silt, clay and some lignite layers, which were probably deposited in interdistributary marshes and minor channels (Young et al., 1976). The Arnak member is a typical example for a non-marine sedimentation in a delta-plain environment (Dixon, 1996; Young & McNeil, 1984). In contrast, the sedimentary composition of the Mackenzie Bay sequence (350-930 m, late Oligocene – middle Miocene), consisting of sand and weakly cemented sandstones with conglomerates and only minor shale interbeds (Dixon, 1996), reflects a sedimentation at the delta-front. The Akpak sequence (middle- upper Miocene), usually occurring in the Mackenzie delta, is absent in the Mallik area due to erosion (Dixon, 1996; Dixon et al., 1992b). The sedimentary peculiarity of the Iperk sequence (0-350 m, Plio- to Pleistocene) is similar to that of the Kugmallit. It consists of unconsolidated sandstones with local intermediary conglomerates, silt and shale layers, and represents delta-plain or even fluvial sediments (Dixon, 1996; Dixon et al., 1992b).

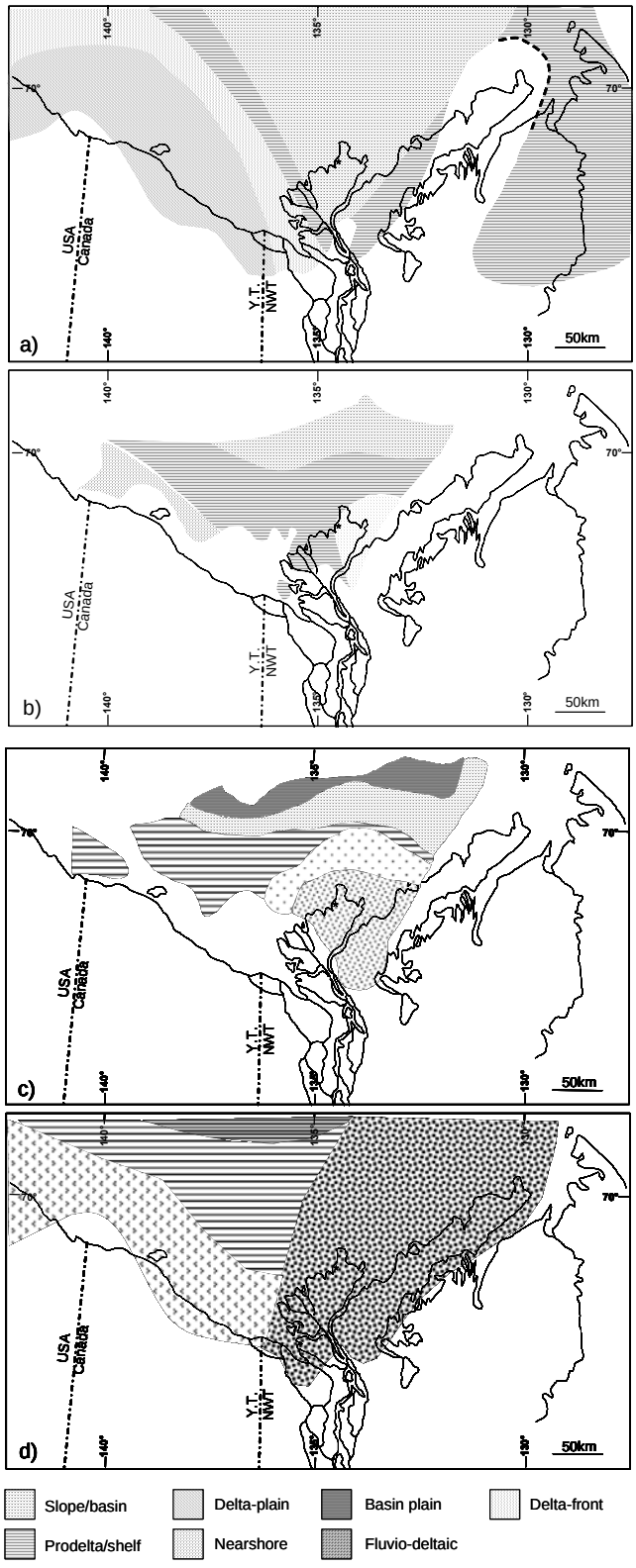

Figure 2.5: Depositional facies maps of sequences after Dixon et al. (1992a); a) Fish River sequence (Early Paleocene), b) Richards sequence (Late Eocene), c) Kugmallit sequence (Oligocene), and d) Iperk sequence (Pliocene).

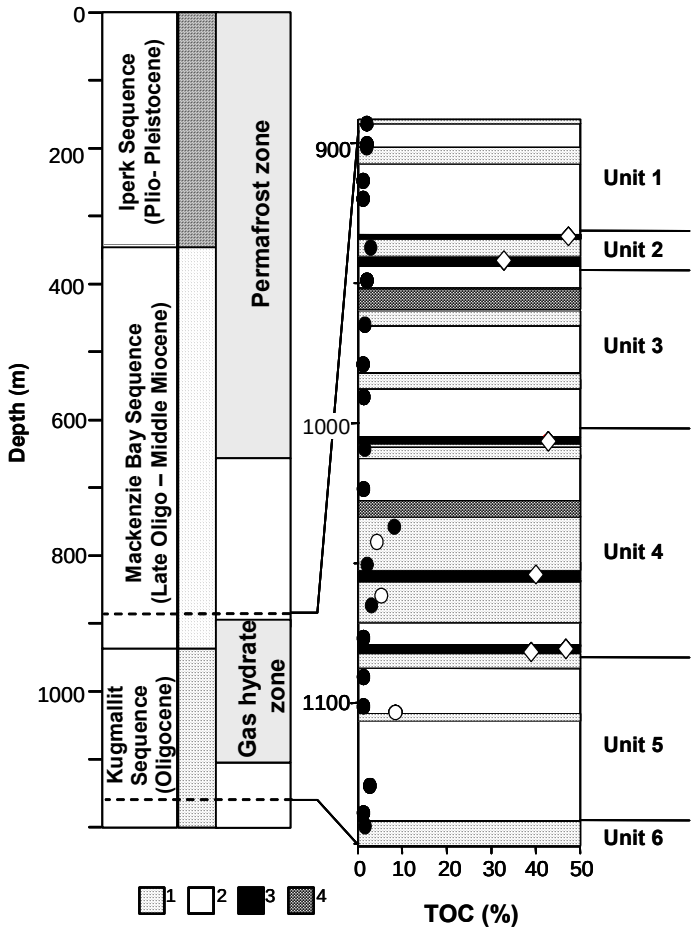

Figure 2.6: Stratigraphic column of the JAPEX/JNOC/GSC et al. Mallik 5L-38 Gas Hydrate production Research Well. Core units after Medioli et al. (2005). Non-lignite samples are indicated with filled circles. Lignites are indicated with diamonds; organic-carbon rich shale samples are indicated with open circles. 1 = silt/clay, 2 = sand, 3 = lignite layer, 4 = conglomerate.

The cored interval (885 -1150 m) of the Mallik well covers only the lower part of the Mackenzie Bay and the upper part of the Kugmallit sequence. The core consists of six units defined after their different litholgical composition (Medioli et al., 2005). The alternating succession of more sand dominated strata with parts dominated by organic-rich clays and lignites is obvious and reflects the deposition in a meandering river system. In the following, these units are described and are combined concerning their lithological properties: Unit 1 (885.63-932.64 m), unit 3 (944.44-1004.65 m) and unit 5 (1087.56- 1142.70 m) are dominated by sandstones, which are weakly laminated or massive with fining-upward cycles in unit 3. Additionally, pebble and silt interbeds occur and in unit 5 some isolated organic-rich layers and amber-bearing horizons are present. Quartz, garnet and pyrite are the most common minerals within these three units. Traces of bioturbation are visible only in unit 1.

Unit 2 (932.64- 944.44 m), unit 4 (1004.65-1087.56 m) and unit 6 (1142.70-1150.79 m, base has not been penetrated) are dominated by weakly to well laminated organic-rich silts and

claystones, with low rank coal or lignites layers, partly amber-bearing. The mineral compositions consist of quartz and clay minerals such as chlorite, kaolinite, smectite and mica. The transition from unit 1 to unit 2 (932.64 m depth) represents the boundary of the Mackenzie Bay sequence and the Kugmallit sequence.

2.3 Paleoclimatic conditions during the Tertiary in the Mackenzie Delta region

The global temperature during the Oligocene was cooler than in the previous Eocene period as discussed by Zachos et al. (2001) based on a compilation of $\delta^{18}O$ isotope data of Cenozoic sediments. Only in the late Oligocene the temperature increased again. These results fit in with the findings of Habicht (1979) who has reported relatively low temperatures in the northern hemisphere during the Oligocene. Palynological data of Ridgway et al. (1995) from the Yukon Territory in northwest Canada indicates a change from angiosperm dominated forest types to those dominated by gymnosperms. This points to a decrease of the relatively warm temperatures during the Eocene to colder conditions during the Oligocene. Tertiary sediment samples (Eocene-Oligocene) from the Rock River coal basin, also located in Yukon Territory, were investigated regarding their palynological characteristics (Long & Sweet, 1994). Long and Sweet (1994) have revealed a dominance of Taxodiaceae-Cupressaceae pollen, indicating a temperate climate and wet-humid conditions. Norris (1982) has shown differences in the distribution of spores between the Ivik member (lower part) and the Arnak member (upper part) of the Kugmallit sequence for the Mackenzie Delta region (Imperial Nuktak C-22 well). In the Eocene and early Oligocene thermophilic angiosperm taxa are common, but they disappear in the lower half of the transition from the early to middle Oligocene. Their absence indicates a cooler interval during the sedimentation of the Ivik member. However, in the late Oligocene (Arnak member) they reappear. It was suggested that the increased diversity of the angiosperm pollen in the Arnak member is due to an amelioration of climate and the re-establishment of warmer temperatures (Norris, 1982).

3 Methods

3.1 Sampling and sample labelling

Drilling with heavy drill equipment in the permafrost area of North Canada is only possible in winter when the ground is frozen and the ice-covered rivers can be used as ice-roads to transport the drill equipment to the drill site. Due to the restricted time window (December 2001 to February 2002) and the fact that apart from the Research well (5L-38) two additional observation wells (3L-38 and 4L-38) were drilled during the Mallik project, only a sediment interval from 880 to about 1160 m, containing the gas hydrate bearing layers, was cored from the Mallik 5L-38 Research well. For the upper 880 m only drill cuttings were available. Thirty sediment samples (18 - 170 g) from different lithologies such as clays, siltstones, sandstones and lignitic carbon-rich layers from above, within and below the gas hydrate zone were collected predominantly from the Kugmallit Sequence (Figure 2.6). In Table 3.1 analytical results of the pore water chemistry and the core temperature are compiled.

To avoid or at least to monitor potential microbial contamination of the core material from the surface stringent microbiological sampling methods were used by the microbiologists at the drill site for the non-lignitic samples. These methods minimized the contact of the sample material with non-sterile, foreign materials and a fluorescent quality control tracer was used during drilling to indicate the penetration depth of the drill fluids into the core material. These tracers, having the size of half a microbe, are Teflon particles bearing a fluorescent group, which enables their detection under a fluorescent microscope. A bag, filled with the tracer, was attached to the top of the core liner and was ripped open immediately during the drilling process when the core penetrates forward into the core liner. After retrieval of the core material the exteriors of core samples were removed and discarded within an anaerobic glovebox on site in order to avoid contaminated outer core sections.

As the coaly lignite layers within the gas hydrate zone may act as a carbon and energy source for microbial communities, nine additional lignite samples were collected. All samples were directly sealed in Teflon receptacles and immediately stored under liquid nitrogen (-196°C) in a cryomoover (Linde Gas AG, Germany) to avoid any post-drilling degradation or post-drilling growth of microbial contaminants or other contamination processes. Samples were stored under these conditions until analysis.

The gathered samples have been labelled using the following nomenclature: The letter combination assigns a specific sampling method (“MB” (microbiology) = samples taken under specific contamination-controlled conditions, see above) or a lithological characterization (“CO”

(coal) = lignite samples). The numbers provide the sample depth in centimetres. Three samples (CO104310, CO106094 and CO110550) were assigned as coals according to initial core descriptions, however, their low organic carbon contents of 3.64, 4.71 and 9.44%, respectively, revealed that these samples are organic-rich shales rather than lignites. In this thesis, these samples are therefore assigned as organic carbon-rich shales.

Table 3.1: Core temperatures and analytical results for interstitial water samples from the JAPEX/JNOC/GSC et al. Mallik 5L-38 gas hydrate production research well. Data from Dallimore et al. (2005a)[1] and Tomaru et al. (2005)[2].

Depth (m)	Core temperature (°C)[1]	SO_4^{2-} (mmol/L)[2]	Cl^- (mmol/L)[2]	$\delta^{18}O$ (‰)[2]	δD (‰)[2]
890-900	0,2- -2,2	1,3-2,9	105,3-416,9	-14,88 - -15,41	-97,7 – 114,2
900-910	0,6 - -1,6	0,8-17,0	147,6-346,9	-13,10 - -14,50	-104,1 - -116,5
910-920	-2,3 - -6,3	0,7-14,9	56,4-333,3	-11,49 - -14,09	-89,6 - -111,5
920-930	-2,3 - -4,7	1,1-4,4	59,3-425,6	-11,62 - -12,64	-98,5 - -109,00
930-940	-0,7 - -4,5	2,3-6,0	248,6-411,6	-12,44 - -14,89	-102,9 - -120,2
940-950	-0,5 - -1,6	0,4-4,5	108,8-436,0	-12,44 - -14,42	-103,0 - -117,3
950-960	2,8 - -3,9	0,5-5,2	54,9-454,7	-9,10 - -13,96	-81,6 - -112,5
960-970	1,4 - - 3,9	1,6-4,5	156,7-471,6	-10,86 - -13,84	-91,6 - -118,2
970-980	-0,3 - -2,5	0,6-3,9	161,3-359,9	-13,14 - -15,14	-100,9 - -113,8
980-990	-0,9 - -2,1	1,5-7,9	83,5-461,5	-12,14 - -13,19	-101,3 - -107,4
990-1000	1,3 - -1,7	0,2-32,0	252,6-1053,9	-10,97 - -11,67	-91,5 - -102
1000-1010	1,5 - -0,1	2,9-9,4	424,8-580,5	-13,22 - -14,89	-111,7 - -171,4
1010-1020	0,0 - -1,6	0,7-5,2	244,8-537,8	-11,17 - -13,80	-95,1 - -110,6
1020-1030	1,2 - -1,5	1,4-3,0	387,7-500,0	-11,84 - -12,56	-87,0 - -113,6
1030-1040	1,6 – 1,3	1,9-3,9	463,2-504,2	-12,06 - -12,42	-103,3 - -112,1
1040-1050	no data	0,7-2,7	456,6-550,5	-11,81 - -13,56	-101,0 - -103,2
1050-1060	0,8 – 0,5	0,2-5,0	480,0-642,9	-12,32 - -13,26	-98,9 - -112,3
1060-1070	2,2 - -0,8	1,6-2,7	472,0-548,6	-10,83 - -12,57	-91,5 - -107,1
1070-1080	0,2 - -3,5	0,8-3,6	162,9-489,5	-9,44 - -12,22	-89,4 - -99,1
1080-1090	-0,4 - -1,9	0,6-4,5	207,1-679,7	-10,04 - -12,33	-85,6 - - 100,7
1090-1100	1,3 - -1,7	0,6-2,2	65,3-508,1	-8,56 - -12,03	-78,3 - -85,2
1100-1110	0,7 - -3,9	1,4-7,5	157,6-538,7	-8,51 - -11,91	-80,2 - -100,9
1110-1120	0,3 - -0,8	7,5-14,2	400,1-629,1	-8,48 - -11,36	-91,0 - -107,3
1120-1130	1,6 – 0,0	6,6-15,0	469,4-573,3	-9,69 - -11,0	-86,8 - -101,2
1130-1140	0,5 - -0,8	6,2-13,9	449,0-489,1	-9,39 - -10,91	-86,2 - -104,6
1140-1150	2,7 - -0,1	6,6-11,4	449,1-537,4	-9,00 - -10,13	-80,1 - -93,8

3.2 Analytical Methods (sample preparation and measurement)

The general workflow of the sample treatment is shown in Figure 3.1.

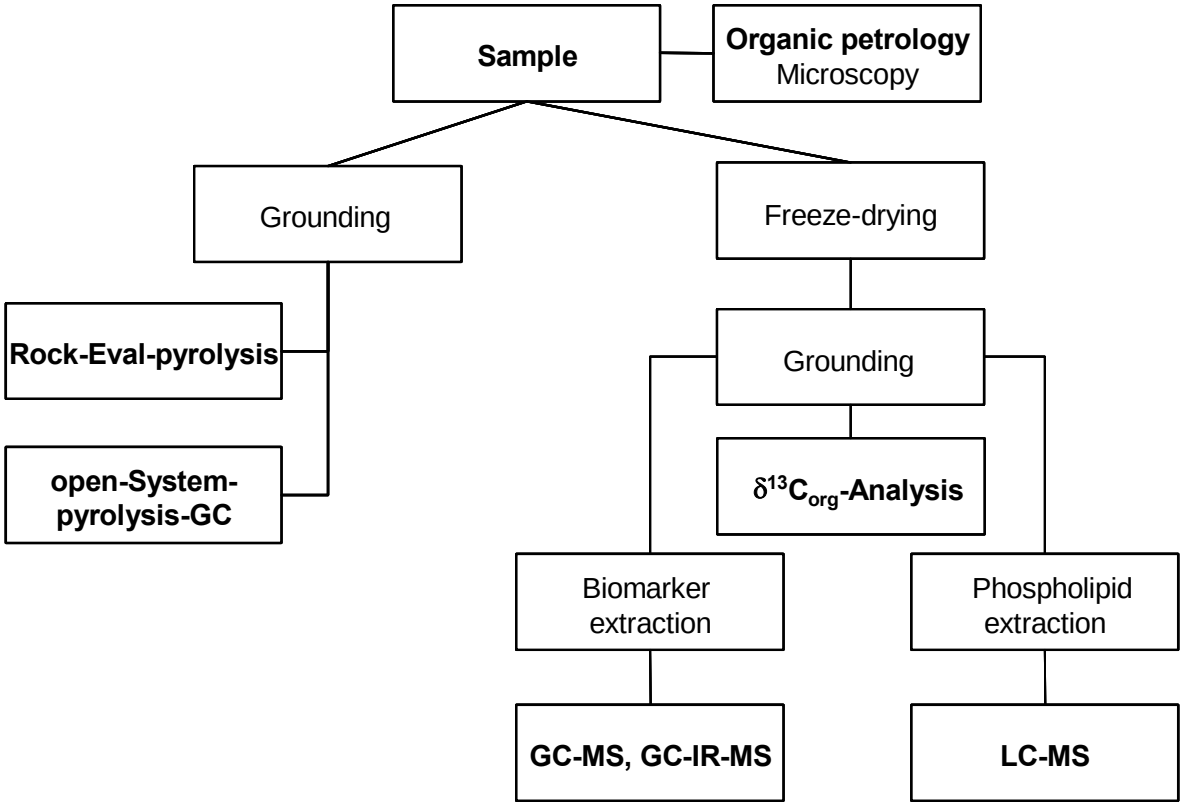

Figure 3.1: General schematic workflow of conducted analysis.

3.2.1 Freeze drying and grounding

Preceding the analyses, the frozen samples have been freeze-dried for 24 to 48 hours according to their water content using a lyophilisation instrument (Piatkowski-Forschungsgeräte, Germany). After freeze-drying, the samples have been grounded to fine powder with a disc mill "Fritsch pulverisette 9" for 30 seconds using a tempered steel grinding set. Alternately, an adequate amount of high-purity silica sand has been grounded for cleaning the grinding set between every new sample.

3.2.2 Rock-Eval-Pyrolysis

The analyses were performed using a Rock-Eval Instrument 6 at Aptec (Norway). The applied procedure is based on the methods established by Espitalié et al. (1977). An external standard (Jet Rock) was used for calibration. Whole rock samples were heated at 300°C for 3 min, and the released thermally distilled products were quantified by flame ionisation detector (FID) as the S1 peak (volatile hydrocarbons). In the following step, the temperature was raised from 300°C to 550°C with a heating rate of 25°C/per min. Generated products resulting from the

thermal breakdown of the kerogen were quantified as the S2 peak. The temperature at which the maximum amount of hydrocarbons is liberated from the kerogen is called Tmax. A third peak (S3) represents the amount of generated carbon dioxide up to a temperature of 390°C. CO_2 was collected in a molecular sieve trap during pyrolysis, then released by ballistic heating and analysed by thermal conductivity detection (TCD). The Hydrogen Index (HI), which is the S2 signal normalised to total organic carbon (TOC) (mg HC/g TOC), corresponds to the pyrolytically released hydrocarbons (HC), and is controlled essentially by the availability of organic hydrogen in the sample. The Oxygen Index (OI) corresponds to the quantity of carbon dioxide (CO_2; S3 signal) normalised to TOC (mg CO_2/g TOC).

3.2.3 $\delta^{13}C_{org}$-analysis of the bulk organic matter

Carbon isotopic compositions of total organic matter were measured after dissolution of carbonates with HCl (10%; at 50°C for 1.5 h), subsequent washing with distilled water and centrifugation for three times. Afterwards the residues were dried at 50°C for 12 hours. For the $\delta^{13}C_{org}$-analysis sample material of about 0.2 to 20 mg, depending on the TOC-value, was placed into small tin cups and combusted at 1000°C in a CN-2500 elemental analyser, oxidizing the organic carbon to carbon dioxide. Prior to the isotopic analyses performed in continuous flow mode on a DELTAplus XL Finnigan mass spectrometer nitrogen oxides were reduced and the water was removed from the combustion gases with a water trap. Isotopic ratios are expressed as $\delta^{13}C_{org}$ values in per mil relative to the Vienna-Pee Dee Belemnite (V-PDB) standard according to equation 1.

Equation 1:
$$\delta_t{}^{13}C\,[‰] = \left(\frac{(^{13}C/^{12}C)_{Sample}}{(^{13}C/^{12}C)_{Standard}} - 1 \right) \cdot 1000 = \left(\frac{R_{Sample}}{R_{Standard}} - 1 \right) \cdot 1000$$

3.2.4 Open System-pyrolysis

Sample aliquots (3 mg to 17 mg) of lignites were analysed by open-system pyrolysis using a Quantum MSSV-2 Thermal Analyzer (cf. Horsfield et al., 1989) interfaced with an Agilent gas chromatograph (GC) 6890A. For analyses, the samples were placed into the central part of a glass tube (26 mm long; inner sleeve diameter 3 mm). The remaining volume was filled with quartz wool cleaned at 630°C in air for 30 min. After flushing with helium at 300°C (5 min) to remove the volatile material, the samples were pyrolysed using a temperature program from 300°C (50°C/min) to 600°C (3 min, isothermal). The products were first cryogenically trapped (liquid nitrogen trap), then analyzed by on-line gas chromatography. A fused

silica capillary column (HP-Ultra 1; 50 m length, inner diameter = 0.32 mm, film thickness = 0.52 µm) connected to a flame ionisation detector (FID) was used with helium as carrier gas. The temperature of the GC oven was programmed from 30°C to 320°C at a rate of 5°C/min, followed by an isothermal phase of 35 min.

3.2.5 Organic petrology

For microscopic studies seven lignite samples and two clay samples with high TOC content were embedded in epoxy resin. The resultant blocks, orientated vertical to the bedding, were ground flat and polished. Qualitative observations were performed in reflected white and fluorescence light (excitation at 365 nm) using a Zeiss Axiophot microscope and oil immersion objectives with 20x and 50x magnifying power. Subsequently, the samples were analysed quantitatively with a point counter, whereas macerals were examined in both reflected white and fluorescence light. Three maceral groups (ten individual macerals) were counted: (1) huminites (ulminite, textinite, and humodetrinite), (2) liptinites (sporinite, fluorinite, cutinite, resinite, and liptodetrinite), and (3) inertinites (inertinite and fusinite). All results are reported in volume percent (vol.-%), on a mineral free basis (without including minerals into the calculation of percentage). Minerals were counted as a separate category in white light mode. A minimum of 200 macerals were measured for each sample. Microscopic investigations have been carried out according to the maceral definitions given by Taylor et al. (1998).

3.2.6 Lipid analysis

The workflow of the lipid analysis is shown in Figure 3.2.

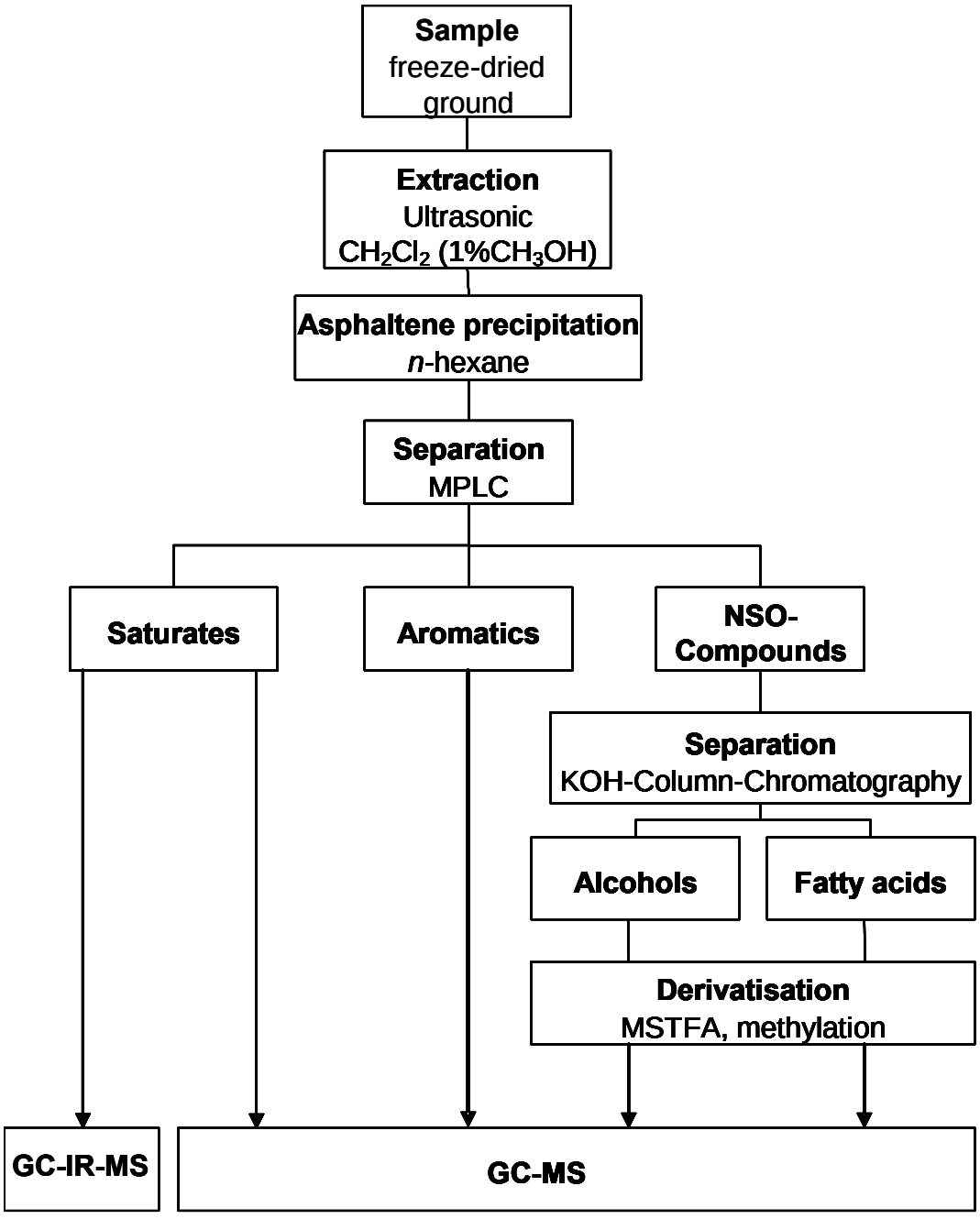

Figure 3.2: Schematic workflow of lipid analysis.

Sample extraction

Freeze-dried and grinded sample aliquots of about 2 g of the lignites and about 10 g to 20 g of the clay and sand samples were extracted ultrasonically using a mixture of dichloromethane (CH_2Cl_2) and methanol (CH_3OH) (99/1, v/v). For the extraction, between 50 and 80 ml of the solvent mixture were added to the sample aliquots. The samples were extracted ultrasonically

(Bandelin Sonorex) for 15 min. After removing of the supernatant the procedure was repeated twice. Subsequently, the volume of the resulting extract was concentrated using a Zymark TurboVap 500 concentrator and finally evaporated to dryness under a nitrogen gas stream.

Asphaltene precipitation and addition of internal standards

The obtained extract was dissolved in 250 µl CH_2Cl_2 and internal standards (5α-androstane, ethylpyrene, 5α-androstan-17-one, eruic acid) were added: 100 µl for the lignite samples and 80 µl of the internal standards (100 µg/ml) for the clay and sand samples. Hence, each sample contained 10 µg or 8 µg of each standard, respectively. Afterwards a 40-fold excess of *n*-hexane was added (10 ml) to precipitate the *n*-hexane unsoluble asphaltenes from the extract. This step was necessary for the subsequent medium pressure liquid chromatography (MPLC), where *n*-hexane is used as the only eluent. The precipitated asphaltenes were removed from the soluble fraction (soluble bitumen) by filtration over sodium sulphate (Na_2SO_4). The *n*-hexane soluble bitumen was concentrated and evaporated to dryness. The asphaltenes were collected by washing the Na_2SO_4 filter with CH_3OH.

Medium pressure liquid chromatography (MPLC) separation

The complex *n*-hexane-soluble fraction was separated by medium-pressure liquid chromatography (MPLC), into three fractions: aliphatic/alicyclic hydrocarbons, aromatic hydrocarbons and hetero-compounds (NSO; nitrogen, sulphur and oxygen) fraction. This semi automatic separation procedure of complex hydrocarbon mixtures has been established by Radke et al. (1980) based on polarity differences of the soluble organic matter. Each extract was dissolved in 1 ml of *n*-hexane. 800 µl of each extract were injected for the separation into a sample loop. The residual 200 µl were withheld as a retain sample. In the initial stage of the MPLC-separation the sample extract is flushed with *n*-hexane through a pre-column, filled with 90% of silica gel 100 (63-200µm) and 10% of silica gel 10 (200-500µm), retaining the hetero-compounds. The mobile compounds are eluted to the main chromatographic column. While the aromatic hydrocarbons are retained at the top of the main column, the aliphatic hydrocarbons are flushed through the column to form the aliphatic/alicyclic hydrocarbon fraction. In order to receive the aromatic hydrocarbon fraction, in a second step the aromatic hydrocarbons are eluted by a reversed flow with an increased flow rate and a longer elution time from the main column. The hetero-compound fraction is eluted separately from the pre-column using a special apparatus and a solvent mixture of CH_2Cl_2 and CH_3OH (95:5). All fractions were concentrated and evaporated to dryness.

Chromatographic separation of the free fatty acid fraction

Carboxylic acids were separated from the hetero-compound fraction using a column filled with KOH-impregnated silica gel prepared by adding 0.5 g KOH in 10 ml isopropanol to 5 g silica gel 100 (63-200 µm). The hetero-compound fractions were dissolved in 1 ml of a mixture of CH_2Cl_2 and CH_3OH (99/1, v/v). 800 µl were placed on the KOH column. The residual 200 µl were withheld as a retain sample. The free fatty acids are immobilized on the KOH-impregnated column by transformation into their potassium salts. The non-acidic compounds (neutral polar fraction) were eluted with 200 ml CH_2Cl_2. Subsequently, the precipitated potassium salts are converted back to free fatty acids using 50 ml of a formic acid (2 %, v/v) CH_2Cl_2 mixture. Subsequently, the fatty acids are obtained with 150 ml CH_2Cl_2. Both fractions were concentrated and evaporated to dryness.

Derivatisation of the sample material prior to GC analysis

In order to increase the compound mobility on the GC-column fatty acids and other compounds in the neutral polar fraction (e.g. alcohols) have to be converted into less polar compounds prior to GC analysis.

Half of the fatty acid fraction was converted into their corresponding methyl esters using diazomethane as methylation reagent. The other half was withheld as a retain sample. The diazomethane reagent was freshly produced from Diazald® (N-Methyl-N-nitroso-4-toluolsulfonacidamide ($CH_3C_6H_4SO_2N(CH_3)NO$), Aldrich) in a so-called Diazald®-apparatus from Aldrich. Therefore 1 g Diazald® were dissolved in 9 ml ether and subsequently added to ethanolic potassium hydroxide (1 g KOH (provided in 1.6 ml $H_2O_{dest.}$) dissolved in 2 ml ethanol). After distillation the obtained diazomethane ether reagent contains approximately 140 mg diazomethane. 500 µl of the diazomethane reagent were added to the fatty acid extract dissolved in CH_2Cl_2. The sample vials were kept closed for 1hour before the ether was evaporated at room temperature.

The neutral polar fraction compounds bearing a hydroxy group were converted into their corresponding trimethylsilyl ethers using trimethylsilyltrifluoroacetamide (MSTFA). For this purpose, the samples were dissolved in 60 µl (lignites) or 40 µl (sands and clays) of CH_2Cl_2 and half of the extract was derivatized with methyl-N-trimethylsilyltrifluoracetamide (F_3C-CO-$N(CH_3)$-$Si(CH_3)_3$, MSTFA) by heating the mixture in a closed vial at 70°C for 1hour. The other half was withheld as a retain sample. Additionally, the same procedures were carried out for the fatty acids fractions, to ensure, that in case of an incomplete chromatographic separation on the KOH-column, non-fatty acid hetero-compounds are detected.

Gas chromatography-mass spectrometry (GC-MS)

Prior to the GC-MS analysis, behenic acid methyl ester (BAME, 100µg/ml) was added as injection standard to the aliphatic hydrocarbon (lignite samples: 4 µg BAME, other samples: 3.2 µg BAME), aromatic hydrocarbon (lignite samples: 4 µg BAME, other samples: 3.2 µg BAME) and neutral polar fractions (lignite samples: 1.6 µg BAME, other samples: 1.28 µg BAME). Squalene was added to the fatty acid fraction (lignite samples: 1.6 µg squalene, other samples: 1.28 µg squalene). The amount of injection standards correspond to the theoretical amounts of the internal standards in each sample after dividing of the samples (retain samples) and conducted to control the quality of sample preparation by comparing the peak area of the injection standard with that of the internal standard.

The samples were analyzed using a gas chromatographic system coupled with a mass spectrometer. Compound separation was performed on a Agilent 6890 Series GC-instrument equipped with a PTV injection system and a fused silica capillary column (SGE BPX5; 50 m length, inner diameter = 0.22 mm, film thickness = 0.25 µm). Helium was used as carrier gas, and the temperature of the GC oven was programmed from 50°C (1 min) to 310°C at a rate of 3°C/min, followed by an isothermal phase of 10 min. The injector temperature was programmed from 52°C to 300°C at a rate of 12°C/s. For compound identification, the gas chromatographic system was linked to a Finnigan MAT 95 XL mass spectrometer operating in the electron impact mode (70 eV). Full scan mass spectra were recorded from *m/z* 50 to 650 at a scan rate of 1 s per decade and an inter scan delay of 0.2 s, resulting in a scan cycle time of 1.3 s.

Qualitative and quantitative analysis of the analytical results

The fractions were analysed with regard to their molecular composition. In this study, *n*-alkanes, *n*-alcohols, *n*-fatty acids, sesqui-, di-, and triterpenoic hydrocarbons were identified and quantified. The identification of compounds of known homologous series (*n*-alkanes, *n*-alcohols, *n*-fatty acids) was carried out by comparing the retention time for these compounds with those of standard mixtures. Other compounds were identified by comparison of their mass spectra with known spectra from literature.

Compound quantification was performed by evaluating the compound peak area of the GC-MS-analysis relative to the peak area of the internal standards. The measured peak areas of the internal standards were assigned to their initial amount (8 µg or 10 µg). Thus, the sample partitions must not be taken into account for the compound quantification. Finally, the

amounts were normalized to the quantity of sediment used for extraction (gSed) or to the content of organic carbon (gTOC) in the sample.

3.2.7 Compound specific carbon isotope analysis (GC-IR-MS)

The carbon isotope composition of the aliphatic fractions was measured with a GC-IR-MS (gas chromatography/combustion/isotope-ratio mass spectrometry) system. Aliquots (3 µl) of the extracts were injected into the GC (Agilent 6890 N, Agilent Technology, USA) in split mode and separated on a fused silica capillary column (HP Ultra 1; 50 m x 0.32 mm x 0.52 µm film thickness, Agilent Technologies, USA). Helium, set to a flow rate of 1.5 ml min^{-1}, was used as carrier gas. The injector temperature was held constant at 250°C. The oven temperature was initially set to 80°C and held for 1 min. The temperature was then increased at a rate of 3°C min^{-1} to 310°C and held for 20 min. The GC unit was connected to a combustion interface (GC-III, Thermo Electron, Germany) with a water removal assembly (Nafion® membrane) coupled to a Finnigan MAT 253 mass spectrometer (Thermo Electron, Germany). Organic substances in the GC effluent stream were oxidised to CO_2 and H_2O in the combustion furnace held at 940°C on a CuO/Ni/Pt catalyst and were transferred online via open split to the isotope ratio mass spectrometer to determine $^{13}C/^{12}C$ ratios of CO_2. The instrument was calibrated using a reference gas (CO_2) with known isotopic composition. Additionally, a mixture of three alkanes (C_{15}, C_{20} and C_{25}) with known isotopic composition (Chiron, Norway) was measured after every fifth run to check the system performance.

3.2.8 Phospholipid analysis

The analytical workflow of the phospholipid analysis is shown in Figure 3.3.

Sample extraction

For the analysis of phospholipids a special method was developed modified after Bligh and Dyer (1959). After sediment samples had been freeze-dried and grinded, sample aliquots of 36 to 75 g (depending on available sample quantity) were extracted using a flow blending system. Prior to the extraction, 100 µl of deuterated lysophosphatidylcholine (500 µg/ml) as internal standard were added. Afterwards, the sample material was stirred at a rotation speed of 16000 min^{-1} using about 100 to 200 ml of a solvent mixture of methanol/dichloromethane/ammonium acetate buffer (pH 7.6) in a ratio of 2:1:0.8 (v/v) for 5 min. The solvent extract was separated from the residual sediment by centrifugation (3500 rpm) for 10 min at a temperature of 15°C. After removal of the supernatant the sediment residue was

re-extracted ultrasonically for 10 min two additional times using 25 ml of the same solvent mixture. The combined solvent extracts were collected in a separation funnel and dichloromethane and water were added to achieve a ratio of 1:1:0.9 (v/v). After phase separation, the organic phase was recovered and the water phase was re-extracted two times with 20 ml dichloromethane. The combined organic phases were concentrated and evaporated to dryness.

Chromatographic separation

Subsequently, the extract (dissolved in 1 ml chloroform/methanol, 9:1 (v/v)) was separated into fractions of different polarity (low polar lipids, free fatty acids, glycolipids and phospholipids) using a pure silica column (1 g silica gel 63-200 µm) and a florisil column (1 g magnesium silica gel 150-250 µm) in sequence(Zink & Mangelsdorf, 2004). The low-polarity lipid fraction was obtained by elution with 20 ml of chloroform, the free fatty acids fraction with 50 ml of methyl formate containing 0.025% glacial acetic acid, the glycolipid fraction with 25 ml of acetone and the phospholipid fraction with 25 ml of methanol. All fractions were concentrated and evaporated to dryness.

HPLC-ESI-MS measurement

Preceding the measurements, the samples were dissolved in 1 ml of CH_3OH and divided in half. The methanol fractions were analysed for intact phospholipids on an HPLC instrument (Shimadzu SCL-10a VP) coupled to a Finnigan MAT TSQ 7000 mass spectrometer equipped with an electrospray interface. Separation of phospholipid classes was achieved with normal-phase HPLC on a pure silica gel column 125 x 2 mm (Hypersil Si-3µm). The HPLC was equipped with a 5 µl sample loop, the flow rate was set to 150 µl/min with a gradient solvent system of chloroform (A), methanol (B), and ammonium acetate buffer (10 mM; C) modified after Aries et al. (2001). The initial mobile phase composition was 30% A, 65% B, 5% C; B was decreased to 55%, and C increased to 15% after 3 min; after 8 min the mobile phase was reset to initial conditions and was held isocratically for 7 min, resulting in a total time of analysis per sample of 15 min. Full scan mass spectra were recorded in the negative ion mode over a *m/z* range of 400 to 1800 at a scan rate of 1 scan every 2 s.

Each sample was measured several times and additionally, a mixture of four different phospholipid standards (phosphatidylglycerol, -ethanolamine, and -choline and the internal standard (lysophosphatidylcholine)) was measured prior to each sample set measured on the same day to check the performance of the system.

For each Mallik sample investigated the same methods were simultaneously applied to reference samples (quartz sand) using the same solvents and chemicals to check for any microbial contamination during the laboratory processes. All reference samples were tested negative with regard to a microbial phospholipid signal.

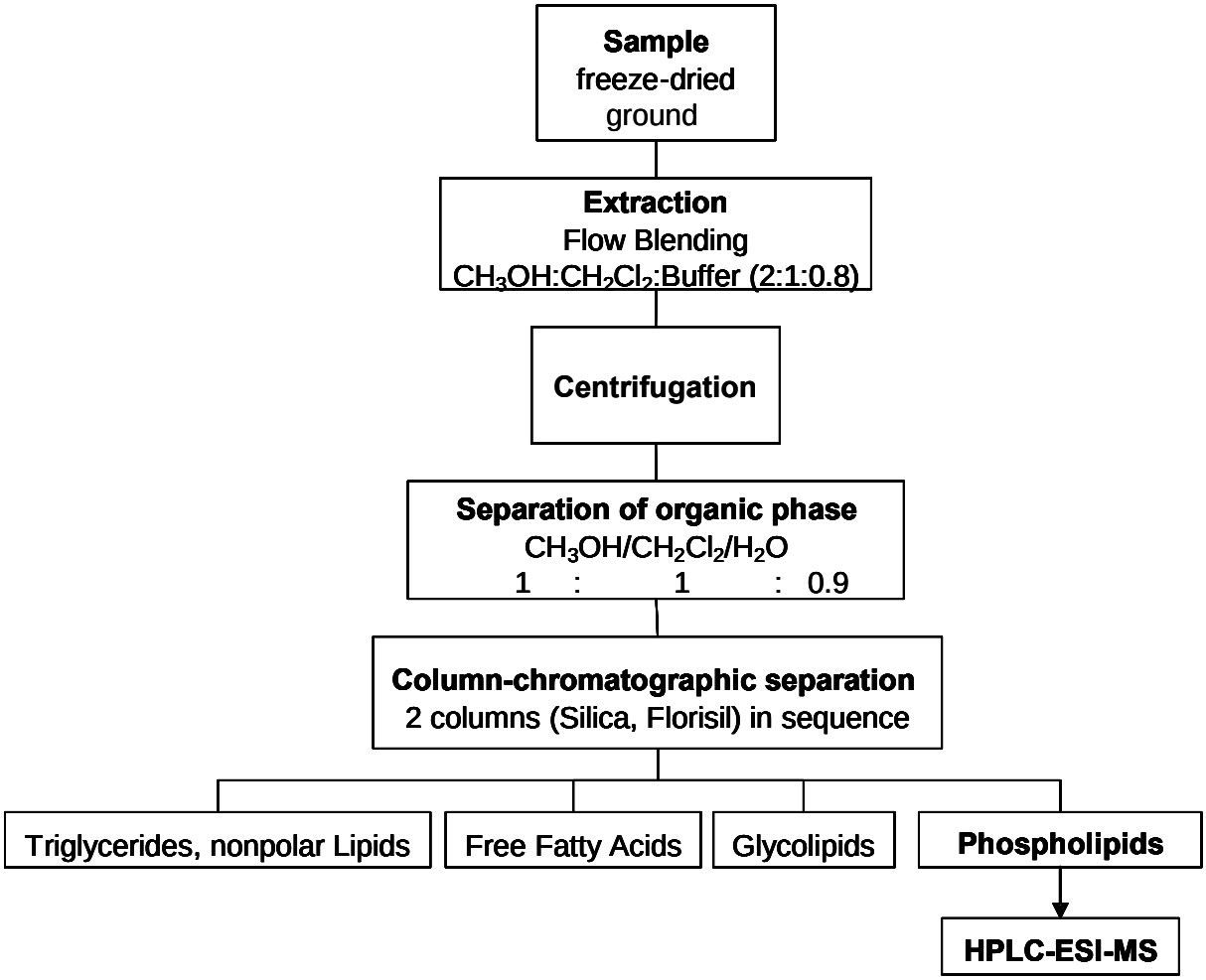

Figure 3.3: Schematic workflow of the phospholipid analysis.

MS-MS experiments

For detailed structural elucidation of individual phospholipids (phospholipid head group, fatty acyl side-chains) collisionally activated dissociation (CAD) tandem quadrupole MS experiments were performed (argon as collision gas, collision energy 30 eV) over a *m/z* range of 100 to 800 at a scan rate of 1 scan/s.

3.2.9 Glycerol etherlipid analysis

For the detection of tetraether lipids the acetone fractions (clay and sand samples) and the neutral polar fractions (lignites) were analysed using an high-performance liquid chromatography/atmospheric pressure chemical ionisation mass spectrometry (HPLC/APCI-MS) method modified after Hopmans et al. (2004). Chromatographic separation was achieved on a Sphere Image 3 CN column (150 x 2 mm, 3 µm; CS-Chromatography, Düren, Germany). The mobile phase consists of *n*-hexane A and isopropanol B (5 min 99% A, 1% B), followed by a linear gradient to 1.4% B within 22.5 min, then within 1 min to 10% B, holding 5 min to clean the column and back to initial conditions in 1 min, held for 6 min for equilibration. The flow rate was set to 200µl/min and injection was performed via autosampler with a 5µl loop. The conditions for the APCI-MS were as follows: corona current 5 µA giving a voltage of around 4 kV; vaporiser temperature 350°C; capillary temperature 200 °C and voltage 7.5V; nitrogen sheath gas at 60 psi (4 bar); without auxiliary gas. Mass spectra were generated by selected (single) ion monitoring (SIM), in the positive ion mode resulting in protonated $[M+H]^+$, $[M+H]^+$+1, and $[M+H]^+$+2 molecular ions, the multiplier voltage was 1500 V, and the scan rate was 2s. For full scan analysis m/z range from 900 to 1400 was used. For semi-quantitative determination of tetraether compounds an external synthetic archaeol standard (AvantiPolarLipids Inc., Al, USA) was used. Linearity and reproducibility was tested on 3 concentrations (0.1, 1, 10 µg/ml) analysed in triplicates and parallel to the sample sequence.

4 Characterisation of the organic matter in lignite layers of the Kugmallit Formation (Oligocene) at the JAPEX/JNOC/GSC et al. Mallik 5L-38 gas hydrate production research well*

*R.M. Haberer, K. Mangelsdorf, V. Dieckmann, A. Fuhrmann, H. Wilkes, B. Horsfield (2005). In: S.R. Dallimore, T.S. Collett (Eds.), Scientific results from Mallik 2005 Gas Hydrate production Research Well Program, Mackenzie Delta, Northwest Territories, Canada, Bulletin 585. Geological Survey of Canada

4.1 Introduction

Organic matter derived from biological precursors is an ubiquitous constituent of sedimentary rocks. Its concentration and composition are known to be controlled by a variety of physical, chemical and biological factors, acting from the time of sedimentation through to deep burial during subsidence. The organic matter, incorporated in the sediments, is composed of two main fractions: the complex macromolecular kerogen, which is insoluble in common organic solvents and typically more than 90% of the organic matter, and the free lipid fraction, or bitumen, soluble in these solvents and typically 1-10% of the organic matter (e.g. Rullkötter, 1992; Summons, 1993). Kerogen is divided into three main types according to its hydrogen content (Type I-III kerogen). Additionally kerogen characterisation gives information on the hydrocarbon potential, and the thermal maturity of the organic material (e.g. Tissot & Welte, 1984). Contrary to the macromolecular kerogen, the in *n*-hexane soluble bitumen consists of lower molecular weight organic compounds. Certain of its constituents, the so-called biomarkers, can be traced to their precursor biomolecules and with that permit conclusions on the origin of the organic material, the degree of diagenetic alteration and also the level of maturity of the organic matter (e.g. Rullkötter, 1992; Summons, 1993).

In this study, we present our preliminary results on the investigation and characterisation of nine organic carbon-rich sediment samples from the Kugmallit Sequence of the JAPEX/JNOC/GSC et al. Mallik 5L-38 gas hydrate production research well using different analytical approaches to examine both the kerogen and the bitumen. This organic geochemical characterisation of subsurface sediments at the Mallik site is the starting point for the authors examination of the nature and the depth range of deep microbial ecosystems using biogeochemical methods (Mangelsdorf et al., 2005a). In this regard, it has been hypothesised that organic carbon-rich lithologies may provide a potential carbon and energy source for deep microbial communities (Krumholz et al., 1997), and the lignite layers of the Kugmallit Sequence (Oligocene) may represent such a carbon and energy source for the deep microbial ecosystems, already detected near the Mallik site (Colwell et al., 1999). Our additional inves-

tigations on specific biomarkers, characteristic of viable microbial communities are outlined in a companion paper (Mangelsdorf et al., 2005a).

4.2 Study area

The Mallik 5L-38 Gas Hydrates Research Well (Figure 4.1) is located at the northern edge of the Mackenzie River Delta (Northwest Territories, Canada). A succession of about 1165 m of Cenozoic sediments has been penetrated (Figure 4.2). The special feature of the Mallik site is a massive permafrost zone from 0-650 m and a zone of numerous gas hydrate bearing layers between 896 m and 1100 m (Dallimore & Collett, 2005).

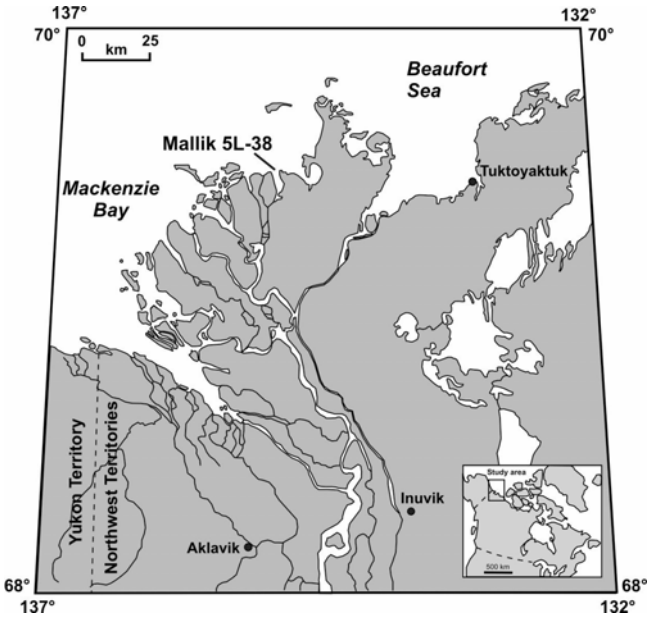

Figure 4.1: Map of the Mackenzie River Delta (Northwest Territories, Canada) and the drilling location of the Mallik 5L-38 Gas Hydrate Production Research Well.

The succession of sediments in the Mallik area reflects a sedimentation dominated by deltaic-processes (Dixon, 1996; Dixon et al., 1992a). The Kugmallit Sequence (930-1165 m, Oligocene) is sand-dominated with interbedded silts, clays and some lignite layers. In the Mallik area, the Kugmallit Sequence represents typically delta-plain deposits (Dixon, 1996). The clays and lignite layers were probably deposited in interdistributary marshes and minor channels (Young et al., 1976). The Mackenzie Bay Sequence (350-930 m, Late Oligocene - Middle Miocene) consists of sand and weakly cemented sandstones with conglomerates. There are only minor silt or shale interbeds. The Mackenzie Bay Sequence is, contrary to the delta-plain deposits of the Kugmallit Sequence, related to sedimentation processes at the delta-front zone (Dixon, 1996). The Akpak Sequence (Middle – Upper Miocene) is absent in the sedimentological succession of the Mallik Well due to erosion (Dixon, 1996; Dixon et al., 1992b).

The Iperk Sequence (0-350 m, Plio- to Pleistocene) is composed of unconsolidated sandstones with local intermediary conglomerates, silt and shale layers. Similar to the Kugmallit Sequence, the Iperk Sequence represents delta-plain or even fluvial sediments (Dixon, 1996; Dixon et al., 1992b).

4.3 Samples and methods

4.3.1 Sampling

The drilling strategy during the Mallik project restricted the coring interval from 880 to about 1160 m (Dallimore *et al.*, 1999; Medioli *et al.*, 2005). Thirty sediment samples (18 - 170 g) from different lithologies such as clays, siltstones, sandstones and lignite carbon-rich layers from above, within and below the gas hydrate zone were collected predominantly from the Kugmallit Sequence (Table 4.1, Figure 4.2). All samples labelled with MB (table 4.1) were gathered, transported and stored, employing specific precautions with a view to avoid any microbial contamination from surface microorganisms (see chapter 3.1 and Mangelsdorf et al. (Mangelsdorf *et al.*, 2005a)). As the coaly lignite layers within the gas hydrate zone may act as a carbon and energy source for microbial communities, we collected nine additional samples (Figure 4.2). The samples were directly sealed in Teflon® receptacles and immediately stored under liquid nitrogen (-196°C) to avoid any degradation or contamination processes. In this study, we present our preliminary results on these nine organic carbon-rich sediments; bulk parameters are reported for all samples taken.

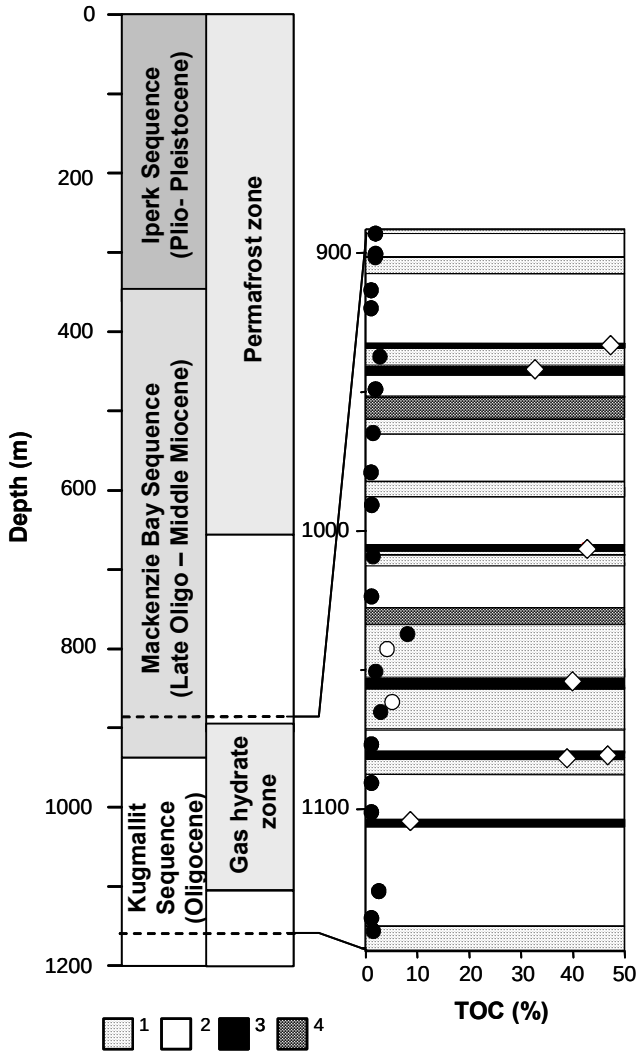

Figure 4.2: Stratigraphic column of the Mallik 5L-38 Gas Hydrate Research Well. The positions of our selected sediment samples are displayed relative to the different lithologies and their total organic carbon (TOC) content. Non-lignite samples are indicated with black dots. Lignites are indicated with diamonds; organic-carbon rich shale samples are indicated with circles. 1 = silt/clay, 2 = sand, 3 = lignite layer, 4 = conglomerate.

4.3.2 Methods

Bulk parameters

After the sediment samples had been freeze-dried and ground, the TOC and $CaCO_3$ (calculated from TIC-values) contents and also the Rock-Eval parameters (hydrogen index (HI) and oxygen index (OI), T_{max} values) (Espitalié *et al.*, 1977) were determined using a Rock-Eval 6 instrument (Table 4.1).

Carbon isotopic composition of the organic matter

Carbon isotopic compositions of total organic matter were measured after dissolution of carbonates with HCl (10%; at 50°C for 1.5 h), subsequently washing with distilled water three

times and drying the residues at 50°C for 12 hours. The isotopic analyses have been performed in continuous flow mode on a DELTAplus XL mass spectrometer in combination with a CA-1500 elemental analyser. Isotopic ratios are expressed as $\delta^{13}C_{org}$ values in per mil relative to the V-PDB standard.

Microscopy

For microscopic studies the lignite samples were embedded in epoxy resin. The resultant blocks, orientated vertical to the bedding, were ground flat and polished. Qualitative observations were performed in reflected white and fluorescence light (excitation at 365 nm) using a Zeiss Axiophot microscope and oil immersion objectives with 20x and 50x magnifying power. Qualitative microscopic investigations have been carried out according to the maceral definitions given by Taylor et al. (1998).

Pyrolysis gas chromatography

Sample aliquots (3 mg to 17 mg) of lignites were analysed by open-system pyrolysis using a Quantum MSSV-2 Thermal Analyzer (cf. Horsfield et al., 1989) interfaced with an Agilent GC 6890A. For this purpose the samples were placed into the central part of a glass tube (26 mm long; inner sleeve diameter 3 mm). The remaining volume was filled with quartz wool cleaned at 630°C in air for 30 min. After flushing at 300°C (5 min) to remove the volatile material, the samples were pyrolysed using a temperature program from 300°C (50°C/min) to 600°C (3 min, isothermal). The products were first cryogenically trapped (liquid nitrogen trap), then analyzed by on-line gas chromatography. A dimethylpolysiloxane capillary column (HP-Ultra 1; 50 m length, inner diameter = 0.32 mm, film thickness = 0.52 µm) connected to a flame ionisation detector (FID) was used with helium as carrier gas. The temperature of the GC oven was programmed from 30°C to 320°C at a rate of 5°C/min, followed by an isothermal phase of 35 min.

Lipid analysis

For lipid analysis, sample aliquots of about 2 g of the lignites were extracted ultrasonically using a mixture of CH_2Cl_2 and methanol (99/1, v/v). Subsequently, the volume of the resulting extract was concentrated using a Zymark TurboVap 500 concentrator and finally evaporated to dryness under a nitrogen gas stream. After addition of internal standards (androstane, ethylpyrene, 5α-androstan-17-one, eruic acid), the extract was dissolved in *n*-hexane to precipitate asphaltenes, which were removed from the soluble fraction by filtration over Na_2SO_4. The *n*-hexane-soluble fraction was separated by medium-pressure liquid chromatography

(Radke et al., 1980) into fractions of aliphatic/alicyclic hydrocarbons (hereafter simply called aliphatic hydrocarbons), aromatic hydrocarbons and nitrogen, sulphur and oxygen (NSO) compounds. Carboxylic acids were separated from the NSO compound fraction using a column filled with KOH-impregnated silica gel prepared by adding 0.5 g KOH in 10 ml isopropanol to 5 g silica gel 100 (63-200 μm). The non-acidic compounds (neutral fraction) were eluted with CH_2Cl_2. Following this the acidic fraction was eluted with 50 ml of a formic acid solution (2% in CH_2Cl_2) and subsequently 100 ml CH_2Cl_2. Prior to GC analysis the acid fraction was methylated with diazomethane and the neutral fraction was silylated with trimethylsilyltrifluoroacetamide (MSTFA). Additionally, behenic acid methyl ester (BAME) was added as injection standard to the aliphatic hydrocarbon, aromatic hydrocarbon and neutral hydrocarbon fractions. Squalene was added to the fatty acid fraction. The fractions of interest were analyzed using a gas chromatographic system coupled with a mass spectrometer. Compound separation was performed on a Agilent 6890 Series GC-instrument equipped with a PTV injection system and a fused silica capillary column (SGE BPX5; 50 m length, inner diameter = 0.22 mm, film thickness = 0.25 μm). Helium was used as carrier gas, and the temperature of the GC oven was programmed from 50°C (1 min) to 310°C at a rate of 3°C/min, followed by an isothermal phase of 20 min.

The injector temperature was fixed at 230°C. For compound identification, the gas chromatographic system was linked to a Finnigan MAT 95 XL mass spectrometer operating in the electron impact mode (70 eV). Full scan mass spectra were recorded from *m/z* 50 to 650 at a scan rate of 1 s per decade and an inter scan delay of 0.2 s, resulting in a scan cycle time of 1.3 s.

Table 4.1: Sample numbers, core depths, lithological description, total organic carbon contents (TOC), carbonate contents, bulk organic carbon isotope values ($\delta^{13}C_{org}$), T_{max}-values, hydrogen index (HI), oxygen index (OI), extract yields of bitumen, and carbon preference index ($CPI_{21\text{-}27}$; $CPI = \frac{1}{2} * \left(\frac{C_{21}+C_{23}+C_{25}}{C_{22}+C_{24}+C_{26}} + \frac{C_{23}+C_{25}+C_{27}}{C_{22}+C_{24}+C_{26}} \right)$) of 30 sediment samples of the Mallik 5L-38 Gas Hydrate Research Well. n.d. = not determined (to date).

Mallik 5L-38	Sample characteristics									
Sample	**Depth (m)**	**Lithology**	**TOC (%)**	**CaCO3(%)**	**$\delta^{13}C_{org}$ (‰)**	**T_{max} (°C)**	**HI (mg HC/g TOC)**	**OI (mg CO_2/g TOC)**	**Extracted Bitumen (mg/g TOC)**	**$CPI_{21\text{-}27}$**
MB89163	891.63 – 891.82	silt/clay	0.92	3.33	n.d.	424	80	215	30.4	n.d.
MB89899	898.99 – 899.16	silt/clay	0.95	4.17	n.d.	426	103	243	51.8	n.d.
MB90020	900.20 – 900.40	silt/clay	0.86	2.50	n.d.	425	77	230	66.5	n.d.
MB91200	912.00 – 912.19	sand	0.05	n.v.d.	n.d.	-	14	n.v.d.	168.6	n.d.
MB91856	918.56 – 918.76	sand	0.05	n.v.d.	n.d.	-	50	100	81.0	n.d.
CO93409	934.09 – 934.10	lignite	46.60	10.83	-24.6	363	195	43	68.4	3.9
MB93589	935.89 – 936.09	silt/clay	1.78	1.67	n.d.	424	177	167	33.1	n.d.
CO94078	940.78 – 940.81	lignite	31.85	16.66	-25.6	392	292	56	59.5	2.4
MB94762	947.62 – 947.84	sand	0.95	0.83	n.d.	406	72	44	100.5	n.d.
MB96334	963.34 – 963.50	silt/clay	0.40	2.50	n.d.	416	42	263	132.8	n.d.
MB97760	977.60 – 977.80	sand	0.09	0.83	n.d.	-	47	n.v.d.	54.5	n.d.
MB98925	989.25 – 989.45	sand	0.10	0.83	n.d.	-	12	410	28.8	n.d.
CO100550	1005.50	lignite	42.03	20.83	-24.9	400	207	56	48.5	3.6
MB100778	1007.78 - 1007.98	silt/clay	0.46	0.83	n.d.	426	111	65	99.3	n.d.
MB102215	1022.15 – 1022.55	sand	0.11	n.v.d.	n.d.	-	134	36	62.0	n.d.
MB103360	1033.60 - 1033.80	silt/clay	7.09	3.33	n.d.	415	175	68	39.6	n.d.
CO104310	1043.10	silt/clay	3.64	1.67	-26.3	430	532	48	114.7	3.3
MB104920	1049.20 – 1049.36	silt/clay	1.01	7.50	-25.5	428	103	898	36.4	n.d.
CO105353	1053.53	lignite	39.19	19.99	-24.3	388	247	55	63.0	2.5
CO106094	1060.94 – 1060.95	silt/clay	4.71	1.67	-26.0	420	165	75	72.4	4.7
MB106380	1063.80 – 1064.00	silt/clay	1.89	2.50	-25.5	417	104	113	37.5	n.d.
MB107960	1079.60 – 1079.81	sand	0.04	n.v.d.	n.d.	-	10	n.v.d.	444.6	n.d.
CO108138	1081.38	lignite	45.93	14.16	-25.8	406	115	62	29.3	4.5
CO108169	1081.69	lignite	38.39	11.66	-24.1	392	220	57	27.9	3.6
MB108924	1089.24 - 1089.39	sand	0.06	n.v.d.	n.d.	-	38	333	77.5	n.d.
MB110494	1104.94 - 1105.14	sand	0.09	0.83	n.d.	-	33	n.v.d.	104.6	n.d.
CO110550	1105.50	lignite	9.44	11.66	-25.1	411	101	99	21.6	n.d.
MB112790	1127.90 - 1128.02	sand	1.57	0.83	-25.8	421	67	127	13.3	n.d.
MB113980	1139.80 - 1139.83	sand	0.17	0.83	n.d.	-	123	459	42.2	n.d.
MB114535	1145.35 - 1145.55	silt/clay	0.53	2.50	n.d.	424	72	340	96.7	n.d.

4.4 Results and discussion

4.4.1 Bulk characteristics

Table 4.1 compiles the bulk data of elemental analysis, Rock-Eval pyrolysis, the extract yields, and the bulk organic carbon isotopic measurements. Additionally, a brief lithological characterisation of each sample is given. The TOC values range between 0.04% and 46.6%. This variation correlates with the lithological difference of the sample material; sand layers reveal the lowest and lignites the highest TOC contents (Figure 4.2). According to initial core descriptions, two samples (CO104310 and CO106094; visualized by circles in Figure 4.2, Figure 4.3 and 4.4.4) were assigned as coal (CO, lignite), however, their obviously low organic carbon contents of 3.64 and 4.71%, respectively, revealed that these samples are organic-rich shales rather than lignites. In this report, these samples are therefore assigned as organic carbon-rich shales. The $\delta^{13}C_{org}$ data of all investigated samples show only minor variations from -24.3 to -26.3‰. Such values are typical for organic carbon from a terrestrial source for Cenozoic age sediments (Hoefs, 1997).

The HI values of most studied samples range between 3 mgHC/gTOC and 300 mgHC/gTOC with the organic carbon-rich samples (diamonds and circles, Figure 4.3) characterized by systematically higher HI values between 100 and 300 mgHC/gTOC and low OI values (<100 $mgCO_2$/gTOC) in comparison to the non-lignite samples (Table 4.1, Figure 4.3a). One sample (CO104310) is characterized by an unusually high HI value (532 mgHC/gTOC) and is therefore classified as kerogen type II.

Interestingly, the soluble bitumen of this sample shows no or only minor variations of its molecular composition in comparison to the other studied samples. As discussed later, in the section of open-system pyrolysis-GC, the kerogen, despite having a type II bulk composition, does not have a marine signature, and appears to be non-marine in original. This begins to help explain the uniformity of biomarker signatures, and further investigations correlating organic petrology, biomarker and molecular kerogen composition are underway.

The HI values from the coarser-grained lithologies (dots, Figure 4.3) range from 10 to 177 mgHC/gTOC. Their OI values range from 44 to 898 $mgCO_2$/gTOC. Figure 4.4.1a shows the characteristics of the studied sample set using the pseudo van Krevelen diagram of the Rock-Eval parameters (Espitalié et al., 1977) in which most samples plot in the area of the terrigenous type III kerogen. The HI vs. T_{max} diagram (fig. 4.4.1b, after Espitalié et al., 1984) also emphasizes the terrestrial character of the investigated organic matter as previously observed in the Mallik area e.g. by Snowdon (1981; 1999). In addition, this diagram indicates

the low maturity of the organic matter taken from the Mallik 5L-38 gas hydrate zone (e.g. Snowdon, 1981;1999).

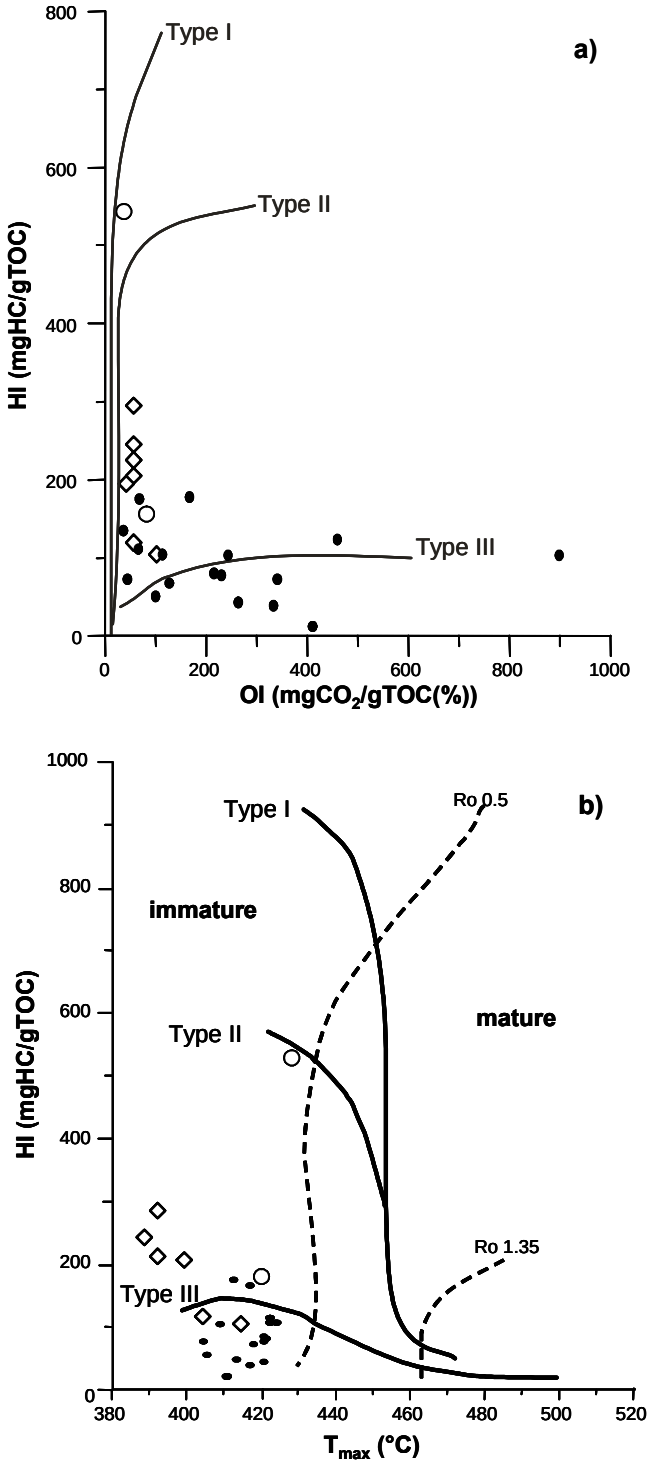

Figure 4.3: a) Cross plot of hydrogen index (HI) vs. oxygen index (OI) in the pseudo van Krevelen diagram after Espitalié et al. (1977). b) Cross plot of hydrogen index (HI) vs. T_{max} after Espitalié et al. (1984). Lignites are indicated with diamonds; organic-carbon rich shale samples are indicated with circles. Non-lignite samples are indicated with black dots. Dashed lines in fig. 3b separate different maturity zones. R_o = vitrinite reflectance.

4.4.2 Microscopic studies

The microscopic investigation supports the assessment of immature terrestrially dominated organic matter in all studied samples as already concluded from the bulk characteristics. The most common maceral group in the organic carbon-rich sediment samples of the Kugmallit sequence is huminite (Figure 4.4a). Huminite is the precursor of vitrinite in immature sediments (Taylor et al., 1998). Although vitrinite reflectance measurements, the most commonly employed maturity indicator of the organic matter, have not been performed yet, the presence of mainly open-textured, ungelified or partly gelified tissues (textinite and texto-ulminite) supports the low maturity level of the studied samples. The immaturity is also corroborated by the occurrence of strongly fluorescing cellulosic material within the plant cell structures. The fact that there is no or only very little inertinite, indicates that charring, oxidation, fungal attack and desiccation were not major processes prior to or during deposition of the sediment (Taylor et al., 1998). A maceral readily recognisable under blue light excitation is fluorinite, which derives from plant resins, balsams or waxes. Another important liptinite maceral is sporinite, which originates from outer cell walls of spores and pollen (Taylor et al., 1998). Figure 4.4b shows an example of a sporangium.

Remnants of the woody material in fluorescence light are shown in Figure 4.4c. The form and the arrangement of the structures (tracheids and pits) suggest that these parts originated from conifers (Uhl, pers. comm.). The qualitative microscopic observations also reveal that the organic-rich sample (CO104310) with a higher HI value is not distinguishable from the lignites investigated.

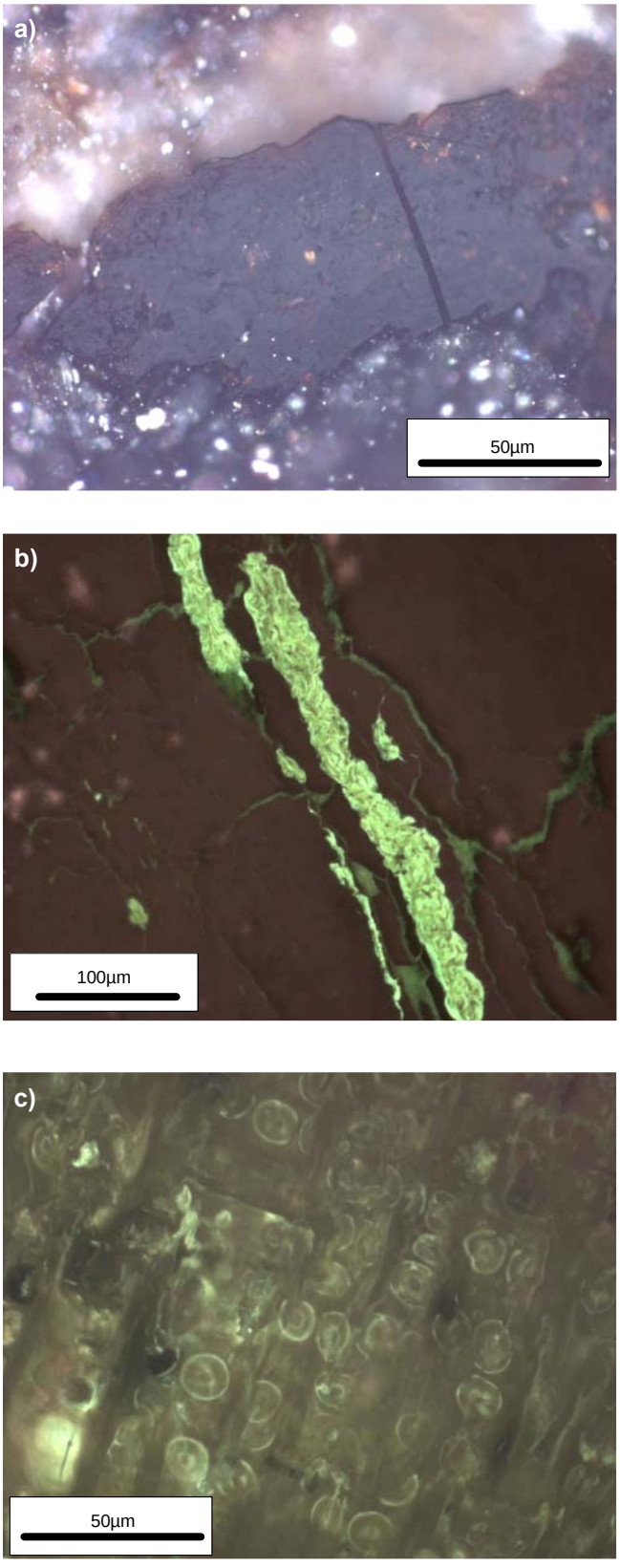

Figure 4.4: Picture a) shows a huminite particle in reflected white light (Mallik sample CO104310). Picture b) displays a sporangium in fluorescence light (Mallik sample CO108138) and in picture c) the form and the arrangement of the structures appearance in fluorescence light (Mallik sample CO93409) points to woody material of conifers (Uhl, pers. comm.).

4.4.3 Open-system pyrolysis-GC

For a more detailed characterisation, the nine selected organic-carbon rich samples were analyzed using open-system pyrolysis-GC experiments. Several different compound groups have been identified in the pyrolysis gas chromatograms (Figure 4.5). The gas chromatograms of the pyrolysates are dominated by phenols and cresols, which are related to the presence of higher land plant debris in the organic matter (Larter, 1984).

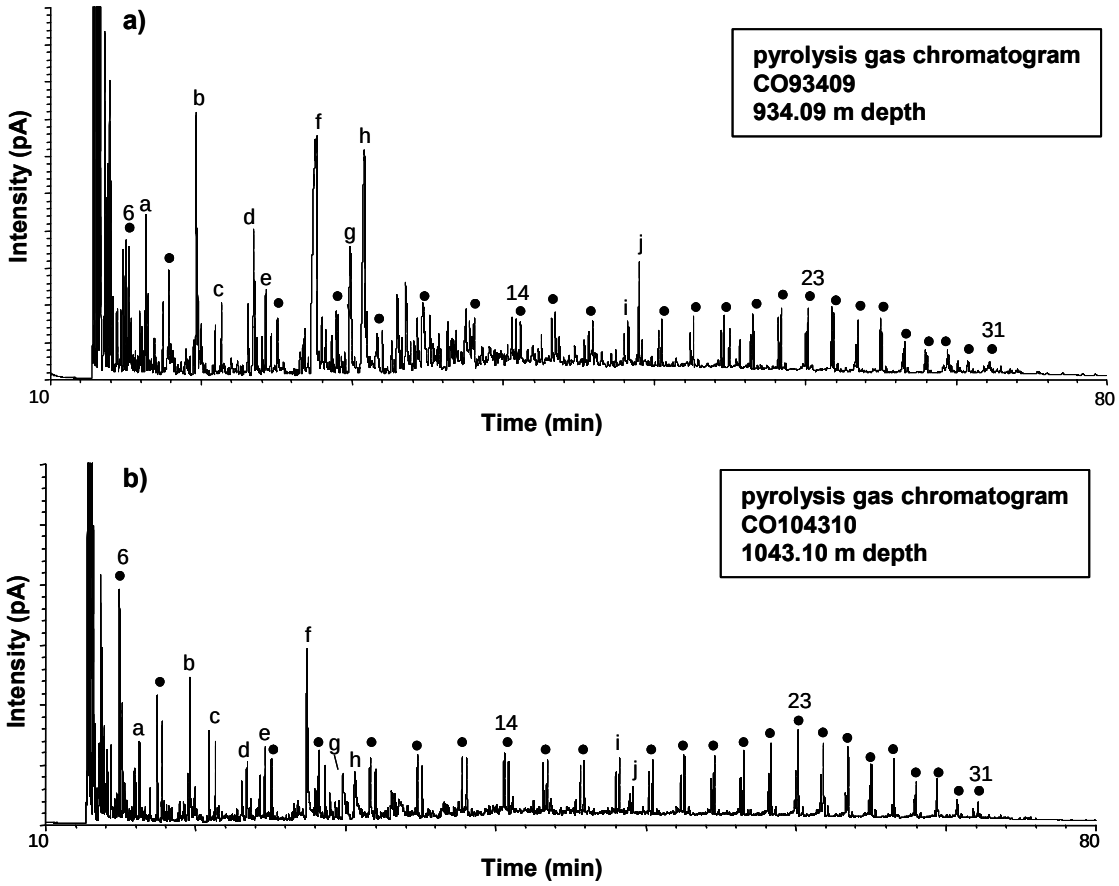

Figure 4.5: Open-system-pyrolysis gas chromatogram of a) the Mallik sample CO93409 (934.09 m depth, lignite sample, TOC value of 46.60 %) and b) the Mallik sample CO104310 (1043.10 m depth, organic carbon rich shale, TOC value of 3.64 %). a = benzene, b = toluene, c = *n*-$C_{8:1}$, d = *m*-*p*-xylene, e = *o*-xylene, f = phenol, g = *o*-cresol, h = *m*-*p*-cresol, i = *n*-$C_{17:1}$ + *n*-$C_{17:0}$, j = prist-1-ene; black dots = aliphatic hydrocarbons, numbers indicate carbon number chain length of *n*-alkanes.

In addition to these compounds, monoaromatic alkylbenzols (benzene, toluene, o-*m*-*p*-xylene) are significant components of the gas chromatographic fingerprint. Figure 4.6a illustrates a ternary plot established by Larter (1984). In this figure, the type of organic matter was defined by the relative enrichment of *n*-octene, *m*-*p*-xylene and phenol in the pyrolysates. This figure shows that the organic matter clearly plots within the range of type III kerogen indicating a mainly terrigenous origin. Phenol as well as its alkylated congeners are enriched as a result of

both the very low maturity of the samples and its origin from higher land plants (Larter, 1984). Additionally, the pyrolysis gas chromatograms of the lignites and the organic-carbon rich shales reveal a notable occurrence of aliphatic hydrocarbons characterized by a multi-modal distribution within the gas chromatogram (peaks marked with a dot in Figure 4.5) indicating a waxy-paraffinic oil potential (Curry & Simpler, 1988; Horsfield, 1989; 1997; Isaksen et al., 1998; Larter, 1984). There is an obvious maximum in the range of 14 to 23 carbon atoms and in most samples a slight even-over-odd carbon number predominance, as shown in Figure 4.5a, in the 22 to 28 carbon number range.

In Figure 4.6b, a ternary diagram after Horsfield (1989) is shown. Based on the distribution of $C_{1\text{-}5}$, *n*-$C_{6\text{-}14}$ and *n*-C_{15+}-alkyl chains in a pyrolysate, different types of depositional environment of the samples as well as the type of petroleum, which may be formed upon the burial of the organic matter preserved in the sediments, can be estimated. In general, the organic matter studied here plots within the "continental" range which is said to have a potential for mainly gas formation. This assignment of facies agrees with the lithological and sequence-stratigraphical analysis of the sedimentary milieu in the Mallik area by Dixon (1996). However, three samples (two organic-carbon rich shales CO104310, CO106094 and a lignite sample CO94078) contain kerogen whose composition shows differences as well as similarities to the kerogen of the other lignite samples. As far as the chain length distribution of kerogen substituents is concerned, the average chain length in these samples is significantly longer than seen in the lignites (Figure 4.6b). According to the calibrations set out by Horsfield (1989), this is equitable with a potential for mixed base high wax oil, and a sedimentary facies lower in the delta plain. The input of ligno-cellulosic materials (vitrinite) to shales as well as lignites is recognisable by the high abundance of phenol relative to light aromatic and aliphatic hydrocarbons (Figure 4.6a). At the time of its publication, calibrations indicated this phenolic signature to be a feature of only type III kerogen (Larter, 1984), but the shale sample CO104310 (filled circle) presented here, classified as type II kerogen by its relative high HI-content (cf. "Bulk characteristics"), shows this is no longer tenable. Terrigenous organic matter components which bring high wax oil potential to the shales may also be responsible in part for raising hydrogen indices to high values. It is important to remember that high hydrogen indices, while pointing to a high generative potential for petroleum, are not unequivocally equitable with marine influence. Additionally, the ternary diagram indicates that the samples shown here are dominated by organic matter, with a potential to form gas/condensate or in case of the three samples, as mentioned above, to form paraffinic-naphthenic-aromatic-rich wax oils.

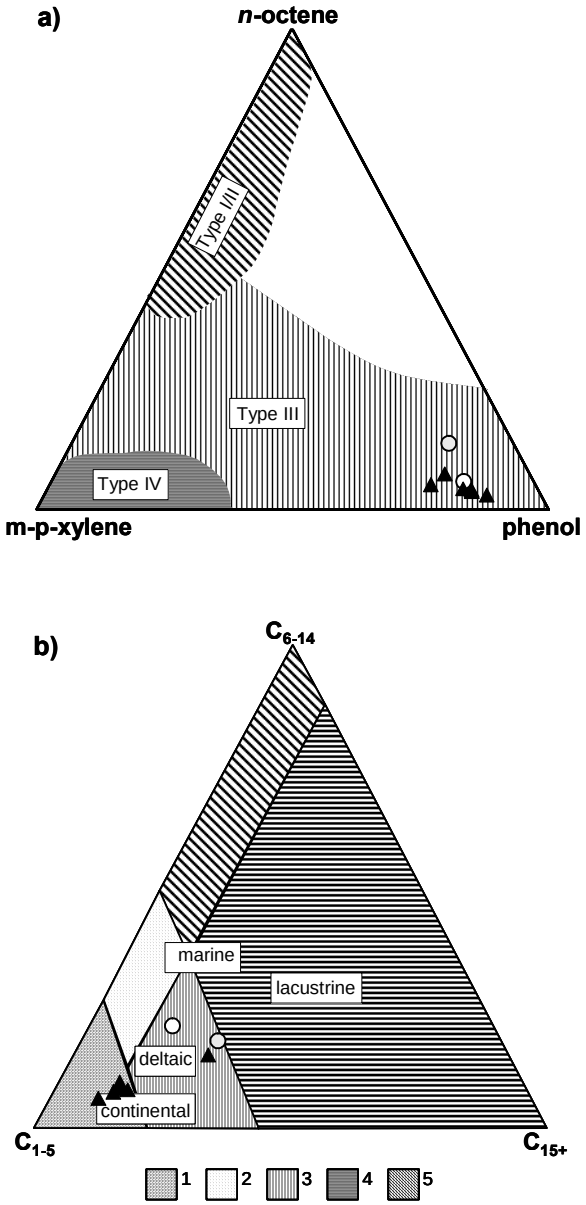

Figure 4.6: a) A ternary diagram of *n*-octene, *m*-*p*-xylene and phenol established by Larter (1984) illustrating different kerogen types of the organic matter from the Kugmallit lignites (black triangles). b) A ternary diagram of *n*-C_{6-14}, *n*-C_{15+} and C_{1-5} after Horsfield (1989) indicating different types of the organic matter in combination with their gas/oil potential. 1 = gas and condensate, 2 = paraffinic-naphthenic-aromatic oil low wax, 3 = paraffinic-naphthenic-aromatic oil high wax, 4 = paraffinic oil high wax, 5 = paraffinic oil low wax. Circles indicate organic carbon rich shales, filled circle = Mallik sample CO104310.

In all organic carbon-rich samples (Figure 4.5a), prist-1-ene is the dominating compound in the carbon number range of *n*-C_{15} to *n*-C_{20} with varying amounts relative to the sum of the *n*-$C_{17:0}$ + *n*-$C_{17:1}$ doublet. Interestingly, prist-1-ene is present only in very low amounts in the pyrolysis gas chromatograms of the two organic carbon-rich shales (Figure 4.5b, CO104310 and CO106094). Curry and Simpler (1988) have reported that decreasing amounts of prist-1-ene relative to the adjacent *n*-$C_{17:0}$ + *n*-$C_{17:1}$ doublet correlate very well with increasing anoxic conditions during sedimentation which may suggest different environmental sedimentary conditions for the organic-carbon rich shales in comparison to the lignite samples. The variation of the organic material between deltaic, terrestrial and lacustrine type of organic matter may be a result of a meandering river system during the delta evolution in the Beaufort Sea area (e.g. Dixon et al., 1992b).

Table 4.2: Compounds identified in the aliphatic hydrocarbon fraction (Figure 4.7a) of a selected Mallik lignite sample (CO93409).

Symbol	Compound name
a	Norisopimarane
b	Fichtelite
c	Norpimarane
d	Norabietane
e	Isopimarane
f	Abietane
g	α-Phyllocladane
h	Olean-12-ene
i	Urs-12-ene
A	Hop-17(21)-ene
B	31-*homo*-17β,21β-hopane

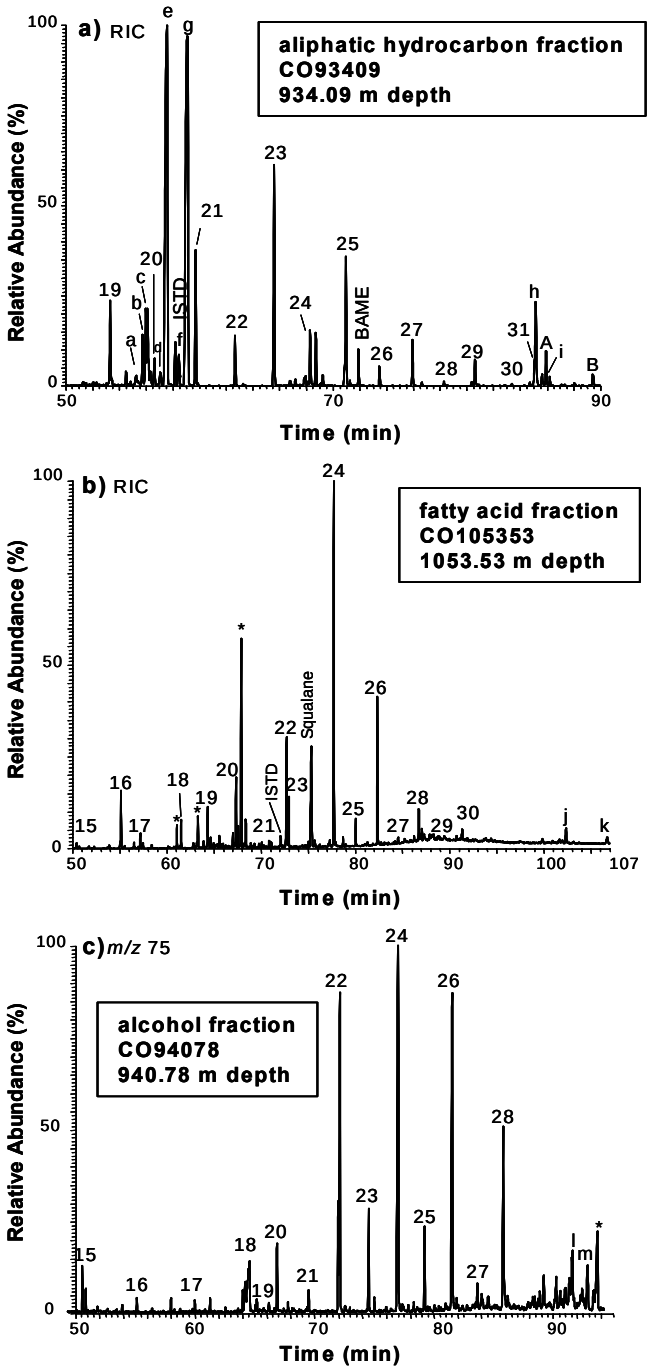

Figure 4.7: a) GC/MS RIC chromatogram (RIC = Reconstructed Ion Current) of a representative aliphatic hydrocarbon fraction of the Mallik sample CO93409 (lignite sample). Numbers indicate chain length of n alkanes. Letters correspond to compound names in table 4.2. Internal standard (ISTD) = androstane, BAME = behenic acid methyl ester. b) GC/MS RIC chromatogram of a representative fatty acid fraction of the Mallik sample CO105353 (lignite sample). The fatty acids are indicated by their carbon numbers. Hopanoic acids are assigned by letters (j = 17α,21β hopanoic acid , k = dihomo 17α,21β hopanoic acid). Internal standard (ISTD) = eruic acid methyl ester. * = unknown compounds c) GC/MS mass chromatogram *m/z* 75 showing the n alcohol distribution of the Mallik sample CO94078. Numbers indicate chain length of n alcohols. Letters indicate the triterpenoid alcohols β amyrine (l = olean 12 ene 3β ol) and α amyrine (m = urs 12 en 3β ol). ISTD = 5α androstan 17 one is not detected in the *m/z* 75 trace. * = unknown compound.

4.4.4 Molecular investigations

A representative gas chromatogram of an aliphatic hydrocarbon fraction of a Kugmallit lignite (CO93409) is shown in Figure 4.7a. The *n*-alkane distributions of all investigated samples reveal a dominance in the long-chain carbon number range from *n*-C_{19} to *n*-C_{31}, which is typical for cuticular waxes of higher land plants (Eglinton & Hamilton, 1967). Contrary to the general observation for *n*-alkanes from terrestrial origin, with a maximum in the carbon number range of *n*-C_{27} to *n*-C_{31}, the Mallik lignite samples show an unusual *n*-alkane maximum at *n*-C_{23}. Figure 4.8 presents the *n*-alkane distribution, normalized to TOC, for three selected samples from different depth (CO93409, CO104310, and CO106094) all showing an *n*-alkane maximum at *n*-C_{23}. A *n*-C_{23} carbon number dominance has been reported for organic matter originating from *Sphagnum* sp. (Baas et al., 2000; Corrigan et al., 1973; Nott et al., 2000). The occurrence of *Sphagnum* sp. has already been detected by White (1999) in the sediment samples of the Mallik 2L-38 well. *Sphagnum* sp. are known to be part of raised bog environments (e.g. Corrigan et al., 1973). This suggests a swampy milieu during formation of the lignitic layers. Furthermore, the *n*-alkane patterns reveal the typical high odd-over-even carbon number predominance as known from immature land plant material (Eglinton & Hamilton, 1967) with carbon preference indices (CPI) (Bray & Evans, 1961) between 2.3 and 4.7 (Table 4.1).

The occurrence of tricyclic diterpenoids is evident in the aliphatic hydrocarbon fraction of the lignites (Figure 4.7a), which was also observed by Snowdon (1981). The dominating compounds are isopimarane and α-phyllocladane, but there is also a distinct diversity of other compounds like norisopimarane, fichtelite, norpimarane, norabietane and abietane (Figure 4.7a, Table 4.2). They are all typical markers for higher land plants (Barrick & Hedges, 1981; Peters & Moldowan, 1993). Especially, α-phyllocladane is a specific marker for conifers (Peters & Moldowan, 1993), whereas isopimarane, norpimarane, norabietane and abietane are specific markers for resins (Philp, 1985). In addition, the terrestrial character of the organic matter is supported by the significant occurrence of pentacylic triterpenoids, e.g. olean-12-ene and urs-12-ene representing a supply of terrigenous organic matter from angiosperms (Chaffee et al., 1986). These results align with previous observations in the Mackenzie Delta area (Kurita & Uchida, 1999; White, 1999).

The two organic carbon-rich shales (CO104310 and CO106094) show the same *n*-alkane distribution pattern as the lignites (Figure 4.8b), but contrary to the lignites they contain only small to negligible traces of the above-mentioned tri- and pentacyclic terpenoids, which suggest again distinct differences in the environmental conditions during sedimentation for both types of samples.

A series of hopanoids, e.g. hop-17(21)-ene and 31-*homo*-hopane in their biogenic 17β,21β configuration (Figure 4.7a, Table 4.2) are clear indicators for the existence of microbial biomass in the subsurface at the Mallik site. For a more detailed discussion on this issue see also chapter 9.

In figure Figure 4.7b a gas chromatogram of a representative fatty acid fraction (CO105353) is depicted. All fatty acids were analyzed as their methylated derivatives upon treatment with diazomethane. The samples show a preference for long-chain fatty acids with a distinct dominance of tetracosanoic acid (*n*-C_{24}). This pattern can be related as well with *Sphagnum* sp. (Lehtonen & Ketola, 1993). The predominance of long-chain fatty acids with even-carbon numbers is again typical for an origin from higher land plants (Eglinton & Hamilton, 1967) and bacterial biomass is indicated by the occurrence of hopanoic acids (17α,21β-hopanoic acid (C_{30}) and *dihomo*-17α,21β-hopanoic acid (C_{32})).

In Figure 4.7c a representative *n*-alcohol distribution (CO100550) is shown by a GC/MS mass chromatogram *m/z* 75 (one of the main fragments of trimethylsilylated ethers (TMS)). The *n*-alcohols, measured as their TMS ethers, reveal a distribution pattern dominated by long even-chain alcohols, which is also typical for higher land plants (Eglinton & Hamilton, 1967), with maxima predominantly at *n*-C_{24}. For two different *Sphagnum* sp., the dominance of the *n*-C_{24} and *n*-C_{26} alcohols has been reported by Ficken et al. (1998). Hence, this agrees well with the results of the *n*-alkane and the *n*-fatty acid distribution. Additionally the terrigenous character of the organic carbon-rich sediments is supported by the occurrence of triterpenoid alcohols such as β-amyrine (olean-12-en-3β-ol) and α-amyrine (urs-12-en-3β-ol) (Chaffee et al., 1986; Otto et al., 1994; ten Haven et al., 1992) (Figure 4.7c) indicating again a supply of terrestrial organic matter from angiosperms (Chaffee et al., 1986). In contrast to the lignitic samples the two organic carbon-rich shales (CO104310 and CO106094) contain no β- or α-amyrine. Nevertheless they show the same alcohol distribution pattern as the lignite samples.

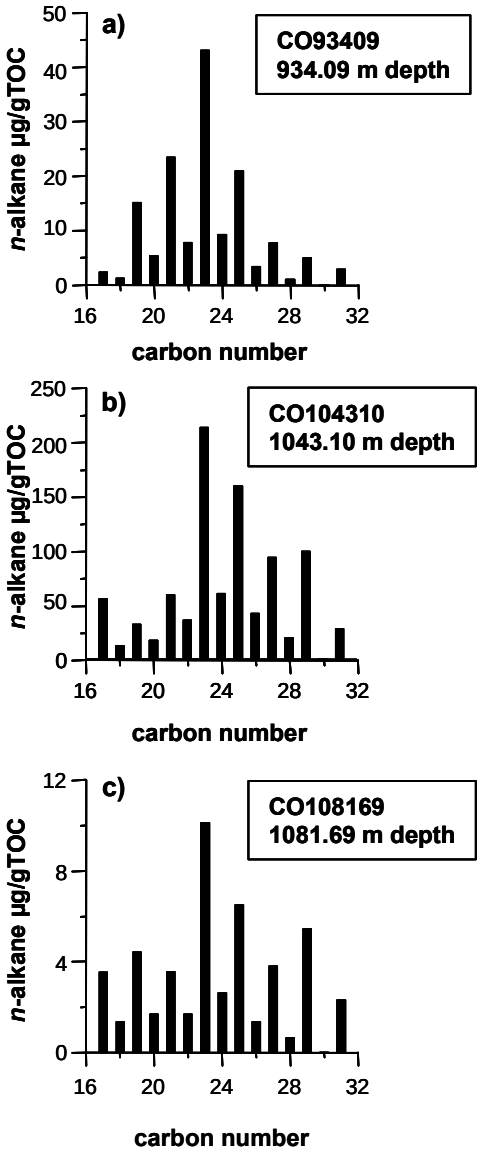

Figure 4.8: Histograms showing the carbon number distributions of n alkanes, normalized to TOC, of three selected Mallik samples a) CO93409 (lignite sample), b) CO104310 (organic carbon rich shale sample), and c) CO108169 (lignite sample).

4.5 Conclusions

Organic carbon-rich terrestrial sediment samples (lignites and shales; 891-1145 m) from the Mallik 5L-38 Gas Hydrate Research Well were investigated with regard to their organic matter composition (kerogen, bitumen) using different organic geochemical approaches. The kerogen composition of these samples has been analysed by Rock-Eval pyrolysis, open-system pyrolysis-GC, and microscopic studies in fluorescence light. All analytical methods indicate a predominantly the terrestrial origin and the prevailing immature character of the organic matter as shown before by Snowdon (1981; 1999). Although, the two organic carbon-rich shale samples show a terrestrial origin, their kerogen composition suggests a lower delta plain or lacustrine-influenced sedimentation environment.

The molecular investigations of the free lipids fraction (bitumen) have revealed a large variety of compounds from land plants and microbial sources (for details on microbial biomarkers see also chapter 9). The terrestrial source of the organic matter in the organic carbon-rich samples at the Mallik site is indicated by the composition of the *n*-alkanes, *n*-fatty acids and *n*-alcohols. Additionally the distribution patterns of these biomarkers support the immature character of the organic matter.

For the lignite samples from the Mallik area, the occurrence of tri- and pentacyclic terpenoids allow conclusions on the plant community during their sedimentation. Gymnosperms (like conifers), angiosperms and moss plants (*Sphagnum* sp.) seem to be important constituents. In recent times *Sphagnum* sp. occur in raised bog regions. Thus, the presence of their lipid biomarkers points to a swampy milieu during sedimentation of the lignitic layers. Probably the lignite layers were deposited in interdistributary marshes and bayous in the Mackenzie Delta system. Contrary to the lignites the occurrence of tri- and pentacyclic terpenoids in the shale samples with high organic carbon-values is negligible. This shows that the sedimentation conditions have been changed probably as a result of a meandering river system during the delta evolution in the Beaufort Sea area.

4.6 Acknowledgments

We acknowledge the international partnership that undertook the Mallik 2002 Gas Hydrate Production Research Well Program: the Geological Survey of Canada (GSC), Japan National Oil Corporation (JNOC), GeoForschungsZentrum Potsdam (GFZ), U.S. Geological Survey (USGS), U.S. Department of Energy (USDOE), India Ministry of Petroleum and Natural Gas (MOPNG)/Gas Authority of India (Gail), and the Chevron-British Petroleum-Burlington joint venture group. The program received financial support from the International Continental Scientific Drilling Program. Also, we wish to thank Dr. B. Mingram (GFZ Potsdam) for the $\delta^{13}C_{org}$-measurements on bulk organic matter, Dr. D. Uhl (University of Tübingen) for his helpful paleobotanic determinations. We are grateful to the anonymous reviewers for their helpful suggestions. The study is funded by the Deutsche Forschungsgemeinschaft (DFG), grant no. Ma 2470/1.

5 Characterisation of the organic matter in samples from different lithologies of the Mackenzie Bay and the Kugmallit Sequence at the JAPEX/JNOC/GSC et al. Mallik 5L-38 Gas Hydrate Production Research Well - supplement to chapter 4

Due to instrument specific problems during the GC-MS-measurements, the signal intensity of compounds eluting after the *n*-C_{24}-alkane was discriminated in the GC-MS-chromatograms. Hence, to ensure the data quality it was necessary to repeat the measurements as well as the quantifications. Complementary the fatty acid and the neutral polar hydrocarbon fraction were evaluated in their entirety. Subsequent to the characterisation of the organic matter in the lignites the organic material in the samples of the other lithologies (silt/clay, sand) has been analysed and interpreted. These additional results are presented in this chapter.

5.1 Microscopic studies – a quantitative maceral analysis

In addition to the qualitative analysis of the maceral composition shown in chapter 4.4.2 here a quantitative evaluation of the maceral composition of six lignite samples and three organic-carbon rich clay samples is provided. The maceral composition has been counted twice (see chapter 3) to confirm the qualitative data shown in chapter 4.4.2. and to extend the examination on the organic-carbon rich silt/clay samples for comparison. Thereby, the interpretation based on the data presented in chapter 4 has been supported in general. Nevertheless, more detailed information on the maceral composition are provided by the quantitative analysis.

In all investigated samples huminites (Figure 4.4a) including ulminite, textinite and humodetrinite are the most common macerals with amounts varying between 56.1 to 98.3 %mfb (mineral free base; Table 5.1). However, there are some distinct differences concerning the composition of the huminites. Within the topmost two lignite samples of the cored section, CO93409 and CO94078, the proportion of textinite (Figure 4.4c) is higher than that of ulminites (70.8 and 59.1 %mfb; Table 5.1). All other samples have higher amounts of ulminite (11.8 to 90.8 %mfb). In two clay samples (MB103360 with 51.5 %mfb and CO104310 with 43.0 %mfb) humodetrinite is the dominant huminite. However, the amount of humodetrinite is in general low with values ranging from 0.6 to 9.7 %mfb. In most samples the amounts of liptinites, including liptodetrinite, cutinite, fluorinite, sporinite and resinite, range between 1.7 and 7.7 %mfb. Exceptional are again the clay samples CO103360 and CO104310 (Table 5.1). Both samples contain a higher amount of sporinite (3.4 and 25.4 %mfb, Table 5.1). In case of

CO1043110 sporinites even account for the highest proportion in the whole liptinite group (Figure 5.1a). The inertinites are not important in the sample set (Table 5.1). They occur only in three samples (MB103360, CO104310, and CO108169; Figure 5.1b) with very low proportions (0.3 to 2.2 %mfb).

Table 5.1: Composition and amounts of the macerals counted in nine organic-rich samples of the Mallik 5L-38 Gas Hydrate Production Research Well.

Mallik 5L-38 Sample		CO93409	CO94078	CO100550	MB103360	CO104310	CO105353	CO108138	CO108169	CO110550
Depth (m)		934.09	940.78	1005.50	1033.60	1043.10	1053.53	1081.38	1081.69	1105.50
Lithology		Lignite	Lignite	Lignite	Silt/Clay	Silt/Clay	Lignite	Lignite	Lignite	Silt/Clay
TOC (%)		46.60	31.85	42.03	7.09	3.64	39.19	45.93	38.39	9.44
Huminites	**Ulminite (%mfb)**	24.6	23.5	90.7	32.2	11.8	67.9	90.2	78.2	75.0
	Textinite (%mfb)	70.8	59.1	6.7	3.9	1.3	25.6	5.2	18.3	13.6
	Humodetrinite (%mfb)	0.0	9.7	0.9	51.5	43.0	0.6	0.0	0.0	6.8
Sum of huminites (%mfb)		95.4	92.3	98.3	87.6	56.1	94.1	95.4	96.5	95.4
Liptinites	**Liptodetrinite (%mfb)**	3.8	4.9	1.2	4.7	5.3	3.4	3.6	0.3	0.0
	Cutinite (%mfb)	0.0	0.4	0.0	0.9	3.5	0.0	0.0	0.0	0.0
	Fluorinite (%mfb)	0.4	0.4	0.6	2.1	7.5	0.3	0.3	1.9	3.6
	Sporinite (%mfb)	0.4	2.0	0.0	3.4	25.4	1.4	0.5	0.0	0.9
	Resinite (%mfb)	0.0	0.0	0.0	0.0	0.0	0.8	0.0	1.3	0.0
Sum of liptinites (%mfb)		4.6	7.7	1.8	11.1	41.7	5.9	4.4	3.5	4.5
Inertinites (%mfb)		0.0	0.0	0.0	1.3	2.2	0.0	0.3	0.0	0.0

The differences of the huminite composition could be related to an increased stage of gelification, because textinite and ulminite differ in their degree of gelification (Taylor et al., 1998). Through biochemical and geochemical gelification textinite alters to ulminite. In addition, the origin of the woody material, from angiosperms or gymnosperms, plays also an important

role. Cellulose-rich leaves, stems and certain woods from angiosperms decompose largely to a humic detritus of cell-wall remains. They are partly decomposed and converted to colloidal humic solutions, which infiltrate the peat and are precipitated on drying as gel particles between the detritus. In contrast, woods from conifers, whose cell walls are impregnated with resin, wax, tannins or pigments, are very resistant to material/structural decomposition and are conserved as textinite (Taylor et al., 1998). The relatively small differences in depth, depositional age and diagenitic conditions for the samples from the Mallik 5L-38 Well argue against a more increased gelification due to enhanced alteration of the organic matter in the sample CO93409 and CO94078. Therefore, the different huminite compositions in the investigated samples are more likely due to a supply of different plant material during time of sedimentation. The assumption that enhanced amounts of gymnosperm material causes the larger amounts of textinite in the samples CO93409 and CO94078 is supported by the interpretation of the aromatic hydrocarbon compounds (chapter 6, Fig. 6.3c), which indicated a conspicuous dominance of gymnosperms for both samples.

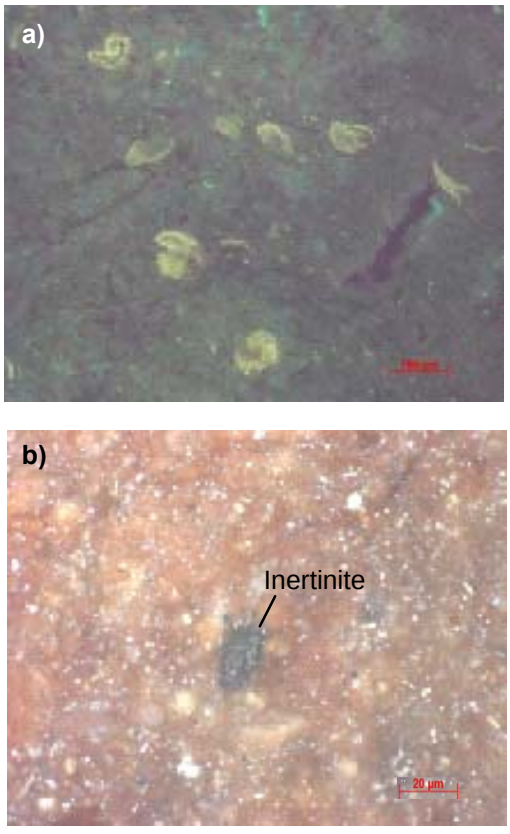

Figure 5.1: Picture a) shows sporinite particles (yellow) in fluorescence light (CO104310). Picture b) displays an inertinite particle in reflected white light (CO104310).

The clay sample CO104310 has an unusual high HI-value (532 mgHC/gTOC) pointing to kerogen type II organic matter (Figure 4.3). However, all other investigations show that the

organic matter is of terrestrial origin. This contrast can presumably be explained with the exceptional high liptinite content of 41.7 %mfb of this sample in contrast to the other samples with liptinite contents of 5.5 %mfb in average. Liptinites especially sporinites are characterised by high aliphatic contents (mainly long-chain *n*-alkanes) resulting in a high hydrogen index value (Figure 5.2) (Diessel, 1992; Tissot & Welte, 1984). The minor relevance of inertinite in the samples indicates that charring, oxidation, fungal attack and desiccation were not major processes prior to or during deposition of the sediment (Taylor et al., 1998).

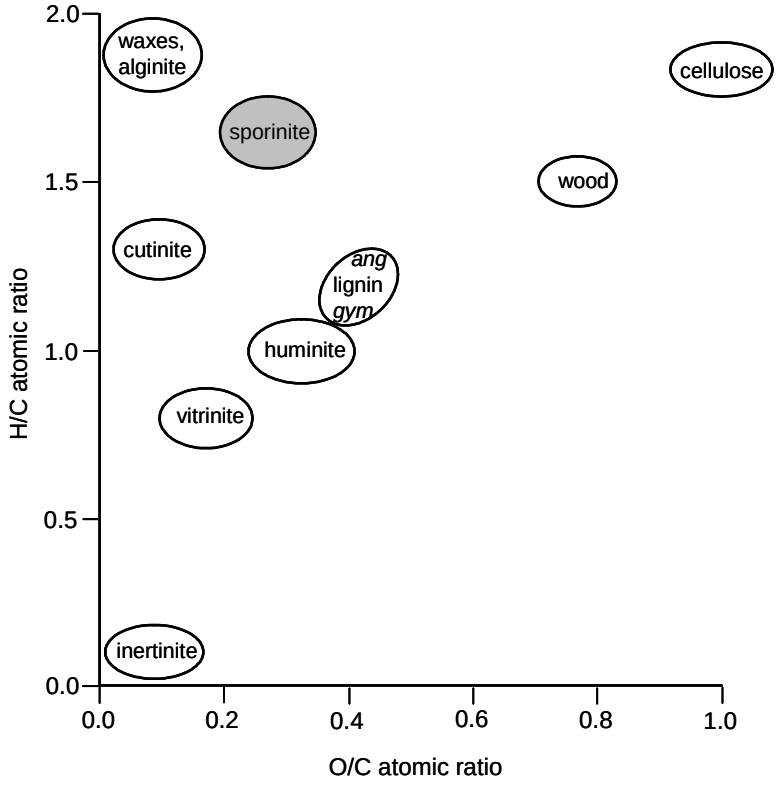

Figure 5.2: Chemical composition of major coal macerals and plant tissues plotted on a van Krevelen diagram after Killops & Killops (2004) (ang = angiosperms, gym = gymnosperms).

5.2 Lipid analysis of the extractable organic matter from the Mallik well

5.2.1 Aliphatic hydrocarbon fractions

Lignite samples

The new results show (Figure 5.3a; CO105353), that the *n*-alkane distribution pattern has been changed to some extent in the range of the high molecular weight compounds. Although, the *n*-alkane patterns still reveal a strong odd-over-even carbon number predominance in the range of the long chain hydrocarbons from *n*-C_{19} to *n*-$C_{31,}$ a second maximum occurs now in the range of *n*-C_{29} to *n*-C_{31}. However, the first maximum at *n*-C_{23} (Figure 5.3a) is still visible. Nonetheless, these new results do not affect the former interpretations. In fact, these chromatograms supports better than before the interpretation of the immature organic matter from terrestrial origin (maximum at *n*-C_{29} or *n*-C_{31}), with an important input of the moss plant *Sphagnum* sp. (maximum at *n*-C_{23}). Also the interpretation concerning the terpenoid composition (Table 5.2, Figure 5.3a) in the lignites has not been changed.

In contrast to the first sample description at the drill site, the sample CO110550, initially assigned as a lignite sample, is, equally to the samples CO104310 and CO106094, defined as a organic-rich shale rather than a lignite due to its low organic carbon content of 9.4%.

Clay samples

A representative gas chromatogram of an aliphatic hydrocarbon fraction of the clay sample MB93589 is shown in Figure 5.3b. The *n*-alkane distributions of all investigated clay samples reveal the dominance in the long-chain carbon number range from *n*-C_{21} to *n*-C_{31} with a maximum at *n*-C_{29} or *n*-C_{31} typically for higher land plant material (Eglinton & Hamilton, 1967). In contrast to the observations in the lignite samples there is no maximum at *n*-C_{23}. Therefore, there is no evidence for an enhanced influence of moss plants as for the clay samples (see chapter 4). Furthermore, the *n*-alkane patterns of the clays display the typical distinct odd-over-even carbon number predominance as known form immature terrestrial organic matter (Eglinton & Hamilton, 1967) with carbon preference indices (CPI, Bray and Evans (1961)) between 2.5 and 7.3.

In most of the clay samples sesquiterpenoid hydrocarbons occur (one undefined sesquiterpene and 4α(H)-Eudesmane). The abundance of tricyclic diterpenoids originating from gymnosperms is lower in the clay samples than in the lignite samples. The dominating compounds in this group are norabietane and α-phyllocladane. However the diterpenes described above in

the lignites like norisopimarane, fichtelite, norpimarane, abietane and isopimarane are also present in the clay samples. Contrary to the lignite samples, the pentacyclic triterpenoids are more important in the clay samples for example olean-12-ene and olean-18-ene, both representing a supply of organic matter from angiosperms (Table 5.2, Figure 5.3b).

Sand samples

Figure 5.3c shows a typical gas chromatogram of an aliphatic hydrocarbon fraction of the Mallik sand sample MB107960. The aliphatic fraction of the sand samples contains very small amounts of biomarkers. The *n*-alkane distribution in the sand samples is different to those of the lignites or clays. The *n*-alkane maximum is in the range of *n*-C_{14} to *n*-C_{18} and no odd-over-even carbon number predominance is detectable.

In the sand no sesquiterpenoic hydrocarbons occur. Tricyclic diterpenoic hydrocarbons occur in the sand samples, but with an in general lower diversity. Norabietane and isopimarane are present in some sand samples and abietane is completely absent. Only in five sand samples pentacyclic triterpenoids, mainly olean-12-ene, are detectable (Table 5.2, Figure 5.3).

5.2.2 Neutral polar hydrocarbon fractions

Lignite samples

As briefly described in chapter 4 the lignite samples (Figure 4.7c and Figure 5.4a) reveal an *n*-alcohol distribution pattern dominated by long even-chain alcohols, with a maximum predominantly at tetracosanol (*n*-C_{24}), indicating higher land plant material with a dominance of *Sphagnum* sp. (Eglinton & Hamilton, 1967; Ficken et al., 1998), because *Sphagnum* sp. often show an abundant *n*-C_{24}-alcohol biomarker signal in their lipid distribution. In addition to the *n*-alcohols, the neutral fractions of the lignite samples contain also branched, not exactly identifiable isomers of the alcohols between tetradecanol (*n*-C_{14}) and heptadecanol alcohol (*n*-C_{17}).

The occurrence of diterpenoid alcohols like ferruginol, 6,7-dehydroferruginol, dehydroabietanol, diverse iso-dehydroabietanols and iso-hinokiol/pisiferol supports the terrestrial character and the supply of gymnosperm derived organic matter (Otto & Simoneit, 2001). The triterpenoid alcohols are represented by δ-amyrin, β-amyrin, α-amyrin and lupanol. Most lignites show a dominance of diterpenoids comparable to the di- to triterpene distribution of the aromatic hydrocarbons (see chapter 6, Table 5.3and Figure 5.4).

In addition to the land plant related biomarkers also some hopanones and hopanols such as 22,29,30-*trinor*-hopan-21-one, 17(α),21(β)-*dihomo*-hopan-32-ol and 17(β),21(β)-*dihomo*-

hopan-32-ol appear in the lignite samples. However, only 17(β),21(β)-*dihomo*-hopan-32-ol occurs in all lignites. 17(β),21(β)-Hopanols are also biomarkers for immature bacterial biomass as well as the 17(β),21(β)-hopanes (see chapter 9).

Clay samples

A representative gas chromatogram of a neutral polar compound fraction of the clay sample MB89899 is shown in Figure 5.4b. The *n*-alcohol distribution patterns of the clay samples display the predominance of long even-chain alcohols in the range from tetracosanol (*n*-C_{24}) to triacontanol (*n*-C_{30}). Between tetradecanol (*n*-C_{14}) and heptadecanol (*n*-C_{17}) also branched alcohols occur.

The diterpenoid alcohols like ferruginol, 6,7-dehydroferruginol, dehydroabietanol, diverse iso-dehydroabietanols and iso-hinokiol/pisiferol occur also in the clay samples. However contrary to the lignites, they are not present in all clays and some samples contain only one or two of the diterpenoid alcohols. Instead, the triterpenoid alcohols, δ-amyrin, β-amyrin, α-amyrin and lupanol, are more relevant in the clay samples than in the lignites (Table 5.3, Figure 5.4).

Concerning the hopanoid alcohols the clay samples show more or less the same pattern as the lignite samples. However, they do not occur in all clay samples.

Sand samples

A representative gas chromatogram of a neutral polar hydrocarbon fraction of the sand sample MB112790 is shown in Figure 5.4c. The *n*-alcohol distribution shows no preference for the long even-chain alcohols. Only negligible branched alcohols have been detected in the sand samples in a negligible abundance. The neutral polar fractions of the sand samples contain neither diterpenoid nor triterpenoid alcohols (Table 5.3, Figure 5.4).

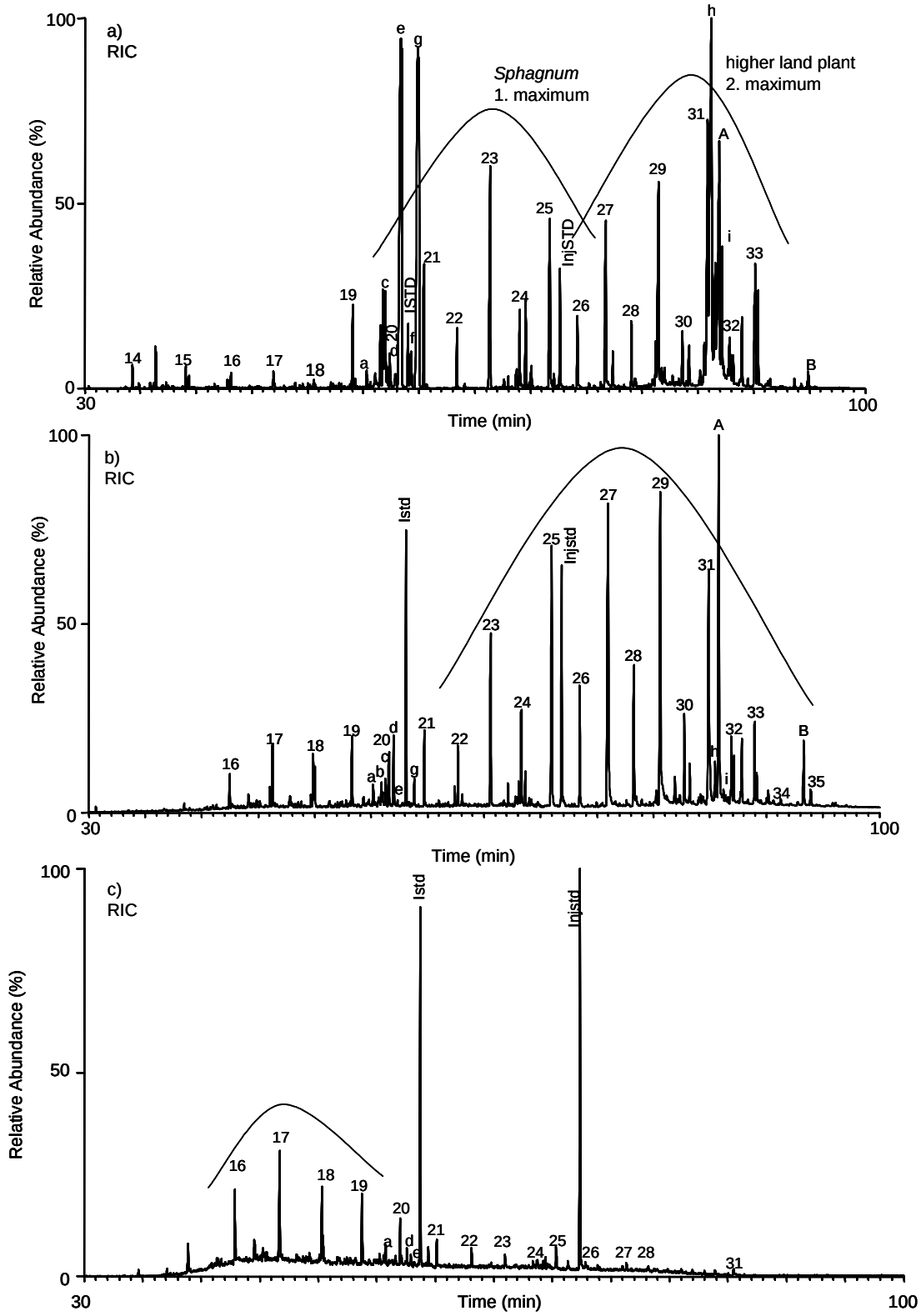

Figure 5.3: GC/MS RIC chromatograms (RIC = Reconstructed Ion Current) of representative aliphatic hydrocarbon fractions of a) sample CO105353 (lignite) b) sample MB93589 (clay) and c) MB107960 (sand). Numbers indicate chain length of *n*-alkanes. Letters correspond to compound names in Table 4.2. Internal standard (ISTD) = androstane, Injection standard (InjSTD) = behenic acid methyl ester (BAME).

Table 5.2: Concentrations of aliphatic sesqui-, di-, and triterpenoic hydrocarbon biomarkers and ratio of di- to di-plus triterpenoids. Dark grey shaded = lignites, light grey shaded = silt/clays, unshaded = sands.

Mallik 5L-38 Sample	Sesqui-terpenoids (µg/gTOC)		Diterpenoids (µg/gTOC)							Triterpenoids (µg/gTOC)					di/(di+tri)
	unid. Sesquiterpene	4α(H)Eudesmane	Isonorpimarane	Fichtelite	Norpimarane	Norabietane	Isopimarane	Abietane	α-Phyllocladane	De-A-Lupane	Olean-(18)-ene	Urs-(12)-ene	Fernene	Olean-(12)-ene	
MB89163	0.0	0.0	4.2	1.6	2.1	3.7	2.3	1.1	5.1	26.6	3.8	1.9	4.8	23.9	0.25
MB89899	7.3	16.1	0.6	1.4	1.7	6.8	1.4	0.7	4.4	4.2	3.9	2.1	0.6	19.7	0.36
MB90020	7.3	21.5	0.7	1.2	2.0	4.5	2.6	0.9	3.8	10.4	2.7	1.4	2.0	18.1	0.31
MB91200	0.0	0.0	100.3	17.6	29.6	0.0	0.0	0.0	44.4	38.9	0.0	0.0	0.0	9.0	0.80
MB91856	0.0	0.0	100.1	36.5	35.6	0.0	0.0	0.0	38.8	0.0	0.0	0.0	0.0	0.0	1.00
CO93409	3.4	0.0	2.2	0.0	12.9	3.6	211.7	6.8	243.4	0.0	0.6	0.8	0.3	7.3	0.98
MB93589	0.0	0.0	4.7	2.7	2.7	14.8	1.2	2.4	5.6	1.1	3.0	2.2	10.6	12.2	0.54
CO94078	15.1	0.0	1.5	0.0	14.5	5.9	36.6	3.4	54.2	1.5	3.6	5.0	0.1	27.2	0.76
MB94762	0.0	0.0	0.0	0.0	0.0	0.0	0.0	0.0	0.0	0.0	0.0	0.0	0.0	0.0	-
MB96334	8.5	36.2	1.9	4.2	3.3	4.5	3.5	0.7	4.4	21.8	5.7	1.4	5.3	18.4	0.30
MB97760	0.0	0.0	34.1	14.8	12.7	0.0	9.5	0.0	13.4	29.5	0.0	0.0	0.0	0.0	0.74
MB98925	0.0	0.0	38.7	12.5	9.5	4.0	5.1	0.0	7.5	16.0	0.0	0.0	0.0	0.0	0.83
CO100550	2.8	1.2	1.9	17.3	3.7	4.5	8.2	5.5	79.5	0.0	0.1	0.2	0.0	0.9	0.99
MB100778	0.0	79.3	1.4	0.0	1.6	9.1	0.8	0.0	1.4	0.0	0.0	0.0	0.0	27.1	0.35
MB102215	0.0	0.0	68.4	12.3	19.4	0.0	0.0	0.0	10.9	20.4	0.0	0.0	0.0	0.0	0.84
MB103360	0.0	0.6	2.1	1.8	6.8	37.6	0.5	1.0	2.3	2.3	1.5	10.6	4.7	10.6	0.64
CO104310	0.0	0.0	3.2	2.1	8.2	66.8	11.4	3.8	31.9	0.0	0.3	0.0	0.8	1.5	0.98
MB104920	0.0	0.0	2.1	1.8	3.1	5.3	5.4	1.8	5.0	19.3	5.0	0.0	0.0	9.2	0.42
CO105353	1.3	0.0	7.9	0.0	20.4	21.2	58.1	6.8	84.8	0.0	0.1	0.0	0.5	0.2	1.00
CO106094	0.0	0.0	0.6	0.0	1.3	2.5	1.9	0.8	3.7	2.1	0.0	0.1	0.0	0.2	0.82
MB106380	0.0	1.6	0.7	2.1	1.0	2.8	1.5	0.6	2.1	2.5	20.9	15.6	6.4	124.2	0.06
MB107960	0.0	0.0	279.4	84.6	139.3	193.8	196.2	0.0	244.4	299.5	0.0	0.0	0.0	141.6	0.72
CO108138	1.3	0.0	1.3	0.0	13.9	0.6	7.9	0.4	34.4	0.0	0.0	2.0	0.0	5.9	0.88
CO108169	1.4	0.0	0.7	3.4	15.1	13.4	1.2	1.3	7.3	0.2	0.0	0.0	0.1	0.1	0.99
MB108924	0.0	0.0	39.1	0.5	7.3	10.9	0.0	0.0	0.5	26.2	0.0	0.0	0.0	0.6	0.69
MB110494	0.0	0.0	279.7	104.7	55.8	87.7	54.7	0.0	114.8	120.0	0.0	0.0	0.0	64.2	0.79
CO110550	0.5	0.0	0.6	0.8	1.2	1.6	4.5	2.5	3.3	17.1	0.0	0.0	0.0	0.0	0.46
MB112790	0.0	3.2	0.5	1.9	0.5	1.1	1.5	0.3	1.6	4.0	0.7	0.3	0.3	1.4	0.53
MB113980	0.0	0.0	46.9	21.6	20.5	14.0	0.0	0.0	7.0	18.9	0.0	0.0	0.0	0.0	0.85
MB114535	3.5	13.2	1.4	5.1	3.9	7.9	9.3	2.4	8.5	25.3	4.7	2.5	8.6	37.8	0.33

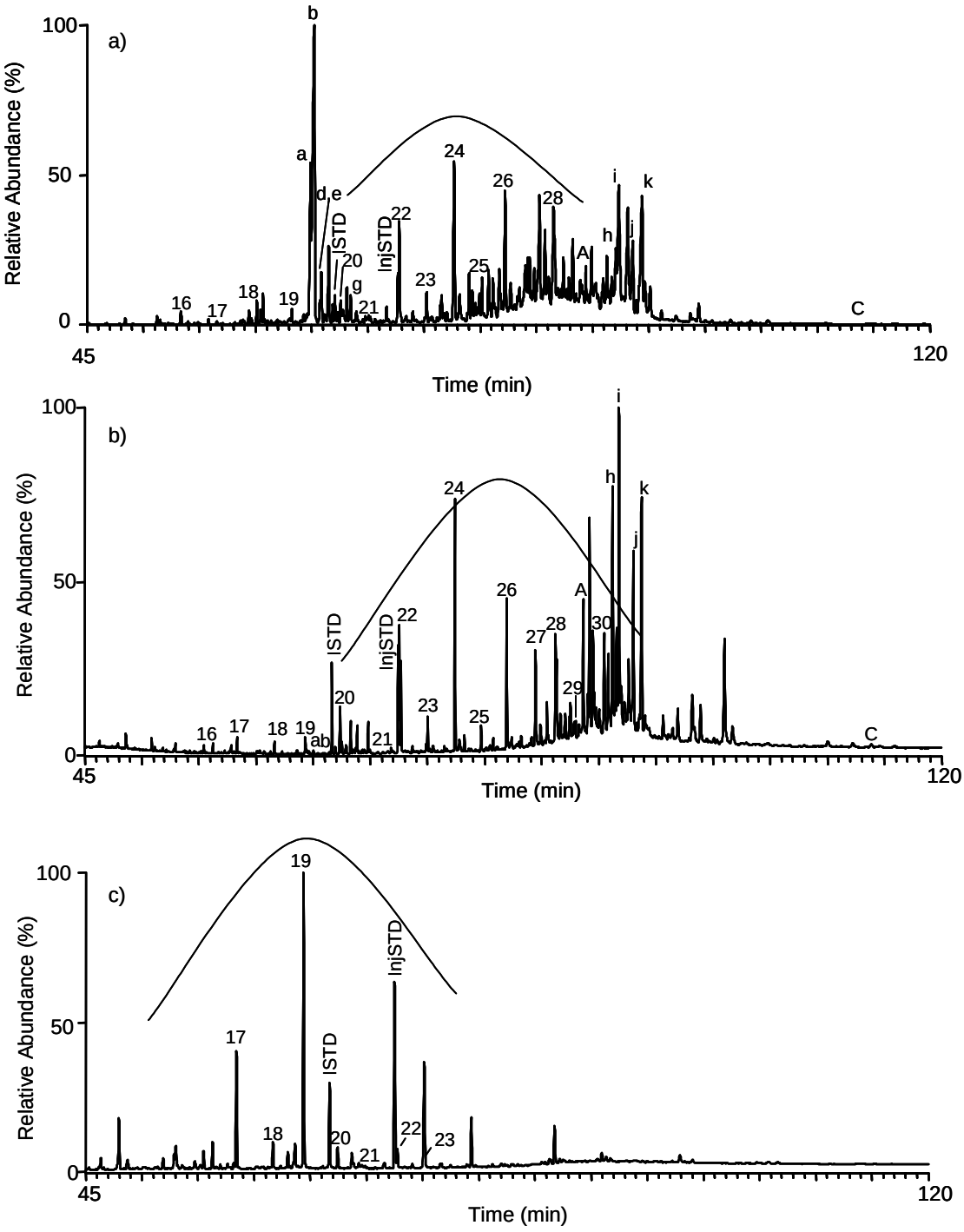

Figure 5.4: GC/MS RIC chromatograms (RIC = Reconstructed Ion Current) of representative neutral polar hydrocarbon fractions of a) sample CO94078 (lignite) b) sample MB89899 (clay) and c) MB112790 (sand). a = iso-dehydroabietanol, b = ferruginol, d = dehydroabietanol, e = iso-dehydroabietanol, g = iso-hinokiol/pisiferol, h = δ-amyrin, i = β-amyrin, j = α-amyrin, k = lupanol; A = 22,29,30-*trinor*-hopan-21-on, C = 17β(H),21β(H)-*dihomo*-hopan-32-ol. Numbers indicate chain length of *n*-alcohols. Internal standard (ISTD) = 5α-androstan-17-one, Injection standard (InjSTD) = behenic acid methyl ester.

Table 5.3: Concentrations of neutral polar sesqui-, di-, and triterpenoic hydrocarbon biomarkers and ratio of di- to di-plus triterpenoids. Dark grey shaded = lignites, light grey shaded = silt/clays, unshaded = sands.

Mallik 5L-38 sample	Diterpenoids (µg/gTOC)						Triterpenoids (µg/gTOC)					di/(di+tri)
	iso-Dehydroabietanol	Ferruginol	6,7-Dehydroferruginol	Dehydroabietanol	iso-Dehydroabietanol	iso-Dehydroabietanol	iso-Hinokiol/Pisiferol	δ-Amyrin	β-Amyrin	α-Amyrin	Lupanol	
MB89163	5.8	2.4	4.0	0.9	0.9	0.7	0.0	9.7	69.9	58.7	0.0	0.10
MB89899	2.6	1.6	1.5	0.0	0.0	0.0	0.0	57.3	199.2	120.9	154.0	0.01
MB90020	0.8	0.0	0.0	0.0	0.0	0.0	0.0	29.6	99.9	88.8	170.8	0.00
MB91200	0.0	0.0	0.0	0.0	0.0	0.0	0.0	0.0	0.0	0.0	0.0	0.00
MB91856	0.0	0.0	0.0	0.0	0.0	0.0	0.0	0.0	0.0	0.0	0.0	0.00
CO93409	158.2	164.3	16.2	12.8	14.6	81.0	29.1	13.7	84.8	63.0	0.0	0.75
MB93589	18.2	28.6	194.6	5.0	9.5	12.2	0.0	44.6	120.5	91.1	171.2	0.39
CO94078	88.0	250.4	1.7	7.3	19.8	3.9	9.6	30.2	73.0	62.6	94.6	0.59
MB94762	0.0	0.0	0.0	0.0	0.0	0.0	0.0	0.0	0.0	0.0	0.0	0.00
MB96334	0.0	0.0	0.0	0.0	0.0	0.0	0.0	11.8	57.4	41.4	66.4	0.00
MB97760	0.0	0.0	0.0	0.0	0.0	0.0	0.0	0.0	0.0	0.0	0.0	0.00
MB98925	0.0	0.0	0.0	0.0	0.0	0.0	0.0	0.0	0.0	0.0	0.0	0.00
CO100550	27.0	99.9	0.1	0.7	2.9	0.8	6.7	20.5	87.7	47.0	0.0	0.47
MB100778	0.8	0.0	0.0	0.0	0.0	0.0	0.0	0.0	4.9	0.0	0.0	0.14
MB102215	0.0	0.0	0.0	0.0	0.0	0.0	0.0	0.0	0.0	0.0	0.0	0.00
MB103360	13.7	35.6	0.0	0.3	1.1	1.9	0.6	56.7	148.5	73.2	134.1	0.11
CO104310	193.4	490.7	5.4	4.6	26.3	24.9	7.5	208.0	261.1	319.3	359.0	0.40
MB104920	1.9	0.0	1.6	0.0	0.0	0.0	0.0	10.5	36.2	24.1	69.6	0.02
CO105353	21.4	92.2	3.5	2.1	6.5	5.6	6.3	11.3	53.5	8.5	13.9	0.61
CO106094	6.2	29.3	0.6	0.5	1.0	2.2	0.6	8.2	23.6	4.0	3.2	0.51
MB106380	0.0	2.1	0.0	0.0	0.0	0.0	0.0	21.2	196.5	79.2	8.6	0.01
MB107960	0.0	0.0	0.0	0.0	0.0	0.0	0.0	0.0	0.0	0.0	0.0	0.00
CO108138	14.7	29.8	0.1	0.5	0.4	1.4	1.4	5.4	98.7	64.2	0.0	0.22
CO108169	15.1	54.4	0.2	0.7	2.4	1.6	3.7	3.5	17.4	7.2	19.7	0.62
MB108924	0.0	0.0	0.0	0.0	0.0	0.0	0.0	0.0	0.0	0.0	0.0	0.00
MB110494	0.0	0.0	0.0	0.0	0.0	0.0	0.0	0.0	0.0	0.0	0.0	0.00
CO110550	0.4	3.2	0.0	0.0	0.2	0.0	0.3	2.4	6.4	0.4	11.2	0.17
MB112790	0.0	0.0	0.0	0.0	0.0	0.0	0.0	0.0	0.0	0.0	0.0	0.00
MB113980	0.0	0.0	0.0	0.0	0.0	0.0	0.0	0.0	0.0	0.0	0.0	0.00
MB114535	26.5	19.1	0.7	0.0	7.1	3.8	0.2	23.6	81.6	61.4	20.6	0.23

5.2.3 Fatty acid fractions

Lignite sample

Figure 5.5a shows the newly measured fatty acid fraction of sample CO105353. As previously described in chapter 4 the lignite samples show a preference for long-chain fatty acids with a dominance of the docosanoic acid (*n*-C_{22}) or the tetracosanoic acid (*n*-C_{24}). This pattern can also be related to an origin from higher land plants (Eglinton & Hamilton, 1967) with *Sphagnum* sp., because *Sphagnum* sp. shows a maximum in the long chain fatty acid range (tetracosanoic acid (*n*-C_{24}) or hexacosanoic acid (*n*-C_{26})) (Lehtonen & Ketola, 1993). The occurrence of diterpenoic acids like dehydroabietanoic acid and of the triterpenoic oleanoic acid supports the terrestrial origin of the organic matter (Table 5.4).

In the range of tetradecanoic acid (*n*-C_{14}) to heptadecanoic acid (*n*-C_{17}) the iso (i) - and anteiso (ai)-isomers of the acids (i-C_{15}, ai-C_{15}, i-C_{16}, ai-C_{16}, i-C_{17}, and ai-C_{17}) occur. Additionaly, 17α,21β-hopanoic acid (C_{30}), 17β,21α-hopanoic acid, 17β,21β-hopanoic acid, 17α,21β-(22S)-*dihomo*-hopanoic acid (C_{32}), 17α,21β-(22R)-*dihomo*-hopanoic acid, 17β,21α-*dihomo*-hopanoic acid, 17β,21β-*dihomo*-hopanoic acid, 17β,21β–*trihomo*-hopanoic acid (C_{33}) are present in nearly all lignite samples. 17β,21β-Hopanoic acids are also biomarker for immature bacterial biomass like the 17β,21β-hopanes or 17β,21β-hopanols.

Clay samples

A representative fatty acid distribution in the clay samples (MB 114535) is shown in Figure 5.5b. In contrast to the lignite samples, it is obvious, that in the clay samples the maximum of the fatty acids is shifted to hexadecanoic acid (*n*-C_{16}). With exception of the samples MB103360, CO104310, CO106094 and CO110550, which show the maximum at the *n*-C_{22} or the *n*-C_{24} fatty acids, this distribution pattern is typical for all clay samples. The terpenoic dehydroabietanoic acid and oleanoic acid appear only in two clay samples (Table 5.4).

Like in the lignite samples, the iso (i) - and anteiso (ai)-isomers of the acids (i-C_{15}, ai-C_{15}, i-C_{16}, ai-C_{16}, i-C_{17}, and ai-C_{17}) occur in the range of tetradecanoic acid (*n*-C_{14}) to heptadecanoic acid (*n*-C_{17}). Hopanoic acids are rare in the clay samples and do not occur as an extensive series like in the lignite samples with the exception of the samples MB90020, CO104310, CO106094 and MB106380, which show the same hopanoic acid distribution as the lignites.

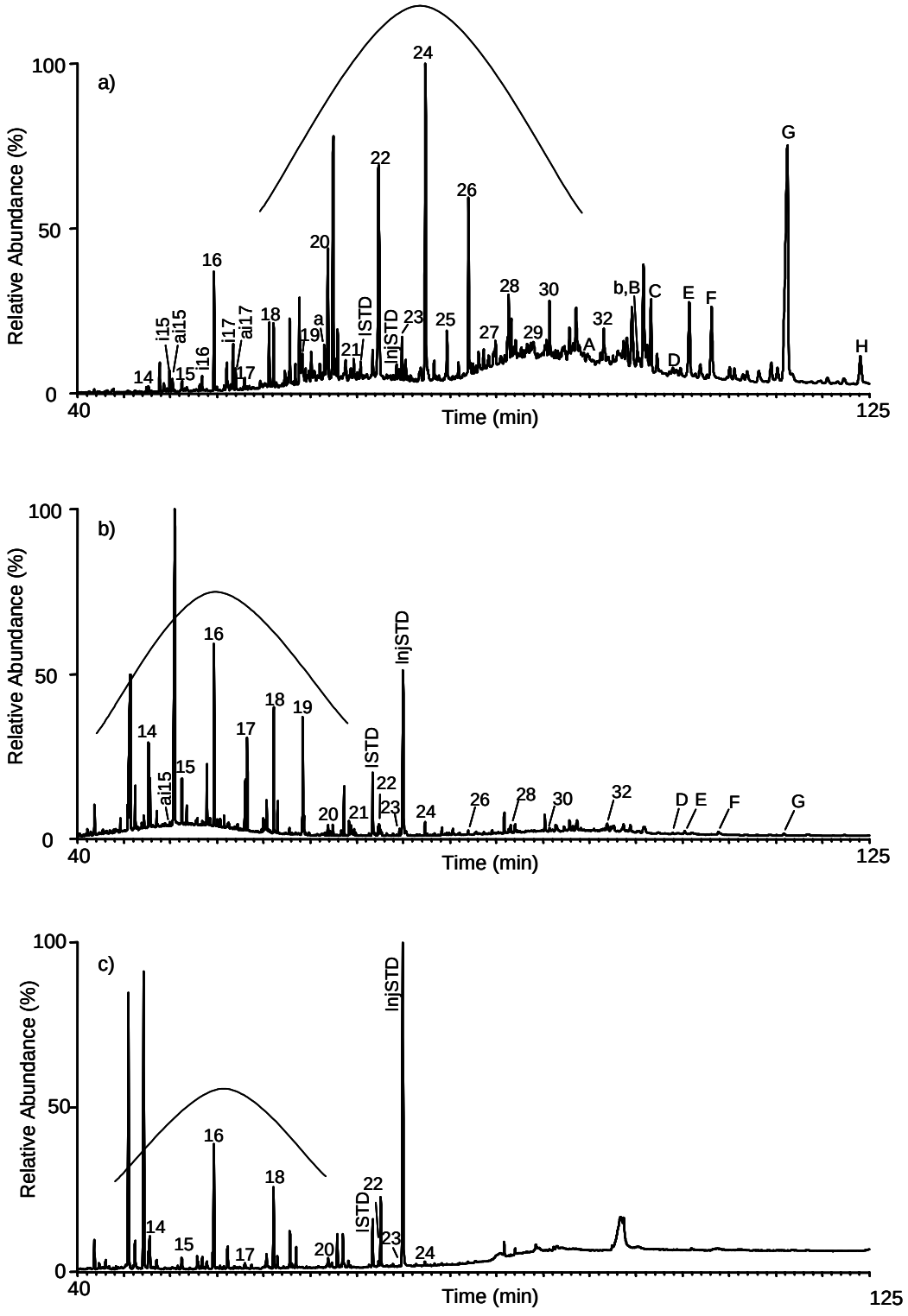

Figure 5.5: GC/MS RIC chromatograms (RIC = Reconstructed Ion Current) of representative fatty acid hydrocarbon fractions of a) sample CO105353 (lignite) b) sample MB114535 (clay) and c) MB112790 (sand). a = dehydroabietanic acid, b = oleanic acid; A = 17α(H),21β(H)–hopanoic acid, B = 17β(H),21β(H)-hopanoic acid, C = 17α(H),21β(H)-(22S)-*dihomo*-hopanoic acid, D = 17α(H),21β(H)–(22R)–*dihomo*-hopanoic acid, E = 17β(H),21α(H)–*dihomo*-hopanoic acid, F = 17β(H),21β(H)-*dihomo*-hopanoic acid, G = 17β(H),21β(H)-*trihomo*-hopanoic acid. Numbers indicate chain length of *n*-fatty acids, i = iso fatty acids, ai = anteiso fatty acids. Internal standard (ISTD) = eruic acid methyl ester, Injection standard (InjSTD) = squalane.

Sand samples

A representative gas chromatogram of a fatty acid fraction of the sand sample MB112790 is shown in Figure 5.5c. The *n*-fatty acid distribution shows a preference for the long even-chain acids with the maximum at *n*-C_{16} fatty acid. Only negligible traces of i- and ai- fatty acids have been detected in the sand samples. The fatty acid fractions of the sand samples contain neither diterpenoic nor triterpenoic fatty acids (Table 5.4).

Table 5.4: Concentrations of fatty acid sesqui-, di-, and triterpenoic hydrocarbon biomarkers. Dark grey shaded = lignites, light grey shaded = silt/clays, unshaded = sands.

Mallik 5L-38 sample	dehydro-abietanoic acid	abietanoic acid	oleanoic acid
MB89163	1.5	-	-
MB89899	-	-	-
MB90020	-	-	-
MB91200	-	-	-
MB91856	-	-	-
CO93409	0.6	1.1	5.4
MB93589	-	-	-
CO94078	-	-	-
MB94762	-	-	-
MB96334	-	-	-
MB97760	-	-	-
MB98925	-	-	-
CO100550	-	-	-
MB100778	-	-	-
MB102215	-	-	-
MB103360	-	-	-
CO104310	9.7	5.3	29.2
MB104920	2.5	-	-
CO105353	2.3	6.0	2.7
CO106094	-	-	-
MB106380	-	-	0.4
MB107960	-	-	-
CO108138	1.2	-	-
CO108169	1.9	3.1	1.6
MB108924	-	-	-
MB110494	-	-	-
CO110550	-	-	-
MB112790	-	-	-
MB113980	-	-	-
MB114535	-	-	-

5.3 Conclusions

The results of the analysis of the outstanding aliphatic, neutral polar and fatty acid hydrocarbon fractions support the general interpretations on the organic matter (terrestrial origin, immaturity) as already explained in chapter 4. In the neutral polar hydrocarbon and particularly in the fatty acid hydrocarbon fractions rather minor proportions of terpenoic hydrocarbon biomarkers occur.

However, in contrast to the lignites, the clay samples do not show any significant input of the moss plant *Sphagnum* and contain a higher proportion of triterpenoic hydrocarbon biomarkers than of diterpenoic hydrocarbons. In general, the sand samples have only small amounts of biomarkers, whereas they contain more diterpenes than triterpenes. For the interpretations of the occurrence of the hopanoids see chapter 9.

6 Occurrence and paleoenvironmental significance of aromatic hydrocarbon biomarkers in Oligocene sediments from the Mallik 5L-38 Gas Hydrate Research Well (Canada)*

*R.M. Haberer, K. Mangelsdorf, H. Wilkes and B. Horsfield (2006). Organic Geochemistry, 37, 519-538.

6.1 Introduction

Aromatic hydrocarbons represent a significant part of the organic matter in terrestrial sediments (Tissot & Welte, 1984). Therefore, their origin and formation have been the object of many studies over the last few decades (Chaffee & Fookes, 1988; Chaffee & Johns, 1983; Tan & Heit, 1981; Wakeham et al., 1980). The use of aromatic hydrocarbons as chemotaxonomic markers for higher land plants has been an important topic of discussion (e.g. Killops et al., 1995; Otto & Simoneit, 2001; Simoneit et al., 1986; Stout, 1992). The structural similarity of sedimentary aromatic biomarkers to the constituents of extant plants allows inferences to be made about the composition of ancient plant communities. Aromatic sesqui-, di- and triterpenoids are significant markers for characterizing paleovegetations (e.g. Killops et al., 1995; Otto & Simoneit, 2001; Otto & Simoneit, 2002; Simoneit et al., 1986; Simoneit et al., 2003). Aromatic biomarkers indicating angiosperms are derivatives of the amyrin triterpenoids. Derivatives of the latter, such as chrysene or picene, have been found for example in Tertiary angiosperm dominated lignites by Stout (1992). However, due to the non-specific occurrence of the precursors in almost all angiosperms these biomarkers do not provide a detailed insight into the angiospermous plant community. Characteristic biogeochemical markers for gymnosperms are represented by the diterpenoids, which are very abundant in the conifer families (Otto & Wilde, 2001). Pimaranes and isopimaranes have been identified in all conifer families except the Cephalotaxaceae. Abietanes and their related aromatic transformation products are the largest class of tricyclic diterpenoids (Otto & Wilde, 2001). They have been described in most conifer families, particularly Cupressaceae s.str., Taxodiaceae, and Podocarpaceae (Otto & Wilde, 2001). Sesquiterpenoids are present in nearly all higher land plants. Most do not provide detailed information about their biological origin (Grantham & Douglas, 1980; Otto & Wilde, 2001). However, there are some specific sesquiterpenes like cuparene, which is a characteristic biomarker for the conifer family *Cupressacea* s.str. (Grantham & Douglas, 1980; Otto & Wilde, 2001) or sativene a specific marker for Pinacea (Otto & Wilde, 2001).

Although both gymno- and angiosperms occur in almost all climate zones, their distribution is influenced by climatic conditions. Even if some angiosperms like *Betula* grow in cool temperate zones, normally the conifer division of gymnosperms is more common in cooler regions. Nowadays, vast regions of the northern temperate boreal forests are conifer dominated, particularly by the *Pinus*, *Picea*, *Abies*, *Thuja* and *Juniperus* families (Walter & Breckle, 1999). Therefore, changes in the plant community composition within a certain area can be used as an indicator of varying climatic conditions.

In addition to the palaeoenvironmental and palaeoclimatic aspects, aromatic hydrocarbons can be used to obtain information on the maturity level of the organic matter on a molecular basis. The extent of aromatization of cyclic hydrocarbons increases with increasing maturity of the organic matter. In particular, in terrestrial organic matter the amounts of aromatic hydrocarbons clearly increase with increasing coalification stage (e.g. Norgate et al., 1999; Radke et al., 1982a; Wilhelms et al., 1998). Furthermore, the distributions of alkylated naphthalenes and phenanthrenes are widely used as aromatic hydrocarbon maturity parameters (Alexander et al., 1995; Alexander et al., 1985; Bastow et al., 2001; Budzinski et al., 1995; Goodarzi et al., 1994; Püttmann & Villar, 1987; Radke et al., 1990; Radke et al., 1994; Radke et al., 1982a; Strachan et al., 1988; Wilhelms et al., 1998). However, as a result of their high degree of aromatization, they occur mainly in relatively mature sediments or crude oils and are not usable with respect to immature sample material. Nevertheless, some aromatic hydrocarbons, like the diterpenoid retene or the amyrin derivatives chrysene and picene, are formed during early diagenesis and can be used as maturity parameters in immature sediments (Tan & Heit, 1981; Wakeham et al., 1980).

Concerning maturation, it has been suggested that hydrogen-rich resin material thermally breaks down to yield either gas condensates (Snowdon, 1980; Snowdon & Powell, 1982) or remains as resoluble aromatic residue (Lewan & Williams, 1987), whereas diterpenoid resinite reacts at lower temperatures than triterpenoid resinite (Fowler et al., 1991). Snowdon's study area was the Mackenzie delta, and in the present study concerning the aromatic hydrocarbon content of the sediments, a deeper insight is given into the composition of the plant communities providing these resins. Specifically, the aromatic hydrocarbon fractions of thirty sediment sample extracts of different lithologies (6 lignite, 13 clay and 11 sand samples) from the JAPEX/JNOC/GSC et al. Mallik 5L-38 Gas Hydrate Production Research Well have been investigated in order to explore the palaeoenvironmental and palaeoclimatic changes in the Mackenzie Delta area as well as the level of thermal maturity of the organic matter on a molecular basis.

6.2 Study area

6.2.1 The Mackenzie Delta

The Mackenzie Delta (Figure 6.1a) is located at the Beaufort Sea margin in northern Canada (Northwest Territories). Since the late Cretaceous-Tertiary it appears not to have experienced any significant tectonic activity (Dixon et al., 1992b) with the result that 12 to 16 km of strata have accumulated in the Beaufort-Mackenzie area, predominantly in a northward-prograding delta (Dixon et al., 1992a; Dixon et al., 1992b). It has been suggested that wave-modified and river-dominated deltas prevailed from the Paleocene to the Oligocene (Dixon et al., 1992b). However, the position of the delta moved through time. Based on a study of the Oligocene Kugmallit Delta, located in the south-central part of the Beaufort shelf area, Lane and Dietrich (1995) proposed that the Tertiary Porcupine River basin provided the clastic sediments draining the northern Cordillera. In the Mallik area, eight deltaic sequences are recognized above the Maastrichtian - Paleocene boundary (e.g. Dixon, 1986; Dixon et al., 1992b; Willumsen & Cote, 1982): The first sequence (Fish River Sequence; late Maastrichtian - early Palaeocene) includes gravity flow deposits composed of conglomerates, sandstones and shales. Subsequently, the widespread thick shale deposits built out into the basin during the formation of the Reindeer Sequence (late Paleocene – middle Eocene), reflecting a transgression. The shale dominated Richards Sequence (late Eocene) represents the continuation of the Reindeer Sequence. The contact between the Richards sequence and the Kugmallit Sequence (early - late Oligocene) is characterised by an erosional unconformity. The overlying Mackenzie Bay (late Oligocene - middle Miocene) and Akpak Sequence (late Miocene) are, in general, shale dominated. In contrast, the Iperk Sequence (early Pliocene – early Pleistocene) consists of sandstones and conglomerates. The Shallow Bay Sequence (Pleistocene – Holocene) is mostly inseparable from the Iperk Sequence.

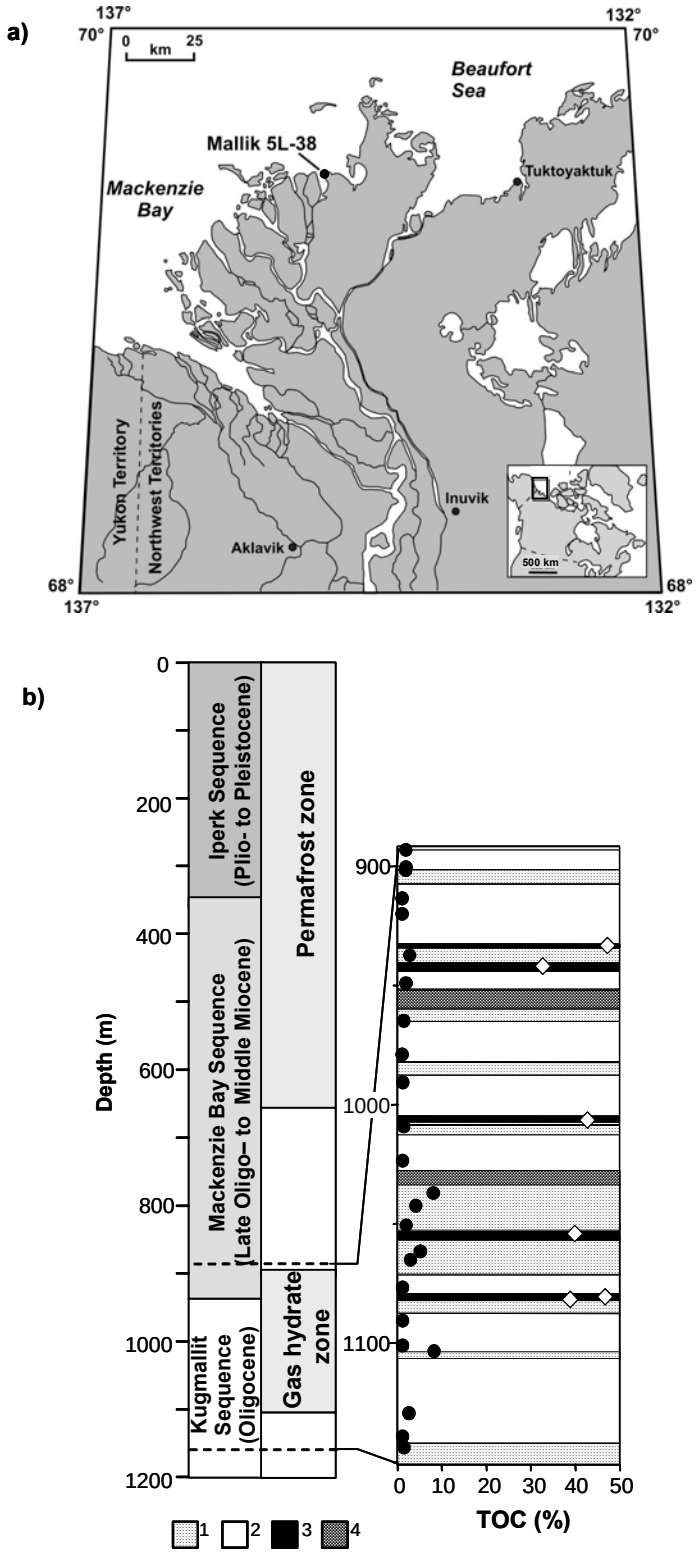

Figure 6.1: a) Map of the Mackenzie River Delta (Northwest Territories, Canada) showing the location of the Mallik 5L-38 Gas Hydrate Research Well. b) Stratigraphic column of the Mallik 5L-38 Gas Hydrate Research Well. The positions of the selected sediment samples are displayed relative to lithology and TOC content. Non-lignite samples are indicated with black dots. Lignites are indicated with diamonds. 1, silt/clay; 2, sand; 3, lignite layer; 4, conglomerate.

6.2.2 Mallik 5L-38 Gas Hydrate Research Well

The Mallik well drilled in January to March 2002, penetrated a permafrost zone from 0 to 650 m and a zone of numerous gas hydrate-bearing layers between 896 and 1100 m depth. The sedimentary succession can be divided into three main sequences: the Kugmallit, the Mackenzie Bay and the Iperk sequence (Figure 6.1b). The sand-dominated Kugmallit Sequence (Oligocene) is subdivided into two parts: the lower Ivik and the upper Arnak members (Young & McNeil, 1984); only sediments from the Arnak member were penetrated by the Mallik well (930-1165 m, late Oligocene). The upper Arnak member is a non-marine, delta-plain deposit (Dixon, 1996; Young & McNeil, 1984) and consists of sand, silt, clay and some lignite layers. The clays and lignite layers were probably deposited in interdistributary marshes and minor channels (Young et al., 1976). Contrary to the Kugmallit sequence, the Mackenzie Bay sequence (350-930 m, late Oligocene - middle Miocene) is related to sedimentation processes at the delta-front. In the Mallik area, it consists mainly of sand and weakly cemented sandstones with conglomerates and only minor silt or shale interbeds (Dixon, 1996).

The Akpak Sequence (Middle – Upper Miocene), which is usually present, is absent from the sedimentological succession in the area of the Mallik Well due to erosion (Dixon, 1996; Dixon et al., 1992b). Similar to the Kugmallit Sequence, the Iperk Sequence (0-350 m, Plio- to Pleistocene) is composed of unconsolidated sandstones with local intermediary conglomerates, silt and shale layers, representing delta-plain or even fluvial sediments (Dixon, 1996; Dixon et al., 1992b).

6.3 Sample material and methods

6.3.1 Sample material

Thirty samples (18 - 170 g) from different lithologies such as clays, siltstones, sandstones and lignitic carbon-rich layers from above, within and below the gas hydrate zone were collected predominantly from the Kugmallit Sequence (Figure 6.1b). Sample names are composed of letters and numbers. The letter combination assigns a specific sampling method [“MB” (microbiology) = samples taken under specific contamination-free conditions (see also chapter 3), or a lithological characterization “CO” (coal) = lignite samples]. The numbers provide the sample depth in cm.

First results for the lignites are already published in Haberer et al. (2005) (see also chapter 4). The major findings are presented in Table 6.1. This table contains a brief lithological description for each sample and bulk elemental data such as the organic carbon content, Rock-Eval

pyrolysis data, and the bulk organic carbon isotopic value, all for an initial sample characterisation. As expected, the six lignite samples contain the highest total organic carbon (TOC) content, up to 46.6%. The thirteen clay samples have lower TOC values from 0.4 to 9.4%, while the portion of organic carbon in the eleven sand samples is very small with an average of 0.3%. According to initial core descriptions, three samples (CO104310, CO106094 and CO110550) were assigned as coals (CO, lignite), however, their comparatively low organic carbon contents of 3.6, 4.7 and 9.4%, respectively, revealed that these samples are organic-rich shales rather than lignites. The Rock-Eval-pyrolysis data (Haberer et al., 2005) of the Mallik samples assign a terrestrial character to the sample set. The HI values of the studied samples range between 3 and 300 mgHC/gTOC with the lignites and organic–rich clays being characterized by systematically higher HI values between 100 and 300 mgHC/gTOC and low OI values (<100 $mgCO_2$/gTOC) in comparison to the coarser-grained lithologies with HI values from 10 to 177 mgHC/gTOC and OI values from 44 to 898 $mgCO_2$/gTOC. In this regard, sample CO104310 shows some remarkable properties. Ithas an unusually HI value (532 mgHC/gTOC) even though the organic matter is of terrestrial origin. One possible explanation for this is the exceptionally high liptinite content of 41.7% on a mineral free basis (mfb) in this sample detected by maceral analysis. In contrast, the liptinite content of the other samples ranges from 1.8 to 11.2%mfb with an average of 5.5%mfb. Liptinites are characterized by a high proportion of aliphatic moieties (mainly long-chain *n*-alkanes) resulting in a high HI value (Diessel, 1992).

Data obtained from the open-system pyrolysis-GC experiments corroborate the origin of the organic matter as being from higher land plants (Haberer et al., 2005) (see also chapter 4). The alkyl-chain distribution in the pyrolysates suggests that the organic material has a potential for mostly gas formation according to the calibrations set out by Horsfield (1989). Three samples show a potential for liquid hydrocarbon generation, falling in the field of paraffinic-naphthenic-aromatic-oils (P-N-A-oil) defined by the same author. A further indicator for the terrestrial origin of the sample material are the $\delta^{13}C_{org}$ data, which show values (~ -25.6‰) typical for organic carbon from a terrestrial source in sediments of Cenozoic age (e.g. Hoefs, 1997).

6.3.2 Methods

After the sediment samples have been freeze-dried and ground, the TOC contents and the Rock-Eval parameters (S_1, S_2, hydrogen index (HI) and oxygen index (OI), T_{max} values; (Espitalié *et al.*, 1977)) were determined using a Rock-Eval 6 instrument (Table 6.1).

For lipid analysis, sample aliquots of about 2 - 25 g (depending on TOC-content) of sediment material were extracted ultrasonically using a mixture of dichlormethane and methanol (99/1, v/v). Subsequently, the volume of the resulting extract was concentrated using a Zymark TurboVap 500 concentrator and finally evaporated to dryness under a nitrogen gas stream. After addition of an internal standard (ethylpyrene) for the aromatic hydrocarbon fraction, the extract was dissolved in *n*-hexane to precipitate asphaltenes, which were removed by filtration over Na_2SO_4. The *n*-hexane-soluble fraction was separated by medium-pressure liquid chromatography (Radke et al., 1980) into fractions of different polarity (aliphatic/alicyclic hydrocarbons, aromatic hydrocarbons and hetero compounds). Prior to GC analysis, behenic acid methyl ester (BAME) was added as injection standard to the aromatic hydrocarbon fractions.

The aromatic hydrocarbon fraction was analyzed using a gas chromatograph coupled with a mass spectrometer. Compound separation was performed on a Agilent 6890 Series GC-instrument equipped with a PTV injection system and a fused silica capillary column (SGE BPX5; 50 m length, inner diameter = 0.22 mm, film thickness = 0.25 µm).

Helium was used as carrier gas, and the temperature of the GC oven was programmed from 50°C (1 min) to 310°C at a rate of 3°C/min, followed by an isothermal phase of 20 min. The mass spectrometer was a Finnigan MAT 95 XL instrument which was operated in the electron ionization mode (70 eV). Full scan mass spectra were recorded from *m/z* 50 to 650 at a scan rate of 1 s per decade and an inter scan delay of 0.2 s, resulting in a scan cycle time of 1.3 s.

6.4 Results

6.4.1 Types of aromatic biomarkers

The major skeleton types in the Mallik samples are related to cyclic sesqui-, di-, and triterpenoids (Table 6.2, Figure 6.2).

Aromatic sesquiterpenoids (Table 6.2, Figure 6.2) are represented by dihydro-*ar*-curcumene [1], cuparene [2] and cadalene [5] and its related compounds calamene [3] and cadina-1(10),6,8-triene [4]. They are in general not very abundant. Sesquiterpenes are used as markers for higher land plants, because they occur in their resinous material. However, due to their occurrence in the resins of conifers (gymnosperms) (e.g. Grantham & Douglas, 1980; Otto et al., 2002; Otto et al., 1997) as well as in dammar resin (van Aarssen et al., 1990), which originates from Dipterocarpaceae (angiosperms), they are often not useful for an unambiguous determination of the precursor plant community. Nevertheless, in contrast to the majority of sesquiterpenes, cuparene (Figure 6.3d) is a characteristic marker for Cupressaceae s.str., a

family of conifers (gymnosperms) including the genera *Cupressus*, *Thuja* and *Juniperus* (Grantham & Douglas, 1980; Otto & Wilde, 2001).

The most abundant type of diterpenoids are members of the abietane group: 18-norabieta-8,11,13-triene [A], 19-norabieta-8,11,13-triene [B], dehydroabietane [C], 1,2,3,4-tetrahydroretene [D], abieta-6,8,11,13-tetraene [E], simonellite [F], retene [H], methylretene [I] (Table 6.2, Figure 6.2).

Additionally, one diaromatic totarane [G] was identified in lower abundance in a few lignite and clay samples (Figure 6.2a, b and Figure 6.3e). Diterpenes are the main constituents of gymnosperm resins and are known to be chemotaxonomic biomarkers, especially for conifers (Otto & Simoneit, 2001; Otto et al., 2003; Otto et al., 1997; Otto & Wilde, 2001; Simoneit, 1977; Simoneit et al., 1986; Stefanova et al., 2002; Wakeham et al., 1980; White & Lee, 1980). Most abundant diterpenes in gymnosperms posses an abietane or pimarane type structure and only a few have a phyllocladane type skeleton. The totaranes, similar to cuparene, are characteristic for the conifer genera Cupressaceae s.str., and additionally for Podocarpaceae (Otto & Simoneit, 2001; Otto et al., 1997; Simoneit, 1977).

The aromatic triterpenoids are mainly of the chrysene and picene type at different stages of aromatiziation. Two isomers of tetramethyloctahydro- and trimethyltetrahydrochrysenes [a-d] (Table 6.2, Figure 6.2), and tetramethyloctahydro- and trimethyltetrahydropicenes [h-k] were identified in addition to hexamethylhexadecahydropicene [g]. In most samples 24,25-dinoroleana-1,3,5(10),12-tetraene [e], and 24,25-dinorursa-1,3,5(10),12-tetraene [f] were detected. Triterpenoids such as amyrins, commonly used as markers for angiosperms (Chaffee & Fookes, 1988; Chaffee et al., 1986; Chaffee & Johns, 1983; Spyckerelle et al., 1977a;b; Stout, 1992; Tan & Heit, 1981; Wakeham et al., 1980), are the precursors of the most abundant aromatic triterpenoids in the samples (Figure 6.4). Although triterpenoids are markers for angiosperms, they provide no specific evidence for the family or the genus.

Analysis of the aromatic fractions reveals the occurrence of specific biomarkers for a gymnosperm and angiosperm plant community in the Mallik area (Table 6.2, Figure 6.2). This agrees with the results of White (1999), who showed in a former study on the Mallik 2L-38 Gas Hydrate Research Well in the same area that gymnosperm and angiosperm pollen and spores were the dominating components in the palynological assemblage. *Picea* spp., *Pinus* spp., and Taxodiaceae-Cupressaceae-Taxaceae were the most common gymnosperm taxa. The angiosperms were represented by Dipterocarpaceae such as *Alnus* spp., Ericales, and betulaeous pollen (White, 1999). Abundant amounts of pollen of gymnosperms (Picea, Pinus, and Taxodiaceae/Cupressaceae) were also identified in a more basinward part of the Kugmal-

lit sequence at the Edlok N-56 well by Dietrich et al. (1989) where angiosperm pollen (e.g. Tsuga, Alnus, Betula, and Ericaceae) were found only in minor amounts.

6.4.2 Occurrence of aromatic hydrocarbon biomarkers in the different lithologies

As illustrated in Figure 6.2 and Figure 6.5, the distribution patterns of aromatic hydrocarbon biomarkers show distinct differences depending on lithology. In the ternary plot of sesqui-, di-, and triterpenoid abundances (Figure 6.5) it appears that the aromatic hydrocarbon fraction of most lignite samples is dominated by diterpenoids. The same can be deduced for the sand samples. In contrast, there is a tendency for clays to be dominated by triterpenoids. The non-specific sesquiterpenoids play only a minor part, which is supported by the quantitative results obtained for the individual aromatic biomarkers (Table 6.3).

Sesquiterpenoids occur in all lignite samples (Figure 6.2a, Table 6.3) and the content ranges from 30 to 80 µg/gTOC. Sesquiterpenoids are more frequent in the lignites than in the samples of other lithologies, although they are not the dominant compound group. The dominating aromatic biomarkers in the lignites are diterpenes, with amounts varying between 21 and 278 µg/gTOC. The values for triterpenes range from 5 to 69 µg/gTOC. With one exception (CO108138), the amounts of triterpenes are always lower than those of diterpenes (Figure 6.3c).

In the clay samples (Figure 6.2b and Table 6.3) sesquiterpenes are only present in four samples (MB89163, MB93589, MB103360, and CO104310), whereas dihydro-*ar*-curcumene occurs only in samples MB103360, and CO104310. The amounts of sesquiterpenoids range between 3 to 5 µg/gTOC with one extreme value of 75 µg/gTOC (CO104310). With exception of three samples (MB 93589, MB100778, and CO104310), the content of diterpenes in the clay samples is lower than in the lignite samples (Figure 6.3a). Moreover, four clay samples (MB89899, MB96334, MB104920, and MB106380) contain diterpenoids near or below the detection limit (Figure 6.3a). In contrast to the lignite samples, triterpenoids are the dominant compounds in most clay samples, with quantities of 20 to 441 µg/gTOC (Figure 6.3b).

Table 6.1: Sample names, lithological description and general elemental parameters for sample characterisation. Dark grey shaded = lignites, light grey shaded = silts/clays and unshaded = sands.

Mallik 5L-38	Sample characteristics								
Sample	**Depth (m)**	**Lithology**	**TOC (%)**	**S_1 (mg HC/g Sed)**	**S_2 (mg HC/g Sed)**	**T_{max} (°C)**	**HI (mg HC/g TOC)**	**OI (mg CO_2/g TOC)**	**$\delta^{13}C_{org}$ (‰)**
MB89163	891.63 – 891.82	silt/clay	0.92	0.03	0.73	424	80	215	-25.21
MB89899	898.99 – 899.16	silt/clay	0.95	0.03	0.97	426	103	243	-25.05
MB90020	900.20 – 900.40	silt/clay	0.86	0.03	0.67	425	77	230	-24.94
MB91200	912.00 – 912.19	sand	0.05	0	0.01	-	14	-	-27.14
MB91856	918.56 – 918.76	sand	0.05	0.01	0.03	-	50	100	-26.49
CO93409	934.09 – 934.10	lignite	46.60	2.52	90.71	363	195	43	-24.6
MB93589	935.89 – 936.09	silt/clay	1.78	0.05	3.15	424	177	167	-25.88
CO94078	940.78 – 940.81	lignite	31.85	4.53	92.97	392	292	56	-25.6
MB94762	947.62 – 947.84	sand	0.95	1.79	0.69	406	72	44	-25.26
MB96334	963.34 – 963.50	silt/clay	0.40	0.01	0.17	416	42	263	-25.91
MB97760	977.60 – 977.80	sand	0.09	0	0.04	-	47	-	-26.02
MB98925	989.25 – 989.45	sand	0.10	0	0.01	-	12	410	-26.83
CO100550	1005.50	lignite	42.03	2.87	87.08	400	207	56	-24.9
MB100778	1007.78 - 1007.98	silt/clay	0.46	0.03	0.51	426	111	65	-25.83
MB102215	1022.15 – 1022.55	sand	0.11	0	0.15	-	134	36	-26.23
MB103360	1033.60 - 1033.80	silt/clay	7.09	0.41	12.44	415	175	68	-26.3
CO104310	1043.10	silt/clay	3.64	0.6	19.36	430	532	48	-26.3
MB104920	1049.20 – 1049.36	silt/clay	1.01	0.03	1.04	428	103	898	-25.5
CO105353	1053.53	lignite	39.19	3.39	96.84	388	247	55	-24.3
CO106094	1060.94 – 1060.95	silt/clay	4.71	0.16	7.79	420	165	75	-26.0
MB106380	1063.80 – 1064.00	silt/clay	1.89	0.06	1.96	417	104	113	-25.5
MB107960	1079.60 – 1079.81	sand	0.04	0.04	0	-	10	-	-26.33
CO108138	1081.38	lignite	45.93	0.73	52.6	406	115	62	-25.8
CO108169	1081.69	lignite	38.39	1.8	84.47	392	220	57	-24.1
MB108924	1089.24 - 1089.39	sand	0.06	0.01	0.02	-	38	333	-26.83
MB110494	1104.94 - 1105.14	sand	0.09	0.01	0.03	-	33	-	-24.74
CO110550	1105.50	silt/clay	9.44	0.21	9.5	411	101	99	-25.1
MB112790	1127.90 - 1128.02	sand	1.57	0.02	1.05	421	67	127	-25.8
MB113980	1139.80 - 1139.83	sand	0.17	0.02	0.21	-	123	459	-25.71
MB114535	1145.35 - 1145.55	silt/clay	0.53	0.02	0.38	424	72	340	-25.47

Table 6.2: Aromatic compounds identified in the aromatic hydrocarbon fractions (Fig. 6.4.1) and their potential as vegetation and maturity indicators. Ses, sesquiterpenes; Di, diterpenes; Tri, triterpenes.

No.	Type	Compound names	Origin/Interpretation	References
1	Ses	Dihydro-ar-curcumene	higher land plants; non-specific	Otto et al. (2002), Otto and Simoneit (2001)
2	Ses	Cuparene	Cupressaceae s.str.	Otto and Wilde (2001), Otto and Simoneit (2001), Grantham and Douglas (1980)
3	Ses	Calamene	higher land plants especially resins of conifers (gymnosperms) and Dipterocarpaceae (dammar resin, angiosperms); non-specific	Otto and Wilde (2001), Simoneit et al. (1986), Otto et al. (1997)
4	Ses	Cadina-1(10),6,8-triene		
5	Ses	Cadalene		
A	Di	18-Norabieta-8,11,13-triene	all conifer families (gymnosperms) except Phyllocladaceae; Cupressaceae s.l.; maturity indicator	Otto and Wilde (2001), Stefanova et al. (2002), Otto et al. (2003), Simoneit (1977), Simoneit et al. (1986), Wakeham et al. (1980), White and Lee (1980)
B	Di	19-Norabieta-8,11,13-triene		
C	Di	Dehydroabietane		
D	Di	1,2,3,4-Tetrahydroretene		
E	Di	Abieta-6,8,11,13-tetraene		
F	Di	Simonellite		
G	Di	diaromatic Totarane	Podocarpaceae, Cupressaceae s.str., (gymnosperms)	Otto et al. (1997), Otto and Simoneit (2001), Simoneit (1977)
H	Di	Retene	all conifer families (gymnosperms) except Phyllocladaceae; Cupressaceae s.l.; maturity indicator	Stefanova et al. (2002), Otto et al. (2003), Simoneit (1977), Simoneit et al. (1986), Wakeham et al. (1980), White and Lee (1980)
I	Di	Methylretene		
a	Tri	3,4,7,12a-Tetramethyl-1,2,3,4,4a,11,12,12a-octahydrochrysene	angiosperms, maturity indicator	Chaffee and Johns (1983), Chaffee and Fookes (1988), Stout (1992), Chaffee et al. (1986), Spyckerelle et al. (1977a; 1977b), Wakeham et al.(1980), Tan & Heit (1981)
b	Tri	3,3,7,12a-Tetramethyl-1,2,3,4,4a,11,12,12a-octahydrochrysene		
c	Tri	3,4,7-Trimethyl-1,2,3,4-tetrahydrochrysene		
d	Tri	3,3,7-Trimethyl-1,2,3,4-tetrahydrochrysene		
e	Tri	24,25-Dinoroleana-1,3,5(10),12-tetraene	angiosperms	Simoneit et al. (2003)
f	Tri	24,25-Dinorursa-1,3,5(10),12-tetraene		
g	Tri	Hexamethylhexadecahydropicene	angiosperms, maturity indicator	Chaffee and Johns (1983), Chaffee and Fookes (1988), Stout (1992), Chaffee et al. (1986), Wakeham et al. (1980), Tan and Heit (1981)
h	Tri	1,2,4a,9-Tetramethyl-1,2,3,4,4a,5,6,15b-octahydropicene		
i	Tri	2,2,4a,9-Tetramethyl-1,2,3,4,4a,5,6,15b-octahydropicene		
j	Tri	1,2,9-Trimethyl-1,2,3,4-tetrahydropicene		
K	Tri	2,2,9-Trimethyl-1,2,3,4-tetrahydropicene		

The clay sample CO104310 with the unusual high HI value of 532 mgHC/gTOC (Table 6.1) also shows some exceptional differences in its aromatic hydrocarbon content compared to other clay samples. It contains an unusually high amount of sesquiterpenes (75 µg/gTOC) and, in contrast to the other clay samples, the diterpenes are the dominant compounds. At 865 µg/gTOC, they are even more abundant than in the lignite samples. Sample CO104310 shows similar amounts of triterpenes to the other clay samples.

The sand samples (Figure 6.2c) contain only low amounts of aromatic hydrocarbons. Sesquiterpenes are only present in two samples (MB107960; 15 µg/gTOC and MB110494; 5 µg/gTOC). Diterpenes occur in all sand samples except sample MB112790, which contains no relevant aromatic hydrocarbons at all. The contents of diterpenes in the sand samples range from 8 to 51 µg/gTOC, with one extreme value of 110 µg/gTOC (MB107960). The values for triterpenes in the sand samples range from 1 to 34 µg/gTOC. As for the diterpenes, sample MB107960 contains also an unusually high amount of triterpenes (225 µg/gTOC). However, sand samples are mainly dominated by aromatic diterpenoids (Figure 6.3c). The abundance of characteristic gymnosperm (cuparene, abietanes and totarane) and angiosperm (chrysenes and picenes) biomarkers in the Mallik samples in relation to lithology is shown in Figure 6.3a and Figure 6.3b. Lignite samples, in general, contain significant amounts of gymnosperm biomarkers (Figure 6.3a).

Many clay samples contain only small amounts of, or even no, gymnosperm biomarkers, although the highest gymnosperm biomarker content was detected in the (in many aspects) remarkable clay sample CO104310 (see above). In contrast, sand samples show higher relative abundances of gymnosperm markers. However, the average aromatic biomarker content in the sand samples is in general fairly low.

Angiosperm markers (Figure 6.3b) are present in all clay and lignite samples in significant amounts, with maxima at 898.99 m, 1007.78 m, 1033.60 m and 1079.60 m depth. Comparing biomarker abundance with lithology, it is obvious that clay samples tend to have the highest amounts of angiosperm markers (Figure 6.3b). In the lignite and especially the sand samples, angiosperm markers appear to be less important.

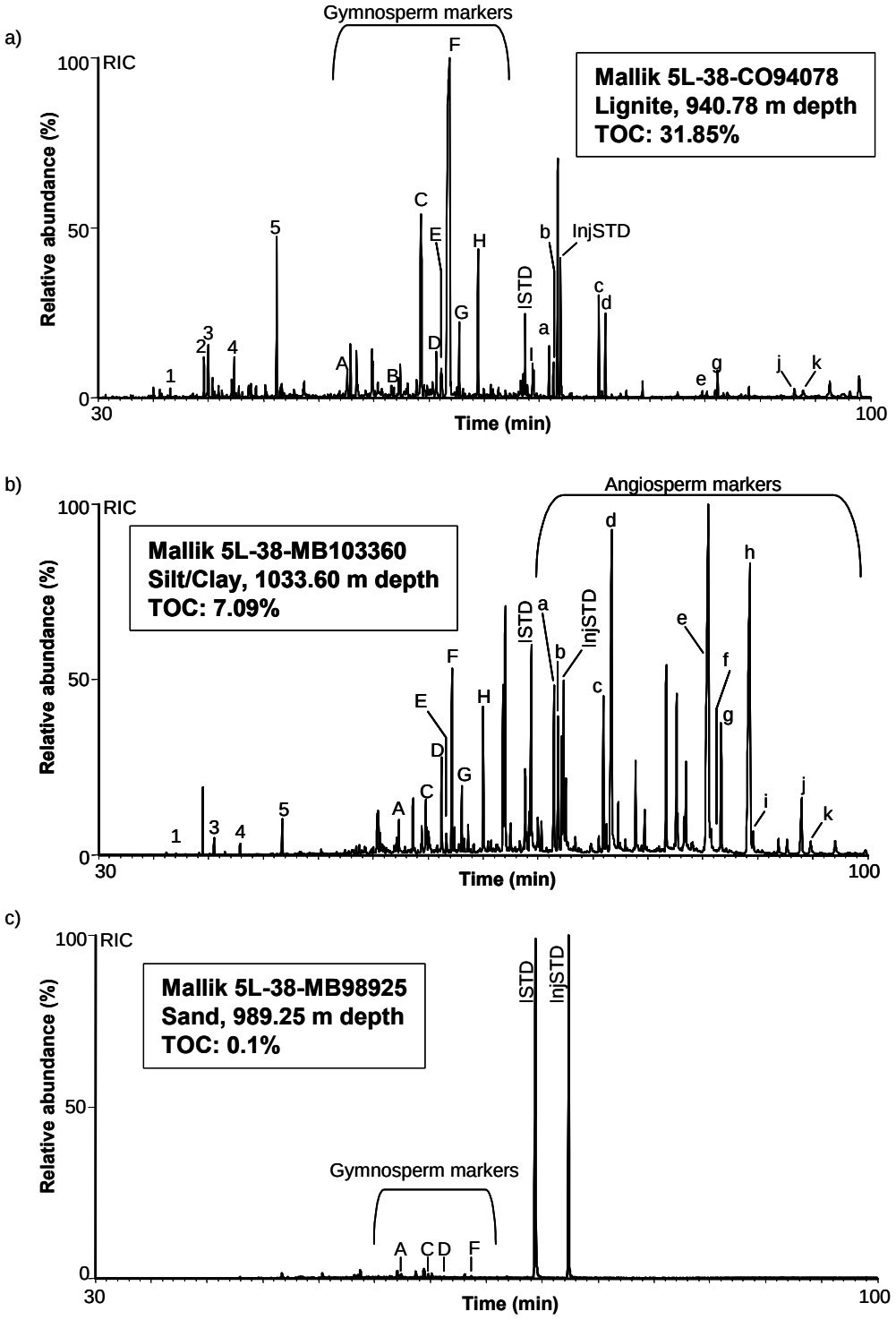

Figure 6.2: GC/MS-RIC-chromatograms of representative aromatic hydrocarbon fractions of a) a lignite sample (CO94078), b) a clay sample (MB103360) and c) a sand sample (MB98925). Numbers and letters correspond to compound names in Table 6.2. Internal standard (ISTD) = ethylpyrene; injection standard (InjSTD) = behenic acid methyl ester (BAME).

6.5 Discussion

6.5.1 Gymnosperm vs. angiosperm occurrence

A new ratio, termed angiosperm-gymnosperm aromatic ratio (AGAR), has been developed to recognise gymnosperm *versus* angiosperm dominated paleoenvironments at the Mallik site. AGAR is defined as the concentration of the aromatic diterpenes divided by the sum of aromatic di- plus triterpene concentrations (Figure 6.3c), and is a modification of the aliphatic hydrocarbon ratio published by Bechtel et al. (2001; 2002).

The ratio reveals a more or less periodical alternation in the dominating plant communities for the Oligocene sediment section with depth (Figure 6.3c). Three major cycles in vegetation type separated by rapid minor fluctuations may be discernable despite the low resolution of the sample set. The top cycle (890-950 m) includes five samples belonging to the Mackenzie Bay Sequence and four samples of the following Kugmallit Sequence. Subsequently, a second cycle (950-1030 m) is visible. In this cycle a strong variability is observed in the paleovegetation signal changing from gymnosperm to angiosperm dominated plant communities. Between 1070 and 1125 m there is a possibility of a third cycle.

As discussed below this apparent cyclicity reflects floral signals from both the site of deposition and the area of sediment provenance.

Gymnosperms dominated the plant community in the Mackenzie Delta area during deposition of the lignite seams. The dominance of gymnosperm biomarkers in the lignites is confirmed by the occurrence of pimaranes, isopimaranes, and phenolic abietanes like ferruginol (Haberer et al., 2005 and unpubl. data) in the aliphatic hydrocarbon and hetero compound fractions of the same sample set (see also chapter 4 and 5). Pimaranes are reported for conifer genera like Pinaceae, Cupressaceae s.str., and Taxodiaceae, whereas isopimaranes are common in all conifer families except Cephalotaxaceae. Non-phenolic abietanes like dehydroabietane also occur in all conifer families except the Phyllocladaceae, whereas the phenolic abietanes like ferruginol or sugiol are characteristic markers for Cupressaceae s.str., Taxodiaceae and Podocarpaceae (Otto & Simoneit, 2001; Otto et al., 2002; Simoneit et al., 2003; Stefanova et al., 2002). One exception to the gymnosperm dominance in the lignites is sample CO108138 (1081.38 m depth), which appears to represent a change in the paleovegetation of the delta system to a more angiosperm dominated plant community and concomitantly a climatic change to presumably warmer conditions in the Mackenzie Delta area during this period.

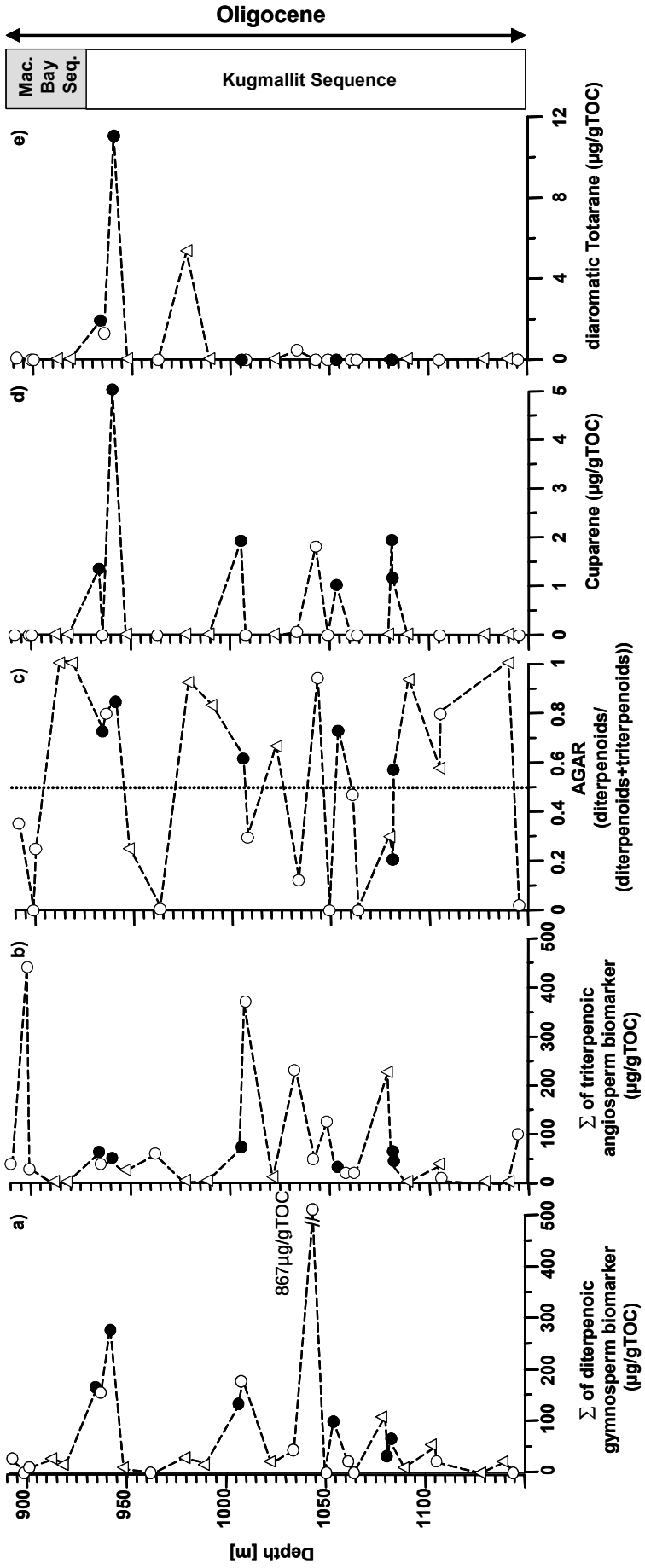
Oligocene
Mac. Bay Seq.
Kugmallit Sequence
e)
diaromatic Totarane (µg/gTOC)
d)
Cuparene (µg/gTOC)
c)
AGAR (diterpenoids/ (diterpenoids+triterpenoids))
b)
Σ of triterpenoic angiosperm biomarker (µg/gTOC)
a)
867µg/gTOC
Σ of diterpenoic gymnosperm biomarker (µg/gTOC)
Depth [m]

Figure 6.3: Depth profile of a) the sum of gymnosperm related biomarkers (cuparene, abietanes, totarane; Table 2) and b) of the sum of angiosperm related biomarkers (chrysenes, picenes; Table 2). c) Ratio of diterpenoid concentration to the sum of di- and triterpenoid concentrations as an indicator for an angio- or gymnosperm dominated paleovegetation (AGAR (angiosperm-gymnosperm-aromatic ratio)). Sample MB112790 is not shown because it contains no relevant aromatic biomarkers. Depth profiles of d) cuparene and e) diaromatic totarane distribution in the Mallik sediments investigated. Triangles = sand samples, open circles = clay samples, filled circles = lignites; Mac. Bay Seq. = Mackenzie Bay Sequence.

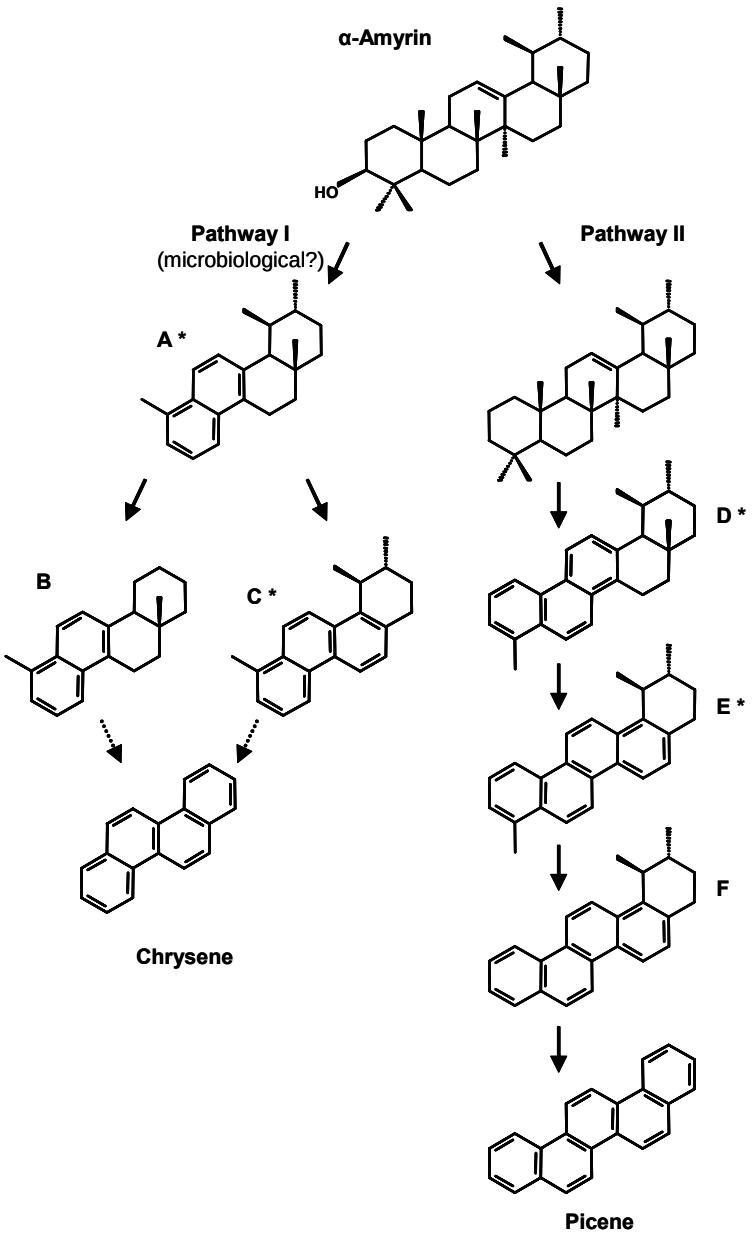

Figure 6.4: Schematic transformation pathways for the formation of aromatic hydrocarbons (chrysene, picene) starting from α-amyrin [adapted from Wakeham (1980) and Tan & Heit (1981)]. A = 3,4,7,12a-tetramethyl-1,2,3,4,4a,11,12,12a-octahydrochrysene, B = 7,12a-dimethyl-1,2,3,4,4a,11,12,12a-octahydrochrysene, C = 3,4,7-trimethyl-1,2,3,4-tetramethylhydrochrysene, D = 1,2,4a,9-tetramethyl-1,2,3,4,4a,5,6,14b octahydro-picene, E = 1,2,9-trimethyl-1,2,3,4-tetrahydropicene, F = 1,2 dimethyl-1,2,3,4-tetrahydropicene. Compounds with an asterisk (*) were detected in the Mallik samples.

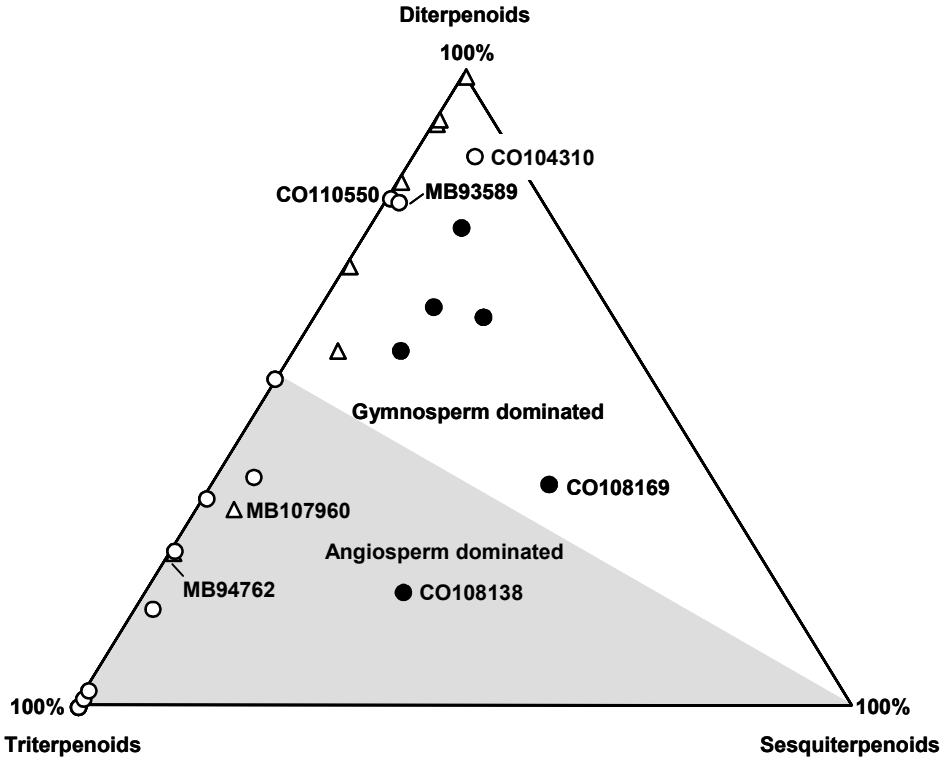

Figure 6.5: Ternary diagram illustrating distribution of sesquiterpenoids (non-specific), diterpenoids (gymnosperms) and triterpenoids (angiosperms). Triangles = sand samples, open circles = clay samples, filled circles = lignites.

Pollen and specific *n*-alkane distribution patterns with a maximum at *n*-C_{23} (Haberer et al., 2005; White, 1999) reveal the occurrence of the peat moss plant *Sphagnum* sp. in the lignite samples of the Mallik site, indicating the formation of lignites in interdistributary swamps of the delta plain (see also chapter 4 and 5).

Most of the clay samples are dominated by biomarkers representing an angiosperm paleovegetation. However, there are three exceptions, whose ratios are consistent with a dominance of gymnosperms. One is the above-mentioned clay sample CO104310 that is rich in liptinites and has a high hydrogen content (Haberer et al., 2005) (see also chapter 5). The other samples are MB93589, which was sandwiched between two lignite layers suggesting that the surrounding paleovegetation was stable, and sample CO110550, which is characterized by an high organic carbon content. Clay samples might represent both an allochthonous floral signal transported by the river to the delta region and an authochthonous signal supplied by the surrounding vegetation to the delta system. The importance of the allochthonous *versus* autochthonous floral signal might vary in the clay samples depending on the dynamics of the river and the position of the site relative to the surrounding vegetation in a meandering delta system. Although one lignite sample shows a dominance of angiosperm markers, most lignite

samples indicate that gymnosperms are the dominating vegetation in the Mackenzie Delta during the time interval investigated. Thus, the three gymnosperm dominated clays might represent a higher autochthonous floral proportion, while the other clay samples illustrate an angiosperm dominated allochthonous floral signal transported by the river from the hinterland (likely the northern Cordillera (Lane & Dietrich, 1995)).

Surprisingly the sand samples, which also should represent fluvial conditions, generally contain only minor amounts of angiosperm markers and are dominated by gymnosperm markers. However, it has to be noted that the total amount of aromatic di- and triterpenoids is fairly low in the sand samples. Sample MB112790 does not even contain any di- or triterpenoids and sample MB113980 contains only one diterpenoic biomarker. Two explanations might be conceivable for the predominance of gymnosperm markers in the sands deposited in channels: (1) sand samples did not transport much organic material from the hinterland to the delta system, which is supported by the low TOC contents, and represent, therefore, a more autochthonous gymnosperm dominated floral signal or (2) sand samples illustrate a gymnosperm dominated floral signal from the hinterland, which would suggest a varying vegetation in the source hinterland between an angiosperm and a gymnosperm dominated paleovegetation during the different times of deposition of clays and sands.

The distribution of cuparene and totarane provides a more detailed insight into the distribution of several conifer families. In Figure 6.3d, the depth profile of cuparene is presented with respect to the different sample lithologies. As mentioned above, cuparene is a characteristic marker for Cupressacea s.str. The depth profile reveals that cuparene is abundant in the lignite samples, indicating that Cupressaceae s.str. were part of the gymnosperm paleovegetation during lignite formation, especially for CO94078. In the clay samples, cuparene occurs only in the liptinite-rich sample CO104310. With exception of the high concentration in sample CO94078, the cuparene contribution to the lignite samples appears quite similar.

Figure 6.3c shows the totarane depth-profile. Totarane is a characteristic marker for Podocarpaceae and Cupressacea s.str.. Obviously, in the upper part of the sedimentary section the cuparene and totarane profiles run parallel, while in the lower part no similarity is observable. This may indicate that cuparene and totarane have a different origin within the conifer genera, at least for the sediments of the lower sedimentary section. Comparing the ratio of gymnosperms to angiosperms (Figure 6.3c) and the distribution of cuparene (Figure 6.3d) it is obvious, that Cupressaceae s.str. were a significant conifer family in the Mallik area during formation of the lignites.

6.5.2 Implication on paleovegetation and paleoclimate

The main geographical extension of conifer gymnosperms is concentrated in the temperate climate zone or the boreal zone. This applies in particular for *Pinus*, *Picea*, *Abies*, and for *Thuja* and *Juniperus*, which are both Cupressaceae. In contrast, most angiosperms prefer warmer conditions with a few exceptions like birches (Walter & Breckle, 1999). The $\delta^{18}O$ isotopic ratios of Cenozoic sediments document that the global temperature during the Oligocene was cooler than in the previous Eocene period. Only during the late Oligocene did the temperature increase again (Zachos et al., 2001). This agrees with the results of Habicht (1979) who reported that the Oligocene was a time of relatively low temperatures in the northern hemisphere. For the Yukon Territory in northwest Canada, the Eocene-Oligocene temperature decrease is supported by palynological data (Ridgway et al., 1995) indicating a change from angiosperm dominated forest types to those dominated by gymnosperms and therefore a decrease from relatively warm temperatures during the Eocene to colder conditions during the Oligocene. The investigations of Long and Sweet (1994) on Eocene-Oligocene sediment samples from the Rock River coal basin, located further south in Yukon Territory, revealed a dominance of Taxodiaceae-Cupressaceae pollen, indicating a temperate climate and wet-humid conditions. For the Mackenzie Delta region (Imperial Nuktak C-22 well), Norris (1982) showed differences in the distribution of spores between the Ivik member (lower part) and the Arnak member (upper part) of the Kugmallit sequence. Thermophilic angiosperms, which are common in the Eocene and early Oligocene disappeared in the lower half of the transition from the early to middle Oligocene (Ivik member). The absence of the thermophilic angiosperm taxa indicates a cooler interval. However, in the late Oligocene (Arnak member) they reappear. Norris (1982) suggests that the increased diversity of angiosperm pollen in the Arnak member is due to an amelioration of climate and the re-establishment of warmer temperatures.

As mentioned before, only sediments of the Arnak member were penetrated by the Mallik well. The occurrence of angiosperm biomarkers in almost all the Mallik sediments confirms the reappearance of angiosperms during the late Oligocene. However, based on biomarker data, angiosperms were not the dominant vegetation in all intervals (Figure 6.3). Especially during the deposition of most of the lignites (and sands), gymnosperm markers obviously played a more important role.

In a river delta the interpretation of these floral variations in terms of paleoclimatic changes is complicated by the fact that the biomarker composition can represent different sources of organic matter either directly from the river delta (autochthonous organic matter) or from the hinterland (allochthonous organic matter) transported by the river into the delta area. In addi-

tion, it is known, that the preservation of plant material in a delta system is related to the different sites of deposition such as channels, levees, floodplains and swamps (Burnham, 1989; Scheihing & Pfefferkorn, 1984).

The organic matter in the lignite samples, some of it originating from the moss plant *Sphagnum*, indicates their formation in swamps (Haberer et al., 2005). Deposition in a swamp suggests that the biomarker composition of the lignites most likely represents an autochthonous plant and climate signal. The dominance of gymnosperm biomarkers points to lower temperatures in the delta system during deposition of the lignites and other periods if the sandstone biomarker signal also represents an autochthonous signal, as suggested above. At least one lignite sample (CO108138), dominated by angiosperms (Figure 6.3c), seems to indicate that a shift to warmer temperatures occasionally occurred in the Mallik area during the late Oligocene.

In contrast to the lignites and sand samples, most clay samples are dominated by angiosperm biomarkers. Clays are assumed to contain a higher allochthonous biomarker signal. Thus, the dominance of angiosperms in many clay samples may point to warmer climatic conditions in the area of the river watershed in the hinterland during deposition.

Overall the variability in the dominance of angiosperm and gymnosperm markers, and the observation that both marker groups are present in almost all samples, indicates varying intermediate climate conditions in the area, which might be typical for a period of slow climate amelioration.

6.5.3 Aromatic hydrocarbons related to diagenesis

The degree of aromatization is a thermal maturity parameter and is well established (Alexander et al., 1987; Alexander et al., 1995; Alexander et al., 1985; Budzinski et al., 1995; Heppenheimer et al., 1992; Püttmann & Villar, 1987; Radke et al., 1990; Radke et al., 1994; Radke et al., 1982a; Radke et al., 1982b; Strachan et al., 1988; Wakeham et al., 1980; Wilhelms et al., 1998). Several parameters, based on the occurrence of diverse methylnaphthalenes or methylphenanthrenes and usually used to evaluate the maturity level of more mature samples (Alexander et al., 1995; Alexander et al., 1985; Budzinski et al., 1995; Püttmann & Villar, 1987; Radke et al., 1990; Radke et al., 1994; Radke et al., 1982a; Strachan et al., 1988; Wilhelms et al., 1998), are not applicable for the Mallik samples because, due to their low rank, they do not contain any methylnaphthalenes or methylphenanthrenes. However, tricyclic diterpenoids are transformed to phenanthrenes in several steps via the formation of simonellite and retene (Figure 6.6). The formation of retene is a fast process, which starts during sedimentation and the early stages of diagenesis (Tan & Heit, 1981; Wakeham et al.,

1980). Therefore, retene occurs in relatively immature organic matter. The increasing degree of aromatization of the abietane derived diterpenoids (Figure 6.6) allows diagenetic changes to be documented at a high level of resolution.

Figure 6.7a illustrates a simple ternary plot in which these early maturity transformation processes are defined by the relative increasing aromatization of abietane type diterpenes in the samples. Different components with the same rank of aromatiziation are combined together to define different alteration steps.

In dehydroabietane, 18- and 19-norabieta-8,11,13-triene only the C-ring is completely aromatized. Simonellite and 1,2,3,4-tetrahydroretene have two aromatized rings (B+C) and methylretene and retene are completely aromatized. The arrow indicates the increasing alteration pathway in relation to increasing degree of aromatization.

Almost all samples plot in the range between one and two ring aromatization indicating a low level of maturity. The MB96334 sample is the only sample plotting between two and three ring aromatization. It contains neither dehydroabietane nor 18- nor 19-norabieta-8,11,13-triene. The position of this sample in the triangular plot is puzzling, because other maturity parameters such as the T_{max} value of 416°C obtained with Rock-Eval-pyrolysis (Haberer et al., 2005) do not indicate enhanced maturity. The generally low level of thermal maturity of the organic matter in the Mallik area, deduced here from the extent of aromatization, has also been shown by Snowdon (1981; 1999) and Haberer et al. (2005); for example Snowdon (1999) reported vitrinite reflectance values (VR_0) between 0.23% and 0.28% for some samples from the adjacent Mallik 2L-38 Gas Hydrate Research Well.

Here, no relationship between increasing diagenetic alteration and increasing depth is detectable (Figure 6.7b); this would not be unexpected for a sedimentary section of only 250 m. In contrast, Figure 6.7b suggests a link between the level of diagenetic alteration and the different facies. Although it has to be kept in mind that the sandstones contain only low amounts of aromatic hydrocarbons, the sand samples tend to show the lowest maturity. In contrast, most of the lignites and claystones show a more advanced level of diagenetic alteration. To explain this observation we can only speculate, but a reason for this might be acidic catalysed diagenetic processes, which have been described for clay minerals by Rubinstein et al. (1975) and Sieskind et al. (1979). The same might be the case for the lignites, also known to be deposited under acidic conditions (Diessel, 1992).

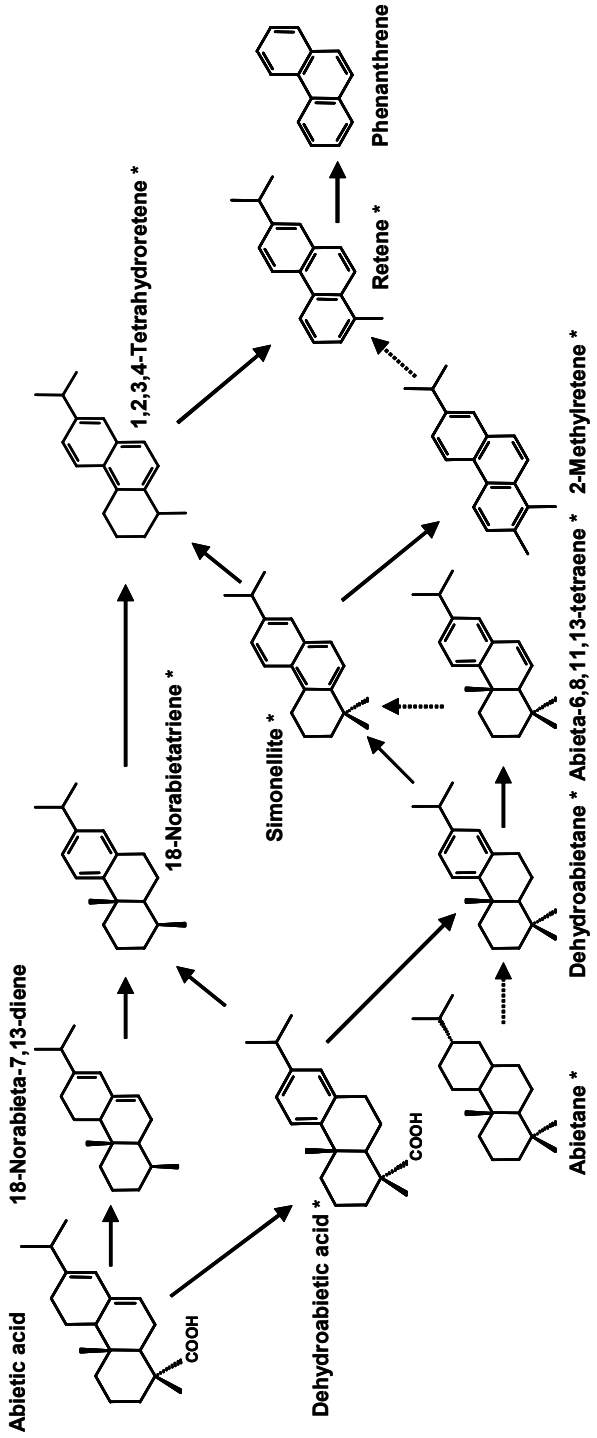

Figure 6.6: Schematic pathway for transformation of tricyclic diterpenoids to phenanthrene via simonellite and retene (adopted from literature (Otto and Simoneit, 2001; 2002; Otto and Wilde, 2001; Simoneit et al., 1986; Wakeham et al., 1980)). Compounds with an asterisk (*) were detected in the Mallik samples.

6.6 Conclusions

Thirty sediment samples (lignites, clays, sands) from the JAPEX/JNOC/GSC et al. Mallik 5L-38 Gas Hydrate Research Well, Canada were analysed with regard to their aromatic hydrocarbon biomarker composition. The samples investigated contain aromatic sesqui-, di-, and triterpenoids in variable amounts. Diterpenoic compounds generally predominate in the lignite and sand samples indicating a gymnosperm dominated paleovegetation. In clay samples, triterpenoids are usually the major constituents of the aromatic hydrocarbon fraction, representing an angiosperm dominated environment. The alternating dominance in the plant communities show varying climatic conditions in the Mallik area (lignites) and in the drainage area of the river (clays) likely related to changing depositional conditions in the delta. The simultaneous occurrence of both biomarker groups in almost all samples suggests intermediate climate condition during the late Oligocene, a phase of slow climate amelioration and re-establishment of warmer temperature conditions. The aromatic hydrocarbons assign a low level of maturity to the organic material at the Mallik site, which is in agreement with the vitrinite reflectance data for comparable samples from the same area (Snowdon, 1999). Additionally, within this low level of maturity, a coherence between the degree of diagenetic alteration and the lithology is suggested.

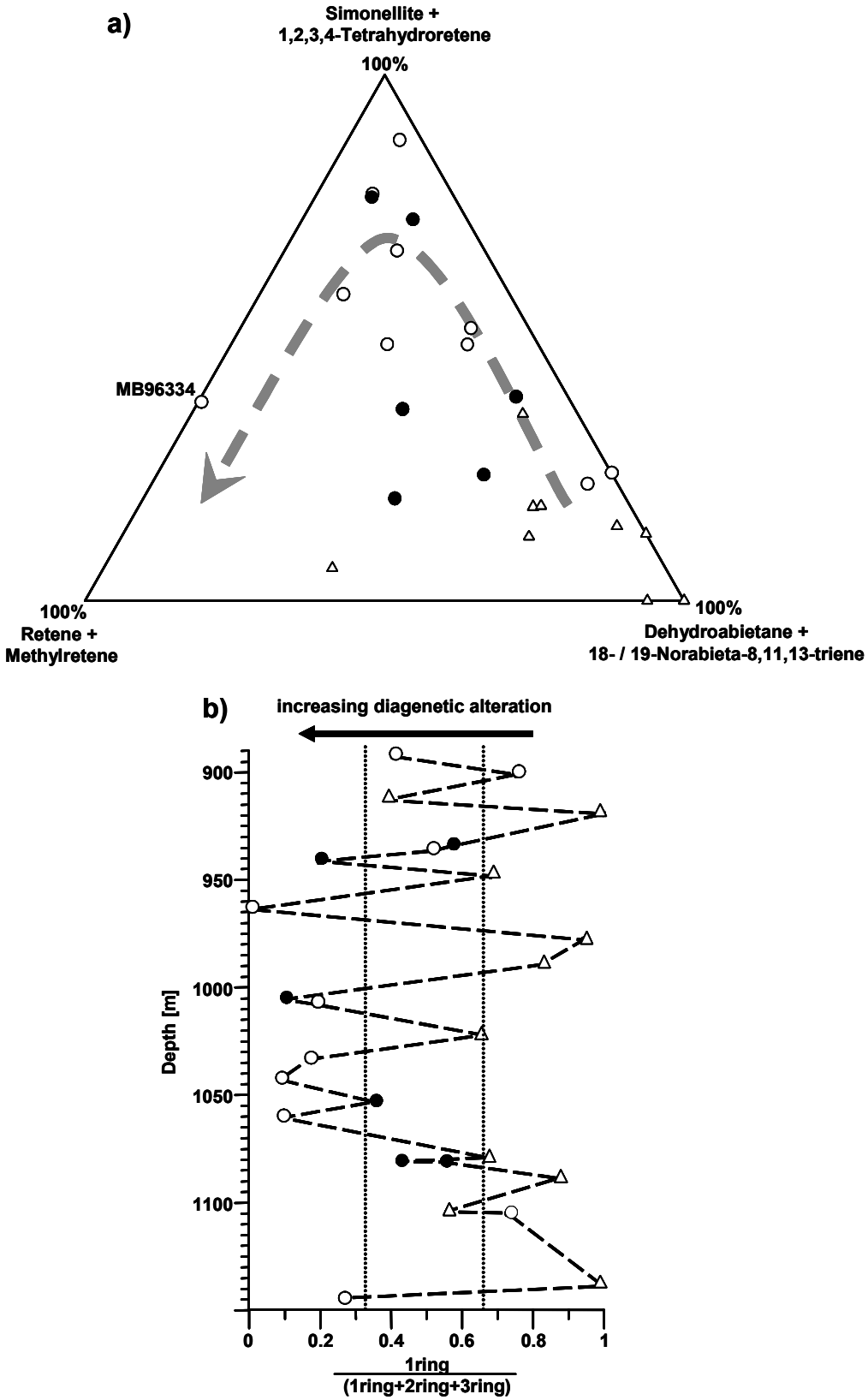

Figure 6.7: a) A ternary diagram of dehydroabietane and 18-/19-norabieta-8,11,13-triene, simonellite and 1,2,3,4-tetrahydroretene, and methylretene and retene illustrating different degrees of aromatization of the aromatic biomarkers. The arrow indicates the increasing maturation. b) Depth profile of the ratio of 1-ring aromatized compounds (dehydroabietane, 18-/19-norabieta-8,11,13-triene) to the sum of 1-, 2- (simonellite, 1,2,3,4-tetrahydroretene), and 3-ring (methylretene, retene) aromatized. Triangles = sand samples, open circles = clay samples, filled circles = lignites. Samples MB89899, MB104920, MB106380, and MB112790 contain no aromatic diterpenoids and are not considered.

Mallik 5L-38	Sesquiterpenoids (µg/gTOC)					Diterpenoids (µg/gTOC)									Triterpenoids (µg/gTOC)										AGAR di/
sample	1	2	3	4	5	A	B	C	D	E	F	G	H	I	a	b	c	d	e	f	g	h	i	j	k	(di+tri)
MB89163	-	-	0.1	1.3	1.5	-	0.1	8.9	1.8	0.5	9.5	0.1	2.8	-	3.8	4.4	4.1	13.6	5.2	1.6	4.1	0.5	1.0	0.1	-	0.35
MB89899	-	-	-	-	-	-	-	-	-	-	-	-	-	-	-	12.8	43.8	264.2	1.7	-	-	-	-	-	118.4	0.00
MB90020	-	-	-	-	-	-	-	7.6	-	-	2.5	-	-	-	1.2	22.4	-	0.2	-	-	6.9	-	-	-	-	0.25
MB91200	-	-	-	-	-	10.5	-	-	-	-	1.7	-	15.3	-	-	-	-	-	-	-	-	-	-	-	-	1.00
MB91856	-	-	-	-	-	9.6	6.8	1.8	-	-	-	-	-	-	-	-	-	-	-	-	-	-	-	-	-	1.00
CO93409	0.9	1.4	7.7	6.3	20.3	9.9	2.7	66.5	2.5	11.5	55.9	1.9	9.7	3.3	8.8	8.9	4.9	17.4	-	-	-	-	-	12.9	5.3	0.73
MB93589	-	-	0.1	1.1	1.4	-	2.3	41.7	2.7	32.6	57.9	1.3	11.3	-	2.3	3.6	10.5	17.1	1.3	0.2	-	-	-	0.1	-	0.80
CO94078	1.2	5.0	8.9	4.8	21.8	3.9	1.5	43.2	6.7	2.9	185.1	11.1	22.3	1.5	6.7	4.4	14.5	11.3	1.2	0.5	3.9	-	-	1.9	2.0	0.85
MB94762	-	-	-	-	-	-	-	5.3	0.9	-	-	-	-	1.5	-	-	8.4	5.6	4.3	2.0	3.1	-	0.3	-	-	0.24
MB96334	-	-	-	-	-	-	-	-	0.2	-	0.1	-	0.5	-	-	1.2	0.7	4.1	15.9	4.3	21.9	4.4	2.7	1.5	1.9	0.01
MB97760	-	-	-	-	-	-	-	20.8	-	1.8	-	5.3	1.4	-	2.1	0.3	-	-	-	-	-	-	-	-	-	0.92
MB98925	-	-	-	-	-	-	8.4	7.3	0.4	0.5	2.3	-	0.8	-	-	-	-	-	-	-	1.5	1.0	1.4	-	-	0.83
CO100550	0.3	1.9	5.8	4.2	18.0	2.8	2.3	6.9	9.0	-	89.4	-	17.6	-	-	-	14.5	31.6	3.1	1.3	0.9	-	-	15.0	2.3	0.62
MB100778	-	-	-	-	-	-	0.9	32.2	56.2	-	65.6	-	26.8	-	-	-	168.3	194.9	0.6	0.5	-	-	-	2.0	2.0	0.30
MB102215	-	-	-	-	-	-	8.8	3.9	2.23	-	1.2	-	3.1	-	-	-	-	-	-	-	1.6	3.2	3.5	-	-	0.66
MB103360	0.1	0.1	1.5	0.8	2.7	-	1.6	4.0	7.9	1.5	16.7	0.5	11.7	-	15.9	10.8	14.4	57.7	21.2	0.3	12.4	85.5	2.9	10.2	2.5	0.12
CO104310	0.6	1.8	33.9	8.6	29.6	-	8.5	62.5	14.5	-	746.9	-	32.8	-	-	-	4.9	46.6	-	-	-	-	-	-	-	0.94
MB104920	-	-	-	-	-	-	-	-	-	-	-	-	-	-	-	3.1	-	4.9	27.3	13.3	43.4	15.4	10.4	2.3	5.3	0.00
CO105353	0.5	1.0	6.2	4.2	22.8	-	8.5	26.5	15.4	-	21.3	-	27.1	1.8	4.1	4.4	0.9	14.5	1.0	-	-	-	-	2.1	0.5	0.73
CO106094	-	-	-	-	-	-	-	1.8	2.9	-	12.9	-	2.7	-	0.9	-	2.3	16.5	-	-	-	-	-	-	-	0.47
MB106380	-	-	-	-	-	-	-	-	-	-	-	-	-	-	-	-	-	10.9	-	-	4.6	-	-	2.2	3.2	0.00
MB107960	-	-	3.9	11.3	-	-	35.7	38.3	-	-	19.9	-	16.4	-	5.4	15.5	13.2	29.3	57.6	9.8	29.1	-	65.1	-	-	0.29
CO108138	-	1.9	-	1.9	36.2	2.5	1.1	5.7	-	-	4.3	-	6.7	1.9	9.5	7.3	3.8	33.2	2.9	1.8	-	-	-	1.1	0.2	0.21
CO108169	-	1.2	1.0	3.6	73.9	2.6	5.9	27.3	-	-	15.7	-	12.2	1.8	13.8	2.8	0.6	14.7	1.8	0.5	5.6	-	-	0.4	-	0.57
MB108924	-	-	-	-	-	-	6.9	2.5	-	-	1.4	-	-	-	-	-	-	-	-	-	-	-	0.8	-	-	0.93
MB110494	-	-	0.1	1.3	3.3	-	9.2	18.8	-	-	17.9	-	4.6	-	6.1	-	9.3	-	2.6	5.0	4.9	2.4	3.1	-	0.8	0.57
CO110550	-	-	-	-	-	-	6.8	8.4	2.3	-	2.4	-	1.1	-	-	-	-	-	-	-	4.3	-	0.8	-	-	0.80
MB112790	-	-	-	-	-	-	-	-	-	-	-	-	-	-	-	-	-	-	-	-	-	-	-	-	-	0.00
MB113980	-	-	-	-	-	-	-	20.7	-	-	-	-	-	-	-	-	-	-	-	-	-	-	-	-	-	1.00
MB114535	-	-	-	-	-	-	-	0.6	0.7	-	0.6	-	0.6	-	0.3	0.5	0.4	-	21.2	5.7	34.5	14.6	13.5	1.4	2.2	0.02

Table 6.3: Concentrations of aromatic sesqui-, di- and triterpenoic hydrocarbon biomarkers. Angiosperm-gymnosperm-aromatic ratio (AGAR): ratio of di- to di- plus triterpenoids. Dark grey shaded = lignites, light grey shaded = silts/clays and unshaded = sands. Numbers and letters correspond to compound names in Table 6.2.

6.7 Acknowledgement

We acknowledge the international partnership that undertook the Mallik 2002 Gas Hydrate Production Research Well Program: the Geological Survey of Canada (GSC), Japan National Oil Corporation (JNOC), GeoForschungsZentrum Potsdam (GFZ), U.S. Geological Survey (USGS), U.S. Department of Energy (USDOE), India Ministry of Petroleum and Natural Gas (MOPNG)/Gas Authority of India (Gail), and the Chevron-British Petroleum-Burlington joint venture group. The program received financial support from the International Continental Scientific Drilling Program (ICDP).

We are grateful to E. Michaels, an anonymous reviewer and M. G. Fowler for their critical review and helpful suggestions. Also, we would like to thank C. Karger, A. Sobotta and I. Schindelwig for technical support. The study was funded by the Deutsche Forschungsgemeinschaft (DFG), grant no. Ma 2470/1.

Appendix: Structures of aromatic hydrocarbons discussed in this paper

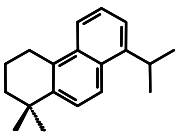

diaromatic Totarane

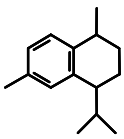

Calamene

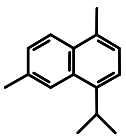

Cadalene

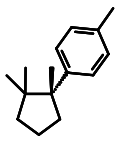

Cuparene

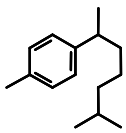

Dihydro-*ar*-curcumene

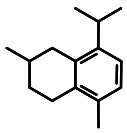

Cadina-1(10),6,8-triene

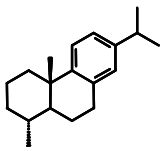

19-Norabietatriene

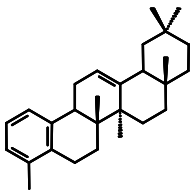

24,25-Dinoroleana-1,3,5(10),12-tetraene

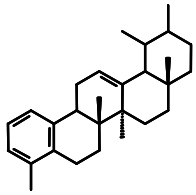

24,25-Dinorursa-1,3,5(10),12-tetraene

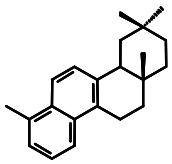

3,3,7,12a-Tetramethyl-1,2,3,4,4a,11,12,12a-octahydrochrysene

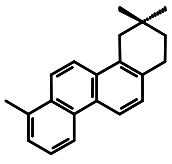

3,3,7-Trimethyl-1,2,3,4-tetrahydrochrysene

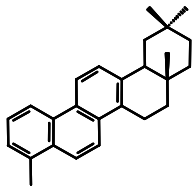

2,2,4ab,9-Tetramethyl-1,2,3,4,4a,5,6,14b-octahydropicene

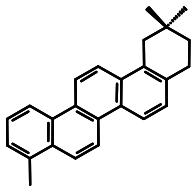

2,2,9-Tetramethyl-1,2,3,4 -tetrahydropicene

7 Occurrence and significance of monomethylated alkanes in the Mallik samples

7.1 Monomethylalkanes in the Mallik samples

Monomethylalkanes with 14 to 16 carbon atoms and different methyl branching positions (3-methyl to 7-methyl) were detected in the range between the *n*-C_{14} and *n*-C_{17}-alkane in the aliphatic fractions of almost all samples investigated. The methyl isomers can be distinguished due to their different fragmentation pattern caused by the different methyl branching positions. Figure 7.1 shows the distribution of the monomethylalkanes in different characteristic mass traces listed in Table 7.1.

Table 7.1: Characteristic fragments for the monomethylalkanes detected in the samples.

characteristic fragments	Carbon number of main chain		
	14	15	16
141 (ω-9)	6-methyl	7-methyl	-
155 (ω-10)	5-methyl	6-methyl	7-methyl
169 (ω-11)	4-methyl	5-methyl	6-methyl
183 (ω-12)	3-methyl	4-methyl	5-methyl
197 (ω-13)	-	3-methyl	4-methyl
211 (ω-14)	-	-	3-methyl

Between *n*-C_{14} and *n*-C_{15}-alkane five different isomers of methyltetradecane occur from the 7-methyl to the 3-methyl isomer (Figure 7.1), whereas the 6-methyltetradecane coelutes with the 7-methyltetradecane. In the range of *n*-C_{15} to *n*-C_{16}-alkane, five isomers from 7- to 3-methylpentadecane occur (Figure 7.1). In this range, there is no co-elution of 7- and 6-methylpentadecane. Similar to the methylpentadecanes, five methylhexadecane isomers occur in the range between *n*-C_{16} and *n*-C_{17}-alkane (Figure 7.1).

The sum of all methylalkanes varies between 19.7µg/gSed in the clay sample CO106094 and 0.1µg/gSed in the sand sample MB98925. The lignites samples as well as the clay samples contain all of the different isomers described above. Only in a few lignite and clay samples, the methyltetradecanes are not represented completely. In these samples the 5-methyl and the co-eluting 6- and 7-methyl isomers are often missing.

Actually, the sand samples contain even less different monomethylalkane isomers as the clays and lignites. The methyltetradecanes and many isomers of the methylpentadecane are com-

pletely lacking in half of the sands and the 7-methylhexadecanes are absent in all sand samples.

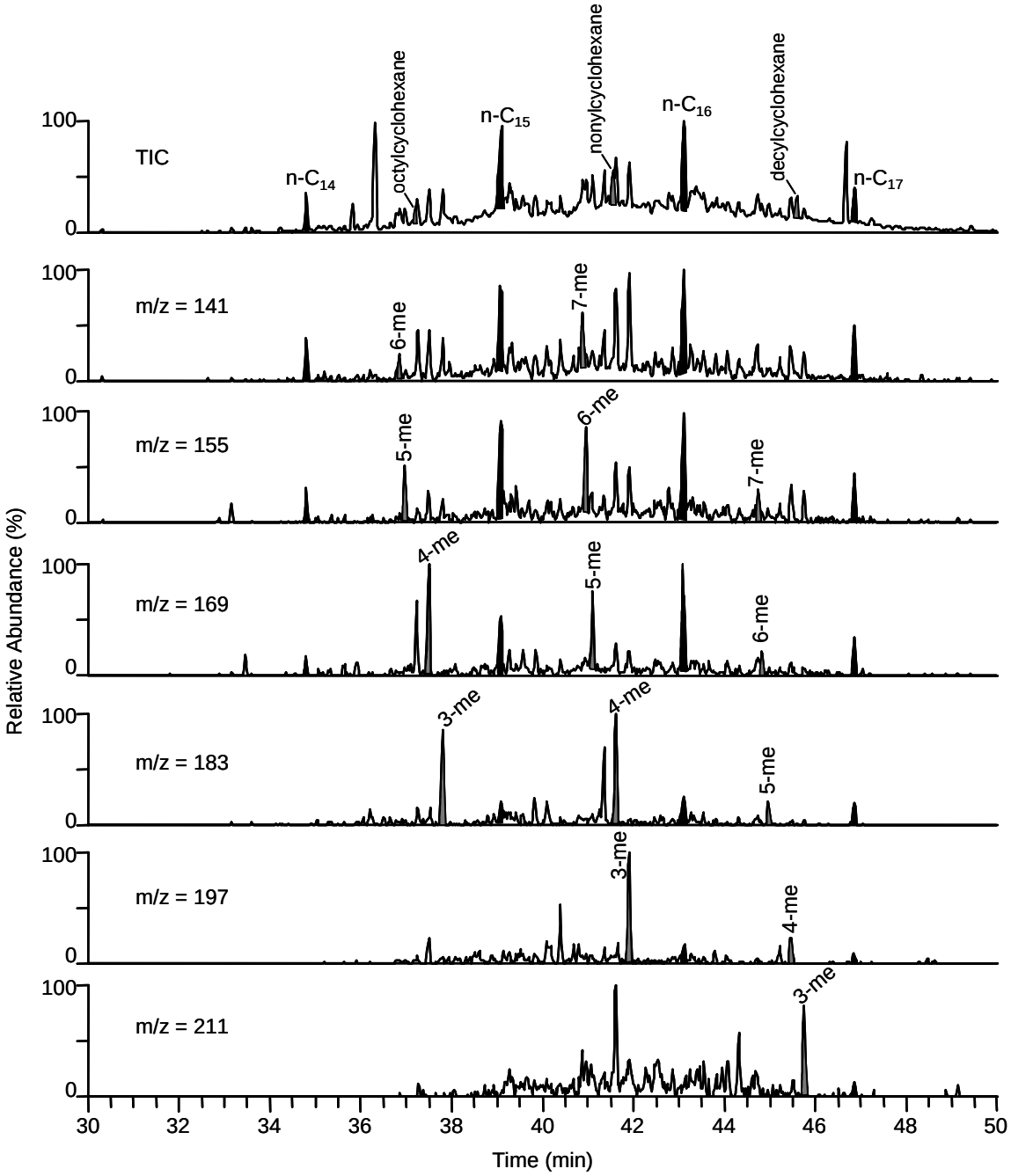

Figure 7.1: Typical distribution of monomethylated alkanes in the Mallik samples (CO94078).

7.2 Possible origins of monomethylated alkanes

7.2.1 Higher land plant material as source for methylalkanes

2- and 3-methylalkanes are associated with *n*-alkenes in plant waxes in the range of *n*-C_{25} to *n*-C_{31} (Kissin, 1987; Kissin & Feulmer, 1986; Tissot & Welte, 1984). Thus, plant waxes, a complex mixtures of long chain alkanes, alcoholes, aldehydes, acetals esters and acids with different numbers and positions of functional groups and chain branching (Eglinton & Hamilton, 1967), could act as sources for methyl branched alkanes in sediments.

7.2.2 Insect cuticles as source for methylalkanes

Additionally, it is well known that cuticles of insect consist in major parts branched hydrocarbons. For example, mono-, tri-, and tetramethyl branched alkanes with a chain length >30 are found in the developing pupae of *Lepidoptera* (*Heliothis virescens*, *Helicoverpa zea*), in the cuticle of the gipsy moth *Lymantria dispar* and in cuticular hydrocarbon from fruit flies larvae (*A. suspense, C. capitata*) (Jurenka & Subchev, 2000; Nelson, 2001; Sutton & Steck, 1994). The proportions of different methylalkanes in insects, for example face flies or termites, vary in relation to the climatic conditions during the different seasons or humidity, and they play probable an important role for the viscosity (Jurenka et al., 1998; Woodrow et al., 2000). Di- and trimethylalkanes are also the significant compounds in beeswax and in the surface wax of eggs and adults of colorado potato beetle (Fröhlich et al., 2000; Nelson et al., 2003).

7.2.3 Cyanobacteria as source for methylalkanes

In cyanobacteria, mid-chain branched alkanes are characteristic components (e.g. Fowler & Douglas, 1987; Gelpi et al., 1970) with a clear preferences for 7- or 8-methylheptadecanes and, in a limited range other isomers depending on the species (e.g. Dachs et al., 1998; Kenig, 2000; Kenig et al., 2001; Kenig et al., 1995; Shiea et al., 1990; Summons et al., 1999). Shiea et al. (1990; 1991) have found a suite of mid-chain branched mono- and multi-methylalkanes in the range from *n*-C_{15} to *n*-C_{21} in recent cyanobacteria mats and lichens, which contain symbiotic cyanobacteria. A suite of specific short-chain (*n*-C_{17} to *n*-C_{21}) and long-chain (*n*-C_{24} to *n*-C_{41}) mono-, di- and trimethylalkanes in recent microbial mats have been reported by Kenig et al. (1995). In the range of C_{16}-C_{29} Kenig (2000) have examinated a homologous series of monomethylalkane isomers with methylgroups at different positions in pyrolysis products of a Holocene microbial mat. In Permian torbanites, four series of monomethylalkanes ranging

from C_{23}-C_{31+} occur and Audino et al. (2001) relate this to a direct input form *Botryococcus braunii*, occurring in the samples.

7.2.4 Microbial sources for methylalkanes

Methylalkanes were also been interpreted as products of diagenetic decarboxylation processes of functionalized lipid precursors such as carboxylic acids (Summons, 1987; Thiel et al., 1999a). In sponges, symbiotic bacterial with an intriguing variety of methyl fatty acids occur (Gillan et al., 1988; Thiel et al., 1999a). In addition to this, mid-chain branched carboxylic acids are reported from non-photothrophic bacteria (Gillan et al., 1988; Thiel et al., 1999a). Furthermore, it is well known, that iso- and anteiso fatty acids are common lipid constituents of anoxygenic bacteria (e.g. Kaneda, 1991) and the preponderance of 2- and 3-methyl alkanes in fossil rock extracts could be related to them as potentials precursors. Kaneda (1991) assumed that branched chain fatty acids in bacteria were synthesized from two different primer sources. The first, most common, type includes branched chain α-keto acids, which are related to valine, leucine and isoleucin. The second type includes short-chain carboxylic acids which are used only by a small proportion of bacteria. Cranwell (1973) assumed also a bacterial origin of mid-chain methyl-branched acids from the gram-positive, aerobic bacteria *Actinomycetales* as biosynthetic precursor for mid-chain methyl branched fatty acids in recent lacustrine sediment from the English Lake District. Investigating the deep biosphere in fluid reservoirs within mid-ocean ridges flanks, Cowen et al. (2003) demonstrated the presence of aliphatic compounds such as long-chain alkanes, iso- and anteiso-alkanes and trace amounts of 9-methylalkanes in escaping fluids, containing nitrate and sulfate reducing bacteria and archaea.

7.2.5 Origin of methylalkanes in oils

In a geological context, monomethyl branched alkanes are found mostly in crude oils from the Palaeozoic or even the late Precambrian (Fowler & Douglas, 1987; Grantham et al., 1988; Höld et al., 1999; Jackson et al., 1986; Kissin, 1987; Kissin & Feulmer, 1986; Klomp, 1986). Several main origins have been stated to explain the presence of these compounds in sediments and crude oils. These are a direct supply of methyl branched alkanes from different sources like cyanobacterial mats and insect cuticles or the defunctionalization of precursor molecules such as branched fatty acids or ketones from bacterial and plant material. Höld et al. (1999) reported the occurrence of mid-chain methyl alkanes with usually two methyl isomers in the range of 16 to 33 carbon numbers in oils from the Infracambrian Huqf Formation

(Oman), whereas the predominant branching position changes with the carbon number. They proposed that compounds with polar head group and a hydrocarbon tail could be precursors for these mid-chain methyl alkanes. In a number of crude oils, suites of branched alkanes with a methyl group from 2-monomethyl- to 6-monomethylalkanes has been described by Kissin (1987). Kissin (1987) interprets their formation as thermal cracking processes of α-olefines transformed in the presences of catalytical acidic clay minerals. Warton *et al.* (1998), conducting laboratory heating experiments, have studied the distribution of monoethylalkanes in late cretaceous sediments and crude oils depending on maturity. Supporting the results of Kissin (1987), the authors propose a reaction mechanism explaining the formation of T-branched alkanes (methyl- up to pentyl) from *n*-alkenes by hydride and alkyl shifts.

7.3 Possible origins of monomethylated alkanes in the Mallik samples

For the samples material from the Mallik Site investigated in this study the origin of the monomethylalkanes are not obvious. There was no correlation with other analyzed parameters; neither with the amount of TOC nor with the Rock-Eval-parameters or the composition of the macerals. Furthermore, there is no link apparent between the abundance of monomethylalkanes and the biomarker composition, in the bitumen fraction indicating enhanced maturity. Also, an important contribution from cyanobacteria is not likely if the results of all other investigations done concerning the biomarker distribution were considered.

Referring to the findings of Höld et al. (1999) it could also be assumed, that phospholipids with branched fatty acid side chains serve as precursors for branched alkanes. However, there was neither a link between the occurrence of monomethylalkanes and the phospholipids nor did the free fatty acid fraction reveal any important supply of methyl branched fatty acids. Therefore, branched fatty acids could not be a source for the monomethylalkanes in the Mallik samples.

The fact, that there is no correlation with other analytical parameters and that there is a complete series of monomethylalkanes and not just some specific isomers, as usually found in cyanobacterial lipids (Kenig et al., 1995) could imply, that the monomethylalkanes found in the sediments from the Mallik 5L-38 Well are part of allochthonous material. The occurrence of monomethylalkanes is usually assigned to crude oils. Thus, migrated crude oil is another possible source for the provenance of the branched alkanes. Recent studies on the geochemistry of the Mackenzie River and its sediments show that the river carries allochthonous organic material from the hinterland into the delta and it has been supposed that this material partly

arise from the Athabaska tar sands or the Norman Wells oils (Yunker et al., 1993). Yunker et al. (2002) have demonstrated that the erosion of the Devonian Canol Formation in the lower Mackenzie River valley, which act as the source rock for the Norman wells oils (Feinstein et al., 1988; Snowdon et al., 1987), supplies material to the Mackenzie River and shelf. Considering this, it appears not unlikely, that there was also a supply of source rock material during the sedimentation of the Kugmallit Formation in the Mallik area and that the methylalkanes derived from this material.

During the Paleogene, the courses of rivers in this region were different from the present-day course. Formerly, the Porcupine River basin has provided the clastic sediments from the northern Cordillera including Ogilvie and Richardson mountains to the Kugmallit delta (Lane & Dietrich, 1995). For the northern Cordillera, the occurrence of crude oils and gas has been described (Link & Bustin, 1989; Norris, 1985a; Norris, 1985b). Hence, the northern Cordillera could have been also a potential source for mature allochthonous organic material deposited in the Mackenzie Delta. Nevertheless, if there was really a supply of crude oil to the Mallik sample material, more indicators for mature organic matter like a broad range of αβ-hopanes and C_{27}-C_{29} steranes, should be detectable in the Mallik sediments. Thus, an embedding of mature oil derived material in the Mallik sediments seems to be unlikely.

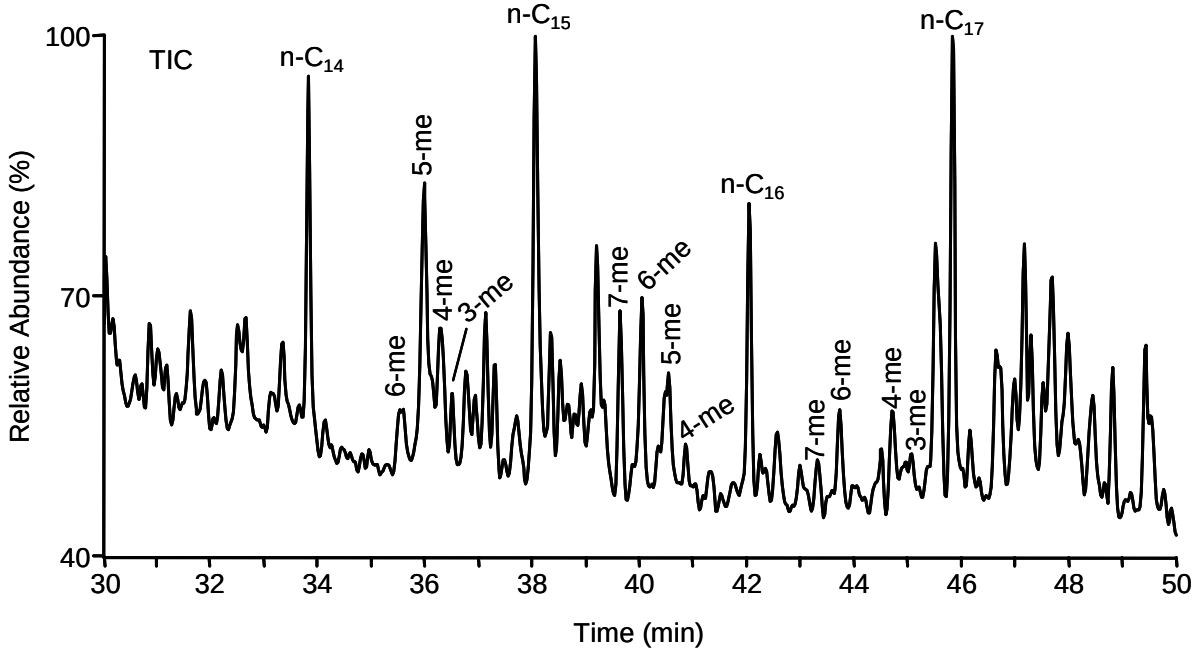

Figure 7.2: Distribution of monomethylated alkanes in the drill mud additive lecithin.

To clarify, whether the monomethylalkanes are an indigenous signal and not a contamination for instance by the drill mud and its additives, samples of the drill mud and the drill mud addi-

tive lecithin were studied. Lecithin was added to the drill fluid to prevent the formation of gas hydrates during the drilling process.

The investigated drill mud and lecithin samples contain also monomethylalkanes and show exactly the same pattern (Figure 7.2), as found in the sediment samples. Unfortunately, the most perspicuous origin of these suites of methylated alkanes in the investigated samples is the contamination of the samples with the drill mud additive lecithine during the drilling process.

8 Characterisation of the organic matter embedded in the Mallik samples: a summary

The characterisation of the organic matter in the sediments from the Mallik 5L-38 Gas Hydrate Production Research well was conducted using different organic geochemical methods to elucidate the origin and the thermal maturity.

A first hint for the terrestrial origin and the immaturity of the organic matter is given by the Rock-Eval pyrolysis data. These results are supported by the maceral analysis and the open-system pyrolysis gas-chromatography of the organic carbon-rich samples. In addition to this, the distributions of the *n*-alkanes, *n*-fatty acids and *n*-alcohols with the maxima in the long-chain carbon number range point clearly to higher land plants as one of the main contributors to the organic matter in the investigated samples. In the lignite samples, the specific feature of the *n*-alkane distributions is the second maximum at *n*-C_{23} indicating an important input of the moss plant *Sphagnum*.

A deeper insight into the terrestrial organic matter is provided by the occurrence of di- and triterpenoic biomarkers. The angiosperm/gymnosperm-aromatic-ratio (AGAR, chapter 6, Figure 6.3c, Figure 8.1b) and the distribution of terpenoic biomarkers in the aliphatic (Figure 8.1a) as well as in the neutral polar hydrocarbon fractions (Figure 8.1c) reveal distinct differences of the dominating plant communities with respect to lithology.

Almost all lignite seams are dominated by gymnosperms (Table 8.1, Figure 8.1) like the conifer genera Pinaceae, Cupressaceae s.str., Taxodiaceae, and Podocarpaceae. In contrast to the lignites most of the clay samples are dominated by an angiosperm paleovegetation (Table 8.1, Figure 8.1). The sand samples contain in general minor amounts of angiosperm markers and are dominated by gymnosperm markers. However, it has to be noted that the total amount of di- and triterpenoids is fairly low in the sand samples. In the neutral polar hydrocarbon fractions of the sand samples even no di- and triterpenoids occur.

Table 8.1: Dominance of gymno- and angiosperms in the paleovegetation at the Mallik site with regard to lithology.

Lithology	aliphatic hydrocarbons		aromatic hydrocarbons		neutral polar hydrocarbons	
	angiosperms	gymnosperms	angiosperms	gymnosperms	angiosperms	gymnosperms
lignites	0	6	1	5	2	4
clays	9	4	10	3	12	1
sands	0	10	2	8	-	-

The compositional differences of the organic matter in the studied Mallik sediments reflect the depositional changes in the meandering river system at the Mackenzie delta. Delta plain sediments were the dominating deposits in the Mallik area. Certainly, the sedimentation took place at the upper delta plain, because there is no marine influence detectable in the samples investigated. The widespread delta plains comprise active and abandoned distributary channels separated by shallow-water environments and by emergent areas.

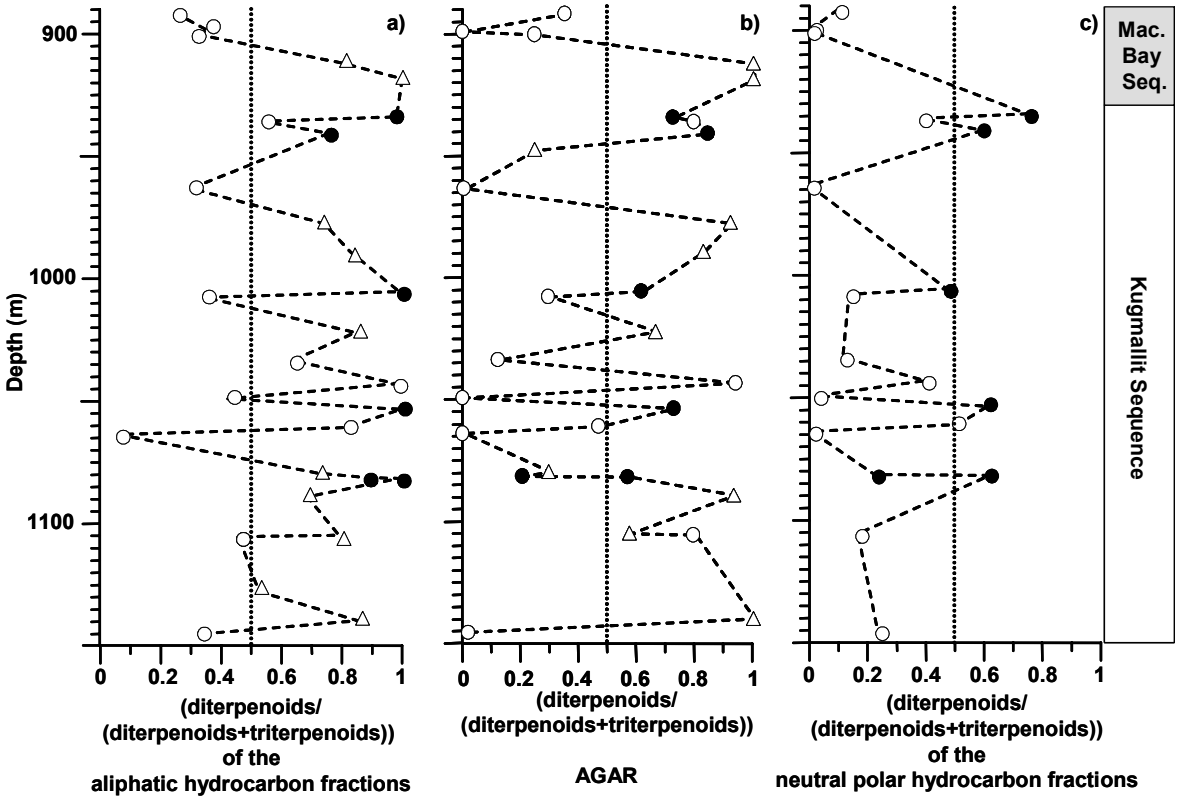

Figure 8.1: Depth profile of the ratio of diterpenoid concentration to the sum of di- and triterpenoid concentrations as an indicator for an angio- or gymnosperm dominated paleovegetation a) in the aliphatic hydrocarbon fractions, b) in the aromatic hydrocarbon fractions (AGAR (angiosperm-gymnosperm-aromatic ratio)), c) in the neutral polar hydrocarbon fractions. Black dots = lignite, open circles = clay, triangles = sand.

The sandstones certainly reflect a very fast sedimentation in such active channels. Due to the rapidity of the sedimentation and the availability of organic material, there is no or only little organic matter embedded. If the sands represent a more autochthonous floral signal or if they demonstrate a vegetational signal from the hinterland, and with that suggesting varying flora (angiosperm and gymnosperm) in the source hinterland remains unclear.

The silts and clays were deposited on floodplains or avulsion belts by a still and slow sedimentation with the possibility to trap more organic matter. They might represent a mixture of both the allochthonous floral signal transported by the river and the authochthonous signal

supplied by the surrounding vegetation into the delta system. The significance of the allochthonous *versus* autochthonous vegetation signal might vary depending on the dynamic of the river and the position of the site relative to the surrounding flora in the meandering river system (Figure 8.2). The lignite layers are residues of former bogs, which were built up in abandoned channels or in shallow pools. They result from interdistributary swamps or peat bogs, which mainly are constituted from *Sphagnum* and *Cupressaceae*, and also from other peat forming plants. Based on the identified plant markers, it is conceivable that the peats were either raised bogs or in the intermediary state between mires and raised bogs (Figure 8.2).

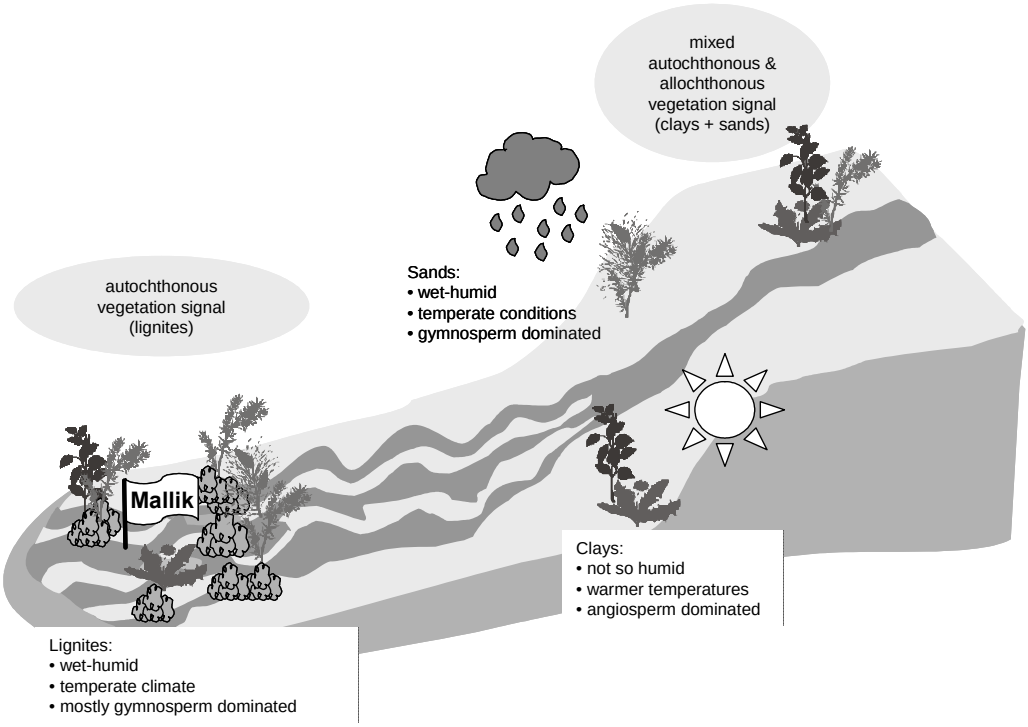

Figure 8.2: Schematic illustration of the paleovegetational and paleoclimatic conditions at the Mallik site.

In addition, obviously, there is an alternation with depth in the dominating plant communities (gymnosperms and angiosperms). The three major cycles in vegetation type separated by rapid minor fluctuations (see chapter 6) is also detectable in the aliphatic and the neutral polar hydrocarbon fraction, with some slight variations (Figure 8.1). These observable alternating sections mirror floral signals from both the site of deposition and the area of sediment provenance.

The changes in the plant communities provide an insight into the climate conditions in the Mallik area during the time of sedimentary deposition. Whereas the gymnosperms prefer cooler temperature, most angiosperms favour warmer conditions. The possible climate

changes indicated by the varieties in the biomarker composition, fit in the results of various studies about the climatic conditions during the Oligocene and Miocene in the northern hemisphere, which reported relatively low temperatures and wet-humid conditions for the Oligocene with an climatic amelioration during the late Oligocene (Habicht, 1979; Long & Sweet, 1994; Norris, 1982; Ridgway et al., 1995; Zachos et al., 2001).

9 Search for microbial life indicators in deep subsurface sediments of the Mallik 5L-38 Gas Hydrate Production Research Well, Canada

[*] This chapter is in process to be published. R.M. Haberer, K. Mangelsdorf, K.-G. Zink. H. Wilkes, and B. Horsfield (in prep.). The short descriptions of the study area, sample material and methods were adapted for this publication.

9.1 Introduction

During the last decades many microbiological and organic geochemical studies have been performed to prove the occurrence of life in the deep subsurface strata and to examine the characteristics of the deep biosphere (Boivin-Jahns et al., 1996; Fredrickson & Onstott, 1996; Head et al., 2003; Krumholz, 2000; Parkes et al., 1994; Pedersen, 1993; Pedersen, 1997; Ringelberg et al., 1997; Wellsbury et al., 2000; Zink et al., 2003).

The abundance of life in the deep subsurface depends on temperature, the presence of water, pore spaces of sediments and rocks, and the availability of nutrients and energy (Fredrickson & Onstott, 1996; Parkes et al., 1994; Pedersen, 1993). Pedersen (1993) suggests that the depth limit is set by temperature if energy is available. Organic matter, embedded into sediments, could act as such an energy source (Krumholz et al., 1997). Krumholz et al. (1997) demonstrate that the main energy source used by microbial communities is organic material trapped within shales. In the shales themselves the microbial activity appears to be reduced, while in the adjacent sandstone layers it was much more abundant. This observation leads the authors to the assumption that microorganisms ferment the organic matter, diffusing from the shales into the more permeable sandstones, and carry out sulphate reduction and acetogenesis. Even if organisms with other metabolic capabilities such as methanogens could be important in such a system, only the occurrence of acetogens was proved in the study of Krumholz et al. (1997).

As an alternative energy source to the organic carbon incorporated into the sediments, gases (e.g. methane and higher hydrocarbon gases) within gas hydrate deposits could be used by microbial ecosystems in depths where energy sources are usually limited. For instance, Wellsbury et al. (2000) could show in deep subsurface sediments from the Blake Ridge that free-gas associated with gas hydrates appears to stimulate both the number and activity rates of microorganisms. In near-surface gas-hydrate bearing sediments at the southern Hydrate Ridge, symbiotic consortia of archaea and sulphate-reducing bacteria have been indicated

(Boetius et al., 2000). These aggregates were abundant in sediments with high rates of methane-based sulphate reduction and evidently mediate anaerobic oxidation of methane. Previously, it has been shown, that certain archaea could reverse the process of methanogenesis by interaction with sulphate-reducing bacteria (Iversen & Joergensen, 1985; Zehnder & Brock, 1979;1980).

Although many information are gathered already on the special feature of microbial communities in deep marine sediments (e.g. Boetius et al., 2000; Parkes et al., 1994; Parkes et al., 2000; Zink et al., 2003), comparatively little is known about the terrestrial deep biosphere (Pedersen, 1993; Pedersen, 1997). In the JAPEX/JNOC/GSC et al. Mallik 5L-38 Gas Hydrate Production Research Well both organic rich lignite layers and gas hydrates occur, therefore it provides the opportunity to investigate the interaction of deep microbial populations with different substrate provided by terrestrial successions. In the previous JAPEX/JNOC/GSC Mallik 2L-38 gas hydrate research well, Colwell et al. (1999) show that methanogenic microorganisms are present in the deep sediments of the Mallik area, and that they are more numerous in the sand than in the silt or clay strata.

From a biogeochemical perspective the commonly used approach to detect microbial communities is the identification of characteristic microbial biomarkers (hopanoids, ether- and phospholipids) and the determination of their carbon isotopic signature (Abraham et al., 1998; Boschker et al., 1998; Cvejic et al., 2000; De Rosa et al., 1971; Fang et al., 2000; Green & Scow, 2000; Hinrichs & Boetius, 2002; Hinrichs et al., 2000; Ourisson & Rohmer, 1992; Ratledge & Wilkinson, 1988; Rohmer et al., 1980; Thiel et al., 2003; Zink et al., 2003). In this paper, the results from the investigations to proof the existence of microbial communities in the deep subsurface sediments of the Mallik Site using molecular organic geochemical approaches are presented.

9.2 Biomarkers used to trace microbial biomass in the Mallik sediments

9.2.1 Hopanoic biomarkers

Pentacyclic triterpenes of the hopanoic family are a very abundant and widespread group of biological marker in sediments and crude oils (e.g. Rohmer et al., 1984; Rohmer et al., 1980; van Dorsselaer et al., 1977; van Dorsselaer et al., 1974). Hopanoids are significant constituents of bacteria. The occurrences of several hopanoic hydrocarbons (diploptene, diploterol and bacteriohopanepolyols) have been proven in almost all cyanobacteria, purple non-sulphur and methylotrophic bacteria, and some Gram-negative or Gram-positive bacteria (De Rosa et al., 1971; Rohmer et al., 1984; Rohmer & Ourisson, 1976a;b). In contrast to this, they appear to be absent in archaea (Rohmer et al., 1984). It is assumed, that they act as reinforcers of the membrane and take on the function of sterols in eukaryotic cells (Kannenberg & Poralla, 1999; Ourisson et al., 1987; Rohmer et al., 1992; Rohmer et al., 1984). But, even if the hopanoids mainly derived from bacteria, it should not be unmentioned that they occur also in cryptogams (algae, mosses, ferns and fungi) and higher land plants (Ourisson et al. 1987; Quirk et al., 1984).

It was thought for long that hopanoids occur only in aerobic bacteria, but recent findings disproved this predication. Thiel et al. (2003) proved the presence of *dihomo*-hopanoic acids (C_{32}) in living anaerobic microbial mats at methane seeps in the Black Sea, Härtner et al. (2005) the occurrence of hop-22(29)-ene (diploptene), hop-21-ene and *dihomo*-hopan-32-ol in two well characterized *Geobacter* species, which are strictly anaerobic bacteria and Sinninghe Damsté et al. (2004) detected hopanoids (bacteriohopantetrol, diploterol diploptene and a C_{27} hopanoid ketone) in the strictly anaerobic anammox bacteria (planctomycetes). Thus, these studies show that the occurrence of hopanoic hydrocarbons is not longer obligatory related to aerobic microorganisms and that hopanoids can also derive from microorganisms living in strictly anoxic environments.

9.2.2 Glycerol ether lipids

Glycerol ether lipids are main membrane constituents of archaea and bacteria. The basic structure of glycerol dialkyl glycerol tetraethers (GDGT's) is composed of two glycerol moieties linked by two carbon chains. Dialkyl glycerol ethers like archaeol or GDGT's such as caldarchaeol or crenarchaeol with an isoprenoid ether chain are used as specific indicators for archaea. GDGT's with non-isoprenoid but branched ether chains are indicators for bacteria (e.g. Weijers et al., 2006). The structures of these different groups of glycerol ether lipids are displayed in Figure 9.1.

Tetraether lipids are known to occur in the membranes of thermophilic and methanogenic archaea and non-thermophilic Crenarchaeota (Hopmans et al., 2000). Schouten et al. (2000) have shown that isoprenoid and branched glycerol dialkyl glycerol tetraethers are widespread in low-temperature environments (< 20°C). As glycerol ether lipids are, like the hopanoic biomarkers, relatively stable against diagenetic degradation, they are not unambiguously biomarkers for living microbial biomass.

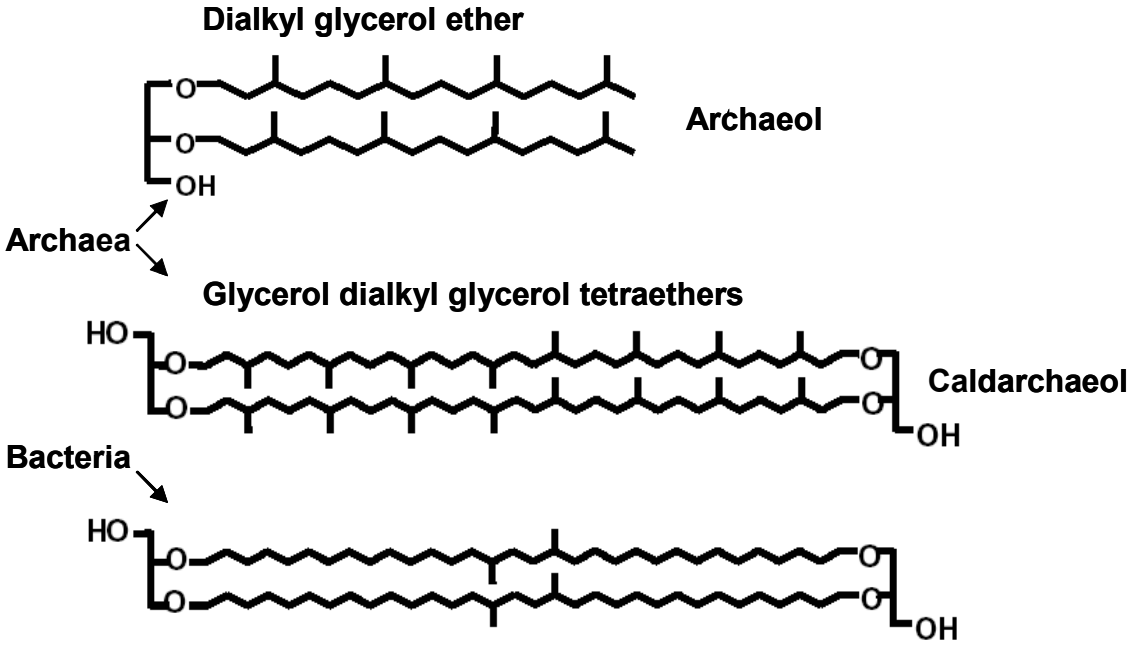

Figure 9.1: Molecular structures of glycerol ether lipids detected in the Mallik sediments.

9.2.3 Phosphoplipids

Phospholipids (PLs) consist of a glycerol unit linked to a phosphatidyl head group and two fatty acyl side chains (or sometimes ether side chains), which can differ concerning their length, alkyl-branches and number of double bonds. The classification of phospholipids is based on the chemical structure of the polar head groups. The head groups form the hydrophilic and the fatty acid side chain the hydrophobic part of the phospholipid molecule. In cellular membranes phospholipids arrange in the form of bilayers with a hydrophobic inner part and a hydrophilic surface. Therefore, phospholipids are the major cell membrane lipids in nearly all organisms.

However, in deeper sedimentary succession only micoorganisms can survive being the source of intact phospholipids, because phospholipids appear to be stable only in living cells for longer periods of time. It was shown that they are rapidly hydrolysed after cell death due to early diagenetic alteration processes (Harvey et al., 1986; White et al., 1979). This makes intact phospholipids to be appropriate indicators for living microbial communities in deep sedimentary systems (White et al., 1979). Therefore, intact phospholipids are used as molecular "life" markers (Zink et al., 2003).

9.3 Samples and methods

9.3.1 Sampling

The Mallik 5L-38 Gas Hydrate Production Research Well drilling campaign was performed in winter 2001/2002 in the Mackenzie Delta (Northwest Territories) in northern Canada (Figure 9.2). Sedimentation in the Beaufort-Mackenzie area was dominated by a predominantly northward-prograding delta systems since the late Cretaceous (Dixon et al., 1992a; Dixon et al., 1992b). Therefore, the sedimentary succession in the Mallik well is composed of sediments typical for deltaic processes such as sand-, silt-, and claystones and some lignite layers. Nowadays, the outstanding feature of the Mallik well is a permafrost zone occurring from 0 to about 600 m and a zone of numerous gas hydrate bearing layers between approximately 896 and 1100 m depth.

Thirty sediment samples (18 - 170 g) have been taken from above, within and below the gas hydrate zone including different lithologies (11 sand, 13 silt/clay and 6 lignite samples). The samples are mainly from the sand-dominated Kugmallit sequence (early - late Oligocene), which reflects delta-plain deposits (Dixon, 1996; Young & McNeil, 1984). From the overlying Mackenzie Bay (350-930 m, late Oligocene - middle Miocene), in general shale domi-

nated, only three samples were collected. In contrast to the Kugmallit sequence, the Mackenzie Bay sequence is related to sedimentation processes at the delta-front (Dixon, 1996). In the Mallik 5L-38 well both, the Kugmallit and the Mackenzie Bay sequence are represented by sands and silts with pebble, clay and lignite interbeds (Medioli et al., 2005). From the uppermost Iperk Sequence (early Pliocene – early Pleistocene) and the Shallow Bay Sequence (Pleistocene – Holocene) both comprised of sandstones and conglomerates no samples were gathered.

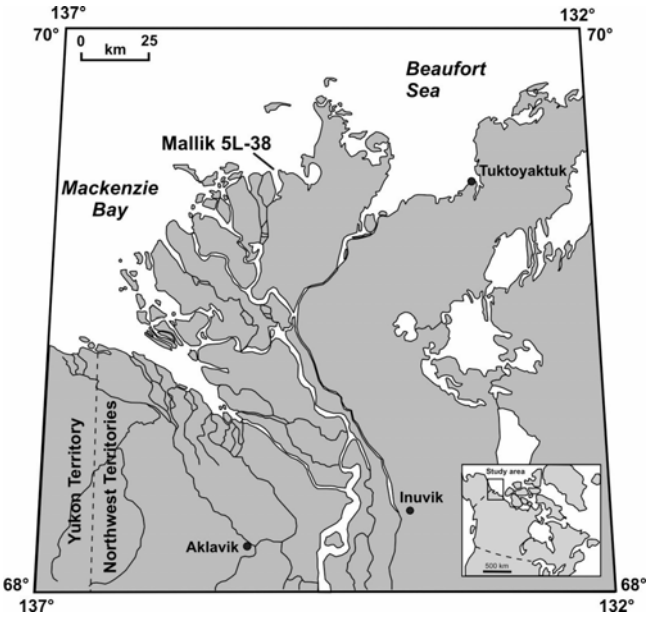

Figure 9.2: Map of the Mackenzie River Delta (Northwest Territories, Canada) showing the drilling location of the Mallik 5L-38 Gas Hydrate Production Research Well.

To avoid microbial contamination of the core material from the surface stringent microbiological sampling methods were used at the drill site for the non lignitic samples. These methods minimized the contact of the sample material with non-sterile, foreign materials and a fluorescent quality control tracer and a compound tracer (lecithin) were used during drilling to indicate the penetration depth of the drill fluids into the core material (Colwell et al., 2005; Dallimore et al., 2005b). After retrieval of the core material the exteriors of core samples were removed and discarded within an anaerobic glovebox on site in order to avoid contaminated outer core sections. All samples were directly sealed in Teflon receptacles and immediately stored under liquid nitrogen (-196°C) to avoid any post-drilling degradation or contamination processes. Samples were stored under these conditions until analysis.

The sample names, given in this paper, are composed of letters and numbers. The letter combination assigns a specific sampling method ("MB" (microbiology) = samples taken under

specific contamination-controlled conditions, see Mangelsdorf et al. (2005b), or a lithological characterization "CO" (coal) = lignite samples). The numbers provide the sample depth in centimeters. According to initial core descriptions, three samples (CO104310, CO106094 and CO110550) were assigned as coals (CO, lignite), however, their comparatively low organic carbon contents of 3.6, 4.7 and 9.4%, respectively, revealed that these samples are organic-rich shales rather than lignites.

As expected, the six lignite samples contain with up to 46.6% the highest contents of organic carbon. The thirteen silty clay samples have lower TOC values from 0.4 to 9.4%, while the portion of organic carbon in the eleven sand samples is very small with an average of 0.3% (Haberer et al., 2005). In former studies the low level of thermal maturity and the terrestrial origin of the organic matter in the sediments of the Mallik area were demonstrated (Haberer et al., 2005; Haberer et al., in press; Snowdon, 1981).

9.3.2 Lipid analysis

For lipid analysis, the sediment samples had been freeze-dried and ground. Sample aliquots of about 2g of the lignites and about 10g to 20g of the clay and sand samples were extracted ultrasonically using a mixture of CH_2Cl_2 and methanol (99/1, v/v). Subsequently, the volume of the resulting extract was concentrated using a Zymark TurboVap 500 concentrator and finally evaporated to dryness under a nitrogen gas stream. After addition of internal standards (androstane, ethylpyrene, 5α-androsta*n*-17-one, eruic acid), the extract was dissolved in *n*-hexane to precipitate asphaltenes, which were removed from the soluble fraction by filtration over Na_2SO_4. The *n*-hexane-soluble fraction was separated by medium-pressure liquid chromatography (Radke et al., 1980) into fractions of aliphatic/alicyclic hydrocarbons, aromatic hydrocarbons and nitrogen, sulphur and oxygen (NSO) compounds. Carboxylic acids were separated from the NSO compound fraction using a column filled with KOH-impregnated silica gel prepared by adding 0.5 g KOH in 10 ml isopropanol to 5 g silica gel 100 (63-200 µm). The non-acidic compounds (neutral fraction) were eluted with CH_2Cl_2. Following this the acidic fraction was eluted with 50 ml of a formic acid solution (2% in CH_2Cl_2) and subsequently 100 ml CH_2Cl_2. Prior to GC analysis the acid fraction was methylated with diazomethane and the neutral fraction was silylated with trimethylsilyltrifluoroacetamide (MSTFA). Additionally, behenic acid methyl ester (BAME) was added as injection standard to the aliphatic hydrocarbon, aromatic hydrocarbon and neutral hydrocarbon fractions. Squalene was added to the fatty acid fraction.

The fractions of interest were analyzed using a gas chromatographic system coupled with a mass spectrometer. Compound separation was performed on a Agilent 6890 Series GC-instrument equipped with a PTV injection system and a fused silica capillary column (SGE BPX5; 50 m length, inner diameter = 0.22 mm, film thickness = 0.25 µm). Helium was used as carrier gas, and the temperature of the GC oven was programmed from 50 °C (1 min) to 310 °C at a rate of 3 °C/min, followed by an isothermal phase of 10 min. The injector temperature was programmed from 52 °C to 300 °C at a rate of 12 °C/sec. For compound identification, the gas chromatographic system was linked to a Finnigan MAT 95 XL mass spectrometer operating in the electron impact ionisation mode (70 eV). Full scan mass spectra were recorded from *m/z* 50 to 650 at a scan rate of 1 s per decade and an inter scan delay of 0.2 s, resulting in a scan cycle time of 1.3 s.

9.3.3 Phopholipid analysis

For the analysis of phospholipids a special method was developed (Zink & Mangelsdorf, 2004) modified after Bligh and Dyer (1959). From the freeze-dried and grounded sediment samples aliquots of 36 to 75 g (depending on available sample quantity) were extracted using a flow blending system with a mixture of methanol/dichloromethane/ammonium acetate buffer (pH 7.6), 2:1:0.8 (v/v) for 5 min. Prior to the extraction, 100 µl of deuterium-labelled lysophosphatidylcholine (500 µg/ml) were added as an internal standard. The solvent extract was separated from the residual sediment by centrifugation (3500 rpm) for 10 min at a temperature of 15°C. After removal of the supernatant, additionally the sediment residue was re-extracted ultrasonically twice using the same solvent mixture. The combined solvent extracts were collected in a separation funnel and dichloromethane and water were added to achieve a ratio of 1:1:0.9 (v/v). After phase separation the organic phase was recovered and the water phase was re-extracted twice with 20 ml dichloromethane. The combined organic phases were concentrated and evaporated to dryness.

Subsequently, the extract was redissolved in 1 ml chloroform/methanol, 9:1 (v/v) and separated into four fractions of different polarity (low polar lipids, free fatty acids, glycolipids and phospholipids) using a pure silica column (1 g silica gel 63-200 µm) and a florisil column (1 g magnesium silica gel 150-250 µm) in sequence. The low polar lipid fraction was obtained by elution with 20 ml of chloroform, the free fatty acids fraction with 50 ml of methyl formiate containing 0.025% glacial acetic acid, the glycolipids fraction with 25 ml of acetone and the phospholipid fraction with 25 ml of methanol.

The methanol fractions were analysed for intact phospholipids on an HPLC instrument (Shimadzu SCL-10a VP) coupled to a Finnigan MAT TSQ 7000 mass spectrometer equipped with an electrospray interface (ESI). Separation of phospholipid classes was achieved with normal phase HPLC on a pure silica gel column 125 x 2 mm (Hypersil Si-3µm). The HPLC was equipped with a 5 µl sample loop, the flow rate was set to 150 µl/min with a gradient solvent system of chloroform (A), methanol (B), and ammonium acetate buffer (10 mM; C) modified after Aries et al. (2001). The initial mobile phase composition was 30% A, 65% B, 5% C; B was decreased to 55%, and C increased to 15% after 3 min; after 8 min the mobile phase was reset to initial conditions and was held isocratically for 7 min, resulting in a total time of analysis per sample of 15 min. Full scan mass spectra were recorded in the negative ion mode over a *m/z* range of 400 to 1800 at a scan rate of 1 scan every 2s. For detailed structural elucidation of individual phospholipids (phospholipid head group, fatty acyl side chains) collisionally activated dissociation (CAD) tandem quadrupole MS experiments were performed (argon as collision gas, collision energy 30 eV) over a *m/z* range of 100 to 800 at a scan rate of 1 scan/s.

For each Mallik sample investigated simultaneously the same methods were applied to quarz sand as reference samples using the same solvents and chemicals to check for any microbial contamination during the laboratory processes. All reference samples were negative with regard to a phospholipid signal.

9.3.4 Glycerol etherlipid analysis

For the detection of tetraether lipids the acetone fractions (clay and sand samples) and the neutral polar fractions (lignites) were analysed using an high-performance liquid chromatography/atmospheric pressure chemical ionisation mass spectrometry (HPLC/APCI-MS) method modified after Hopmans et al. (2004). Chromatographic separation was achieved on a Sphere Image 3 CN column (150 x 2 mm, 3 µm; CS-Chromatography, Düren, Germany). The mobile phase consists of *n*-hexane A and isopropanol B (5 min 99% A, 1% B), followed by a linear gradient to 1.4% B within 22.5 min, then within 1 min to 10% B, holding 5 min to clean the column and back to initial conditions in 1 min, held for 6 min for equilibration. The flow rate was set to 200µl/min and injection was performed via autosampler with a 5µl loop. The conditions for the APCI-MS were as follows: corona current 5 µA giving a voltage of around 4 kV; vaporiser temperature 350°C; capillary temperature 200 °C and voltage 7.5V; nitrogen sheath gas at 60 psi (4 bar); without auxiliary gas. Mass spectra were generated by selected (single) ion monitoring (SIM), in the positive ion mode resulting in protonated

$[M+H]^+$, $[M+H]^+$+1, and $[M+H]^+$+2 molecular ions, the multiplier voltage was 1500 V, and the scan rate was 2s. For full scan analysis m/z range from 900 to 1400 was used. For semi-quantitative determination of tetraether compounds an external synthetic archaeol standard (AvantiPolarLipids Inc., Al, USA) was used. Linearity and reproducibility was tested on 3 concentrations (0.1, 1, 10 µg/ml) analysed in triplicates and parallel to the sample sequence.

9.3.5 Carbon isotopic analysis of individual biomarkers

The carbon isotope composition of the aliphatic fractions was measured with a gas-chromatograph coupled via a combustion interface to an isotope ratio mass spectrometer (GC-C-IRMS system). Double measurements were performed. Aliquots (3 µl) of the extracts were injected into the GC (Agilent 6890 N, Agilent Technology, USA) in split mode and separated on a capillary column (HP Ultra 1; 50 m x 0.32 mm x 0.52 µm film thickness, Agilent Technologies, USA). Helium, set to a flow rate of 1.5 ml min^{-1}, was used as carrier gas. The injector temperature was held constant at 250 ^oC. The oven temperature was initially set to 80 °C and held for 1 min. The temperature was then increased at a rate of 3 °C min^{-1} to 310 °C and held for 20 min. The GC unit was connected to a combustion device (GC-III, Thermo Electron, Germany) coupled to a MAT 253 mass spectrometer (Thermo Electron, Germany). Organic substances in the GC effluent stream were oxidised to CO_2 and H_2O in the combustion furnace held at 940 ^oC on a CuO/Ni/Pt catalyst and were transferred online via open split to the isotope ratio mass spectrometer to determine $^{13}C/^{12}C$ ratios of CO_2. The instrument was calibrated using a reference gas (CO_2) with known isotopic composition. Additionally, a mixture of three *n*-alkanes (C_{15}, C_{20} and C_{25}) with known isotopic composition (Chiron, Norway) was measured every 5 runs to check the performance of the whole system. The carbon isotope composition is reported in the δ-notation (per mill) relative to Vienna Pee Dee Belemnite standard (V-PDB).

9.4 Results

9.4.1 Hopanoic hydrocarbons occurring in the Mallik samples

The investigated samples of the Mallik 5L-38 well contain a wide variety of hopanes, hopenes, methylhopenes, hopanols and hopanoic acids (Table 9.1). The hopanoid composition varies from sample to sample but only one sample (MB91856) contains no hopanoic hydrocarbons at all (MB91856, Table 9.2). Figure 9.3 displays a typical distribution of hopanes and hopenes in the aliphatic hydrocarbon fraction from the Mallik Site (clay sample MB106380). The representative *m/z* 191 mass chromatogram (Figure 9.3b) shows the predominance of hopanoids with the 17β(H) (C_{27}) and 17β(H),21β(H)-configuration (C_{29}-C_{32}) and of hopenes (compounds listed in Table 9.1). Additionally, hopanes with the 17α(H) (C_{27}) and 17α(H),21β(H)-configuration (C_{29}-C_{31}) occur in the Mallik samples, although with a lower variability and abundance (Figure 9.4). Only one hopanoid with a 17β(H),21α(H)-configuration (moretanes, C_{29}) is present. Another interesting hopanoic hydrocarbon group found in the investigated samples are the methylhop-17(21)-enes. Four different isomers are detected: two congeners of 2-methylhop-17(21)-enes, one 3-methylhop-17(21)-ene and one hop-17(21)-ene methylated probably at the C-ring. Their typical distribution in the Mallik samples is illustrated in the characteristic *m/z* 245 trace (sample MB106380; Figure 9.3c).

The distribution and abundance of hopanoids differ with the lithological differences of the sample material investigated (Figure 9.4). In the lignites and clays the 17β(H),21β(H)-hopanes and the hopenes are the dominating hopanoic hydrocarbons. In contrast, in the sand samples the 17α(H),21β(H)-hopanes are the most common hopanoids with highest abundance relative to the total organic carbon (TOC) in samples MB107960 and MB110494. Other hopanoids occur only in four sand samples (MB91200, MB107960, MB110494, and MB112790, Table1). While methylhop-17(21)-enes are present in significant amounts in the lignites and clay samples, methylhopenes are completely absent in the sand samples (Figure 9.4, Table 9.2).

Table 9.1: Sample numbers, core depths, lithological description, total organic carbon (TOC) contents, and totals (µg/gTOC) of the hopanoic hydrocarbons identified in the aliphatic, fatty acid and neutral fractions of the samples. n.d.l. = near detection limit.

Mallik 5L-38	sample characteristics			aliphatic hopanoids					hopanoic acids /alcohols				
Samples	Depth (m)	Lithology	TOC (%)	∑ hopenes (µg/gTOC)	∑ ββ-hopanes (µg/gTOC)	∑ αβ-hopanes (µg/gTOC)	∑ βα-hopanes (µg/gTOC)	∑ methylhopenes (µg/gTOC)	∑αβ-hopanoic acids (µg/gTOC)	∑ββ-hopanoic acids (µg/gTOC)	∑βα-hopanoic acids (µg/gTOC)	∑ hopanons/-ols (µg/gTOC)	∑ all hopanoids (µg/gTOC)
MB89163	891.63 – 891.82	silt/clay	0.92	56.4	0.0	0.0	0.0	0.4	0.0	4.4	0.0	15.3	76.5
MB89899	898.99 – 899.16	silt/clay	0.95	103.6	81.6	16.5	7.1	0.5	2.5	4.8	1.6	51.0	269.2
MB90020	900.20 – 900.40	silt/clay	0.86	73.0	60.2	13.9	7.0	0.3	1.3	3.7	0.8	4.2	164.4
MB91200	912.00 – 912.19	sand	0.05	8.0	0.0	17.3	0.0	0.0	0.0	0.0	0.0	0.0	25.3
MB91856	918.56 – 918.76	sand	0.05	0.0	0.0	0.0	0.0	0.0	0.0	0.0	0.0	0.0	0
CO93409	934.09 – 934.10	lignite	46.60	89.1	72.2	73.4	2.2	1.4	137.4	312.1	83.7	n.d.l	771.5
MB93589	935.89 – 936.09	silt/clay	1.78	110.5	0.0	0.0	0.0	0.1	14.2	21.0	0.0	0.8	146.6
CO94078	940.78 – 940.81	lignite	31.85	85.1	159.3	100.0	10.8	1.0	2.6	28.0	0.5	n.d.l	387.3
MB94762	947.62 – 947.84	sand	0.95	0.0	0.0	29.8	0.0	0.0	0.0	0.0	0.0	0.0	29.8
MB96334	963.34 – 963.50	silt/clay	0.40	65.1	64.9	24.3	8.9	0.4	0.0	1.0	0.0	3.4	168
MB97760	977.60 – 977.80	sand	0.09	0.0	0.0	33.2	0.0	0.0	0.0	0.0	0.0	0.0	33.2
MB98925	989.25 – 989.45	sand	0.10	0.0	0.0	7.8	0.0	0.0	0.0	0.0	0.0	0.0	7.8
CO100550	1005.50	lignite	42.03	44.0	31.7	32.4	4.4	1.1	310.9	685.0	101.7	n.d.l	1211.2
MB100778	1007.78 - 1007.98	silt/clay	0.46	153.2	99.1	41.4	6.2	0.4	0.0	0.0	0.0	1.1	301.4
MB102215	1022.15 – 1022.55	sand	0.11	0.0	0.0	13.8	0.0	0.0	0.0	0.0	0.0	0.0	13.8
MB103360	1033.60 - 1033.80	silt/clay	7.09	92.8	0.0	0.0	0.0	2.0	0.0	1.7	0.3	2.5	99.3
CO104310	1043.10	silt/clay	3.64	546.8	592.5	141.7	74.3	2.9	61.9	1088.9	136.8	83.9	2729.7
MB104920	1049.20 – 1049.36	silt/clay	1.01	36.0	48.2	50.6	4.0	0.2	0.0	0.0	0.0	0.0	139
CO105353	1053.53	lignite	39.19	158.6	283.8	50.8	6.3	2.7	137.1	427.1	116.4	n.d.l	1182.8
CO106094	1060.94 – 1060.95	silt/clay	4.71	93.1	94.0	13.9	4.4	0.3	13.9	87.7	17.5	0.2	325
MB106380	1063.80 – 1064.00	silt/clay	1.89	89.1	118.6	27.3	9.0	0.2	4.1	14.0	4.6	0.0	266.9
MB107960	1079.60 – 1079.81	sand	0.04	99.4	213.6	656.1	42.1	0.0	0.0	0.0	0.0	0.0	1011.2
CO108138	1081.38	lignite	45.93	75.2	23.7	6.2	1.6	1.0	42.8	232.7	21.0	n.d.l	404.2
CO108169	1081.69	lignite	38.39	25.0	17.6	39.7	1.0	0.4	27.4	121.7	6.7	n.d.l	239.5
MB108924	1089.24 - 1089.39	sand	0.06	0.0	0.0	6.0	0.0	0.0	0.0	0.0	0.0	0.0	6
MB110494	1104.94 - 1105.14	sand	0.09	28.8	188.1	159.2	0.0	0.0	0.0	0.0	0.0	0.0	376.1
CO110550	1105.50	silt/clay	9.44	6.9	7.5	7.1	1.5	0.1	0.0	2.5	0.0	1.5	27.1
MB112790	1127.90 - 1128.02	sand	1.57	1.8	3.3	0.1	0.6	0.0	0.0	0.0	0.0	0.0	5.8
MB113980	1139.80 - 1139.83	sand	0.17	0.0	0.0	16.0	0.0	0.0	0.0	0.0	0.0	0.0	16
MB114535	1145.35 - 1145.55	silt/clay	0.53	56.8	102.8	35.9	9.0	0.0	8.8	9.9	2.6	0.0	225.8

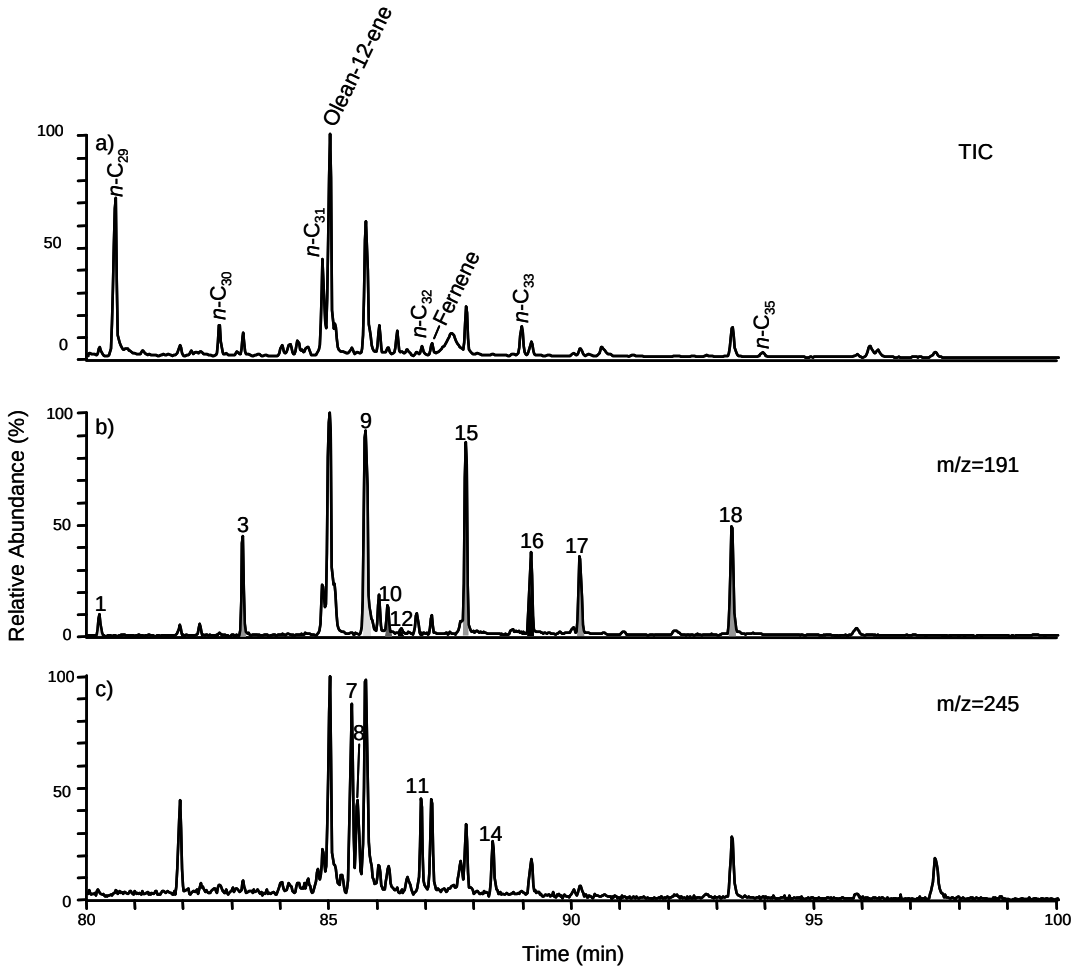

Figure 9.3: a) GC/MS RIC chromatogram (RIC = Reconstructed Ion Current) of a representative aliphatic hydrocarbon fraction (silty clay sample MB106380), b) GC/MS-mass chromatogram *m/z* 191 showing the distribution of hopanes and c) GC/MS-mass chromatogram *m/z* 245 showing the distribution of methylhop-17(21)-enes. Numbers correspond to compound names in Table 9.1.

The chromatogram in Figure 9.5a shows the distribution of the hopanoic fatty acids in the sample MB106380. The major compounds are the three isomers of the *dihomo*-hopanoic acids with the (22R)-17α(H),21β(H), 17β(H),21α(H), and 17β(H),21β(H) (compounds 24, 25 and 26). With exception of all sand samples and two clay samples (MB100778 and MB104920), which do not contain any hopanoic fatty acids at all (Table 9.1), *dihomo*-hopanoic acids can be observed in all studied samples from the Mallik well in high proportions. Furthermore, the (22R)-17α(H),21β(H)-hopanoic acid, the 17β(H),21β(H)-hopanoic acid and the 17β(H),21β(H)-*trihomo*-hopanoic acid occur in all lignite and some clay samples (Table 9.2).

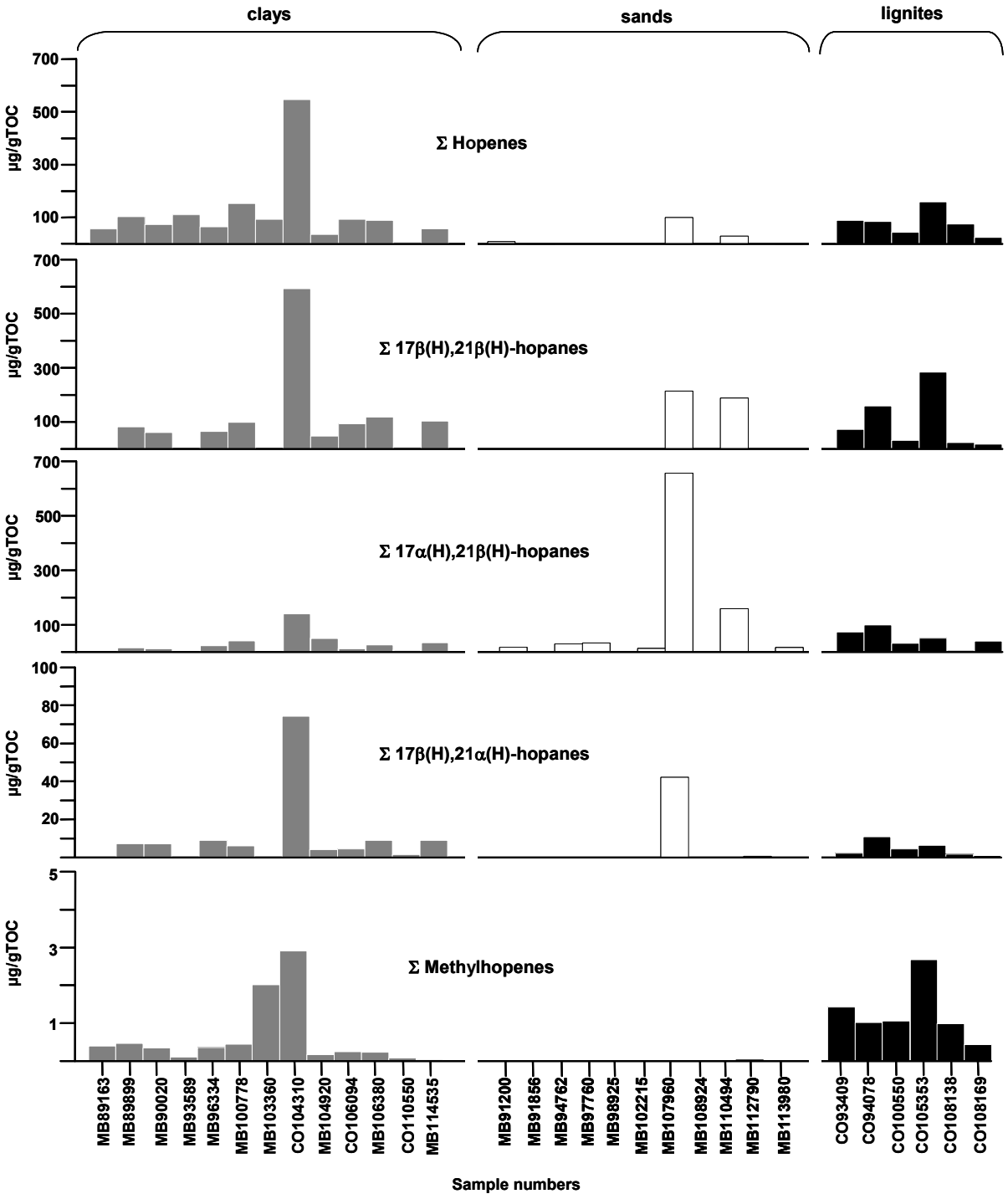

Figure 9.4: Distribution and abundance of hopanoids occurring in the Mallik samples with regard to different lithologies.

In the neutral polar lipid fraction of the studied lignite and clay samples, also hopanoic hydrocarbons occur (Figure 9.5b, Table 9.1, Table 9.2). However, in most samples only the 17β(H),21β(H)-*dihomo*-hopan-32-ol is present, although in the lignites they are only near the detection limit. Therefore, they are not noted in Table 9.1.

Table 9.2: Hopanoic hydrocarbon compounds identitied in the aliphatic, fatty acid and neutral fractions of the Mallik samples.

No.	Compound names
1	22,29,30-*trinor*-hop-13(18)-en
2	17α(H)–22,29,30–*trinor*-hopane
3	17β(H)–22,29,30–*trinor*-hopane
4	28,30–*dinor*-17α(H),18α(H),21β(H)–hopane
5	30-*nor*-hop-17(21)-en
6	17α(H),21β(H)-*nor*-hopane
7	Hop-17(21)-ene
8	17β(H),21α(H)–30–*nor*-hopane
9	17α(H),21β(H)–hopane
10	*Neo*-hop-13(18)-ene
11	17(H)β,21β(H)–*nor*-hopane
12	(22R)–17α(H),21β(H)–*homo*-hopane
13	17(H)β,21β(H)-hopane
14	17β(H),21β(H)-*homo*-hopane
15	(22R)-17α(H),21β(H)-*trihomo*-hopane
16	17(H)β,21β(H)-*dihomo*-hopane
17	2-Methyl-hop-17(21)-ene
18	2-Methyl-hop-17(21)-ene
19	Methyl-hop-17(21)-ene
20	3-Methyl-hop-17(21)-ene
21	(22R)–17α(H),21β(H)–hopanoic acid
22	17β(H),21β(H)-hopanoic acid
23	(22S)–17α(H),21β(H)-*dihomo*-hopanoic acid
24	(22R)–17α(H),21β(H)–*dihomo*-hopanoic acid
25	17β(H),21α(H)–*dihomo*-hopanoic acid
26	17β(H),21β(H)-*dihomo*-hopanoic acid
27	17β(H),21β(H)-*trihomo*-hopanoic acid
28	22,29,30-*trinor*-hopan-21-on
29	17α(H),21β(H)-*dihomo*-hopan-32-ol
30	17β(H),21β(H)-*dihomo*-hopan-32-ol

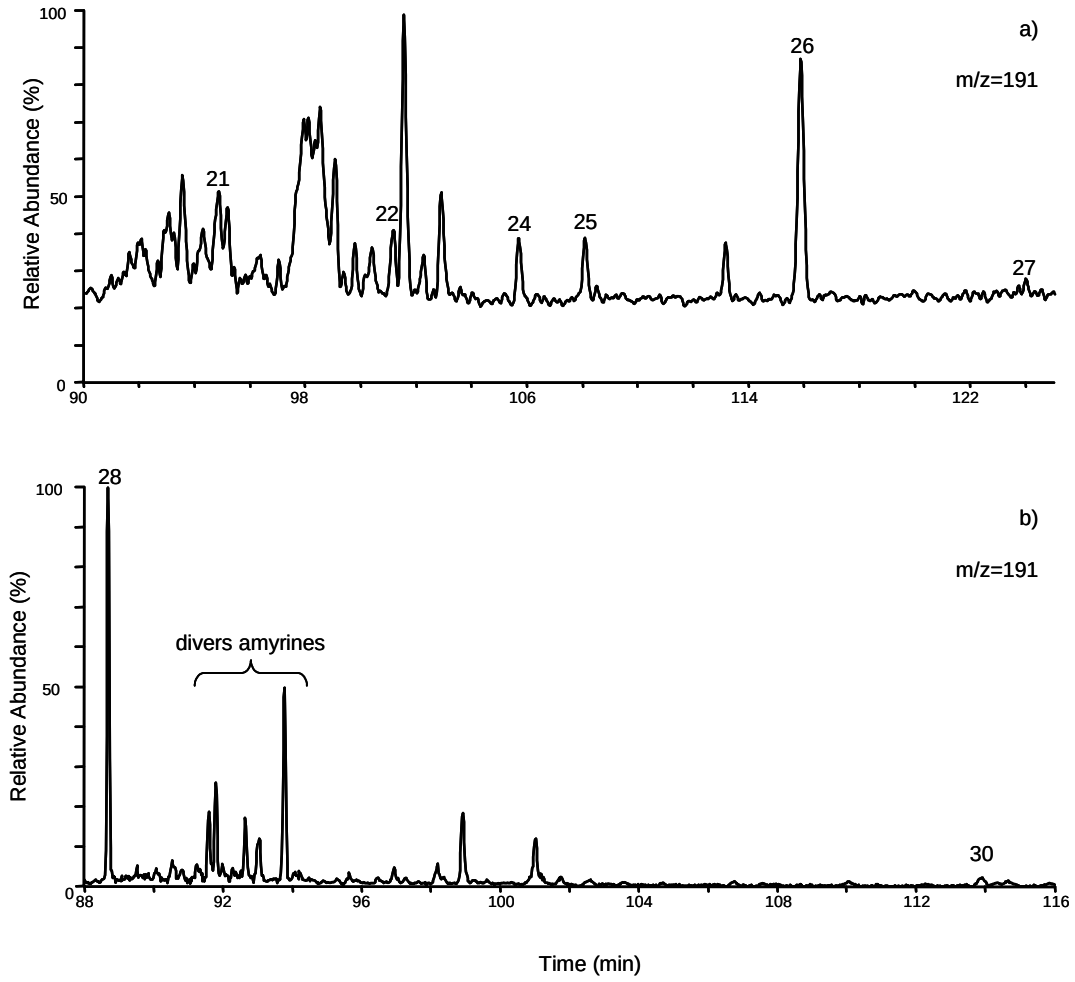

Figure 9.5: a) GC/MS mass chromatogram *m/z* 191 of a representative fatty acid fraction (silty clay sample MB106380). Hopanoic acids are assigned by letters corresponding to compound names in Table 2. b) GC/MS mass chromatogram *m/z* 191 of a representative neutral polar fraction (silty clay sample MB89899). Letters correspond to compound names in Table 9.1.

Figure 9.6 shows the depth profile of the sum of hopanoids occurring in the Mallik samples normalized to their TOC contents and relative to the methane contents of the Mallik sediments obtained from mud log data (Dallimore et al., 2005a). High methane contents indicate the presence of gas hydrates as indicated by the gas hydrate saturation record (Collett & Lee, 2005). It can be assumed that free-gas associated to this gas hydrates most likely occur at the transition to the surrounding sediments as shown for other gas hydrate formations (Valentine, 2002; Wellsbury et al., 2000). The investigated lignites and silty clays plot mainly within the sedimentary sections, where no gas hydrates occur or where the gas contents are low. In contrast the sand samples often fall into the range of the gas hydrate sections. The larger pore space of the sands and in some cases of the silty clays availing the formation of gas hydrates might be the reason for this observation. Comparing the hopanoid signal with the methane profile it can be observed that in many cases the hopanoid contents are highest in sediments

with no gas hydrates or at transition zones. This indicates that a comparable higher proportion of the organic matter in the non gas hydrate bearing layers is from microbial origin, compared to samples within the gas hydrate formations. Thus, in most cases lignites and silty clay samples show high hopanoid contents. In most sand samples plotting mainly within the gas hydrates the hopanoid contents are relatively low. However, two sand samples contain very high hopanoid concentrations. Interestingly, these samples are at the transition zone of gas hydrate layers, where the occurrence of free-gas associated to the gas hydrates is very likely.

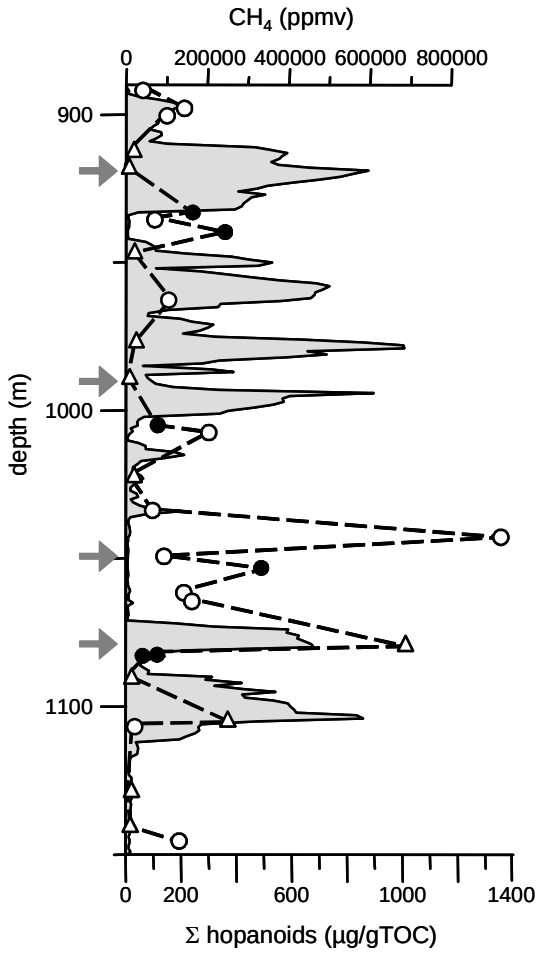

Figure 9.6: Depth profile of the sum of hopanoids detected in the Mallik sample compared to the methane content of the cored Mallik sediments representing gas hydrate bearing layers (data from Dallimore et al., 2005). Black dots: lignites, triangles: sands, circles: silt/clays.

9.4.2 Intact phospholipids occurring in the Mallik samples

With exception of the lignite samples, which were not taken under specific contamination-controlled conditions, all samples were analysed for their phospholipid contents. To prevent the formation of gas hydrates during the drilling process lecithin was added to the drill mud. Lecithin consists of mainly phospholipids with a phosphatidylcholine head group (PCs). Due to the characteristic structure and composition of the lecithin phospholipids drill mud contaminated samples could be easily distinguished from non-contaminated samples using our applied sample preparation method. Although the drill mud lecithin signal could be observed in some samples, this does not necessarily mean that the sample material is contaminated with surface microorganisms in a number detectable with our method, because the drill mud did not contain any other phospholipids than those from the lecithin. A post grow of surface microorganisms on the sample material after contamination with the drill mud can be excluded, because the samples were immediately frozen down to -196°C with liquid nitrogen and stored under these conditions until analysis. Anyway, to be on the safe side samples containing any lecithin phospholipids were not taken into account for further phospholipids analysis. Additionally, the varying biomarker signal of the hopanoids, which is completely different from those of the drill mud containing the typical hopanoic distribution of mature oil-derived hydrocarbons (C_{27}, C_{29}-C_{35} hopanoids in the 17α(H),21β(H)-configuration and with the C_{30}-hopane as maximum compound in the *m/z* 191 trace) indicates that the hopanoid signal is an indigenous biomarker signal of the Mallik samples. Even if there is a small contamination by the drill mud hopanoids these contaminants did not significantly influence the indigenous hopanoid signal.

Although the phospholipid signal in the Mallik samples is in general small, at least in four of the non-contaminated samples (MB91858, MB98925, MB104920, and MB107960) phosphatidylglycerols (PGs), phosphatidylethanolamines (PEs) with different acyl side chains (with 16 and 18 carbon atoms) were detected. Three of these samples containing detectable amounts of PLs are sand samples, whereas the fourth is a silty clay sample.

As an example for the PL distribution in the Mallik samples the PL results of sample MB91856 are presented in Figure 9.7. This sand sample from 918.56 m depth contains phosphatidylglycerols (PGs) and phosphatidylethanolamines (PEs). The reconstructed ion current (RIC) chromatogram of the deprotonated molecular ions of the PGs (1.6 - 2.1 min) and the PEs (2.8 - 3.6 min) is shown in Figure 9.7a. In sample MB91856, the PE signal is very small and near the detection limit.

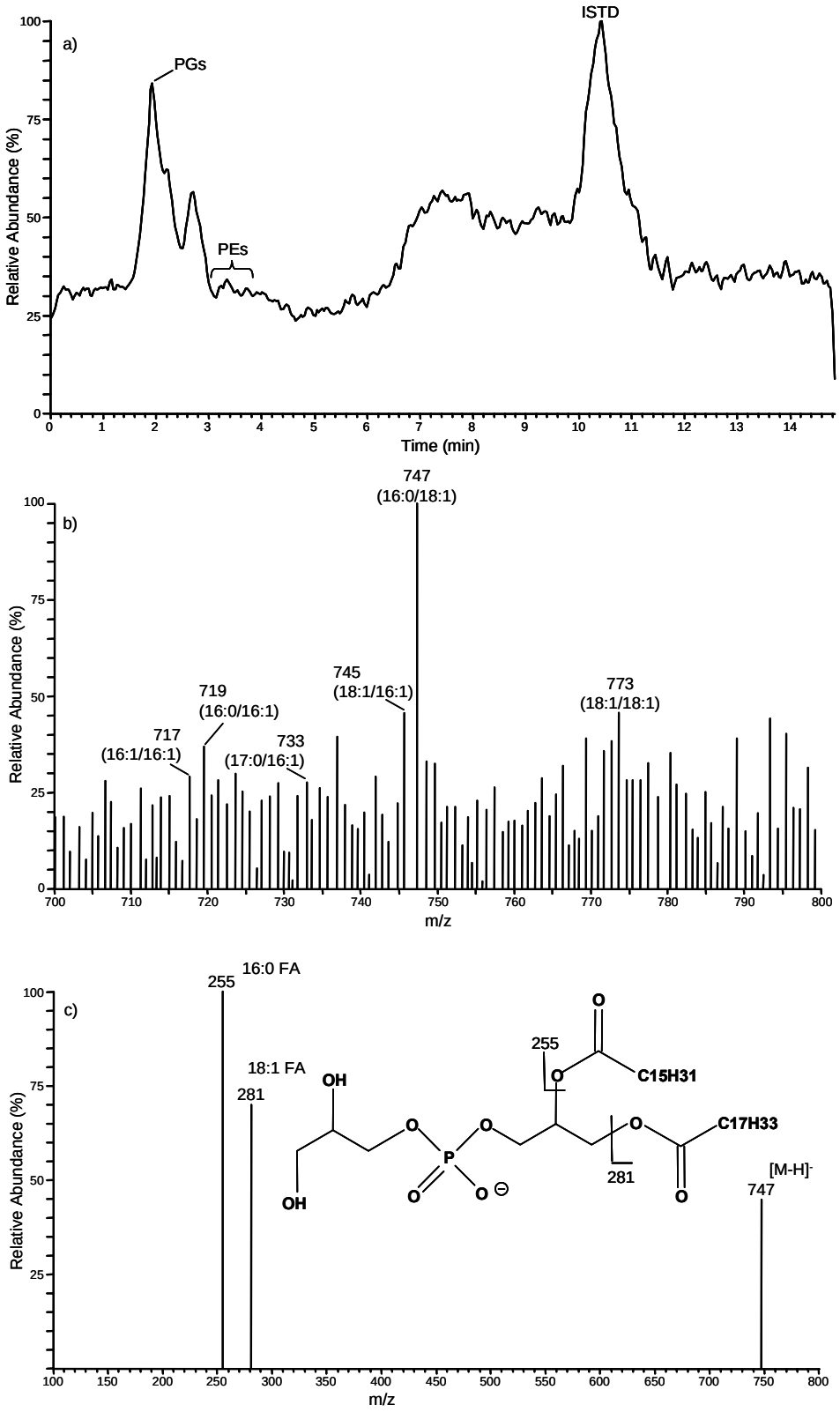

Figure 9.7: a) HPLC-ESI-MS RIC-chromatogram (negative ion mode) of the phosphatidylglycerols (PGs) and phosphatidylethanolamines (PEs) detected in the sand sample MB91856. ISTD = Internal standard (deuterium-labelled palmitoyl-D31- lysophosphatidylcholine) b) Average mass spectrum of the phosphatidylglycerols from 1.7-2.1 min. c) Collisionally activated dissociation mass spectrum on *m/z* 747.4 (PG(16:0/18:1), 1 hexadecanyl-2-octadecenyl-phoshatidylglycerol) during the time interval from 1.9-2.0 min, (sand sample MB98925). Collision energy 30 eV.

Table 9.3: Phosphatidylglycerols and phosphatidylethanolamines detected in the Mallik 5L-38 samples, their pseudomolecular ions and their predominantly fatty acid side chain composition. unshaded = sand, grey shaded = silt/clay.

	PG							PE				
Mallik 5L-38 samples	717 16:1/16:1	719 16:0/16:1	721 16:0/16:0	733 17:0/16:1	745 18:1/16:1	747 18:1/16:0	773 18:1/18:1	686 16:1/16:1	688 16:0/16:1	690 16:0/16:0	714 16:1/18:1	716 16:0/18:1
MB91858	x	x		x	x	x	x	x	x	x	x	x
MB98925	x	x	x	x	x	x	x			x	x	x
MB104920		x	x					x	x		x	x
MB107960	x	x	x	x	x	x	x	x	x			x

However, an example for the composition and structure of PEs in the Mallik sediments has already been shown by Mangelsdorf et al. (2005b). Figure 9.7b presents a more detailed insight into the PG distribution in sample MB91856 demonstrating that the PG signal consists at least of six deprotonated molecular ions (*m/z* 717.7, 719.5, 733.0, 745.6, 747.8 and 773.6) being significantly above the detection limit. The different masses suggest variable composition in the ester linked fatty acids side chain composition in terms of different chain length and number of double bonds (Table 9.3).

More detailed structural information on the linked fatty acids was gained by collisionally activated dissociation (CAD) tandem MS experiments carried out on the PG and PE deprotonated molecular ions. Both, the PGs and the PEs show a wide diversity, with C_{16}, C_{17} and C_{18} fatty acid side chains with no or one double bond per acyl side chain (Table 9.3). For instance, Figure 9.7c illustrates the results of the tandem MS experiment on the deprotonated molecular PG ion *m/z* 747 over the elution time range of 1.9-2.1 min for sample MB98925 (collision energy 30eV). In addition to the deprotonated molecular ion $[M-H]^-$ *m/z* 747 the mass spectrum shows two supplementary fragments (*m/z* 255 and 281) which represent the formerly linked saturated C_{16} and monounsaturated C_{18} fatty acid side chains. The dominance of the *m/z* 255 fragment implies that the saturated C_{16} fatty acid was linked predominantly to the *sn2*-position in the glycerol backbone, because the fatty acids in the *sn2*-position are preferentially removed resulting in higher fragment ion intensity (Cole & Enke, 1991; Fang & Barcelona, 1998).

Additionally to the PGs and the PEs, in ten samples compound signals can be detected, which MS/MS fragmentation spectra can be interpreted as lyso-phosphatidylglycerol ethers (LPGs). Figure 9.8a shows the mass chromatogram of the clay sample MB106380 (1063 m depth). The compound signal consists of six deprotonated molecular ions (Figure 9.8b) with masses

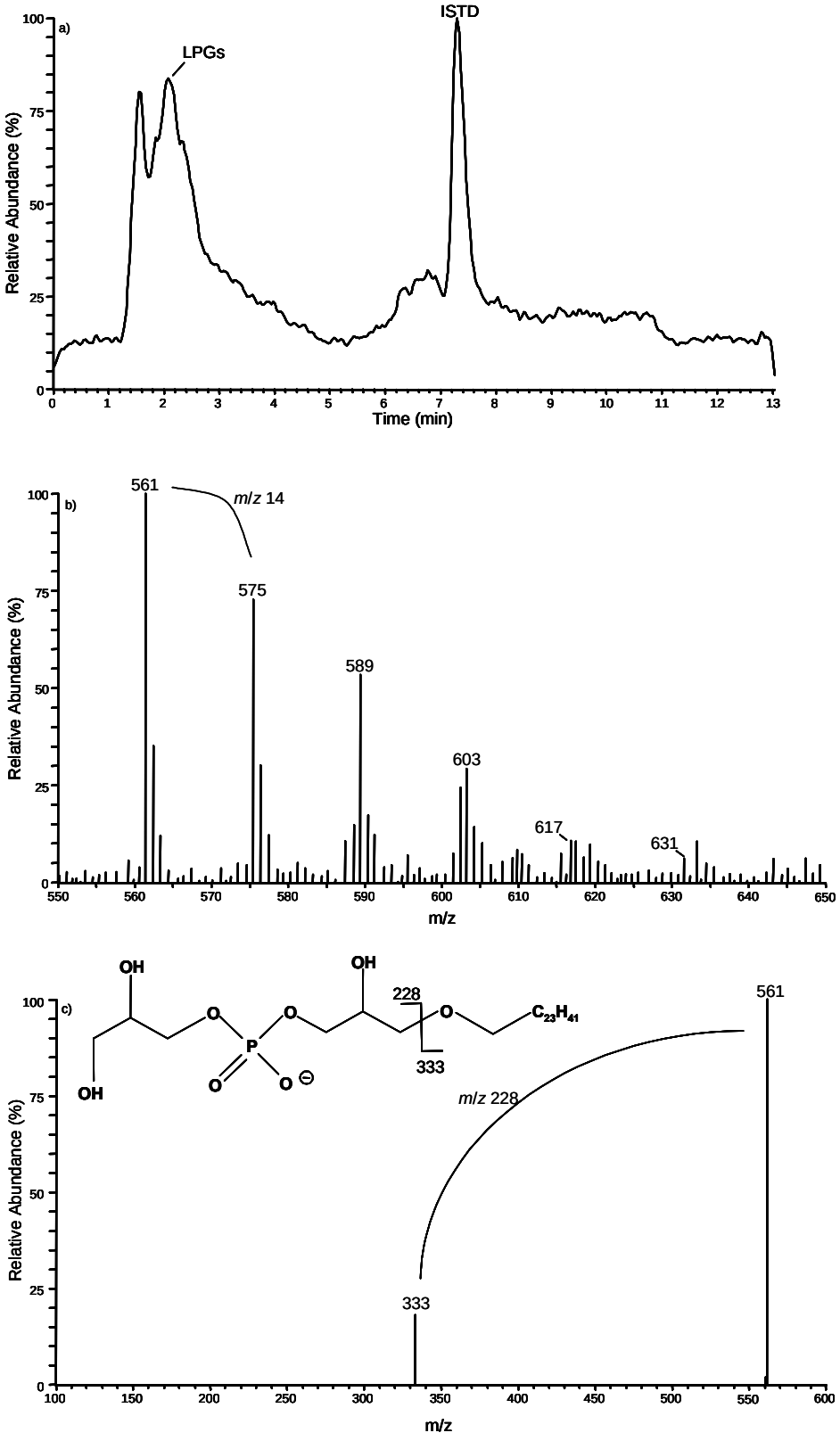

Figure 9.8: a) Mass chromatogram of the pseudomolecular ions (negative ion mode) of the lysophosphatidyl-glycerol-ethers (LPGs) detected in the ESI/MS run of the sample MB10638. ISTD = Internal standard (deuterium-labelled lysophosphatidyl-d32-choline) b) Average mass spectrum of the lysophosphatidylglycerol-ethers from 1.2-1.6 min. c) Collisionally activated tandem mass spectrum on m/z 561 (LPG (23:3), 1-hydroxyl-2-tricosatrienyl-phoshatidylglycerolether) during the time interval from 1.5-1.6 min. Collision energy 40 eV.

suggesting different carbon chain lengths. In contrast to the PGs (Figure 9.7) and PEs (Mangelsdorf et al., 2005a) it is very conspicuous for these compounds, that the individual ion masses always differ by *m/z* 14 corresponding to the mass of a CH_2-group.

Furthermore these compounds show a different behaviour during the MS/MS experiment compared to the PL esters. Even with enhanced collision energy (40eV and 60eV), the fragmentation mass spectrum of the MS/MS experiments (Figure 9.8c) performed on the deprotonated molecular ion *m/z* 561 over the time range of 1.5-1.6 min reveal only one small fragment (*m/z* 333) in addition to the $[M-H]^-$ *m/z* 561. The difference of *m/z* 228 between the deprotonated molecular ion *m/z* 561 and the *m/z* 333 fragment corresponds to a headgroup of a lyso-phosphatidylglycerol (LPG). In contrast to the cleavage of the PL ester, where only a relatively small amount of energy is required to produce distinct fatty acid fragments (Figure 9.7) more energy (40 to 60 eV) was needed to fragment these compounds and despite this higher energy supply only a small fragment was produced. All this point to an ether bound, which is more stable than an ester bound. Thus, the *m/z* 333 fragment would indicate an ether side chain with 23 carbon atoms and 3 double bonds ($C_{23:3}$).

9.4.3 Glycerol ethers occurring in the Mallik sediments

Dialkyl glycerol ethers like archaeol or glycerol dialkyl glycerol tetraethers such as caldarchaeol could be detected in nearly all samples investigated. Figure 9.9 shows the HPLC/APCI-SIM mass chromatograms of selected ions of the clay sample MB96334 (963 m depth).

Although the bacterial ether lipids are more abundant than the archaeal ones both compound groups vary in the same way with regard to the different sample lithologies (

Figure 9.10, Table 9.4). High abundance of these biomarkers is observed in the non gas hydrate bearing sediments (silt/clay and lignite samples). In general the amounts of archaeal etherlipids are higher in the lignite samples than in the clay samples. The distribution of bacterial etherlipids shows no differences between the clays and the lignites. Only clay sample CO110550 does not contain any ether lipids. In contrast to the lignites and clays the sand samples from the gas hydrate bearing strata contain only low amounts of ether lipids.

If the ether lipids at least partly represent a viable microbial population, this observation agrees with the suggestion of Valentine (2002) that microorganisms might preferentially colonise the non gas hydrate bearing sediments using the free-gas as a carbon and energy source.

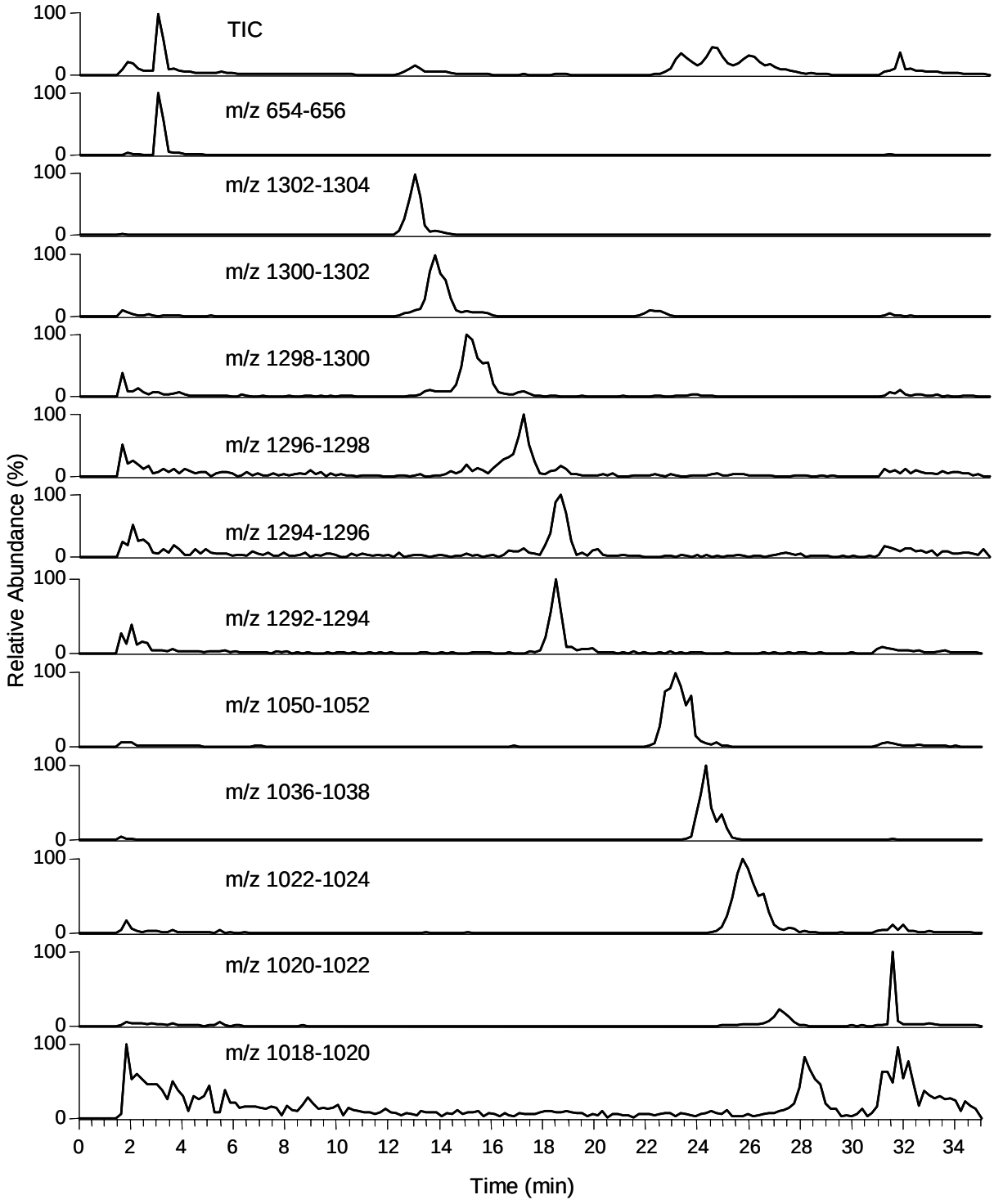

Figure 9.9: HPLC/APCI-SIM mass chromatograms of the selected ions of different ether lipids detected in the sample MB96334.

Table 9.4: Sample numbers, core depths, totals (ng/gSed) of all ether lipids (EL), the glycerol ethers (archaea. Ar-EL), the glycerol dialkyl glycerol tetraethers (bacteria, B-EL), and archaeol (Aol). grey shaded = silt/clay, dark grey shaded = lignite, unshaded = sand.

Mallik 5L-38 Samples	Depth (m)	EL (ng/gSed)	Ar-EL (ng/gSed)	B-EL (ng/gSed)	Aol (ng/gSed)
MB89163	891.63	161.3	78.1	83.2	52.5
MB89899	898.99	200.5	84.3	116.2	61.3
MB90020	900.2	258.0	129.4	128.7	101.9
MB91200	912	15.7	11.1	4.6	2.6
MB91856	918.56	9.2	8.0	1.2	2.3
CO93409	934.09	4898.5	2493.4	2405.0	1647.7
MB93589	935.89	112.8	60.9	51.9	48.1
CO94078	940.78	404.0	404.0	0.0	404.0
MB94762	947.62	15.6	10.9	4.7	7.8
MB96334	963.34	194.9	101.2	93.8	76.0
MB97760	977.6	11.5	9.2	2.4	5.7
MB98925	989.25	7.8	5.7	2.2	3.7
CO100550	1005.5	448.4	448.4	0.0	448.4
MB100778	1007.78	4.2	1.6	2.5	1.1
MB102215	1022.15	16.3	9.6	6.6	3.9
MB103360	1033.6	1002.0	340.4	661.6	197.2
CO104310	1043.1	1118.1	285.4	832.8	167.3
MB104920	1049.2	223.0	50.2	172.8	30.1
CO105353	1053.53	315.3	315.3	0.0	315.3
CO106094	1060.94	1410.1	338.5	1071.7	96.8
MB106380	1063.8	337.1	92.3	244.8	48.4
MB107960	1079.6	7.5	6.5	1.0	1.4
CO108138	1081.38	498.6	498.6	0.0	498.6
CO108169	1081.69	53.7	53.7	0.0	53.7
MB108924	1089.24	4.6	3.7	0.9	1.1
MB110494	1104.94	11.9	6.6	5.2	3.5
CO110550	1105.5	-	-	-	-
MB112790	1127.9	16.4	9.1	7.4	6.5
MB113980	1139.8	9.1	6.6	2.5	4.2
MB114535	1145.35	158.7	68.8	89.9	48.4

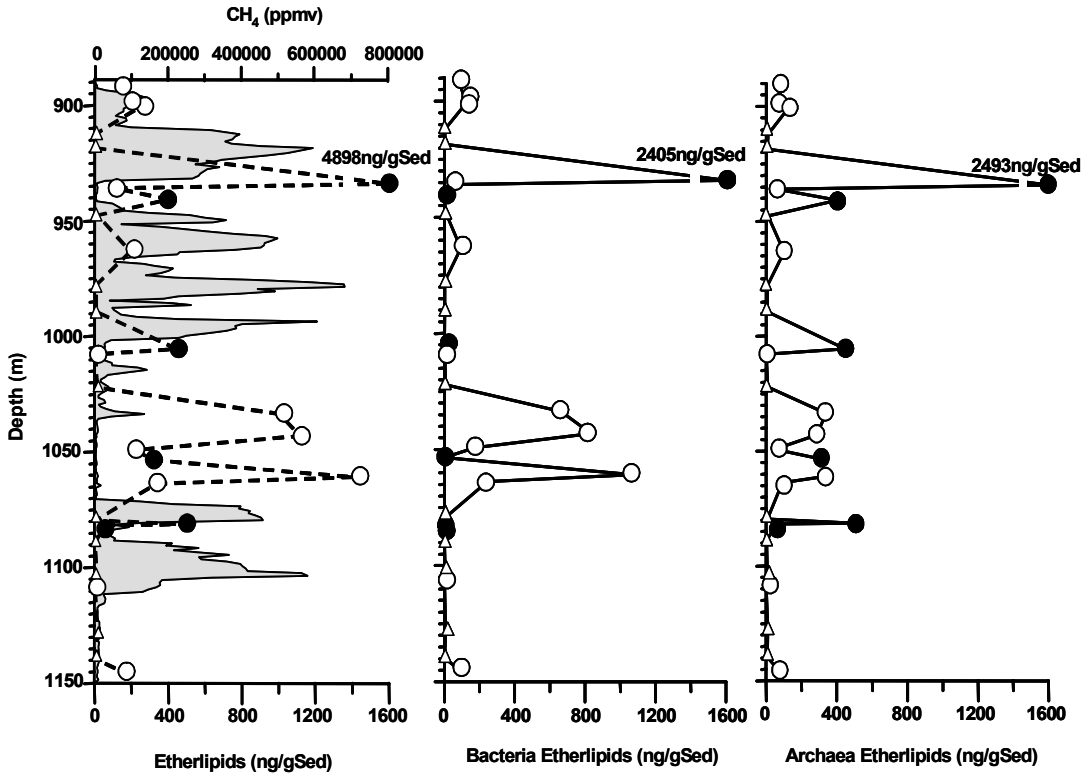

Figure 9.10: Depth profile of the sum of dialkyl glycerol ethers (archaea) and glycerol dialkyl glycerol tetraethers (bacteria) detected in the Mallik samples compared to the methanecontent (grey shaded area) of the cored Mallik sediments representing gas hydratebearing layers (data from Dallimore et al. (2005a)). Black dots: lignites, triangles: sands,circles: silts/clays.

9.4.4 Compound specific $\delta^{13}C$ analysis of microbial biomarkers

The aliphatic fractions of seventeen samples from different lithologies have been analysed to determine their compound-specific $\delta^{13}C$-isotopic composition. The most abundant microbial lipids detected in the aliphatic fractions were the hopanoids. However, compared to other compounds within the aliphatic hydrocarbon fractions the hopanoid biomarker signal is relatively small, which makes the evaluation of the isotopic carbon composition of single hopanoids difficult. The most abundant hopanoid in all Mallik samples is the hop-17(21)-ene, an indicator for relative immature microbial biomass. Therefore, its isotopic carbon values could be determined in all samples investigated.

The $\delta^{13}C$-values obtained for the hop-17(21)-enes range from -26.7 to -49.6‰ with an average value of -36.7‰ (Table 9.5). In comparison, the $\delta^{13}C$-ratio for other compounds such as diterpenoic, and non-hopanoic triterpenoic hydrocarbons occurring in the aliphatic fraction, representing terrestrial organic material, reveal values from -21.3 to -30.5‰ with an average value of -26.5‰, the *n*-alkanes show an average value of -30.4‰ (Table 9.5). Thus, the hop-17(21)-enes are in average depleted in ^{13}C by more than 8‰ in comparison to the

Table 9.5: Compound specific $\delta^{13}C$ data of *n*-alkanes, di- and triterpenoids and hopanoids from selected samples. grey shaded = silt/clay, dark grey shaded = lignite.

Samples	*n*-C_{16}	*n*-C_{17}	*n*-C_{18}	*n*-C_{19}	Isonorpimarane	Norpimarane	Norabietane	*n*-C_{20}	Isopimarane	α-Phyllocladane	*n*-C_{21}	*n*-C_{22}	*n*-C_{23}	*n*-C_{24}
MB89163	-27.1	-28.2	-28.9	-30.4							-23.5	-28.8	-29.8	-24.9
MB89899	-30.3	-25.6	-30.4	-23.7			-21.3	-27.9		-37.0	-28.3	-29.1	-29.5	-30.1
MB90020	-29.8	-30.5	-20.2	-26.4				-27.8			-28.2	-32.0	-29.7	-31.9
CO93409	-30.1	-31.1	-33.9	-29.7	-24.6	-25.1			-24.7	-27.2	-29.3	-29.4	-29.5	-32.9
MB93589	-30.4	-31.1	-29.6	-28.9				-29.4			-28.3	-32.0	-31.5	-27.2
CO94078	-29.5	-30.8	-28.1	-22.1	-24.3	-24.8	-28.8	-28.5	-26.3	-26.9	-31.2	-31.5	-30.4	-29.9
MB96334	-28.1	-28.5	-17.4	-27.5				-27.7			-24.	-24.7	-25.3	-23.9
CO100550	-30.1	-30.1	-34.1	-31.8	-24.5	-26.8		-19.6	-23.8	-24.4	-30.4	-28.9	-29.8	-24.3
MB103360	-31.5	-29.2	-31.2	-39.3			-26.9	-26.7			-30.1	-32.7	-30.6	-32.1
CO104310	-30.1	-33.1	-26.8	-30.9			-22.5		-32.9	-27.9	-30.5	-33.1	-28.3	-24.4
MB104920	-29.9	-28.3	-28.7	-29.5				-29.6			-32.3	-31.8	-30.4	-30.8
CO105353	-29.7	-30.2	-31.7		-29.1				-23.3	-26.0	-35.9	-34.7	-18.8	-22.1
MB106380	-31.5	-31.6	-31.3	-30.3				-31.1			-31.9	-29.9	-31.5	-31.1
CO108138	-31.6	-30.7	-34.0	-29.4		-27.3	-38.9	-28.5	-29.3	-27.3	-30.8	-32.7	-30.0	-29.9
CO110550														
MB114535														

Samples	*n*-C_{25}	*n*-C_{26}	*n*-C_{27}	*n*-C_{28}	*n*-C_{29}	*n*-C_{30}	Olean-12-ene	Hop-17(21)-ene	*n*-C_{31}	*n*-C_{32}	17(H)β,21β(H)–*nor*-hopane	*n*-C_{33}	17β(H),21β(H)-*homo*-hopane	*n*-C_{35}
MB89163	-28.3	-30.4	-24.0	-29.9	-29.8									
MB89899	-30.2	-28.7	-29.4	-32.2	-33.2	-33.5		-37.9	-41.2		-32.7	-31.7		-32.9
MB90020	-29.1	-31.8	-28.9	-30.7	-29.6	-25.4		-36.4	-35.2		-46.4	-34.6		
CO93409	-30.8	-39.5	-23.4		-29.9		-26.5	-36.5	-27.8		-20.4	-28.1		
MB93589	-31.1	-26.2	-31.2	-30.2	-31.8	-33.1		-49.6	-36.2		-40.1	-33.6	-39.9	
CO94078	-30.1	-27.9	-31.1	-29.5	-31.2	-30.3	-26.5	-31.3	-30.1			-32.6	-35.1	
MB96334	-27.1	-25.7	-31.7	-34.7	-30.1	-25.8		-36.4	-36.9		-39.2	-35.1		
CO100550	-30.7	-36.4	-25.6	-51.2	-33.2	-23.7	-28.8	-26.5	-34.2		-35.9	-32.3		
MB103360	-31.6	-32.1	-34.1		-31.3	-33.2		-43.9	-32.3		-37.1	-35.3	-31.1	-31.9
CO104310	-31.0	-33.0	-33.1	-35.9	-32.4	-34.1		-34.5	-35.8		-34.5	-28.0	-28.2	-32.2
MB104920	-34.0	-31.3	-32.3	-30.6	-27.5	-34.9	-26.6	-30.7	-47.3		-31.8	-29.4	-32.2	-28.8
CO105353	-27.3	-38.3	-36.9	-40.1	-33.0	-40.6		-38.9	-37.9		-34.8	-32.5	-36.4	-30.5
MB106380	-33.0	-36.4	-33.6	-33.4	-33.7	-34.9	-30.1	-40.2	-39.1	-28.5	-35.3	-32.4	-35.9	
CO108138	-28.2	-30.7	-31.3		-32.4	-28.7	-30.6	-38.7	-30.4		-30.9	-28.7	-29.5	
CO110550					-33.9			-32.3	-27.5				-33.3	-33.9
MB114535					-33.9		-33.7	-37.4	-29.6					

terrestrial biomarker signal. Other microbial lipids like the isoprenoids crocetane (2,6,11,15-tetramethylhexadecane) and PMI (2,6,10,15,19-pentamethylicosane) (Thiel et al., 1999b; Zhang et al., 2003) and often observed in the lipid inventory of surface near gas hydrate formations (Zhang et al., 2003) and at submarine gas seeps (Hinrichs et al., 2000; Thiel et al., 2001; Thiel et al., 1999b) were not detected in the very deep gas hydrate bearing sediments of the Mallik Site.

The phospholipid contents within the Mallik samples were abundant enough to be detected by HPLC-ESI-MS; however, they were too small to obtain sufficient fatty acid material after alkaline hydrolytic cleavage of the PLs to determine the isotopic carbon values of the liberated phospholipid fatty acids (PLFA). Concerning the PL analysis it would have been desirable to get more sample material for the lipid extraction.

9.5 Discussion

9.5.1 Occurrence of microbial biomass in the Mallik sediments

Four main groups of hopanoids were detected in the Mallik samples: hopenes, hopanes, hopanoic acids and hopanoic alcohols. The saturated hopanoids occurred in two main configurations at the C-17 and C-21 position: the 17β(H),21β(H) und the 17α(H),21β(H)-configuration. The 17β(H),21β(H)-configuration can be found in living microorganisms and consequently was thought to be the biogenic form (van Dorsselaer et al., 1974). Therefore, together with unsaturated hopanes (hopenes), the presence of hopanes in their biogenic 17β(H),21β(H)-form points to a high proportion of immature microbial biomass in the studied samples from the deep subsurface of the Mallik site.

Hopanoids in the 17α(H),21β(H)-configuration were considered to be characteristic for an enhanced maturity and are usually found in oil samples. However, it has been proven that such hopanoids with the "geological" configuration occur already during the first stages of diagenesis. For example, in recent peat samples, Quirk et al. (1984) found high proportion of (22R)-17α(H),21β(H)-*homo*-hopane which they explain with bacterial decay of plant matter in a very early stage of diagenesis and they assumed that *dihomo*-hopanoic acids occurring in peat samples, are originated from oxidative cleavage (microbial or abiotic) of bacteriohopane precursor polyols with 35 carbon atoms. Thiel et al. (2003) demonstrate clearly that the 17α(H),21β(H)-hopanoids can also be generated biologically. They proved the occurrence of (22R)-*dihomo*-hopanoic acids (C_{32}) in their "geological" 17α(H),21β(H)-configuration in

living anaerobic microbial mats at methane seeps in the Black Sea. Therefore, if not the typical oil-type hopanoid distribution (17α(H),21β(H)-C_{27}, C_{29}-C_{35} with S and R epimers from C_{31} to C_{35}) can be observed, it can be suggested that α,β configured hopanoids (mainly with 31 carbon atoms) also represent immature microbial biomass.

Furthermore, Thiel et al. (2003) showed that the 17α(H),21β(H)-hopanoids can not only be generated biologically but also in a strictly anaerobic environment. These results are approved by the finding of hopanoids in other strictly anaerobic microorganisms (Härtner et al., 2005; Sinninghe Damsté et al., 2004). In addition to the Mallik Site, we were able to detect the 17α(H),21β(H)-C_{31}-hopanes together with 17β(H),21β(H)-hopanes and hopenes in several deeper sedimentary systems in marine sediments e.g. offshore Ireland (IODP-Integrated Ocean Drilling Program Leg 307) and terrestrial sediments e.g. on the North Island of New Zealand (DEBITS-Deep Biosphere in Terrestrial Systems-Project) indicating that this biomarkers are widely spread in deeper sedimentary successions on Earth. All these results give indication that the hopanoic signal in deeper sediments can also be the biomarker signal of living deep microbial populations and not only the remnants of surface microorganisms preserved and subsided to deeper depth during sedimentation or at least it could be a mixture of both sources.

An indication for the existence of viable deep microbial populations in the Mallik sediments is provided by the finding of intact phospholipids acting as “life” markers in several samples. The composition of phospholipids observed in the studied samples corresponds to the pattern known to occur in microorganisms (e.g. Ratledge & Wilkinson, 1988). In the Mallik samples, PGs and PEs were detected with the PGs being the major phospholipids group. Recently, Mangelsdorf et al. (2005b) analysed the phospholipids composition of piezosensitive bacteria isolated from deep subsurface marine sediments and cultivated under different pressure conditions. They could demonstrate that in the culture grown under higher pressure the percentage of PGs increases relative to the PEs. This observation in the phospholipids composition was interpreted as a restructuring of the cell membrane to withstand higher pressure conditions and to maintain the cell membrane fluidity. The higher proportion of PGs in the Mallik samples might, therefore, be an expression for the higher pressure conditions in the deep sediments of the Mallik Site (890-1150m).

The finding of the LPGs and glycerol ethers is interesting, because it is known that glycerolether occur in archaeal biomass (Chappe & Albrecht, 1982; Chappe et al., 1979; Nichols et al., 1993; Tornabene & Langworthy, 1979; Tornabene et al., 1978). In particular the detection of ethers in methanotrophic archaea (Kates, 1997) is of interest for the investigation of the

deep biosphere in the Mallik area. If the LPGs and GDGTs detected in the samples are constituents of methanotrophic archaea, their detection supports the results of Colwell et al. (2005) and Jain et al. (2005), which shown already the existence of archaea and methane consuming microorganisms in sediments of the Mallik 5L-38 well. In addition it could be assumed that the methane trapped in the gas hydrates is used as energy source from these archaea.

9.5.2 Possible carbon and energy sources

An intriguing question investigating deep microbial ecosystems is which feedstock microorganisms can use as a carbon and energy source in their, from a surface perspective, inhospitable life habitat. In the Mallik Site the gas hydrate formation represents a natural collector or concentrator of biochemicals in a depth where, with exception of several distinct lignite layers, other potential substrates are relatively low. Free hydrocarbon gases especially methane associated to gas hydrates and gas seeps are recognized to be important carbon and energy sources for microorganisms in marine settings via methanotrophic processes (e.g. Hinrichs et al., 1999; Wellsbury et al., 2000). In marine environments it is thought that anaerobic oxidation of methane was mediated by aggregates consisting of archaea, which were able to reverse the process of methanogenesis (Iversen & Joergensen, 1985; Zehnder & Brock, 1979;1980), and sulphate-reducing bacteria (Boetius et al., 2000). Thus, the specific attraction for studying microbial life in the Mallik sediments was whether gas hydrates, obviously stimulating microbial life in surface near marine sediments (Boetius et al., 2000; Boetius & Suess, 2004; Cragg et al., 1996; Elvert et al., 2000; Hinrichs et al., 1999; Hinrichs et al., 2000; Wellsbury et al., 2000; Zhang & Lanoil, 2004; Zhang et al., 2003) could also stimulate an enhanced microbial life in deep terrestrial sediments.

It is obvious from Figure 9.6 that the contents of methane and with that the occurrence of gas hydrates proceeds in an opposite trend to the record of the sum of the hopanoids related to the total organic carbon content. Also the distribution of the glycerol ether lipids shows an opposite trend to the methane contents (Figure 9.10). Wellsbury et al. (2000) and Lanoil et al. (2001) showed that methane hydrates themselves not harbour many microorganisms. Hence, the observation that in strata containing less methane, a higher proportion of the organic matter is of microbial origin corresponds to these results. Additionally, Wellsbury et al. (2000) and Valentine (2002) show that microbial life is stimulated in the vicinity or transition from the gas hydrate to the surrounding sediments where most likely free gas occurs. Interestingly, the only two sand samples gathered from a transition (MB110494, MB107960) contain, com-

pared to the other samples, unusual high proportions of microbial biomass, maybe indicating a stimulation of microbial life at this horizon. In samples MB107960 also phospholipids were detected. However, this is not to say that the hopanoids are part of the biomass of a methanotrophic consortium using the transitional free gas as a substrate source, but they might be part of microbial communities living on the waste products or biomass of microorganisms consuming the methane. The carbon isotopic investigation of the hop-17(21)-ene might give an indication for this assumption. The isotopic data vary from -26.7 to -49.6‰ and might resemble a mixture between a heavier and a lighter carbon source. Data around -30‰ might represent a higher proportion of the heavier terrestrial organic matter while data around -40‰ or ligther could indicate a higher proportion from biomass of microorganisms involved in methanotrophic process.

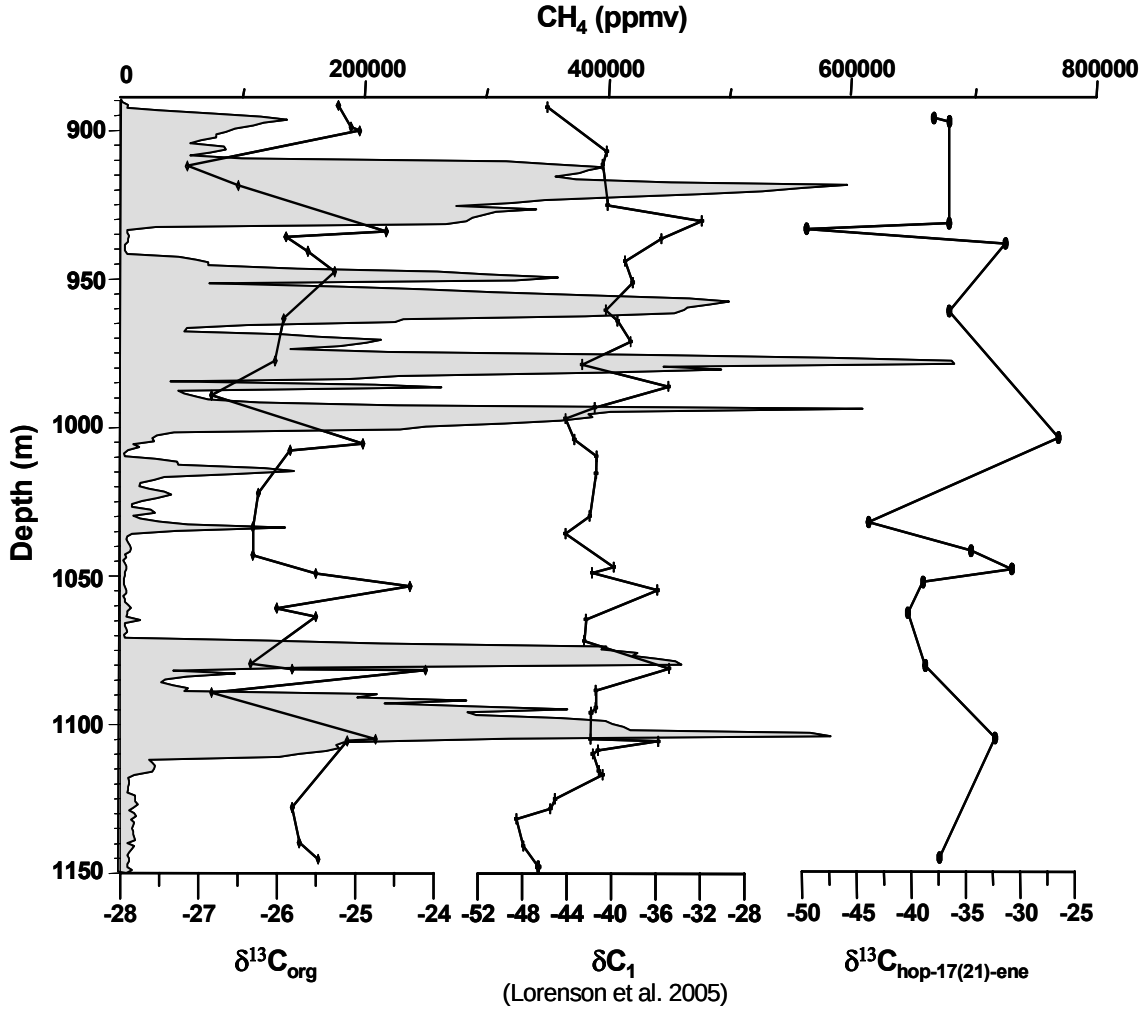

Figure 9.11: Depth profile of the carbon isotopic signal of the total organic matter, the core methane (Lorenson et al., 2005) and of hop-17(21)-ene relative to the methane content (grey shaded area) of the cored Mallik sediments representing gas hydrate bearing layers (data from Dallimore et al. (2005a)). Black dots: lignites, triangles: sands, circles: silts/clays.

Overall the microbial biomarker signal in the Mallik samples is relatively small and seems to represent the typical small abundance of deep microbial populations. Especially, the PL signals in the Mallik samples are in general not very abundant and only in a limited number of samples phospholipids are above the detection limit. This must not necessarily mean that microbial life is absent in the other samples. It could also mean that the applied method might have reached it sensitivity limit. If available, higher amounts of sample material should be taken and extracted in future studies for the phospholipid investigations. Although some isotopically lighter biomarkers were detected indicating a process where gas hydrates may be involved, there is no real indication that an intense anaerobic oxidation of methane (AOM) as observed in marine gas hydrates (Boetius et al., 2000; Hinrichs et al., 1999) takes place in the Mallik sediments. Thus, deep microbial organisms, suggested to keep viable under low metabolic rates, appear not to be stimulated by the huge carbon pool represented by the gas hydrates in the deep sediments of the Mallik site as known from marine sediments.

These findings from the molecular biogeochemical investigations are confirmed by the results provided from microbiological investigations of sediment material from the Mallik 5L-38 Gas Hydrate Production Research well. Colwell et al. (2005) detected small quantities of archaea and low methanogenic activities in the deep sediments of the Mallik well and Jain et al. (2005) also pointed out that the Mallik sediments contain only low contents of methane producing and consuming microorganisms.

In the deep subsurface in the Mallik area all conditions assumed to be needed for the existence of microbial life such as nutrients (organic carbon, methane), terminal electron acceptors (e.g. sulphate (Chen et al., 2005; Dallimore et al., 2005a; Tomaru et al., 2005)), water, low temperatures were available. Therefore, for the reasons why marine surface near gas hydrates stimulates microbial activity and deep terrestrial gas hydrates not we can only speculate at this time.

9.6 Conclusions

Thirty sediment samples from the Mallik 5L-38 Gas Hydrate Production Research Well have been investigated using organic geochemical methods to proof the existence of microbial communities in the deep subsurface in the Mallik area. The presence of microbial biomarkers like hopanoids and glycerol etherlipids in the samples points to a widely disseminated microbial biomass. The finding of intact phospholipids (PEs, PGs) even suggests evidence of the occurrence of a viable microbial ecosystem. However it seems that there are important differences concerning their dispersion between the microbial communities in the terrestrial deep

subsurface and with those –already better known- occurring in the deep subsurface in oceanic sediments. Admittedly, the feeding processes in the terrestrial deep subsurface are not comparable to those in marine settings and not yet well understood.

9.7 Acknowledgment

We acknowledge the international partnership that undertook the Mallik 2002 Gas Hydrate Production Research Well Program: the Geological Survey of Canada (GSC), Japan National Oil Corporation (JNOC), GeoForschungsZentrum Potsdam (GFZ), U.S. Geological Survey (USGS), U.S. Department of Energy (USDOE), India Ministry of Petroleum and Natural Gas (MOPNG)/Gas Authority of India (Gail), and the Chevron-British Petroleum-Burlington joint venture group. The program received financial support from the International Continental Scientific Drilling Program.

Also, we would like to thank M. Gabriel, C. Karger, T. Mohr, I. Schindelwig, A. Sobotta and A. Vieth for technical support. The study was funded by the Deutsche Forschungsgemeinschaft (DFG), grant no. Ma 2470/1.

10 Conclusions

For the current study, sediments samples of the JAPEX/JNOC/GSC et al. Mallik 5L-38 Gas Hydrate Production Research Well, located at the northern edge of the Mackenzie River Delta, Northwest Territories, Canada, were investigated using organic-geochemical methods. The well penetrates a succession of Cenozoic sediments (sand- and siltstones, clays and lignites) of about 1166 m and includes a massive permafrost zone in the upper ca. 600 m and a zone of numerous gas hydrate bearing layers from about 896 to 1100 m, the so-called gas hydrate zone. Above, within and below this gas hydrate zone 30 core samples have been collected from the different lithologies.

In addition to the characterisation of the origin and nature of the organic matter embedded in the sediments at the Mallik site the main goal of this study was to elucidate the occurrence and nature of deep microbial ecosystems in the well and to investigate whether there is any interaction between the gas hydrates and a deep biosphere (formation or consumption of methane) as known from surface near marine gas hydrate formations. Both the chemical and isotopic compositions of individual biomarkers were employed to identify the sources of organic matter detritus and the type of living biomass.

Characteristics of the organic matter

The TOC values of the samples vary with the lithology between less than 1 to more than 40% (sandstones: 0.04-1.57%, clay samples: up to 7.09%, lignites: 9.4-46.6%). The immaturity and the terrestrial origin of the organic matter in the investigated samples has been proven by the Rock-Eval-parameters (i.e. hydrogen index (HI), oxygen index (OI) and T_{max}), the open-system pyrolysis-GC experiments, the $\delta^{13}C_{org}$ data and the maceral analysis.

The molecular lipid analysis confirmed the results of the bulk organic geochemical investigations. The distribution of the *n*-alkanes with an odd-over-even carbon number predominance and a maximum in the range of *n*-C_{29} to *n*-C_{31} in the lignite and silt/clay samples is typical for immature land plant material. The second *n*-alkane maximum at *n*-C_{23} in the lignite samples indicates the presence the moss plant *Sphagnum*, a main constituent of raised bogs, during the sedimentation of these layers. The organic carbon poor sandy sample material reveals only few and small biomarker signals. In contrast to all other samples, they show the maximum of *n*-alkanes in the range of *n*-C_{15} to *n*-C_{17} with no odd-over-even carbon number predominance. This suggests an allochthonous supply of crude oil or erosion of uplifted source rock transported by the river from the hinterland. In the organic carbon rich silt/clay and lignite samples

this mature hydrocarbon signal may be overprinted by the organic matter of the surrounding vegetation.

More detailed information about the plant communities contributing to the sedimentary organic matter are provided by terpenoids. The predominance of diterpenoids points to a major influence of gymnosperms at the Mallik site during the formation of the lignites with a minor supply of angiosperms markers. The terpenoic hydrocarbon biomarkers were detected although in lower abundance in the silt/clay samples from the Mallik well, but were almost absent in the sand samples. However, the clay samples contain more triterpenoids than diterpenoids. This suggests a change in the plant community to a more angiosperms in comparison to the lignites. Whereas the material in the lignites is from autochthonous origin from higher land plant growing in the delta area, the clastic lithologies (clays and sandstones) transported also plant material from the hinterland. Hence, the signals from the climatic conditions in the delta area are overprinted with signals from the river watershed. Therefore, the interpretation of vegetational variations in terms of paleoclimatic changes is complicated in a delta system, partiaculary is it known that the preservation of plant material in a delta system is related to the different sites of deposition such as channels, levees, floodplains and swamps. Both, paleoclimatic changes influencing the paleovegetation and the dislocation of the river channels in a meandering river system may have supported the formation of different litholocigal successions with different paleovegetational compositions.

Characteristics of the microbial ecosystem

For the occurrence of microbial biomass in the Mallik sediments first indications are given by the hopanoic compounds. Hopanoids were found in significant amounts in almost all sediment samples investigated indicating a widely disseminated microbial biomass in the deep sediments of the Mallik site. Hopenes and hopanes in their biogenic 17β(H),21β(H) configuration confirm, thereby, the immature character of the microbial biomass. In addition, the C_{30}- and C_{31}-hopanes are also present in their most stable 17α,21β configuration which is usually regarded as the mature form. However, the absence of other elongated hopanoids in the "geological form" suggests that these hopanoids are also biomarkers from immature microbial biomass rather than from mature geologically altered organic matter.

Even if hopanoids are mainly related to various aerobic bacteria, they also occur in anaerobic bacteria. Thus, the hopanoids detected in the Mallik sediments may also originate from indigenous yet unknown anaerobic bacteria. However, it can not be excluded that hopanoids are

part of the embedded organic matter and therefore, they are not unequivocally biomarkers for living microbial biomass.

For the detection of viable microbial communities of the deep biosphere phospholipids (PLs) were used as target molecules due to their rapid degradation after cell. The indigenous PL ester signals are in general low and often near the detection limit. The low abundance of PL ester may indicate that a larger amount of sediment has to be sampled and extracted in future to be well above the detection limit. Nevertheless, in four samples the presence of phosphatidylglycerols and phosphatidylethanolamines are proved.

Additionally, a series of specific compound signals are detectable in almost all samples investigated, which are probably lyso-phosphatidylglycerols ethers. The finding of lyso-phosphatidylglycerols may point to a microbial community of archaea (methanogens or methanotrophs) in the deep subsurface of the Mallik site. These interpretations are supported by the detection of dialkyl glycerol ethers and glycerol dialkyl glycerol tetraethers known as membrane constituents of archaea. Thus, there are molecular indications for the existence of a deep biosphere at the Mallik site. However, the low abundance of these molecular indicators suggests only minor importance of this deep biosphere for the formation of the Mallik gas hydrate.

The $\delta^{13}C$-signal can also be used to identify whether the Mallik gas hydrate is used as a carbon source by deep microbial communities. Due to the isotopic fractionation during biosynthesis microorganisms, participating in this methanotrophic process, consist of biomarkers with a very light isotopic carbon signal (about < -70‰). However, biomarkers with such very low $\delta^{13}C$-signals could not be detected in the Mallik sediments. Although some extremely lighter isotopic values of indicators for bacterial biomass might indicate a process where gas hydrates may be involved, there is no real indication that an intense anaerobic oxidation of methane (AOM) as known from marine gas hydrates takes place in the Mallik sediments. Thus, deep microbial organisms, suggested to keep viable under low metabolic rates, appear not to be stimulated by the huge carbon pool represented by the gas hydrates in the deep sediments of the Mallik site as known from marine sediments.

11 References

Abraham, W.-R., Hesse, C., Pelz, O., 1998. Ratios of carbon isotopes in microbial lipids as an indicator of substrate usage. Applied and Environmental Microbiology, 64, 4202-4209.

Alexander, G., Hazai, I., Grimalt, J.O., Albaiges, J., 1987. Occurrence and transformation of phyllocladanes in brown coals from Nograd Basin, Hungary. Geochimica et Cosmochimica Acta, 51, 2065-2073.

Alexander, R., Bastow, T.P., Fisher, S.J., Kagi, R.I., 1995. Geosynthesis of organic compounds; II, Methylation of phenanthrene and alkylphenanthrenes. Geochimica et Cosmochimica Acta, 59, 4259-4266.

Alexander, R., Kagi, R.I., Rowland, S.J., Sheppard, P.N., Chirila, T.V., 1985. The effects of thermal maturity on distributions of dimethylnaphthalenes and trimethylnaphthalenes in some ancient sediments and petroleums. Geochimica et Cosmochimica Acta, 49, 385-395.

Aries, E., Doumenq, P., Artaud, J., Molinet, J., Bertrand, J.C., 2001. Occurrence of fatty acids linked to non-phospholipid compounds in the polar fraction of a marine sedimentary extract from Carteau Cove, France. Organic Geochemistry, 32, 193-197.

Audino, M., Grice, K., Alexander, R., Boreham, C.J., Kagi, R.I., 2001. Unusual distribution of monomethylalkanes in Botryococcus braunii-rich samples; origin and significance. Geochimica et Cosmochimica Acta, 65, 1995-2006.

Baas, M., Pancost, R., van Geel, B., Sinninghe Damsté, J.S., 2000. A comparative study of lipids in *Sphagnum* species. Organic Geochemistry, 31, 535-541.

Barrick, R.C., Hedges, J.I., 1981. Hydrocarbon geochemistry of the Puget Sound region; Sedimentary diterpenoid, steroid and triterpenoid hydrocarbons. Geochimica et Cosmochimica Acta, 45, 381-392.

Bastow, T.P., Singh, R.K., van Aarssen, B.G.K., Alexander, R., Kagi, R.I., 2001. 2-methylretene in sedimentary material; a new higher plant biomarker, Selected papers from the 2000 Australian organic geochemistry conference, 32; 10, pp. 1211-1217. Pergamon, Oxford-New York, International.

Bechtel, A., Gruber, W., Sachsenhofer, R.F., Gratzer, R., Puettmann, W., 2001. Organic geochemical and stable carbon isotopic investigation of coals formed in low-lying and raised mires within the Eastern Alps (Austria). Organic Geochemistry, 32, 1289-1310.

Bechtel, A., Sachsenhofer, R.F., Kolcon, I., Gratzer, R., Otto, A., Puttmann, W., 2002. Organic geochemistry of the lower Miocene Oberdorf Lignite (Styrian Basin, Austria); its relation to petrography, palynology and the palaeoenvironment. International Journal of Coal Geology, 51, 31-57.

Bishnoi, P.R., Natarajan, V., 1996. Formation and decompostion of gas hydrates. Fluid Phase Equilibria, 117, 168-177.

Bligh, E.G., Dyer, W.J., 1959. A rapid method of total lipid extraction and purification. Canadian Journal of Biochemistry and Physiology, 37, 911-917.

Blöchl, E., Rachel, R., Burggraf, S., Hafenbradl, D., Jannasch, H.W., Stetter, K.O., 1997. *Pyrolobus fumarii*, gen. and sp. nov., represents a novel group of archaea, extending the upper temperature limit for life to 113°C. Extremophiles, 1, 14-21.

Boetius, A., Ravenschlag, K., Schubert, C.J., Rickert, D., Widdel, F., Gieseke, A., Amann, R., Jorgensen, B.B., Witte, U., Pfannkuche, O., 2000. A marine microbial consortium apparently mediating anaerobic oxidation of methane. Nature, 407, 623-626.

Boetius, A., Suess, E., 2004. Hydrate Ridge: a natural laboratory for the study of microbial life fueled by methane from near-surface gas hydrates. Chemical Geology, 205, 291-310.

Boivin-Jahns, V., Ruimy, R., Bianchi, A., Daumas, S., Christen, R., 1996. Bacterial diversity in a deep-subsurface clay environment. Applied and Environmental Microbiology, 62, 3405-3412.

Boschker, H.T.S., Nold, S.C., Wellsbury, P., Bos, D., de Graaf, W., Pel, R., Parkes, R.J., Cappenberg, T.E., 1998. Direct linking of microbial populations to specific biogeochemical processes by (super 13) C-labelling of biomarkers. Nature, 392, 801-804.

Bray, E.E., Evans, E.D., 1961. Distribution of *n*-paraffins as a clue to recognition of source beds. Geochimica et Cosmochimica Acta, 22, 2-15.

Budzinski, H., Garrigues, P., Connan, J., Devillers, J., Domine, D., Radke, M., Oudin, J.L., 1995. Alkylated phenanthrene distributions as maturity and origin indicators in crude oils and rock extracts. Geochimica et Cosmochimica Acta, 59, 2043-2056.

Burnham, R.J., 1989. Relationships between standing vegetation and leaf litter in a paratropical forest; implications for paleobotany. Review of Palaeobotany and Palynology, 58, 5-32.

Chaffee, A.L., Fookes, C.J.R., 1988. Polycyclic aromatic hydrocarbons in Australian coals - III. Structural elucidation by proton nuclear magnetic resonance spectroscopy. Organic Geochemistry, 12, 261-271.

Chaffee, A.L., Hoover, D.S., Johns, R.B., Schweighardt, F.K., 1986. Biological markers extractable from coal. In: R.B. Johns (Ed.), Biological markers in the sedimentary record, 24 (Ed. by R.B. Johns), pp. 311-345. Elsevier, Amsterdam.

Chaffee, A.L., Johns, R.B., 1983. Polycyclic aromatic hydrocarbons in Australian coals. I. Angularly fused pentacyclic tri- and tetraaromatic components of Victorian brown coal. Geochimica et Cosmochimica Acta, 47, 2141-2155.

Chappe, B., Albrecht, P., 1982. Polar lipids of archaebacteria in sediments and petroleums. Science, 217, 65-66.

Chappe, B., Michaelis, W., Albrecht, P., Ourisson, G., 1979. Fossil evidence for a novel series of archaebacterial lipids. Naturwissenschaften, 66, 522-523.

Chen, Y.F., Matsumoto, R., Tomaru, H., Anton, D., 2005. Organic carbon, nitrogen, sulphur, and $\delta^{34}S$ compositions of pyrite and pore waters in the JAPEX/JNOC/GSC et al. Mallik 5L-38 gas hydrate production research well. In: S.R. Dallimore, T.S. Collett (Eds.), Scientific Results from Mallik 2002 Gas Hydrate Production Research Well Program, Mackenzie Delta, Northwest Territories, Canada, Bulletin 585 (Ed. by S.R. Dallimore, T.S. Collett). Geological Survey of Canada.

Cole, M.J., Enke, C.G., 1991. Direct determination of phospholipid structures in microorganisms by fast atom bombardment triple quadropole mass spectrometry. Analytical Chemistry, 63, 1032-1038.

Collett, T.S., Lee, M.W., 2005. Electrical-resistivity well-log analysis of gas hydrate saturations in the JAPEX/JNOC/GSC et al Mallik 5L-38gas hydrate production research well. In: S.R. Dallimore, T.S. Collett (Eds.), Scientific Results from Mallik 2002 Gas Hydrate Production Research Well Program, Mackenzie Delta, Northwest Territories, Canada, Bulletin 585 (Ed. by S.R. Dallimore, T.S. Collett). Geological Survey of Canada.

Colwell, F.S., Delwiche, M.E., Blackwelder, D., Wilson, M.S., Lehman, R.M., Uchida, T., 1999. Microbial communities from core intervals, JAPEX/ JNOC/ GSC Mallik 2L-38 gas hydrate research well. In: S.R. Dallimore, T. Uchida, T.S. Collett (Eds.), Scientific results from JAPEX/ JNOC/ GSC Mallik 2L-38 gas hydrate research well, Mackenzie Delta, Northwest Territories, Canada (Ed. by S.R. Dallimore, T. Uchida, T.S. Collett), pp. 189-195. Geological Survey of Canada, Ottawa, ON, Canada.

Colwell, F.S., Nunoura, T., Delwiche, M.E., Boyd, S., Bolton, R., Reed, D.W., Takai, K., Lehmann, R.M., Horikoshi, K., Elias, D.A., Phelps, T.J., 2005. Evidence of minimal methanogenic numbers and activity in sediments collected from the JAPEX/JNOC/GSC et al. Mallik 5L-38 gas hydrate production research well. In: S.R. Dallimore, T.S. Collett (Eds.), Scientific Results from Mallik 2002 Gas Hydrate Production Research Well Program, Mackenzie Delta, Northwest Territories, Canada, Bulletin 585 (Ed. by S.R. Dallimore, T.S. Collett). Geological Survey of Canada.

Corrigan, D., Kloos, C., O'Connor, C.S., Timoney, R.F., 1973. Alkanes from four types of *Sphagnum* moss. Phytochemistry, 12, 213-214.

Cowen, J.P., Giovannoni, S.J., Kenig, F., Johnson, H.P., Butterfield, D., Rappe, M.S., Hutnak, M., Lam, P., 2003. Fluids from aging ocean crust that support microbial life. Science, 299, 120-123.

Cragg, B.A., Parkes, R.J., Fry, J.C., Weightman, A.J., Rochelle, P.A., Maxwell, J.R., 1996. Bacterial populations and processes in sediments containing gas hydrates (ODP Leg 146; Cascadia margin), Seismic indications of gas hydrates in continental margins, 139; 3-4, pp. 497-507. Elsevier, Amsterdam, Netherlands.

Cranwell, P.A., 1973. Branched-chain and cyclopropanoid acids in a recent sediment. Chemical Geology, 11, 307-313.

Curry, D.J., Simpler, T.K., 1988. Isoprenoid constituents in kerogens as a function of depositional environment and catagenesis. Organic geochemistry, 13, 995-1001.

Cvejic, J.H., Bodrossy, L., Kovacs, K.L., Rohmer, M., 2000. Bacterial triterpenoids of the hopane series from the methanotrophic bacteria Methylocaldum spp.: phylogenetic implications and first evidence for an unsaturated aminobacteriohopanepolyol. FEMS Microbiology Letters, 182, 361-365.

Dachs, J., Bayona, J.M., Fowler, S.W., Miquel, J.C., Albaiges, J., 1998. Evidence for cyanobacterial inputs and heterotrophic alteration of lipids in sinking particles in the Alboran Sea (SW Mediterranean). Marine Chemistry, 60, 189-201.

Dallimore, S.R., Collett, T.S., 1999. Regional gas hydrate occurrences, permafrost conditions, and Cenozoic geology, Mackenzie Delta area, Scientific results from JAPEX/ JNOC/ GSC Mallik 2L-38 gas hydrate research well, Mackenzie Delta, Northwest Territories, Canada, pp. 31-43. Geological Survey of Canada, Ottawa, ON, Canada.

Dallimore, S.R., Collett, T.S., 2005. Summary and implications of the Mallik 2002 Gas HydrateProduction Research Well Program. In: S.R. Dallimore, T.S. Collett (Eds.), Scientific Results from Mallik 2002 Gas Hydrate Production Research Well Program, Mackenzie Delta, Northwest Territories, Canada, Bulletin 585 (Ed. by S.R. Dallimore, T.S. Collett). Geological Survey of Canada.

Dallimore, S.R., Collett, T.S., Uchida, T., 1999. Overview of science program, JAPEX/ JNOC/ GSC Mallik 2L-38 gas hydrate research well, Scientific results from JAPEX/ JNOC/ GSC Mallik 2L-38 gas hydrate research well, Mackenzie Delta, Northwest Territories, Canada, pp. 11-17. Geological Survey of Canada, Ottawa, ON, Canada.

Dallimore, S.R., Medioli, B.E., Laframboise, R.R., Giroux, D.c., 2005a. Mallik 2002 Gas Hydrate Production Research Well Program, Mackenzie Delta, Northwest Territories: well data and interactive data viewer; Appendix A. In: S.R. Dallimore, T.S. Collett (Eds.), Scientific Results from the Mallik 2002 Gas Hydrate Production Research Well Program, Mackenzie Delta, Northwest Territories, Canada, Bulletin 585 (Ed. by S.R. Dallimore, T.S. Collett). Geological Survey of Canada.

Dallimore, S.R., Taylor, A.E., Wright, J.F., Nixon, F.M., Collett, T.S., Uchida, T., 2005b. Overview of the coring program for the JAPEX/JNOC/GSC et al. Mallik 5L-38 gas hydrate production research well. In: S.R. Dallimore, T.S. Collett (Eds.), Scientific Results from Mallik 2002 Gas Hydrate Production Research Well Program, Mackenzie Delta, Northwest Territories, Canada, Bulletin 585 (Ed. by S.R. Dallimore, T.S. Collett). Geological Survey of Canada.

De Rosa, M., Gambacorta, A., Minale, L., Bu'Lock, J.D., 1971. Bacterial triterpanes. Journal of Chemical Society, Chemical Communications, 2, 619-620.

Dickens, G.R., 2001. Modeling the global carbon cycle with a gas hydrate capacitor: Significance for the Latest Paleocene Thermal Maximum. In: C.K. Paull, W.P. Dilloan (Eds.), Natural Gas Hydrates: Occurrence, Distribution, and Detection, Geophysical monograph 124 (Ed. by C.K. Paull, W.P. Dilloan), pp. 19-38. American Geophysical Union.

Dickens, G.R., Castillo, M.M., Walker, J.C.G., 1997. A blast of gas in the latest paleocene; simulating first-order effects of massive dissociation of oceanic methane hydrate. Geology, 25, 259-262.

Diessel, C.F.K., 1992. Coal-bearing depositional systems. Springer-Verlag, Berlin Heidelberg.

Dietrich, J.R., Dixon, J., McNeil, D.H., (1985) Sequence analysis and nomenclature of Upper Cretaceous to Holocene Strata in the Beaufort-Mackenzie Basin, pp. 613-628. Geological Survey of Canada, Ottawa.

Dietrich, J.R., Dixon, J., McNeil, D.H., McIntyre, D.J., Snowdon, L.R., Cameron, A.R., 1989. The geology, biostratigraphy and organic geochemistry of the Natsek E-56 and Edlok N-56 wells, western Beaufort Sea, Frontier Geoscience Program, Arctic Canada - Programme geoscientifique des regions pionnieres, region arctique du Canada, 89-1G, pp. 133-157. Geological Survey of Canada, Ottawa.

Dixon, J., 1986. Cretaceous to Pleistocene stratigraphy and paleogeography, Northern Yukon and Northwestern District of Mackenzie. Bulletin of Canadian Petroleum Geology, 34, 49-70.

Dixon, J., 1996. Depositional facies. In: J. Dixon (Ed.), Geological Atlas of the Beaufort-Mackenzie Area, 59 (Ed. by J. Dixon), pp. 89-98. Geological Survey of Canada, Miscellaneous report, Ottawa, Ontario.

Dixon, J., Dietrich, J., Snowdon, L.R., Morrell, G., McNeil, D.H., 1992a. Geology and petroleum potential of Upper Cretaceous and Tertiary strata, Beaufort-Mackenzie area, Northwest Canada. AAPG Bulletin, 76, 927-947.

Dixon, J., Dietrich, J.R., 1990. Canadian Beaufort Sea and adjacent land areas, The Arctic Ocean region. Geol Soc, Am.

Dixon, J., Dietrich, J.R., McNeil, D.H., 1992b. Upper Cretaceous to Pleistocene sequence stratigraphy of the Beaufort-Mackenzie and Banks Island areas, Northwest Canada. Geological Survey of Canada Bulletin, 407, 90.

Eglinton, G., Hamilton, R.J., 1967. Leaf epicuticular waxes. Science, 156, 1322-1334.

Elvert, M., Suess, E., Greinert, J., Whiticar, M.J., 2000. Archaea mediating anaerobic methane oxidation in deep-sea sediments at cold seeps of the eastern Aleutian subduction zone. Organic Geochemistry, 31, 1175-1187.

Espitalié, J., Laporte, J.L., Madec, M., Marquis, F., Leplat, P., Paulet, J., Boutefeu, A., 1977. Méthode rapide de caractérisation des roches mères, de leur potentiel pétrolier et de leur degré d'évolution. Revue de l'Institut Francais du Petrole et Annales des Combustibles Liquides, 32, 23-42.

Espitalié, J., Marquis, F., Barsony, I., 1984. Geochemical logging. In: K.J. Voorhees (Ed.), Analytical pyrolysis techniques and applications (Ed. by K.J. Voorhees), pp. 276-304. Butterworth and Co., London.

Fang, J., Barcelona, M.J., 1998. Structural determination and quantitative analysis of bacterial phospholipids using liquid chromatography / electrospray ionization / mass spectrometry. Journal of Microbiological Methods, 33, 23-35.

Fang, J., Barcelona, M.J., Alvarez, P.J.J., 2000. A direct comparison between fatty acid analysis and intact phospholipid profiling for microbial identification. Organic Geochemistry, 31, 881-887.

Feinstein, S., Brooks, P.W., Fowler, M.G., Snowdon, L.R., Williams, G.K., 1988. Families of oils and source rocks in the central Mackenzie Corridor; a geochemical oil-oil and oil-source rock correlation, Sequences, stratigraphy, sedimentology; surface and subsurface, 15;, pp. 543-552. Canadian Society of Petroleum Geologists, Calgary, AB, Canada.

Ficken, K.J., Barber, K.E., Eglinton, G., 1998. Lipid biomarker, $\delta^{13}C$ and plant macrofossil stratigraphy of a Scottish montane peat bog over the last two millennia. Organic Geochemistry, 28, 217-237.

Fowler, M.G., Douglas, A.G., 1987. Saturated hydrocarbon biomarkers in oils of late Precambrian age from Eastern Siberia. Organic Geochemistry, 11, 201-213.

Fowler, M.G., Gentzis, T., Goodarzi, F., Foscolos, A.E., 1991. The petroleum potential of some Tertiary lignites from northern Greece as determined using pyrolysis and organic petrological techniques. Organic Geochemistry, 17, 805-826.

Fredrickson, J.K., Onstott, T.C., 1996. Microbes deep inside the Earth. Scientific American, 68-73.

Fröhlich, B., Riederer, M., Tautz, J., 2000. Comb wax discrimination by honeybees tested with the proboscis extension reflex. Journal of experimental Biology, 203, 1581-1587.

Gelpi, E., Schneider, H., Mann, J., Oro, J., 1970. Hydrocarbons of geochemical significance in microscopic algae. Phytochemistry, 9, 603-612.

Gillan, F.T., Stoilov, I.L., Thompson, J.E., Hogg, R.W., Wilkinson, C.R., Djerassi, C., 1988. Fatty acids as biological markers for bacterial symbionts in sponges. Lipids, 23, 1139-1145.

Goodarzi, F., Snowdon, L.R., Gentzis, T., Pearson, D., 1994. Petrological and chemical characteristics of liptinite-rich coals from Alberta, Canada. Marine and Petroleum Geology, 11, 307-319.

Grantham, P.J., Douglas, A.G., 1980. The nature and origin of sesquiterpenoids in some Tertiary fossil resins. Geochimica et Cosmochimica Acta, 44, 1801-1810.

Grantham, P.J., Lijmbach, G.W.M., Posthuma, J., Clarke, M.W.H., Willink, R.J., 1988. Origin of crude oils in Oman. Journal of Petroleum Geology, 11, 61-80.

Green, C.T., Scow, K.M., 2000. Analysis of phospholipid fatty acids (PLFA) to characterize microbial communities in aquifers. Hydrogeology Journal, 8, 126-141.

Haberer, R.M., Mangelsdorf, K., Dieckmann, V., Fuhrmann, A., Wilkes, H., Horsfield, B., 2005. Characterization of the organic matter in lignites of the Kugmallit Formation (Oligocene) at the JAPEX/JNOC/GSC et al. Mallik 5L-38 gas hydrate production research well. In: S.R. Dallimore, T.S. Collett (Eds.), Scientific Results from Mallik 2002

Gas Hydrate Production Research Well Program, Mackenzie Delta, Northwest Territories, Canada, Bulletin 585 (Ed. by S.R. Dallimore, T.S. Collett). Geological Survey of Canada.

Haberer, R.M., Mangelsdorf, K., Wilkes, H., Horsfield, B., in press. Occurrence and paleoenvironmental significance of aromatic hydrocarbon biomarkers in Oligocene sediments from the Mallik 5L-38 Gas Hydrate Production Research Well (Canada). Organic Geochemistry.

Habicht, J.K.A., 1979. Paleoclimate, Paleomagnetism, and Continental drift. American Association of Petroleum Geologists, Tulsa.

Härtner, T., Straub, K.L., Kannenberg, E., 2005. Occurrence of hopanoid lipids in anaerobic *Geobacter* species. FEMS Microbiology Letters, 243, 59-64.

Harvey, H.R., Fallon, R.D., Patton, J.S., 1986. The effect of organic matter and oxygen on the degradation of bacterial membrane lipids in marine sediments. Geochimica et Cosmochimica Acta, 50, 795-804.

Head, I.M., Jones, D.M., Larter, S.R., 2003. Biological activity in the deep subsurface and the origin of heavy oil. Nature, 426, 344-352.

Heppenheimer, H., Steffens, K., Puttman, W., Kalkreuth, W., 1992. Comparison of resinite-related aromatic biomarker distributions in Cretaceous-Tertiary coals from Canada and Germany. Organic Geochemistry, 18, 273-287.

Hinrichs, K.U., Boetius, A., 2002. The anaerobic oxidation of methane: new insights in microbial ecology and biogeochemistry. In: G. Wefer, D. Billet, D. Hebbeln, B.B. Jorgensen, S. M, T. van Weering (Eds.), Ocean Margin Systems (Ed. by G. Wefer, D. Billet, D. Hebbeln, B.B. Jorgensen, S. M, T. van Weering), pp. 457-477. Springer-Verlag, Berlin Heidelberg.

Hinrichs, K.U., Hayes, J.M., Sylva, S.P., Brewer, P.G., DeLong, E.F., 1999. Methane-consuming archaebacteria in marine sediments. Nature (London), 398, 802-805.

Hinrichs, K.U., Summons, R.E., Orphan, V., Sylva, S.P., Hayes, J.M., 2000. Molecular and isotopic analysis of anaerobic methane-oxidizing communities in marine sediments. Organic Geochemistry, 31, 1685-1701.

Hoefs, J., 1997. Stable isotope geochemistry. Springer-Verlag, Berlin.

Höld, I.M., Schouten, S., Jellema, J., Sinninghe Damsté, J.S., 1999. Origin of free and bound mid-chain methyl alkanes in oils, bitumens and kerogens of the marine, Infracambrian Huqf Formation (Oman). Organic Geochemistry, 30, 1411-1428.

Hopmans, E.C., Schouten, S., Pancost, R.D., van der Meer, M.T.J., Sinninghe Damste, J.S., 2000. Analysis of intact tetraether lipids in archaeal cell material and sediments by high performance liquid chromatography/atmospheric pressure chemical ionization mass spectrometry. Rapid communications in Mass Spectrometry, 14, 585-589.

Hopmans, E.C., Weijers, J.W.H., Schefuß, E., Herfort, L., Sinninghe Damste, J.S., Schouten, S., 2004. A novel proxy for terrestrial organic matter in sediments based on branched and isoprenoid tetraether lipids. Earth and Planetary Science Letters, 224, 107-116.

Horsfield, B., 1989. Practical criteria for classifying kerogens: Some observations from pyrolysis-gas chromatography. Geochimica et Cosmochimica Acta, 53, 891-901.

Horsfield, B., 1997. The bulk composition of first-formed petroleum in source rocks. In: D.H. Welte, B. Horsfield, D.R. Baker (Eds.), Petroleum and basin evolution; insights from petroleum geochemistry, geology and basin modeling (Ed. by D.H. Welte, B. Horsfield, D.R. Baker), pp. 335-402. Springer-Verlag, Berlin.

Horsfield, B., Disko, U., Leistner, F., 1989. The micro-scale simulation of maturation; outline of a new technique and its potential applications. Geologische Rundschau, 78, 361-374.

Isaksen, G.H., Curry, D.J., Yeakel, J.D., Jenssen, A.I., 1998. Controls on the oil and gas potential of humic coals. Organic geochemistry, 29, 23-44.

Iversen, N., Joergensen, B.B., 1985. Anaerobic methane oxidation rates at the sulfate-methane transition in marine sediments from Kattegat and Skagerrak (Denmark). Limnology and Oceanography, 30, 944-955.

Jackson, M.J., Powell, T.G., Summons, R.E., Sweet, I.P., 1986. Hydrocarbon shows and petroleum sources rocks in sediments as old as 1.7X10 (sub 9* years. Nature (London), 322, 727-729.

Jurenka, R.A., Holland, D., Krafsur, E.S., 1998. Hydrocarbon profiles of diapausing and reproductive adult face flies (Musca autumnalis). Archives of insects biochemistry and physiology, 37, 206-214.

Jurenka, R.A., Subchev, M., 2000. Identification of cuticular hydrocarbons and the alkene precursor to the pheromone in hemolymph of the female gypsy moth, lymantria dispar. Archives of insects biochemistry and physiology, 43, 108-115.

Kaneda, T., 1991. Iso- and anteiso-fatty acids in bacteria: Biosynthesis, function, and taxonomic significance. Microbiological Reviews, 55, 288-302.

Kannenberg, E.L., Poralla, K., 1999. Hopanoid biosynthesis and function in bacteria. Naturwissenschaften, 86, 168-176.

Kates, M., 1997. Diether and tetraether phospholipids and glycolipids as molecular markers for Archaebacteria (Archaea), Molecular markers in environmental geochemistry, 671;, pp. 35-48. American Chemical Society, Washington, DC, United States.

Katz, M.E., Pak, D.K., Dickens, G.R., Miller, K.G., 1999. The source and fate of massive carbon input during the latest Paleocene thermal maximum. Science, 286, 1531-1533.

Kenig, F., 2000. C (sub 16) -C (sub 29) homologous series of monomethylalkanes in the pyrolysis products of a Holocene microbial mat. Organic Geochemistry, 31, 237-241.

Kenig, F., Simons, D.J.H., Anderson, K.B., 2001. Distribution and origin of ethyl-branched alkanes in a Cenomanian transgressive shale of the Western Interior Seaway (USA). Organic Geochemistry, 32, 949-954.

Kenig, F., Sinninghe Damsté, J.S., Kock, v.D.A.C., Rijpstra, W.I.C., Huc, A.Y., de, L.J.W., 1995. Occurrence and origin of mono-, di-, and trimethylalkanes in modern and Holocene cyanobacterial mats from Abu Dhabi, United Arab Emirates. Geochimica et Cosmochimica Acta, 59, 2999-3015.

Kennicutt II, M.C., Brooks, J.M., Cox, H.B., 1993. The origin and distribution of gas hydrates in marine sediments. In: M.H. Engel, S.A. Macko (Eds.), Organic geochemistry: Principles and applications (Ed. by M.H. Engel, S.A. Macko), pp. 535-544. Plenum Press, New York.

Killops, S.D., Killops, V.J., 1993. An introduction to organic geochemistry. John Wiley & Sons, New York.

Killops, S.D., Killops, V.J., 2004. An introduction to organic geochemistry. Blackwell science, Oxford.

Killops, S.D., Raine, J.I., Woolhouse, A.D., Weston, R.J., 1995. Chemostratigraphic evidence of higher-plant evolution in the Taranaki Basin, New Zealand. Organic Geochemistry, 23, 429-445.

Kissin, Y.V., 1987. Catagenesis and composition of petroleum; origin of n-alkanes and isoalkanes in petroleum crudes. Geochimica et Cosmochimica Acta, 51, 2445-2457.

Kissin, Y.V., Feulmer, G.P., 1986. Gas chromatographic analysis of alkyl-substituted paraffins. Journal of Chromatography Science, 24, 53-56.

Klomp, U.C., 1986. The chemical structure of a pronounced series of iso-alkanes in South Oman crudes, Advances in organic geochemistry 1985; Part II, Molecular and general organic geochemistry, 10; 4-6, pp. 807-814. Pergamon, Oxford-New York, International.

Krumholz, L.R., 2000. Microbial communities in the deep subsurface. Hydrogeology Journal, 8, 4-10.

Krumholz, L.R., McKinley, J.P., Ulrich, G.A., Suflita, J.M., 1997. Confined subsurface microbial communities in Cretaceous rock. Nature, 386, 64-66.

Kurita, H., Uchida, T., 1999. Dinoflagellate cysts from the JAPEX/ JNOC/ GSC Mallik 2L-38 gas hydrate research well. In: S.R. Dallimore, T. Uchida, T.S. Collett (Eds.), Scientific results from JAPEX/ JNOC/ GSC Mallik 2L-38 gas hydrate research well, Mackenzie Delta, Northwest Territories, Canada (Ed. by S.R. Dallimore, T. Uchida, T.S. Collett), pp. 77-80. Geological Survey of Canada, Ottawa.

Kvenvolden, K.A., 1993. Gas hydrates, geological perspective and global change. Reviews of Geophysics, 31, 173-187.

Kvenvolden, K.A., 1994. Natural gas hydrates occurrence and issues. In: E.D. Sloan, J. Happel, M.A. Hnatow (Eds.), International conference on natural gas hydrates, 715 (Ed. by E.D. Sloan, J. Happel, M.A. Hnatow), pp. 232-246. New York Academy of Sciences, New York.

Kvenvolden, K.A., 1998. A primer on the geological occurrence of gas hydrate, Gas hydrates; relevance to world margin stability and climate change, 137;, pp. 9-30. Geological Society of London, London, United Kingdom.

Kvenvolden, K.A., 2002. Methane hydrate in the global organic carbon cycle. Terra Nova, 14, 302-306.

Lane, L.S., Dietrich, J.R., 1995. Tertiary structural evolution of the Beaufort Sea - Mackenzie Delta region, Arctic Canada. Bulletin of Canadian Petroleum Geology, 43, 293-314.

Lanoil, B.D., Sassen, R., La, D.M.T., Sweet, S.T., Nealson, K.H., 2001. Bacteria and Archaea physically associated with Gulf of Mexico gas hydrates. Applied and Environmental Microbiology, 67, 5143-5153.

Larter, S.R., 1984. Application of analytical pyrolysis techniques to kerogen characterization and fossil fuel exploration exploitation. In: K.J. Voorhees (Ed.), Analytical pyrolysis techniques and applications (Ed. by K.J. Voorhees), pp. 212-275. Butterworth and Co., London.

Lehtonen, K., Ketola, M., 1993. Solvent-extractable lipids of *Sphagnum*, *Carex*, *Bryales* and *Carex-Bryales* peats; content and compositional features vs peat humification. Organic Geochemistry, 20, 363-380.

Lewan, M.D., Williams, J.A., 1987. Evaluation of petroleum generation from resinites by hydrous pyrolysis. AAPG Bulletin, 71, 207-214.

Link, C.M., Bustin, R.M., 1989. Maturation and thermal history of Phanerozoic strata in northern Yukon and northwestern District of Mackenzie. Bulletin of Canadian Petroleum Geology, 37, 266-292.

Long, D.G.F., Sweet, A.R., 1994. Age and depositional environment of the Rock River coal basin, Yukon Territory, Canada. Canadian Journal of Earth Sciences, 31, 865-880.

Lorenson, T.D., Whiticar, M.J., Collett, T.S., Dallimore, S.R., Dougherty, J.A., 2005. Complete gas composition and isotopic geochemistry from the JAPEX/JNOC/GSC et al. Mallik 5L-38 gas hydrate production research well: cuttings, core, gas hydrate, and production testing results. In: S.R. Dallimore, T.S. Collett (Eds.), Scientific Results from Mallik 2002 Gas Hydrate Production Research Well Program, Mackenzie Delta, Northwest Territories, Canada, Bulletin 585 (Ed. by S.R. Dallimore, T.S. Collett). Geological Survey of Canada.

Mangelsdorf, K., Haberer, R.M., Zink, K.G., Dieckmann, V., Wilkes, H., Horsfield, B., 2005a. Molecular indicators for the occurrence of deep microbial communities at the JAPEX/JNOC/GSC et al. Mallik 5L-38 Gas Hydrate Research Well. In: S.R. Dallimore, T.S. Collett (Eds.), Scientific Results from Mallik 2002 Gas Hydrate Production Re-

search Well Program, Mackenzie Delta, Northwest Territories, Canada, Bulletin 585 (Ed. by S.R. Dallimore, T.S. Collett). Geological Survey of Canada.

Mangelsdorf, K., Zink, K.-G., Birrien, J.-L., Toffin, L., 2005b. A quantitative assessment of pressure dependent adaptive changes in the membrane lipids of a piezosensitive deep sub-seafloor bacterium. Organic Geochemistry, 36, 1459-1479.

Medioli, B.E., Wilson, N., Dallimore, S.R., Pare, D., Brennan-Alpert, P., Oda, H., 2005. Sedimentology of the cored interval, Mallik 5L-38 gas hydrate research well, Mackenie Delta, Northwest Territories. In: S.R. Dallimore, T.S. Collett (Eds.), Scientific Results from Mallik 2002 Gas Hydrate Production Research Well Program, Mackenzie Delta, Northwest Territories, Canada, Bulletin 585 (Ed. by S.R. Dallimore, T.S. Collett). Geological Survey of Canada.

Nelson, D.R., 2001. Discovery of novel trimethylalkanes in the internal hydrocarbons of developing pupae of Heliothis virescens and Helicoverpa zea. Comparative Biochemistry and Physiology part B, 128, 647-659.

Nelson, D.R., Adams, T.S., Fatland, C.L., 2003. Hydrocarbons in the surface wax of eggs and adults of the Colorado potato beetle, Leptinotarsa decemlineata. Comparative Biochemistry and Physiology part B, 134, 447-466.

Nichols, P.D., Shaw, P.M., Mancuso, C.A., Franzmann, P.D., 1993. Analysis of archaeal phospholipid-derived di- and tetraether lipids by high temperature capillary gas chromatography. Journal of Microbiological Methods, 18, 1-9.

Nisbet, E.G., 1990. The end of ice age. Canadian Journal of Earth Sciences, 27, 148-157.

Norgate, C.M., Boreham, C.J., Wilkins, A.J., 1999. Changes in hydrocarbon maturity indices with coal rank and type, Buller Coalfield, New Zealand. Organic Geochemistry, 30, 985-1010.

Norris, A.W., 1985a. Stratigraphy of Devonian outcrop belts in Northern Yukon Territory and Northwestern District of Mackenzie (Operation Porcupine area). Geological Survey of Canada, Ottawa.

Norris, D.K., 1985b. Eastern Cordilleran Foldbelt of northern Canada; its structural geometry and hydrocarbon potential. AAPG Bulletin, 69, 788-808.

Norris, G., 1982. Spore-pollen evidence for early Oligocene high-latitude cool climatic episode in northern Canada. Nature (London), 297, 387-389.

Nott, C.J., Xie, S., Avsejs, L.A., Maddy, D., Chambers, F.M., Evershed, R.P., 2000. *n*-Alkane distributions in ombrotrophic mires as indicators of vegetation change related to climatic variation. Organic Geochemistry, 31, 231-235.

Otto, A., Simoneit, B.R.T., 2001. Chemosystematics and diagenesis of terpenoids in fossil conifer species and sediment from the Eocene Zeitz Formation, Saxony, Germany. Geochimica et Cosmochimica Acta, 65, 3505-3527.

Otto, A., Simoneit, B.R.T., 2002. Biomarkers of Holocene buried conifer logs from Bella Coola and North Vancouver, British Columbia, Canada. Organic Geochemistry, 33, 1241-1251.

Otto, A., Simoneit, B.R.T., Rember, W.C., 2003. Resin compounds from the seed cones of three fossil conifer species from the Miocene Clarkia flora, Emerald Creek, Idaho, USA, and from related extant species. Review of Palaeobotany and Palynology, 126, 225-241.

Otto, A., Simoneit, B.R.T., Wilde, V., Kunzmann, L., Puettmann, W., 2002. Terpenoid composition of three fossil resins from Cretaceous and Tertiary conifers. Review of Palaeobotany and Palynology, 120, 203-215.

Otto, A., Walther, H., Puettmann, W., 1997. Sesqui- and diterpenoid biomarkers preserved in Taxodium-rich Oligocene oxbow lake clays, Weisselster Basin, Germany. Organic Geochemistry, 26, 105-115.

Otto, A., Walther, H., Püttmann, W., 1994. Molecular composition of a leaf- and root-bearing Oligocene oxbow lake clay in the Weisselster Basin, Germany. Organic Geochemistry, 22, 275-286.

Otto, A., Wilde, V., 2001. Sesqui-, Di-, and Triterpenoids as chemosystematic markers in extant conifers - a review. The botanical Review, 67, 141-238.

Ourisson, G., Rohmer, M., 1992. Hopanoids. 2. Biohopanoids: A novel class of bacterial lipids. Accounts of Chemical Research, 25, 403-408.

Ourisson, G., Rohmer, M., Poralla, K., 1987. Prokaryotic hopanoids and other polyterpenoid sterol surrogates. Annual Review of Microbiology, 41, 301-333.

Parkes, R.J., Cragg, B.A., Bale, S.J., Getlifff, J.M., Goodman, K., Rochelle, P.A., Fry, J.C., Weightman, A.J., Harvey, S.M., 1994. Deep bacterial biosphere in Pacific Ocean sediments. Nature, 371, 410-413.

Parkes, R.J., Cragg, B.A., Wellsbury, P., 2000. Recent studies on bacterial populations and processes in subseafloor sediments: A review. Hydrogeology Journal, 8, 11-28.

Pedersen, K., 1993. The deep subterranean biosphere. Earth-Science Reviews, 34, 243-260.

Pedersen, K., 1997. Microbial life in deep granitic rock. FEMS Microbiology Reviews, 20, 399-414.

Peters, K.E., Moldowan, J.M., 1993. The biomarker guide - Interpreting molecular fossils in petroleum and ancient sediments. Prentice Hall, New Jersey.

Philp, R.P., 1985. Fossil fuel biomarkers. Elsevier, Amsterdam.

Püttmann, W., Villar, H., 1987. Occurrence and geochemical significance of 1,2,5,6-tetramethylnaphthalene. Geochimica et Cosmochimica Acta, 51, 3023-3029.

Quirk, M.M., Wardroper, A.M.K., Wheatley, R.E., Maxwell, J.R., 1984. Extended hopanoids in peat environments. Chemical Geology, 42, 25-43.

Radke, M., Garrigues, P., Willsch, H., 1990. Methylated dicyclic and tricyclic aromatic hydrocarbons in crude oils from the Handil field, Indonesia. Organic Geochemistry, 15, 17-34.

Radke, M., Rullkotter, J., Vriend, S.P., 1994. Distribution of naphthalenes in crude oils from the Java Sea: Source and maturation effects. Geochimica et Cosmochimica Acta, 58, 3675-3689.

Radke, M., Welte, D.H., Willsch, H., 1982a. Geochemical study on a well in the Western Canada Basin: relation of the aromatic distribution pattern to maturity of organic matter. Geochimica et Cosmochimica Acta, 46, 1-10.

Radke, M., Willsch, H., Leythaeuser, D., Teichmuller, M., 1982b. Aromatic components of coal: relation of distribution pattern to rank. Geochimica et Cosmochimica Acta, 46, 1831-1848.

Radke, M., Wilsch, H., Welte, D.H., 1980. Preparative hydrocarbon group type determination by automated medium pressure liquid chromatography. Analytical Chemistry, 52, 406-411.

Ratledge, C., Wilkinson, S.G., 1988. Microbial Lipids. Academic Press, London.

Reading, H.G., Collinson, J.D., 1996. Clastic coasts. In: H.G. Reading (Ed.), Sedimentary environments; processes, facies and stratigraphy (Ed. by H.G. Reading), pp. 154-231. Blackwell Science, Oxford.

Ridgway, K.D., Sweet, A.R., Cameron, A.R., 1995. Climatically induced floristic changes across the Eocene-Oligocene transition in the northern high latitudes, Yukon Territory, Canada. Geological Society of America Bulletin, 107, 676-696.

Ringelberg, D.B., Sutton, S., White, D.C., 1997. Biomass, bioactivity and biodiversity: microbial ecology of the deep subsurface: analysis of ester-linked phospholipid fatty acids. FEMS Microbiology Reviews, 20, 371-377.

Ripmeester, J.A., Lu, H., Moudrakovski, I.L., Dutrisac, R., Wilson, L.D., Wright, F., Dallimore, S.R., 2005. Structure and composition of gas hydrate in sediment recovered from the JAPEX/JNOC/GSC et al. Mallik 5L-38 gas hydrate production research well, determined by X-ray diffraction and Raman and solid-state nuclear magnetic resonance spectroscopy. In: S.R. Dallimore, T.S. Collett (Eds.), Scientific Results from Mallik 2002 Gas Hydrate Production Research Well Program, Mackenzie Delta, Northwest Territories, Canada, Bulletin 585 (Ed. by S.R. Dallimore, T.S. Collett). Geological Survey of Canada.

Rohmer, M., Bisseret, P., Neunlist, S., 1992. The hopanoids, prokaryotic triterpenoids and precursors of ubiquitous molecular fossils, Biological markers in sediments and petroleum; a tribute to Wolfgang K Seifert. Prentice Hall, Englewood Cliffs, NJ, United States.

Rohmer, M., Bouvier-Nave, P., Ourisson, G., 1984. Distribution of hopanoid triterpenes in prokaryotes. Journal of General Microbiology, 130, 1137-1150.

Rohmer, M., Dastillung, M., Ourisson, G., 1980. Hopanoids from C_{30} to C_{35} in recent muds - Chemical markers for bacterial activity. Naturwissenschaften, 67, 456-458.

Rohmer, M., Ourisson, G., 1976a. Dérives du bactériohopane: variations structurales et répartition. Tetrahedron Letters, 40, 3637-3640.

Rohmer, M., Ourisson, G., 1976b. Structures des bactériohopanetétrols d'Acétobacter xylinum. Tetrahedron Letters, 40, 3633-3636.

Rullkötter, J., 1992. Organic geochemistry. In: R.A. Meyer (Ed.), Encyclopedia of physical science and technology, 7 (Ed. by R.A. Meyer), pp. 165-192. Academic Press.

Scheihing, M.H., Pfefferkorn, H.W., 1984. The taphonomy of land plants in the Orinoco Delta; a model for the incorporation of plant parts in clastic sediments of Late Carboniferous age of Euramerica. Review of Palaeobotany and Palynology, 41, 205-240.

Schouten, S., Hopmans, E.C., Pancost, R.D., Sinninghe Damste, J.S., 2000. Widespread occurence of structurally diverse tetraether membrane lipids: Evidence for the ubiquitous presence of low-temperature relatives of hyperthermophiles. National Academy of Sciences Proceedings, 97, 14421-14426.

Selley, R.C., 1992. Applied sedimentology. Academic Press, London.

Shiea, J., Brassell, S.C., Ward, D.M., 1990. Mid-chain branched mono- and dimethyl alkanes in hot spring cyanobacterial mats; a direct biogenic source for branched alkanes in ancient sediments? Organic Geochemistry, 15, 223-231.

Shiea, J., Brassell, S.C., Ward, D.M., 1991. Comparative analysis of extractable lipids in hot spring microbial mats and their component photosynthetic bacteria. Organic Geochemistry, 17, 309-319.

Simoneit, B.R.T., 1977. Diterpenoid compounds and other lipids in deep-sea sediments and their geochemical significance. Geochimica et Cosmochimica Acta, 41, 463-476.

Simoneit, B.R.T., Grimalt, J.O., Wang, T.G., Cox, R.E., Hatcher, P.G., Nissenbaum, A., 1986. Cyclic terpenoids of contemporary resinous plant detritus and of fossil woods, ambers and coals, Advances in organic geochemistry 1985; Part II, Molecular and general organic geochemistry, 10, pp. 877-889. Pergamon, Oxford-New York, International.

Simoneit, B.R.T., Otto, A., Wilde, V., 2003. Novel phenolic biomarker triterpenoids of fossil laticifers in Eocene brown coal from Geiseltal, Germany. Organic Geochemistry, 34, 121-129.

Sinninghe Damsté, J.S., Rijpstra, W.I.C., Schouten, S., Fuerst, J.A., Jetten, M.S.M., Strous, M., 2004. The occurrence of hopanoids in planctomycetes: implications for the sedimentary biomarker record. Organic Geochemistry, 35, 561-566.

Sloan, E.D., 2003. Fundamental principles and applications of natural gas hydrates. Nature, 426, 353-359.

Snowdon, L.R., 1980. Resinite; a potential petroleum source in the Upper Cretaceous/ Tertiary of the Beaufort-Mackenzie Basin, Facts and principles of world petroleum occurrence, 6, pp. 509-520. Canadian Society of Petroleum Geologists, Calgary.

Snowdon, L.R., 1981. Organic Geochemistry of the Upper Cretaceous-Tertiary Delta Complexes of the Beaufort-Mackenzie sedimentary Basins, Northwest Territories. Geological Survey of Canada, Bulletin 291.

Snowdon, L.R., 1999. Methane and carbon dioxide gas-generation kinetics, JAPEX/ JNOC/ GSC Mallik 2L-38 gas hydrate research well. In: S.R. Dallimore, T. Uchida, T.S. Collett (Eds.), Scientific results from JAPEX/ JNOC/ GSC Mallik 2L-38 gas hydrate research well, Mackenzie Delta, Northwest Territories, Canada (Ed. by S.R. Dallimore, T. Uchida, T.S. Collett), pp. 125-141. Geological Survey of Canada, Ottawa.

Snowdon, L.R., Brooks, P.W., Williams, G.K., Goodarzi, F., 1987. Correlation of the Canol Formation source rock with oil from Norman Wells. Organic Geochemistry, 11, 529-548.

Snowdon, L.R., Powell, T.G., 1982. Immature oil and condensate; modification of hydrocarbon generation model for terrestrial organic matter. AAPG Bulletin, 66, 775-788.

Spyckerelle, C., Greiner, A.C., Albrecht, P., Ourisson, G., 1977a. Hydrocarbures aromatiques d'origine géologique; III, Un tetrahydrochrysène, derive de triterpenes, dans des sediments recents et anciens; 3, 3, 7 - triméthyl 1, 2, 3, 4 - tetrahydrochrysène. Journal of Chemical Research, 12, 3746-3777.

Spyckerelle, C., Greiner, A.C., Albrecht, P., Ourisson, G., 1977b. Hydrocarbures aromatiques d'origine géologique; IV, Un octa-hydrochrysène, derive de triterpenes, dans un schiste bitumineux. Journal of Chemical Research, 12, 3801-3828.

Stach, E., Mackowsky, M.-T., Teichmüller, M., Taylor, G.H., Chancra, D., Teichmüller, R., 1982. Stach's Textbook of coal petrology. Borntraeger, Berlin Stuttgart.

Stefanova, M., Oros, D.R., Otto, A., Simoneit, B.R.T., 2002. Polar aromatic biomarkers in the Miocene Maritza-East Lignite, Bulgaria. Organic Geochemistry, 33, 1079-1091.

Stout, S.A., 1992. Aliphatic and aromatic triterpenoid hydrocarbons in a Tertiary angiospermous lignite. Organic Geochemistry, 18, 51-66.

Strachan, M.G., Alexander, R., Kagi, R.I., 1988. Trimethylnaphthalenes in crude oils and sediments: Effects of source and maturity. Geochimica et Cosmochimica Acta, 52, 1255-1264.

Summons, R.E., 1987. Branched alkanes from ancient and modern sediments; isomer discrimination by GC/ MS with multiple reaction monitoring. Organic Geochemistry, 11, 281-289.

Summons, R.E., 1993. Biogeochemical cycles: A review of fundamental aspects of organic matter formation, preservation and composition. In: M.H. Engel, S.A. Macko (Eds.), Organic geochemical: Principles and applications (Ed. by M.H. Engel, S.A. Macko), pp. 3-21. Plenum Press, New York.

Summons, R.E., Jahnke, L.L., Hope, J.M., Logan, G.A., 1999. 2-methylhopanoids as biomarkers for cyanobacterial oxygenic photosynthesis. Nature, 400, 554-557.

Sutton, B.D., Steck, G.J., 1994. Discrimination of caribbean and mediterranean fruit fly larvae (Diptera: Tephritidae) by cuticular hydrocarbon analysis. Florida entomologist, 77, 231-237.

Tan, Y.L., Heit, M., 1981. Biogenic and abiogenic polynuclear aromatic hydrocarbons in sediments from two remote Adirondack lakes. Geochimica et Cosmochimica Acta, 45, 2267-2279.

Taylor, G.H., Teichmüller, M., Davis, A., Diessel, C.F.K., Littke, R., Robert, P., 1998. Organic petrology. Borntraeger, Berlin Stuttgart.

ten Haven, H.L., Peakman, T.M., Rullkötter, J., 1992. Early diagenetic transformation of higher-plant triterpenoids in deep-sea sediments from Baffin Bay. Geochimica et Cosmochimica Acta, 56, 2001-2024.

Thiel, V., Blumenberg, M., Pape, T., Seifert, R., Michaelis, W., 2003. Unexpected occurrence of hopanoids at gas seeps in the Black Sea. Organic Geochemistry, 34, 81-87.

Thiel, V., Jenisch, A., Worheide, G., Lowenberg, A., Reitner, J., Michaelis, W., 1999a. Mid-chain branched alkanoic acids from "living fossil" demosponges: a link to ancient sedimentary lipids? Organic Geochemistry, 30, 1-14.

Thiel, V., Peckmann, J., Richnow, H.H., Luth, U., Reitner, J., Michaelis, W., 2001. Molecular signals for anaerobic methane oxidation in Black Sea seep carbonates and a microbial mat. Marine Chemistry, 73, 97-112.

Thiel, V., Peckmann, J., Seifert, R., Wehrung, P., Reitner, J., Michaelis, W., 1999b. Highly isotopically depleted isoprenoids; molecular markers for ancient methane venting. Geochimica et Cosmochimica Acta, 63, 3959-3966.

Tissot, B.P., Welte, D.H., 1984. Petroleum formation and occurrence. Springer-Verlag, Berlin.

Tomaru, H., Matsumoto, R., Chen, Y.F., Clark, I.D., 2005. Evolution of a gas hydrate system as recorded by oxygen and hydrogen isotopes of the interstitial waters of the JAPEX/JNOC/GSC et al. Mallik 5L-38 gas hydrate production research well. In: S.R. Dallimore, T.S. Collett (Eds.), Scientific Results from Mallik 2002 Gas Hydrate Production Research Well Program, Mackenzie Delta, Northwest Territories, Canada, Bulletin 585 (Ed. by S.R. Dallimore, T.S. Collett). Geological Survey of Canada.

Tornabene, T.G., Langworthy, T.A., 1979. Diphytanyl and dibiphytanyl glycerol ether lipids of methanogenic Archeabacteria. Science, 203, 51-53.

Tornabene, T.G., Wolfe, R.S., Balch, W.E., Holzer, G., Fox, G.E., Oró, J., 1978. Phytanyl-Glycerol ethers and Squalenes in the Archaebacterium *Methanobacterium thermoautotrophicum*. Journal of molecular evolution, 11, 259-266.

Uchida, T., Ochiai, K., Waseda, A., Sawamura, F., 2005. Occurrence of natural gas hydrate and associated gas-hydrate-bearing sedimnets in the JAPEX/JNOC/GSC et al. Mallik 5L-38 gas hydrate production research well. In: S.R. Dallimore, T.S. Collett (Eds.), Scientific Results from Mallik 2002 Gas Hydrate Production Research Well Program, Mackenzie Delta, Northwest Territories, Canada, Bulletin 585 (Ed. by S.R. Dallimore, T.S. Collett). Geological Survey of Canada.

Valentine, D.L., 2002. Biogeochemistry and microbial ecology of methane oxidation in anoxic environments: a review. Antonie van Leeuwenhoek, 81, 271-282.

van Aarssen, B.G.K., Cox, H.C., Hoogendoorn, P., De Leeuw, J.W., 1990. A cadinene biopolymer in fossil and extant dammar resins as a source for cadinanes and bicadinanes in crude oils from South East Asia. Geochimica et Cosmochimica Acta, 54, 3021-3031.

van Dorsselaer, A., Albrecht, P., Ourisson, G., 1977. Identification of novel (17αH)-hopanes in shales, lignites, sediments and petroleum. Bulletin de la Society Chimique de France, 1, 165-170.

van Dorsselaer, A., Ensminger, A., Spyckerelle, C., Dastillung, M., Sieskind, O., Arpino, P., Albrecht, P., Ourisson, G., 1974. Degraded and extent hopane derivatives (C_{27} to C_{35}) as ubiquitous geochemical markers. Tetrahedron Letters, 14, 1349-1352.

Wakeham, S.G., Schaffner, C., Giger, W., 1980. Polycyclic aromatic hydrocarbons in recent lake sediments; II, Compounds derived from biogenic precursors during early diagenesis. Geochimica et Cosmochimica Acta, 44, 415-430.

Walter, H., Breckle, S.-W., 1999. Vegetation und Klimazonen. Ulmer, Stuttgart.

Warton, B., Alexander, R., Kagi, R.I., 1998. The effect of maturation on the distribution of monoethylalkanes in Late Cretaceous sedimentary rocks and crude oils from the Gippsland Basin, Australia, Advances in organic geochemistry 1997; proceedings of the 18th international meeting on Organic geochemistry; Part 1, Petroleum geochemistry, 29; 1-3, pp. 593-604. Pergamon, Oxford-New York, International.

Weijers, J.W.H., Schouten, S., Hopmans, E.C., Geenevasen, J.A.J., David, O.R.P., Coleman, J.M., Pancost, R.D., Sinninghe Damste, J.S., 2006. Membrane lipids of mesophilic anaerobic bacteria thriving in peats have typical archaeal traits. Environmental Microbiology, 8, 648-657.

Wellsbury, P., Goodman, K., Cragg, B.A., Parkes, R.J., 2000. The geomicrobiology of deep marine sediments from Blake Ridge containing methane hydrate (sites 994, 995, and 997), Proceedings of the Ocean Drilling Program; 164; scientific results; gas hydrate sampling on the Blake Ridge and Carolina Rise; covering Leg 164 of the cruises of the drilling vessel JOIDES Resolution, Halifax, Nova Scotia, to Miami, Florida, sites 991-997, 31 October-19 December 1995, 164, pp. 379-391. Texas A & M University Ocean Drilling Program, College Station, TX, United States.

White, C.M., Lee, M.L., 1980. Identification and geochemical significance of some aromatic components of coal. Geochimica et Cosmochimica Acta, 44, 1825-1832.

White, D.C., Davis, W.M., Nickels, J.S., King, J.D., Bobbie, R.J., 1979. Determination of the sedimentary microbial biomass by extractable liquid phosphate. Oecologia, 40, 51-62.

White, D.C., Ringelberg, D.B., MacNaughton, S.J., Alugupalli, S., Schram, D., 1997. Signature lipid biomarker analysis for quantitative assessment in situ of environmental microbial ecology, Molecular markers in environmental geochemistry, 671, pp. 22-34. American Chemical Society, Washington, DC, United States.

White, J.M., 1999. Palynology, age, and paleoenvironmental interpretations from the JAPEX/ JNOC/ GSC Mallik 2L-38 gas hydrate research well. In: S.R. Dallimore, T. Uchida, T.S. Collett (Eds.), Scientific results from JAPEX/ JNOC/ GSC Mallik 2L-38 gas hydrate research well, Mackenzie Delta, Northwest Territories, Canada (Ed. by S.R. Dallimore, T. Uchida, T.S. Collett), pp. 81-93. Geological Survey of Canada, Ottawa.

Wilhelms, A., Telnaes, N., Steen, A., Augustson, J., 1998. A quantitative study of aromatic hydrocarbons in a natural maturity shale sequence - the 3-methylphenanthrene/retene ratio, a pragmatic maturity parameter. Organic Geochemistry, 29, 97-105.

Willumsen, P.S., Cote, R.P., 1982. Tertiary sedimentation in the southern Beaufort Sea, Canada, Studies in continental margin geology, 34, pp. 283-293. American Association of Petroleum Geologists, Tulsa.

Woodrow, R.J., Grace, J.K., Nelson, L.J., Haverty, M.I., 2000. Modification of cuticular hydrocarbons of Cryptotermes brevis (Isoptera: Kalotermitidae) in response to temperature and relative humidity. Physiological and chemical ecology, 29, 1100-1107.

Young, F.G., McNeil, D.H., 1984. Cenozoic stratigraphy of the Mackenzie Delta, Northwest Territories. Geological Survey of Canada Bulletin 336, Ottawa.

Young, F.G., Myhr, D.W., Yorath, C.J., 1976. Geology of the Beaufort-Mackenzie Basin. Geological Survey of Canada Paper 76/11, Ottawa.

Yunker, M.B., Backus, S.M., Graf Pannatier, E., Jeffries, D.S., Macdonald, R.W., 2002. Sources and significance of alkane and PAH hydrocarbons in canadian arctic river. Estuarine, Coastal and Shelf Sciences, 55, 1-31.

Yunker, M.B., Macdonald, R.W., Cretney, W.J., Fowler, B.R., McLaughlin, F.A., 1993. Alkane, terpene, and polycyclic aromatic hydrocarbon geochemistry of the Mackenzie River and Mackenzie Shelf; riverine contributions to Beaufort Sea coastal sediment. Geochimica et Cosmochimica Acta, 57, 3041-3061.

Zachos, J., Pagani, M., Sloan, L., Thomas, E., Billups, K., 2001. Trends, Rhythms, and Aberrations in Global Climate 65 Ma to Present. Science, 292, 686-693.

Zehnder, A.J., Brock, T.D., 1979. Methane formation and methane oxidation by methanogenic bacteria. Journal of Bacteriology, 137, 420-432.

Zehnder, A.J., Brock, T.D., 1980. Anaerobic methane oxidation: Occurrence and ecology. Applied and Environmental Microbiology, 39, 194-204.

Zhang, C.L., Lanoil, B., 2004. Geomicrobiology and biogeochemistry of gas hydrates and cold seeps. Chemical Geology, 205, 187-194.

Zhang, C.L., Pancost, R.D., Sassen, R., Qian, Y., Macko, S.A., 2003. Archaeal lipid biomarkers and isotopic evidence of anaerobic methane oxidation associated with gas hydrates in the Gulf of Mexico. Organic Geochemistry, 34, 827-836.

Zink, K.-G., Mangelsdorf, K., 2004. Efficient and rapid method for extraction of intact phospholipids from sediments combined with molecular structure elucidation using LC-ESI-MS-MS analysis. Analytical and Bioanalytical Chemistry, 380, 798-812.

Zink, K.G., Wilkes, H., Disko, U., Elvert, M., Horsfield, B., 2003. Intact phospholipids; microbial "life markers" in marine deep subsurface sediments. Organic Geochemistry, 34, 755-769.

12 Appendix

Mallik 5L-38 Samples	GFZ sample number	S1 (mg/g)	S2 (mg/g)	S3 (mg/g)	Tmax (°C)	PP (mg/g)	PI (wt ratio)	HI (mg HC/g TOC)	OI (mg CO2/g TOC)	TOC (%)	TC (%)
MB89163	G000270	0.03	0.73	1.98	424	0.76	0.04	80	215	0.92	1.32
MB89899	G000271	0.03	0.97	2.31	426	1.01	0.03	103	243	0.95	1.45
MB90020	G000272	0.03	0.67	1.98	425	0.69	0.04	77	230	0.86	1.16
MB91200	G000273	0	0.01	0	413	0.01	0.36	14		0.05	0.05
MB91856	G000274	0.01	0.03	0.05	407	0.03	0.19	50	100	0.05	0.05
CO93409	G000275	2.52	90.71	20.15	363	93.23	0.03	195	43	46.6	47.9
MB93589	G000276	0.05	3.15	2.98	424	3.2	0.02	177	167	1.78	1.98
CO94078	G000277	4.53	92.97	17.84	392	97.5	0.05	292	56	31.85	33.85
MB94762	G000278	1.79	0.69	0.42	406	2.47	0.72	72	44	0.95	1.05
MB96334	G000279	0.01	0.17	1.05	416	0.18	0.07	42	263	0.4	0.7
MB97760	G000280	0	0.04	0.78	561	0.05	0.09	47		0.09	0.19
MB98925	G000281	0	0.01	0.41	449	0.02	0.25	12	410	0.1	0.2
CO100550	G000282	2.87	87.08	23.47	400	89.95	0.03	207	56	42.03	44.53
MB100778	G000283	0.03	0.51	0.3	426	0.54	0.05	111	65	0.46	0.56
MB102215	G000284	0	0.15	0.04	600	0.15	0.03	134	36	0.11	0.11
MB103360	G000285	0.41	12.44	4.79	415	12.85	0.03	175	68	7.09	7.49
CO104310	G000286	0.6	19.36	1.76	430	19.96	0.03	532	48	3.64	3.84
MB104920	G000287	0.03	1.04	9.07	428	1.07	0.03	103	898	1.01	1.91
CO105353	G000288	3.39	96.84	21.65	388	100.23	0.03	247	55	39.19	41.59
CO106094	G000290	0.16	7.79	3.55	420	7.95	0.02	165	75	4.71	5.01
MB106380	G000289	0.06	1.96	2.13	417	2.02	0.03	104	113	1.89	2.09
MB107960	G000291	0.04	0	0	297	0.04	0.91	10		0.04	0.04
CO108138	G000292	0.73	52.6	28.47	406	53.32	0.01	115	62	45.93	47.63
CO108169	G000293	1.8	84.47	21.91	392	86.27	0.02	220	57	38.39	39.79
MB108924	G000294	0.01	0.02	0.2	424	0.03	0.18	38	333	0.06	0.06
MB110494	G000295	0.01	0.03	0.98	420	0.04	0.19	33		0.09	0.19
CO110550	G000296	0.21	9.5	9.37	411	9.71	0.02	101	99	9.44	10.84
MB112790	G000297	0.02	1.05	2	421	1.07	0.02	67	127	1.57	1.67
MB113980	G000298	0.02	0.21	0.78	584	0.23	0.08	123	459	0.17	0.27
MB114535	G000299	0.02	0.38	1.8	424	0.4	0.04	72	340	0.53	0.83

Table A1: Rock-eval-data, and list of the GFZ sample numbers linked to the Mallik 5L-38 sample numbers.

Samples	*n*-C_{13}	*n*-C_{14}	*n*-C_{15}	*n*-C_{16}	*n*-C_{17}	*n*-C_{18}	*n*-C_{19}	*n*-C_{20}	*n*-C_{21}	*n*-C_{22}	*n*-C_{23}	*n*-C_{24}	*n*-C_{25}	*n*-C_{26}	*n*-C_{27}	*n*-C_{28}	*n*-C_{29}	*n*-C_{30}	*n*-C_{31}	*n*-C_{32}	*n*-C_{33}	*n*-C_{34}	*n*-C_{35}
MB89163	0.0	0.3	1.9	8.6	16.0	8.1	8.0	9.0	12.6	10.3	34.4	29.9	46.7	19.8	73.2	20.9	113.2	17.9	60.4	5.7	17.1	0.4	3.1
MB89899	0.0	13.8	17.5	17.7	9.6	9.0	11.8	11.4	23.4	19.8	55.2	34.2	65.0	36.8	89.4	35.0	103.6	25.8	61.7	9.5	23.1	1.8	3.9
MB90020	0.0	6.6	17.1	35.8	24.6	9.5	8.8	8.4	15.7	13.1	47.6	38.9	64.5	29.7	87.6	28.7	105.9	20.1	63.1	7.2	19.3	0.5	4.3
MB91200	78.0	318.5	461.7	666.3	877.2	588.6	475.2	420.0	339.3	250.0	266.5	298.4	185.3	113.9	137.4	76.2	90.3	53.7	43.2	0.0	0.0	0.0	0.0
MB91856	404.9	1845.5	3200.8	3550.6	4711.4	3154.7	1672.7	1049.8	510.2	351.2	217.1	155.4	114.7	119.7	71.3	23.0	25.8	12.2	13.7	0.0	0.0	0.0	0.0
CO93409	0.0	1.0	2.7	3.9	9.6	4.1	16.1	5.6	25.8	7.8	42.5	13.9	40.0	9.9	32.3	7.9	46.5	5.8	58.9	9.2	42.3	0.2	0.1
MB93589	0.0	0.3	1.1	7.1	14.9	10.5	14.0	2.6	15.8	12.7	44.6	21.0	87.2	29.0	118.2	35.3	123.4	20.7	61.7	15.4	22.2	0.5	5.0
CO94078	0.0	5.2	15.0	16.0	5.4	1.9	7.8	3.5	13.8	7.6	23.8	12.2	24.2	14.3	34.0	14.1	55.9	10.6	42.2	6.3	22.7	1.1	2.9
MB94762	0.0	8.2	16.9	28.8	15.5	4.0	6.3	1.8	3.6	3.4	4.2	3.8	6.9	7.4	7.7	5.6	9.3	4.4	10.9	2.4	1.5	0.0	0.0
MB96334	0.0	5.1	30.4	66.1	42.0	16.1	11.6	8.8	9.0	8.4	14.6	17.0	33.7	23.4	81.4	38.6	140.3	29.9	102.7	15.6	43.4	0.5	11.1
MB97760	32.3	66.7	117.0	183.4	323.3	179.1	115.3	86.7	71.3	58.7	45.0	40.7	29.4	23.1	37.6	18.2	32.4	11.2	32.6	0.0	0.0	0.0	0.0
MB98925	17.4	6.9	39.0	54.1	141.4	124.7	108.6	96.9	64.0	44.3	36.4	36.1	18.1	19.2	22.1	13.9	11.5	4.3	9.9	6.1	0.2	0.0	0.0
CO100550	0.0	0.9	3.4	4.0	4.3	1.9	9.9	3.2	11.1	4.7	14.7	15.9	17.5	4.5	18.6	5.2	51.0	8.0	81.5	7.5	48.0	1.0	1.5
MB100778	2.5	21.9	35.0	70.6	49.8	17.7	11.9	9.4	9.9	12.1	47.3	15.2	61.3	14.7	127.3	17.0	138.8	15.7	72.6	4.4	13.6	0.0	0.0
MB102215	7.9	14.6	77.7	173.1	280.1	175.3	121.0	84.8	56.0	36.4	31.8	26.4	18.4	22.3	19.7	22.4	14.0	9.1	9.3	6.0	0.0	0.0	0.0
MB103360	0.0	1.0	1.5	4.1	7.9	5.7	9.3	7.0	14.2	9.4	35.7	23.6	63.1	29.6	85.7	40.7	100.8	20.3	44.6	14.5	18.9	0.1	17.6
CO104310	0.0	35.5	111.1	126.6	40.3	13.1	31.2	22.3	79.3	43.8	240.0	119.3	305.0	133.5	379.5	165.3	704.3	144.4	405.2	64.6	110.2	9.1	84.1
MB104920	0.0	6.1	20.3	64.8	43.2	15.5	12.8	9.3	12.0	9.9	22.7	12.0	29.8	13.6	44.0	13.4	59.1	10.5	27.4	4.6	10.1	0.9	1.7
CO105353	0.0	0.9	4.7	5.4	4.1	2.0	11.3	3.8	10.0	5.6	24.2	12.0	22.1	7.8	24.5	9.9	79.1	10.0	82.7	8.1	45.4	3.2	32.8
CO106094	0.0	30.9	114.3	131.6	37.3	7.4	6.7	5.3	16.8	9.7	44.2	20.9	56.7	10.6	68.3	8.8	58.5	6.2	19.9	2.0	2.8	1.1	2.4
MB106380	0.0	5.7	12.2	28.6	24.3	11.9	11.6	2.1	23.1	17.7	69.6	25.7	84.9	30.7	99.6	28.7	104.6	15.4	49.1	5.5	14.8	0.5	3.6
MB107960	24.3	58.6	175.6	561.7	1004.7	727.4	517.4	344.3	236.5	162.7	141.6	209.3	109.5	85.3	184.1	116.9	250.9	45.2	46.9	28.5	0.0	0.0	0.0
CO108138	0.0	0.1	2.3	3.5	2.7	1.0	10.8	2.0	6.2	1.9	7.9	7.3	6.7	2.0	10.6	2.8	21.1	2.5	25.5	1.6	14.8	0.3	1.0
CO108169	0.0	1.2	5.0	6.3	2.8	0.9	4.0	1.2	3.4	1.4	7.7	1.9	6.4	1.8	7.6	2.2	16.4	1.5	12.9	1.3	26.3	3.4	38.0
MB108924	10.7	16.5	40.0	129.7	287.8	245.5	153.4	109.6	68.8	46.1	40.3	45.7	39.1	31.0	41.5	26.6	31.5	14.9	15.5	0.0	0.0	0.0	0.0
MB110494	10.0	29.5	148.2	462.0	745.6	762.9	450.3	302.7	244.7	186.2	147.6	143.7	118.2	152.7	77.3	55.0	58.6	29.5	24.0	32.6	29.4	13.7	8.2
CO110550	0.0	13.4	35.9	42.6	8.6	1.2	0.9	0.4	0.7	0.4	0.6	0.9	0.9	0.6	1.9	0.7	2.8	0.3	1.1	0.5	1.3	0.2	1.2
MB112790	0.0	3.1	13.4	42.2	34.4	9.8	11.6	5.5	4.0	4.9	6.5	9.7	14.3	13.3	11.2	7.8	10.1	4.2	9.9	2.0	6.9	0.1	1.4
MB113980	2.7	53.4	71.3	306.1	639.0	1131.2	911.3	592.7	440.6	311.8	210.4	129.6	74.8	41.4	22.5	6.0	8.4	3.1	3.2	4.6	5.2	0.0	0.0
MB114535	0.0	2.8	22.3	64.3	45.1	13.0	7.1	5.4	4.0	4.3	6.3	11.4	12.8	9.9	17.0	8.5	22.5	5.9	80.0	5.1	11.0	0.4	5.0

Table A2: Concentrations of *n*-alkanes in µg/gTOC

Samples	*n*-C_{13}	*n*-C_{14}	*n*-C_{15}	*n*-C_{16}	*n*-C_{17}	*n*-C_{18}	*n*-C_{19}	*n*-C_{20}	*n*-C_{21}	*n*-C_{22}	*n*-C_{23}	*n*-C_{24}	*n*-C_{25}	*n*-C_{26}	*n*-C_{27}	*n*-C_{28}	*n*-C_{29}	*n*-C_{30}	*n*-C_{31}	*n*-C_{32}	*n*-C_{33}	*n*-C_{34}	*n*-C_{35}
MB89163		0.0	0.0	0.1	0.1	0.1	0.1	0.1	0.1	0.1	0.3	0.3	0.4	0.2	0.7	0.2	1.0	0.2	0.6	0.1	0.2	0.0	0.0
MB89899	0.0	0.1	0.2	0.2	0.1	0.1	0.1	0.1	0.2	0.2	0.5	0.3	0.6	0.4	0.8	0.3	1.0	0.2	0.6	0.1	0.2	0.0	0.0
MB90020		1.4	0.3	0.7	0.4	0.2	0.1	0.1	0.2	0.2	0.6	0.5	0.8	0.3	1.0	0.3	1.2	0.2	0.7	0.1	0.2	0.0	0.0
MB91200	0.0	0.2	0.2	0.3	0.4	0.3	0.2	0.2	0.2	0.1	0.1	0.2	0.1	0.1	0.1	0.0	0.0	0.0	0.0	0.0	0.0	0.0	0.0
MB91856	0.2	0.9	1.6	1.8	2.4	1.6	0.8	0.5	0.3	0.2	0.1	0.1	0.1	0.1	0.0	0.0	0.0	0.0	0.0	0.0	0.0		
CO93409		0.5	1.3	1.8	4.5	1.9	7.5	2.6	12.0	3.6	19.8	6.5	18.6	4.6	15.0	3.7	21.7	2.7	27.4	4.3	19.7	0.1	0.0
MB93589		0.0	0.0	0.1	0.3	0.2	0.2	0.0	0.3	0.2	0.8	0.4	1.6	0.5	2.1	0.6	2.2	0.4	1.1	0.3	0.4	0.0	0.1
CO94078		1.7	4.8	5.1	1.7	0.6	2.5	1.1	4.4	2.4	7.6	3.9	7.7	4.5	10.8	4.5	17.8	3.4	13.4	2.0	7.2	0.4	0.9
MB94762		0.1	0.2	0.3	0.1	0.0	0.1	0.0	0.0	0.0	0.0	0.0	0.1	0.1	0.1	0.1	0.1	0.0	0.1	0.0	0.0	0.0	0.0
MB96334		0.0	0.1	0.3	0.2	0.1	0.0	0.0	0.0	0.0	0.1	0.1	0.1	0.1	0.3	0.2	0.6	0.1	0.4	0.1	0.2	0.0	0.0
MB97760	0.0	0.1	0.1	0.2	0.3	0.2	0.1	0.1	0.1	0.1	0.0	0.0	0.0	0.0	0.0	0.0	0.0	0.0	0.0	0.0	0.0	0.0	
MB98925	0.0	0.0	0.0	0.1	0.1	0.1	0.1	0.1	0.1	0.0	0.0	0.0	0.0	0.0	0.0	0.0	0.0	0.0	0.0	0.0	0.0	0.0	0.0
CO100550		0.4	1.4	1.7	1.8	0.8	4.2	1.3	4.7	2.0	6.2	6.7	7.4	1.9	7.8	2.2	21.5	3.4	34.3	3.1	20.2	0.4	0.6
MB100778	0.0	0.1	0.2	0.3	0.2	0.1	0.1	0.0	0.0	0.1	0.2	0.1	0.3	0.1	0.6	0.1	0.6	0.1	0.3	0.0	0.1	0.0	0.0
MB102215	0.0	0.0	0.1	0.2	0.3	0.2	0.1	0.1	0.1	0.0	0.0	0.0	0.0	0.0	0.0	0.0	0.0	0.0	0.0	0.0	0.0	0.0	0.0
MB103360		0.1	0.1	0.3	0.6	0.4	0.7	0.5	1.0	0.7	2.5	1.7	4.5	2.1	6.1	2.9	7.1	1.4	3.2	1.0	1.3	0.0	1.2
CO104310		1.3	4.0	4.6	1.5	0.5	1.1	0.8	2.9	1.6	8.7	4.3	11.1	4.9	13.8	6.0	25.6	5.3	14.7	2.4	4.0	0.3	3.1
MB104920		0.1	0.2	0.7	0.4	0.2	0.1	0.1	0.1	0.1	0.2	0.1	0.3	0.1	0.4	0.1	0.6	0.1	0.3	0.0	0.1	0.0	0.0
CO105353		0.3	1.8	2.1	1.6	0.8	4.4	1.5	3.9	2.2	9.5	4.7	8.7	3.1	9.6	3.9	31.0	3.9	32.4	3.2	17.8	1.3	12.9
CO106094		1.5	5.4	6.2	1.8	0.3	0.3	0.3	0.8	0.5	2.1	1.0	2.7	0.5	3.2	0.4	2.8	0.3	0.9	0.1	0.1	0.1	0.1
MB106380		0.1	0.2	0.5	0.5	0.2	0.2	0.0	0.4	0.3	1.3	0.5	1.6	0.6	1.9	0.5	2.0	0.3	0.9	0.1	0.3	0.0	0.1
MB107960	0.0	0.0	0.1	0.2	0.4	0.3	0.2	0.1	0.1	0.1	0.1	0.1	0.0	0.0	0.1	0.0	0.1	0.0	0.0	0.0	0.0	0.0	0.0
CO108138		0.1	1.1	1.6	1.2	0.4	5.0	0.9	2.8	0.9	3.6	3.3	3.1	0.9	4.9	1.3	9.7	1.1	11.7	0.7	6.8	0.1	0.5
CO108169		0.5	1.9	2.4	1.1	0.4	1.5	0.5	1.3	0.6	3.0	0.7	2.4	0.7	2.9	0.9	6.3	0.6	5.0	0.5	10.1	1.3	14.6
MB108924	0.0	0.0	0.0	0.1	0.2	0.1	0.1	0.1	0.0	0.0	0.0	0.0	0.0	0.0	0.0	0.0	0.0	0.0	0.0				
MB110494	0.0	0.0	0.1	0.4	0.7	0.7	0.4	0.3	0.2	0.2	0.1	0.1	0.1	0.1	0.1	0.0	0.1	0.0	0.0	0.0	0.0	0.0	0.0
CO110550		1.3	3.4	4.0	0.8	0.1	0.1	0.0	0.1	0.0	0.1	0.1	0.1	0.1	0.2	0.1	0.3	0.0	0.1	0.0	0.1	0.0	0.1
MB112790	0.0	0.2	0.7	0.5	0.2	0.2	0.1	0.1	0.1	0.1	0.2	0.2	0.2	0.2	0.1	0.2	0.1	0.2	0.0	0.1	0.0	0.0	
MB113980	0.0	0.1	0.1	0.5	1.0	1.8	1.5	1.0	0.7	0.5	0.3	0.2	0.1	0.1	0.0	0.0	0.0	0.0	0.0	0.0	0.0	0.0	0.0
MB114535		0.0	0.1	0.3	0.2	0.1	0.0	0.0	0.0	0.0	0.0	0.1	0.1	0.1	0.1	0.0	0.1	0.0	0.4	0.0	0.1	0.0	0.0

Table A3: Concentrations of *n*-alkanes in µg/gSed

Mallik 5L-38 Samples	22,29,30-*trinor*-hop-13(18)-en	17α(H)–22,29,30 –*trinor*-hopane	17β(H)–22,29,30 –*trinor*-hopane	28,30–*dinor*-17α(H),18α(H), 21β(H)–hopane	30-*nor*-hop-17(21)-en	17α(H),21β(H)-*nor*-hopane	2-Methyl-hop-17(21)-ene	2-Methyl-hop-17(21)-ene	Hop-17(21)-ene	17β(H),21α(H)–30–*nor*-hopane	Methyl-hop-17(21)-ene	17α(H),21β(H)–hopane	*Neo*-hop-13(18)-ene	3-Methyl-hop-17(21)-ene	17(H)β,21β(H)–*nor*-hopane	(22R)–17α(H), 21β(H)–*homo*-hopane	17(H)β,21β(H)-hopane	17β(H),21β(H)-*homo*-hopane	(22R)-17α(H),21β(H)-*trihomo*-hopane	17(H)β,21β(H)-*dihomo*-hopane
MB89163	0.0	0.0	0.0	0.0	0.0	0.0	0.2	0.1	56.4	0.0	0.1	0.0	0.0	0.0	0.0	0.0	0.0	0.0	0.0	0.0
MB89899	0.1	0.0	0.5	0.0	0.0	0.0	0.2	0.1	2.1	0.2	0.1	0.0	0.0	0.1	0.5	0.3	0.3	0.5	0.0	0.0
MB90020	3.5	0.0	14.5	0.0	0.0	0.0	0.2	0.1	68.2	7.0	0.1	1.9	1.3	0.0	14.0	12.0	11.5	14.8	0.0	5.4
MB91200	0.0	0.0	0.0	0.0	0.0	0.0	0.0	0.0	8.0	0.0	0.0	0.0	0.0	0.0	0.0	17.3	0.0	0.0	0.0	0.0
MB91856	0.0	0.0	0.0	0.0	0.0	0.0	0.0	0.0	0.0	0.0	0.0	0.0	0.0	0.0	0.0	0.0	0.0	0.0	0.0	0.0
CO93409	6.2	0.0	12.0	0.0	0.0	0.0	0.8	0.3	82.8	2.2	0.3	1.5	0.0	0.0	22.7	71.9	22.7	13.2	0.0	1.7
MB93589	0.0	0.0	0.0	0.0	0.0	0.0	0.0	0.0	110.5	0.0	0.0	0.0	0.0	0.1	0.0	0.0	0.0	0.0	0.0	0.0
CO94078	13.9	0.0	36.4	0.0	0.0	0.0	0.5	0.1	71.2	10.8	0.4	1.8	0.0	0.1	30.5	98.2	39.1	48.2	0.0	5.1
MB94762	0.0	29.8	0.0	0.0	0.0	0.0	0.0	0.0	0.0	0.0	0.0	0.0	0.0	0.0	0.0	0.0	0.0	0.0	0.0	0.0
MB96334	5.2	0.0	29.2	0.0	0.0	0.0	0.2	0.1	57.9	8.9	0.1	1.2	2.1	0.1	19.3	23.1	16.4	0.0	0.0	0.0
MB97760	0.0	0.0	0.0	0.0	0.0	30.2	0.0	0.0	0.0	0.0	0.0	0.0	0.0	0.0	0.0	3.0	0.0	0.0	0.0	0.0
MB98925	0.0	0.0	0.0	0.0	0.0	7.8	0.0	0.0	0.0	0.0	0.0	0.0	0.0	0.0	0.0	0.0	0.0	0.0	0.0	0.0
CO100550	4.1	0.0	11.5	0.0	0.0	0.0	0.5	0.4	37.4	4.4	0.2	0.0	2.6	0.0	18.2	32.4	0.0	18.5	0.0	1.7
MB100778	5.1	0.0	22.7	0.0	25.0	5.9	0.3	0.0	117.4	6.2	0.1	7.4	5.7	0.1	31.9	28.2	16.6	27.8	0.0	0.0
MB102215	0.0	0.0	0.0	0.0	0.0	13.8	0.0	0.0	0.0	0.0	0.0	0.0	0.0	0.0	0.0	0.0	0.0	0.0	0.0	0.0
MB103360	0.0	0.0	0.0	0.0	0.0	0.0	0.7	0.4	0.1	0.0	0.9	0.0	0.0	0.1	0.0	0.0	0.0	0.0	0.0	0.0
CO104310	18.6	0.0	159.3	0.0	0.0	0.0	1.7	0.6	528.2	74.3	0.3	10.7	0.0	0.3	159.7	131.0	120.4	145.2	0.0	8.0
MB104920	4.3	0.0	27.5	35.4	0.0	0.0	0.1	0.0	28.5	4.0	0.0	4.5	3.2	0.0	7.6	10.7	5.3	7.8	0.0	0.0
CO105353	4.8	0.0	20.2	0.0	0.0	0.0	1.2	0.5	153.8	6.3	0.9	0.0	0.0	0.1	16.5	50.8	20.8	226.3	0.0	0.0
CO106094	4.0	0.0	15.4	0.0	0.0	0.0	0.1	0.0	87.2	4.4	0.1	0.0	1.9	0.0	23.1	13.9	19.5	33.2	0.0	2.8
MB106380	6.4	0.0	29.5	0.0	0.0	0.0	0.1	0.1	82.7	9.0	0.1	1.9	0.0	0.0	63.6	25.5	25.5	0.0	0.0	0.0
MB107960	0.0	128.6	151.3	121.6	0.0	405.9	0.0	0.0	86.6	42.1	0.0	0.0	12.7	0.0	43.7	0.0	18.6	0.0	0.0	0.0
CO108138	5.1	0.0	4.8	0.0	0.0	0.0	0.5	0.3	59.6	1.6	0.1	0.0	10.5	0.1	4.5	6.2	6.5	6.3	0.0	1.7
CO108169	3.9	0.0	3.1	0.0	0.0	0.0	0.2	0.1	21.1	1.0	0.2	0.0	0.0	0.1	2.3	39.7	4.3	7.9	0.0	0.0
MB108924	0.0	0.0	0.0	0.0	0.0	6.0	0.0	0.0	0.0	0.0	0.0	0.0	0.0	0.0	0.0	0.0	0.0	0.0	0.0	0.0
MB110494	0.0	0.0	35.2	0.0	0.0	124.1	0.0	0.0	28.8	0.0	0.0	0.0	0.0	0.0	0.0	0.0	0.0	28.8	35.2	124.1
CO110550	0.0	0.0	3.2	0.0	0.0	0.0	0.0	0.0	6.6	1.5	0.0	0.0	0.3	0.0	1.0	7.1	1.4	1.9	0.0	0.0
MB112790	0.3	0.0	0.9	0.0	0.0	0.0	0.0	0.0	1.3	0.6	0.0	0.1	0.2	0.0	1.2	0.0	0.5	0.5	0.0	0.2
MB113980	0.0	0.0	0.0	0.0	0.0	16.0	0.0	0.0	0.0	0.0	0.0	0.0	0.0	0.0	0.0	0.0	0.0	0.0	0.0	0.0
MB114535	3.8	0.0	41.4	0.0	0.0	0.0	0.0	0.0	52.1	9.0	0.0	1.7	1.0	0.0	40.5	34.2	20.9	0.0	0.0	0.0

Table A3: Concentrations of hopanoic hydrocarbons in the aliphatic fractions in µg/gTOC.

Mallik 5L-38 Samples	7-methyl -C_{14}	5-methyl -C_{14}	4-methyl -C_{14}	3-methyl -C_{14}	7-methyl -C_{15}	6-methyl -C_{15}	5-methyl -C_{15}	4-methyl -C_{15}	3-methyl -C_{15}	7-methyl -C_{16}	6-methyl -C_{16}	5-methyl -C_{16}	4-methyl -C_{16}	3-methyl -C_{16}
MB89163	0.00	0.00	0.02	0.01	0.01	0.01	0.02	0.02	0.02	0.02	0.01	0.02	0.03	0.02
MB89899	0.14	0.05	0.23	0.12	0.10	0.07	0.12	0.08	0.11	0.04	0.02	0.06	0.06	0.04
MB90020	0.08	0.07	0.25	0.16	0.08	0.13	0.24	0.20	0.19	0.05	0.04	0.07	0.09	0.04
MB91200	0.00	0.00	0.03	0.02	0.00	0.00	0.00	0.04	0.02	0.04	0.00	0.00	0.04	0.00
MB91856	0.00	0.00	0.16	0.12	0.00	0.00	0.15	0.16	0.17	0.00	0.40	0.07	0.18	0.08
CO93409	0.10	0.13	0.08	0.21	0.09	0.07	0.10	0.31	0.11	0.00	0.15	0.08	0.16	0.20
MB93589	0.00	0.00	0.05	0.03	0.03	0.02	0.05	0.07	0.04	0.03	0.01	0.03	0.07	0.02
CO94078	1.60	1.16	2.42	2.58	2.69	1.82	2.69	4.14	3.45	0.68	0.39	1.07	1.20	0.40
MB94762	0.13	0.07	0.13	0.06	0.05	0.07	0.11	0.12	0.13	0.00	0.00	0.19	0.19	0.00
MB96334	0.02	0.04	0.16	0.13	0.07	0.06	0.16	0.16	0.13	0.04	0.03	0.08	0.09	0.04
MB97760	0.00	0.00	0.01	0.01	0.00	0.00	0.01	0.02	0.01	0.00	0.03	0.01	0.03	0.01
MB98925	0.00	0.00	0.00	0.00	0.00	0.00	0.00	0.00	0.00	0.00	0.01	0.02	0.02	0.01
CO100550	0.13	0.17	0.15	0.29	0.25	0.16	0.30	0.48	0.32	0.22	0.08	0.20	0.35	0.13
MB100778	0.13	0.09	0.30	0.16	0.13	0.09	0.17	0.29	0.29	0.00	0.00	0.15	0.12	0.04
MB102215	0.00	0.00	0.00	0.00	0.00	0.00	0.13	0.14	0.11	0.00	0.35	0.22	0.31	0.12
MB103360	0.00	0.00	0.06	0.06	0.04	0.04	0.07	0.09	0.08	0.10	0.02	0.05	0.08	0.04
CO104310	1.61	1.20	2.59	2.12	3.00	2.89	3.59	4.32	4.53	0.58	0.29	1.35	1.85	0.20
MB104920	0.03	0.02	0.07	0.08	0.16	0.12	0.15	0.17	0.22	0.11	0.07	0.13	0.20	0.09
CO105353	0.57	0.79	0.47	0.95	0.46	0.47	0.69	1.13	0.85	0.26	0.14	0.35	0.36	0.15
CO106094	1.11	1.22	2.96	2.73	3.18	2.92	5.02	4.73	5.19	1.26	0.47	2.16	2.31	0.48
MB106380	0.08	0.06	0.13	0.13	0.27	0.24	0.31	0.42	0.42	0.17	0.11	0.30	0.35	0.13
MB107960	0.00	0.00	0.00	0.00	0.00	0.00	0.01	0.02	0.03	0.00	0.05	0.04	0.04	0.00
CO108138	0.38	0.10	0.36	0.31	0.44	0.47	0.73	0.72	0.87	0.26	0.11	0.32	0.35	0.15
CO108169	0.59	0.30	0.46	0.54	0.79	0.66	0.86	1.59	1.08	0.27	0.21	0.58	0.62	0.20
MB108924	0.00	0.00	0.00	0.01	0.00	0.00	0.00	0.00	0.00	0.00	0.03	0.01	0.02	0.01
MB110494	0.00	0.00	0.00	0.00	0.00	0.00	0.10	0.14	0.10	0.00	0.62	0.15	0.29	0.10
CO110550	0.43	0.52	1.03	1.04	1.29	1.42	1.81	2.65	1.63	0.81	0.45	0.79	0.82	0.32
MB112790	0.00	0.00	0.06	0.05	0.12	0.12	0.19	0.25	0.24	0.17	0.20	0.17	0.20	0.00
MB113980	0.00	0.00	0.00	0.00	0.00	0.00	0.00	0.00	0.00	0.00	0.25	0.00	0.01	0.03
MB114535	0.00	0.00	0.20	0.00	0.09	0.06	0.14	0.17	0.00	0.08	0.05	0.11	0.11	0.07

Table A4: Concentrations of methylalkanes in µg/gSed.

Samples	*n*-C_{12}	*n*-C_{13}	*n*-C_{14}	C_{15} branched	C_{15} branched	*n*-C_{15}	C_{16} branched	C_{16} branched	*n*-C_{16}	C_{17} branched	C_{17} branched	*n*-C_{17}	*n*-C_{18}	C_{20} branched	*n*-C_{19}	*n*-C_{20}	*n*-C_{21}	*n*-C_{22}	*n*-C_{23}	*n*-C_{24}	*n*-C_{25}	*n*-C_{26}	*n*-C_{27}	*n*-C_{28}	*n*-C_{29}	*n*-C_{30}
MB89163	0.00	0.00	0.02	0.00	0.00	0.02	0.01	0.00	0.02	0.00	0.09	0.09	0.08	0.00	0.02	0.02	0.02	0.28	0.04	0.62	0.05	0.37	0.03	0.27	0.02	0.38
MB89899	0.00	0.00	0.02	0.05	0.02	0.02	0.01	0.01	0.03	0.00	0.02	0.07	0.05	0.00	0.06	0.22	0.02	0.50	0.14	1.10	0.11	0.70	0.05	0.47	0.11	0.57
MB90020	0.00	0.00	0.02	0.01	0.01	0.03	0.01	0.01	0.08	0.00	0.02	0.15	0.09	0.00	0.03	0.05	0.04	0.30	0.11	0.87	0.13	0.68	0.05	0.45	0.04	0.51
MB91200	0.00	0.00	0.00	0.00	0.00	0.00	0.00	0.00	0.01	0.00	0.00	0.00	0.10	0.02	0.00	0.01	0.00	0.04	0.00	0.02	0.00	0.01	0.00	0.00	0.00	0.00
MB91856	0.00	0.00	0.00	0.00	0.00	0.00	0.00	0.00	0.00	0.00	0.00	0.01	0.04	0.00	0.00	0.00	0.00	0.05	0.00	0.01	0.00	0.00	0.00	0.00	0.00	0.00
CO93409	0.00	0.00	0.07	0.99	0.88	0.65	0.20	0.26	0.49	0.28	0.09	1.32	0.75	0.00	2.07	6.09	1.90	22.76	1.48	26.94	3.07	15.14	0.00	29.70	0.00	0.00
MB93589	0.00	0.00	0.03	0.03	0.04	0.05	0.03	0.02	0.09	0.10	0.02	0.10	0.22	0.00	0.49	0.18	0.00	0.24	0.12	1.23	0.28	1.10	0.19	0.75	0.45	0.00
CO94078	0.00	0.00	0.09	0.97	0.55	0.11	0.24	0.04	0.59	0.14	0.10	0.40	0.41	0.00	1.01	2.42	0.63	13.13	3.64	27.38	3.49	18.45	0.00	14.61	0.00	0.00
MB94762	0.00	0.00	0.02	0.01	0.02	0.02	0.01	0.01	0.07	0.00	0.01	0.10	0.09	0.11	0.03	0.01	0.04	0.02	0.02	0.01	0.03	0.00	0.05	0.00	0.00	
MB96334	0.00	0.00	0.02	0.01	0.01	0.03	0.01	0.01	0.08	0.00	0.02	0.09	0.07	0.00	0.04	0.23	0.02	0.08	0.01	0.13	0.03	0.14	0.02	0.18	0.02	0.14
MB97760	0.00	0.00	0.00	0.00	0.00	0.00	0.00	0.00	0.01	0.00	0.00	0.00	0.03	0.00	0.00	0.01	0.00	0.03	0.00	0.01	0.00	0.01	0.00	0.00	0.00	0.00
MB98925	0.00	0.00	0.00	0.00	0.00	0.00	0.00	0.00	0.01	0.00	0.00	0.00	0.05	0.01	0.00	0.01	0.00	0.02	0.00	0.01	0.00	0.00	0.00	0.00	0.00	0.00
CO100550	0.00	0.00	0.05	0.59	0.35	0.25	0.05	0.01	0.44	0.05	0.05	0.15	0.24	0.00	0.38	3.15	0.58	24.24	2.97	29.26	2.42	13.19	0.00	9.08	0.00	0.00
MB100778	0.00	0.00	0.01	0.00	0.00	0.02	0.01	0.01	0.03	0.00	0.01	0.09	0.04	0.00	0.03	0.01	0.03	0.05	0.00	0.02	0.01	0.02	0.01	0.06	0.01	0.03
MB102215	0.00	0.00	0.01	0.00	0.00	0.00	0.00	0.00	0.02	0.00	0.00	0.01	0.09	0.00	0.00	0.00	0.00	0.04	0.00	0.01	0.02	0.01	0.00	0.00	0.00	0.00
MB103360	0.00	0.00	0.08	0.09	0.06	0.12	0.03	0.04	0.09	0.01	0.06	0.18	0.28	0.00	0.12	0.13	0.05	0.31	0.14	2.01	0.28	2.22	0.30	2.68	0.00	1.22
CO104310	0.00	0.00	0.11	0.09	0.12	0.28	0.10	0.14	0.22	0.00	0.13	1.55	0.38	0.00	1.62	0.40	0.32	4.42	1.45	11.78	2.47	8.57	1.20	8.81	1.53	7.18
MB104920	0.00	0.00	0.14	0.00	0.00	0.23	0.13	0.09	0.25	0.00	0.04	1.23	0.35	0.00	0.67	1.08	0.26	0.15	1.04	0.44	0.05	0.54	0.07	0.48	0.11	0.26
CO105353	0.00	0.00	0.05	0.81	0.51	0.64	0.07	0.09	0.53	0.33	0.30	0.34	0.97	0.00	1.23	7.33	0.66	20.60	2.42	39.64	2.99	17.21	0.00	4.45	0.00	0.00
CO106094	0.00	0.00	0.12	0.10	0.04	0.37	0.10	0.06	0.16	0.00	0.10	1.49	0.59	0.00	2.13	0.13	0.06	0.50	0.14	1.50	0.94	3.08	0.00	2.68	0.00	0.00
MB106380	0.00	0.00	0.07	0.01	0.02	0.08	0.00	0.02	0.11	0.00	0.00	0.05	0.14	0.00	0.05	0.02	0.01	0.12	0.64	0.46	0.13	0.77	0.21	0.91	0.16	0.23
MB107960	0.00	0.00	0.03	0.00	0.00	0.00	0.00	0.00	0.02	0.00	0.00	0.01	0.07	0.01	0.01	0.01	0.04	0.00	0.02	0.01	0.00	0.00	0.00	0.00	0.00	0.00
CO108138	0.00	0.00	0.01	0.10	0.03	0.22	0.01	0.01	0.34	0.03	0.02	0.11	0.17	0.00	0.71	1.01	0.07	3.32	0.45	10.16	0.78	4.30	0.00	5.09	0.00	0.00
CO108169	0.00	0.00	0.05	0.24	0.25	0.63	0.07	0.04	0.70	0.40	0.06	0.68	0.27	0.00	1.81	6.31	0.11	3.52	0.67	19.37	3.34	14.83	0.00	8.94	0.00	0.00
MB108924	0.00	0.00	0.01	0.00	0.00	0.00	0.00	0.00	0.01	0.00	0.00	0.01	0.05	0.00	0.01	0.01	0.81	0.00	0.01	0.00	0.00	0.00	0.00	0.00	0.00	0.00
MB110494	0.01	0.00	0.01	0.00	0.00	0.00	0.00	0.00	0.01	0.00	0.00	0.01	0.08	0.00	0.03	0.01	0.00	0.03	0.01	0.09	0.07	0.55	0.02	0.03	0.00	0.00
CO110550	0.00	0.00	0.10	0.04	0.00	0.05	0.01	0.03	0.07	0.00	0.07	0.19	0.09	0.00	0.09	0.08	0.00	0.34	0.16	0.24	0.04	1.01	0.00	1.88	0.00	0.00
MB112790	0.00	0.00	0.05	0.00	0.01	0.12	0.02	0.04	0.19	0.01	0.01	1.21	0.27	3.09	0.21	0.03	0.08	0.02	0.02	0.01	0.02	0.01	0.05	0.01	0.03	
MB113980	0.01	0.00	0.01	0.00	0.00	0.00	0.00	0.00	0.06	0.00	0.00	0.02	0.09	0.02	0.01	0.00	0.00	0.04	0.00	0.01	0.00	0.01	0.00	0.00	0.00	0.00
MB114535	0.00	0.00	0.02	0.01	0.01	0.06	0.02	0.04	0.07	0.01	0.02	0.24	0.11	0.00	0.29	0.05	0.02	0.10	0.04	0.22	0.03	0.18	0.03	0.18	0.02	0.12

Table A5: Concentrations of the *n*-alcohols and the branched alcohlic hydrocarbons (µg/gSed).

Samples	*n*-C_{12}	*n*-C_{13}	*n*-C_{14}	C_{15} branched	C_{15} branched	*n*-C_{15}	C_{16} branched	C_{16} branched	*n*-C_{16}	C_{17} branched	C_{17} branched	*n*-C_{17}	*n*-C_{18}	C_{20} branched	*n*-C_{19}	*n*-C_{20}	*n*-C_{21}	*n*-C_{22}	*n*-C_{23}	*n*-C_{24}	*n*-C_{25}	*n*-C_{26}	*n*-C_{27}	*n*-C_{28}	*n*-C_{29}	*n*-C_{30}
MB89163			2.7	0.4	0.5	2.6	1.2	0.4	1.7	0.5	9.6	9.6	8.9	0.0	2.6	2.6	2.2	30.2	4.0	67.4	5.8	40.0	3.2	28.8	2.7	41.2
MB89899			1.6	5.0	2.1	2.3	1.3	1.1	3.1	0.5	1.6	6.9	4.9	0.0	6.6	22.8	2.3	52.6	15.0	116.1	11.7	73.9	5.7	49.9	11.2	59.9
MB90020			1.9	0.9	1.3	3.3	1.5	1.4	9.4	0.4	2.7	17.5	10.9	0.0	3.6	6.4	4.6	34.8	13.3	101.0	14.9	78.6	5.9	52.5	4.6	59.3
MB91200	4.5	1.7	9.6	0.0	0.0	3.5	0.0	0.0	26.4	0.0	0.0	7.9	202.2	43.3	0.0	24.4	0.0	82.9	1.9	37.8	6.6	28.8	1.1	6.4	0.0	3.4
MB91856	4.1	0.8	6.4	0.0	0.0	1.6	0.0	0.0	9.1	0.0	0.0	13.9	88.4	0.0	0.0	1.4	0.0	103.1	2.3	14.9	2.4	2.5	0.0	1.7	0.0	0.0
CO93409			0.1	2.1	1.9	1.4	0.4	0.5	1.1	0.6	0.2	2.8	1.6	0.0	4.4	13.1	4.1	48.8	3.2	57.8	6.6	32.5	0.0	63.7	0.0	0.0
MB93589			1.7	1.8	2.2	3.0	1.7	1.3	5.0	5.6	0.9	5.7	12.6	0.0	27.7	10.0	0.0	13.5	6.5	68.9	15.7	62.0	10.7	41.9	25.2	0.0
CO94078			0.3	3.0	1.7	0.3	0.7	0.1	1.8	0.4	0.3	1.3	1.3	0.0	3.2	7.6	2.0	41.2	11.4	86.0	11.0	57.9	0.0	45.9	0.0	0.0
MB94762			1.8	0.8	1.6	1.7	1.2	0.9	7.2	0.0	0.9	11.0	9.6	0.0	11.8	3.2	1.1	4.2	2.2	2.1	1.1	3.1	0.0	5.5	0.0	0.0
MB96334			5.5	2.3	1.8	7.0	3.4	3.1	19.7	0.0	5.1	23.0	17.2	0.0	9.6	57.0	5.5	19.4	3.1	32.0	6.3	35.0	4.6	45.8	5.1	34.6
MB97760	2.6	0.6	3.8	0.0	0.0	1.1	0.0	0.0	7.1	0.0	0.0	2.7	37.9	3.5	0.0	7.5	0.0	35.5	1.2	14.3	2.2	6.9	0.0	1.8	0.0	0.0
MB98925	1.8	0.4	3.8	0.0	0.0	0.7	0.0	0.0	8.2	0.0	0.0	3.4	48.6	6.8	2.6	10.7	0.0	20.7	1.0	6.1	0.4	1.5	0.4	0.5	0.0	0.0
CO100550			0.1	1.4	0.8	0.6	0.1	0.0	1.1	0.1	0.1	0.4	0.6	0.0	0.9	7.5	1.4	57.7	7.1	69.6	5.7	31.4	0.0	21.6	0.0	0.0
MB100778			2.7	0.7	0.9	4.2	1.6	2.5	6.6	0.0	2.7	20.0	9.4	0.0	7.4	2.6	6.5	9.8	0.3	4.7	1.9	3.4	2.5	12.9	1.4	7.2
MB102215	2.9	0.0	6.4	0.0	0.0	0.0	0.0	0.0	17.5	0.0	0.0	9.6	83.4	0.0	0.0	3.9	0.0	34.0	2.9	11.4	22.5	4.8	0.0	1.5	0.0	0.0
MB103360			1.2	1.3	0.8	1.7	0.4	0.6	1.2	0.1	0.9	2.5	3.9	0.0	1.7	1.8	0.7	4.4	2.0	28.3	3.9	31.3	4.2	37.8	0.0	17.2
CO104310			3.1	2.5	3.2	7.8	2.8	3.7	5.9	0.0	3.6	42.6	10.6	0.0	44.5	11.1	8.9	121.3	39.9	323.6	67.9	235.5	32.9	242.1	41.9	197.1
MB104920			13.5	0.0	0.0	22.3	12.6	9.1	25.0	0.0	4.3	121.7	35.0	0.0	66.7	107.0	25.3	15.2	103.0	43.5	5.1	53.3	6.8	47.8	10.5	25.5
CO105353			0.1	2.1	1.3	1.6	0.2	0.2	1.3	0.9	0.8	0.9	2.5	0.0	3.1	18.7	1.7	52.6	6.2	101.1	7.6	43.9	0.0	11.4	0.0	0.0
CO106094			2.5	2.1	0.9	7.9	2.1	1.2	3.3	0.1	2.2	31.7	12.5	0.0	45.1	2.8	1.2	10.6	3.0	31.7	19.9	65.4	0.0	56.8	0.0	0.0
MB106380	0.0	0.0	3.6	0.6	1.2	4.4	0.0	0.8	5.8	0.0	0.0	2.8	7.7	0.0	2.6	1.2	0.6	6.3	34.1	24.3	6.8	40.5	11.0	48.0	8.3	12.2
MB107960	7.2	3.1	83.4	0.0	0.0	3.6	0.0	0.0	57.5	0.0	0.0	34.7	182.0	34.5	17.4	30.3	99.8	3.2	50.5	14.9	0.0	0.0	0.0	0.0	0.0	0.0
CO108138			0.0	0.2	0.1	0.5	0.0	0.0	0.7	0.1	0.0	0.2	0.4	0.0	1.5	2.2	0.2	7.2	1.0	22.1	1.7	9.4	0.0	11.1	0.0	0.0
CO108169			0.1	0.6	0.7	1.7	0.2	0.1	1.8	1.0	0.2	1.8	0.7	0.0	4.7	16.4	0.3	9.2	1.7	50.5	8.7	38.6	0.0	23.3	0.0	0.0
MB108924	7.7	1.4	19.6	0.0	0.0	1.7	0.0	0.0	13.9	0.0	0.0	21.1	76.6	5.1	9.8	9.4	1355	2.4	9.5	0.8	2.1	1.1	1.6	0.0	0.0	0.0
MB110494	6.3	2.0	13.8	0.0	0.0	1.2	0.0	0.0	13.6	0.0	0.0	13.6	88.8	0.0	29.6	7.0	0.0	27.9	7.6	102.4	82.3	606.5	20.3	30.9	0.0	0.0
CO110550			1.0	0.4	0.0	0.6	0.1	0.4	0.8	0.0	0.8	2.0	1.0	0.0	1.0	0.8	0.0	3.6	1.7	2.5	0.4	10.7	0.0	20.0	0.0	0.0
MB112790			3.0	0.2	0.9	7.5	1.4	2.7	12.2	0.5	0.9	77.4	17.1	0.0	196.7	13.6	1.7	5.4	1.4	1.6	0.8	1.5	0.6	3.0	0.6	2.1
MB113980	3.6	0.7	5.4	0.0	0.0	1.0	0.0	0.0	32.7	0.0	0.0	12.8	55.8	11.6	4.5	0.0	0.0	25.5	1.2	8.6	0.0	8.5	0.0	0.0	0.0	0.0
MB114535			4.6	2.4	2.2	12.0	4.3	7.8	12.3	1.2	3.4	46.2	20.8	0.0	55.2	9.9	3.5	19.2	7.1	41.4	6.3	33.3	4.8	33.3	4.1	23.1

Table A6: Concentrations of the *n*-alcohols and the branched alcohlic hydrocarbons (µg/gTOC).

Samples	*n*-C_{14}	*n*-C_{15}	*n*-C_{16}	*n*-C_{17}	*n*-C_{18}	*n*-C_{19}	*n*-C_{20}	*n*-C_{21}	*n*-C_{22}	*n*-C_{23}	*n*-C_{24}	*n*-C_{25}	*n*-C_{26}	*n*-C_{27}	*n*-C_{28}	*n*-C_{29}	*n*-C_{30}	*n*-C_{31}	*n*-C_{32}	iC_{15}	aiC_{15}	iC_{16}	aiC_{16}	iC_{17}	aiC_{17}
MB89163	28.7	18.4	57.4	3.8	30.4	0.4	1.3	0.4	1.1	0.6	4.8	1.5	2.6	0.3	1.2	0.2	1.1	0.0	0.5	1.2	1.9	0.0	3.3	0.4	0.7
MB89899	37.7	18.7	68.3	4.9	52.8	1.0	2.2	0.8	2.8	1.9	14.4	2.3	6.1	1.0	3.3	0.5	1.9	0.0	0.9	2.8	2.4	2.5	0.0	0.9	1.3
MB90020	30.3	20.7	92.6	4.5	46.9	0.7	1.6	0.4	1.6	1.0	6.5	1.0	4.3	0.5	1.8	0.4	1.7	0.0	0.7	2.7	1.9	2.7	0.0	0.8	1.1
MB91200	234.6	173.0	962.4	42.4	407.2	7.2	23.5	1.1	23.7	1.9	0.0	43.4	5.1	11.9	0.0	0.0	0.0	0.0	0.0	0.0	0.0	0.0	0.0	0.0	0.0
MB91856	1109.5	1022.6	8457.0	967.6	5202.2	0.0	143.4	0.0	108.6	0.0	0.0	236.1	0.0	0.0	0.0	0.0	0.0	0.0	0.0	0.0	0.0	0.0	0.0	0.0	0.0
CO93409	1.5	1.3	16.1	1.4	6.2	0.8	11.3	1.9	46.1	3.4	41.2	3.0	13.3	0.8	4.3	0.0	2.9	0.0	0.0	1.1	0.6	1.1	0.2	2.5	1.1
MB93589	20.5	7.3	77.3	5.0	33.4	12.2	1.6	2.4	4.6	1.8	30.7	5.5	41.5	3.8	25.0	0.0	11.0	0.0	0.0	1.2	46.3	1.4	0.0	0.0	0.9
CO94078	1.3	0.7	9.7	0.5	4.2	0.4	7.7	0.9	14.6	2.1	12.8	1.7	7.9	0.5	3.4	0.3	1.7	0.0	0.0	0.5	0.3	0.3	0.0	0.1	0.3
MB94762	18.8	9.7	95.6	3.1	46.2	0.6	1.5	0.5	1.4	0.6	3.6	0.6	2.1	0.3	1.2	0.3	0.0	0.0	0.0	1.7	0.0	0.0	0.0	0.0	0.0
MB96334	0.2	0.0	0.8	0.0	0.4	0.0	0.0	0.0	0.0	0.0	4.3	0.0	0.0	0.0	0.0	0.0	0.0	0.0	0.0	5.1	0.0	0.0	0.0	0.0	0.0
MB97760	50.1	26.7	287.0	9.4	133.6	1.6	4.7	1.8	5.7	0.4	0.0	12.7	2.1	5.1	0.0	0.0	0.0	0.0	0.0	0.0	0.0	0.0	0.0	0.0	0.0
MB98925	40.8	22.7	313.2	6.7	126.8	0.6	4.5	0.6	8.0	0.0	0.0	24.5	2.3	4.9	0.0	0.0	0.0	0.0	0.0	0.0	0.0	0.0	0.0	0.0	0.0
CO100550	18.1	8.5	85.9	5.1	27.1	2.5	21.7	4.9	64.8	15.3	163.0	20.0	80.9	5.8	37.5	22.3	0.0	0.0	0.0	10.5	4.2	0.0	0.0	2.4	2.1
MB100778	172.6	0.0	597.8	19.6	120.5	0.0	6.6	0.0	6.5	3.6	11.1	3.7	5.2	0.0	0.0	0.0	0.0	0.0	0.0	16.4	16.9	88.0	0.0	0.0	0.0
MB102215	115.9	92.9	537.9	19.6	187.7	1.3	4.2	0.0	9.9	0.0	0.0	14.9	0.0	2.4	0.0	0.0	0.0	0.0	0.0	0.0	0.0	0.0	0.0	0.0	0.0
MB103360	0.0	0.0	0.2	0.0	0.1	0.0	0.0	0.0	0.1	0.0	0.3	0.0	0.1	0.0	0.0	0.0	0.0	0.0	0.0	0.0	0.0	0.0	0.0	0.0	0.0
CO104310	7.7	3.4	49.1	1.7	36.2	1.2	5.8	1.8	24.4	9.3	137.4	12.7	71.3	5.2	28.9	3.5	20.1	0.0	7.7	1.3	0.9	0.9	0.0	0.7	0.7
MB104920	30.4	14.3	141.1	32.8	48.9	46.6	0.8	1.8	4.1	1.4	6.1	0.9	3.8	3.7	2.7	0.0	2.7	0.0	0.0	1.4	15.1	1.6	0.0	0.0	1.5
CO105353	13.2	23.9	104.5	20.7	80.2	12.0	86.9	26.1	130.3	64.8	183.1	67.2	130.8	13.1	71.5	7.4	71.8	0.0	37.7	41.9	16.5	29.5	0.0	67.3	34.3
CO106094	24.3	14.6	177.4	5.8	78.0	1.6	7.4	2.3	280.8	5.3	58.0	6.2	55.1	2.8	41.2	0.0	20.3	0.0	4.1	1.8	2.3	1.7	4.5	1.4	0.7
MB106380	9.7	4.7	67.2	1.9	26.5	0.0	1.5	0.8	5.8	2.9	19.0	2.3	9.6	1.1	4.6	0.8	2.5	0.0	0.7	0.4	0.7	0.0	0.0	0.0	0.8
MB107960	123.8	138.0	782.6	17.8	417.6	0.0	0.0	0.0	66.0	0.0	0.0	141.1	0.0	46.2	0.0	24.3	0.0	0.0	0.0	0.0	0.0	0.0	0.0	0.0	0.0
CO108138	34.3	21.0	67.3	4.8	27.4	3.3	42.9	6.7	87.3	35.3	104.6	38.4	69.9	6.0	44.4	2.8	27.0	0.0	11.4	28.0	13.4	14.9	1.4	19.2	6.1
CO108169	57.1	41.7	102.1	13.5	65.7	5.7	61.5	11.0	112.5	34.4	138.8	17.4	75.6	2.9	29.0	1.8	17.9	0.0	5.7	59.9	36.5	29.4	2.6	46.6	14.9
MB108924	1179.1	1220.0	9032.0	429.5	3834.6	160.6	289.4	61.4	437.9	0.0	138.2	900.1	80.0	309.0	12.6	54.4	0.0	0.0	0.0	0.0	0.0	0.0	0.0	0.0	0.0
MB110494	41.0	15.6	180.6	11.5	174.6	2.8	6.2	0.0	10.7	0.0	0.0	30.3	6.7	24.4	0.7	1.6	0.0	0.0	0.0	0.0	0.0	0.0	0.0	0.0	0.0
CO110550	8.3	4.3	60.5	1.6	15.6	0.2	0.8	0.3	140.1	0.4	5.7	0.6	3.5	0.3	2.3	0.0	1.6	0.0	0.8	0.5	0.7	0.4	1.8	0.2	0.5
MB112790	18.2	9.3	131.7	2.8	74.9	0.0	7.2	0.0	4.2	0.5	2.5	0.4	1.3	0.0	0.7	0.0	0.4	0.0	0.0	0.7	1.3	0.0	1.0	0.0	0.8
MB113980	191.5	91.0	717.0	32.5	442.0	3.8	15.3	2.2	17.5	5.3	39.6	0.0	6.4	11.7	0.0	1.4	0.0	0.0	0.0	0.0	0.0	0.0	0.0	0.0	0.0
MB114535	215.5	102.5	273.6	45.3	237.6	4.0	16.6	4.1	20.8	7.3	26.4	4.6	9.5	2.0	7.3	1.1	5.2	0.0	2.3	7.8	9.5	3.1	60.1	0.0	5.0

Table A7: Concentrations of the *n*-fatty acids, the i- and ai-fatty acids (µg/gTOC).

Samples	*n*-C_{14}	*n*-C_{15}	*n*-C_{16}	*n*-C_{17}	*n*-C_{18}	*n*-C_{19}	*n*-C_{20}	*n*-C_{21}	*n*-C_{22}	*n*-C_{23}	*n*-C_{24}	*n*-C_{25}	*n*-C_{26}	*n*-C_{27}	*n*-C_{28}	*n*-C_{29}	*n*-C_{30}	*n*-C_{31}	*n*-C_{32}	iC_{15}	aiC_{15}	iC_{16}	aiC_{16}	iC_{17}	aiC_{17}
MB89163	0.3	0.2	0.5	0.0	0.3	0.0	0.0	0.0	0.0	0.0	0.0	0.0	0.0	0.0	0.0	0.0	0.0	0.0	0.0	0.0	0.0	0.0	0.0	0.0	0.0
MB89899	0.4	0.2	0.6	0.0	0.5	0.0	0.0	0.0	0.0	0.0	0.1	0.0	0.1	0.0	0.0	0.0	0.0	0.0	0.0	0.0	0.0	0.0	0.0	0.0	0.0	0.0
MB90020	0.3	0.2	0.8	0.0	0.4	0.0	0.0	0.0	0.0	0.0	0.1	0.0	0.0	0.0	0.0	0.0	0.0	0.0	0.0	0.0	0.0	0.0	0.0	0.0	0.0	0.0
MB91200	0.1	0.1	0.5	0.0	0.2	0.0	0.0	0.0	0.0	0.0	0.0	0.0	0.0	0.0	0.0	0.0	0.0	0.0	0.0	0.0	0.0	0.0	0.0	0.0	0.0	0.0
MB91856	0.6	0.5	4.2	0.5	2.6	0.0	0.1	0.0	0.1	0.0	0.0	0.1	0.0	0.0	0.0	0.0	0.0	0.0	0.0	0.0	0.0	0.0	0.0	0.0	0.0	0.0
CO93409	0.7	0.6	7.5	0.7	2.9	0.4	5.2	0.9	21.5	1.6	19.2	1.4	6.2	0.4	2.0	0.0	1.4	0.5	0.3	0.5	0.1	1.2	0.5		
MB93589	0.4	0.1	1.4	0.1	0.6	0.2	0.0	0.0	0.1	0.0	0.5	0.1	0.7	0.1	0.4	0.0	0.2	0.0	0.0	0.0	0.8	0.0	0.0	0.0	0.0
CO94078	0.4	0.2	3.1	0.1	1.3	0.1	2.5	0.3	4.7	0.7	4.1	0.5	2.5	0.2	1.1	0.1	0.5	0.2	0.1	0.1	0.0	0.0	0.1		
MB94762	0.2	0.1	0.9	0.0	0.4	0.0	0.0	0.0	0.0	0.0	0.0	0.0	0.0	0.0	0.0	0.0	0.0	0.0	0.0	0.0	0.0	0.0	0.0	0.0	0.0	0.0
MB96334	0.2	0.0	0.8	0.0	0.4	0.0	0.0	0.0	0.0	0.0	0.0	0.0	0.0	0.0	0.0	0.0	0.0	0.0	0.0	0.0	0.0	0.0	0.0	0.0	0.0	0.0
MB97760	0.0	0.0	0.3	0.0	0.1	0.0	0.0	0.0	0.0	0.0	0.0	0.0	0.0	0.0	0.0	0.0	0.0	0.0	0.0	0.0	0.0	0.0	0.0	0.0	0.0	0.0
MB98925	0.0	0.0	0.3	0.0	0.1	0.0	0.0	0.0	0.0	0.0	0.0	0.0	0.0	0.0	0.0	0.0	0.0	0.0	0.0	0.0	0.0	0.0	0.0	0.0	0.0	0.0
CO100550	7.6	3.6	36.1	2.1	11.4	1.0	9.1	2.1	27.2	6.4	68.5	8.4	34.0	2.4	15.8	9.4	0.0	4.4	1.8	0.0	0.0	1.0	0.9	0.0	0.0
MB100778	0.8	0.0	2.8	0.1	0.6	0.0	0.0	0.0	0.0	0.0	0.1	0.0	0.0	0.0	0.0	0.0	0.0	0.0	0.0	0.1	0.1	0.4	0.0	0.0	0.0
MB102215	0.1	0.1	0.6	0.0	0.2	0.0	0.0	0.0	0.0	0.0	0.0	0.0	0.0	0.0	0.0	0.0	0.0	0.0	0.0	0.0	0.0	0.0	0.0	0.0	0.0	0.0
MB103360	0.7	0.5	2.7	0.2	1.1	0.1	0.3	0.1	1.1	0.4	4.6	0.5	1.9	0.1	0.7	0.0	0.1	0.1	0.1	0.1	0.0	0.0	0.0	0.0	0.0	0.0
CO104310	0.3	0.1	1.8	0.1	1.3	0.0	0.2	0.1	0.9	0.3	5.0	0.5	2.6	0.2	1.1	0.1	0.7	0.0	0.3	0.0	0.0	0.0	0.0	0.0	0.0	0.0
MB104920	0.3	0.1	1.4	0.3	0.5	0.5	0.0	0.0	0.0	0.0	0.1	0.0	0.0	0.0	0.0	0.0	0.0	0.0	0.2	0.0	0.0	0.0	0.0	0.0	0.0	0.0
CO105353	5.2	9.4	40.9	8.1	31.4	4.7	34.1	10.2	51.1	25.4	71.7	26.3	51.2	5.1	28.0	2.9	28.1	0.0	14.8	16.4	6.5	11.6	0.0	26.4	13.4
CO106094	1.1	0.7	8.4	0.3	3.7	0.1	0.3	0.1	13.2	0.2	2.7	0.3	2.6	0.1	1.9	0.0	1.0	0.0	0.2	0.1	0.1	0.1	0.2	0.1	0.0
MB106380	0.2	0.1	1.3	0.0	0.5	0.0	0.0	0.0	0.1	0.1	0.4	0.0	0.2	0.0	0.1	0.0	0.0	0.0	0.0	0.0	0.0	0.0	0.0	0.0	0.0	0.0
MB107960	0.0	0.1	0.3	0.0	0.2	0.0	0.0	0.0	0.0	0.0	0.0	0.1	0.0	0.0	0.0	0.0	0.0	0.0	0.0	0.0	0.0	0.0	0.0	0.0	0.0	0.0
CO108138	15.7	9.7	30.9	2.2	12.6	1.5	19.7	3.1	40.1	16.2	48.0	17.7	32.1	2.8	20.4	1.3	12.4	0.0	5.2	12.9	6.2	6.8	0.6	8.8	2.8
CO108169	21.9	16.0	39.2	5.2	25.2	2.2	23.6	4.2	43.2	13.2	53.3	6.7	29.0	1.1	11.1	0.7	6.9	0.0	2.2	23.0	14.0	11.3	1.0	17.9	5.7
MB108924	0.7	0.7	5.4	0.3	2.3	0.1	0.2	0.0	0.3	0.0	0.1	0.5	0.0	0.2	0.0	0.0	0.0	0.0	0.0	0.0	0.0	0.0	0.0	0.0	0.0	0.0
MB110494	0.0	0.0	0.2	0.0	0.2	0.0	0.0	0.0	0.0	0.0	0.0	0.0	0.0	0.0	0.0	0.0	0.0	0.0	0.0	0.0	0.0	0.0	0.0	0.0	0.0	0.0
CO110550	0.8	0.4	5.7	0.2	1.5	0.0	0.1	0.0	13.2	0.0	0.5	0.1	0.3	0.0	0.2	0.0	0.1	0.0	0.1	0.1	0.1	0.0	0.2	0.0	0.0
MB112790	0.3	0.1	2.1	0.0	1.2	0.0	0.1	0.0	0.1	0.0	0.0	0.0	0.0	0.0	0.0	0.0	0.0	0.0	0.0	0.0	0.0	0.0	0.0	0.0	0.0	0.0
MB113980	0.3	0.2	1.2	0.1	0.8	0.0	0.0	0.0	0.0	0.0	0.1	0.0	0.0	0.0	0.0	0.0	0.0	0.0	0.0	0.0	0.0	0.0	0.0	0.0	0.0	0.0
MB114535	1.1	0.5	1.5	0.2	1.3	0.0	0.1	0.0	0.1	0.0	0.1	0.0	0.1	0.0	0.0	0.0	0.0	0.0	0.0	0.0	0.1	0.0	0.3	0.0	0.0

Table A7: Concentrations of the *n*-fatty acids, the i- and ai-fatty acids (µg/gSed).

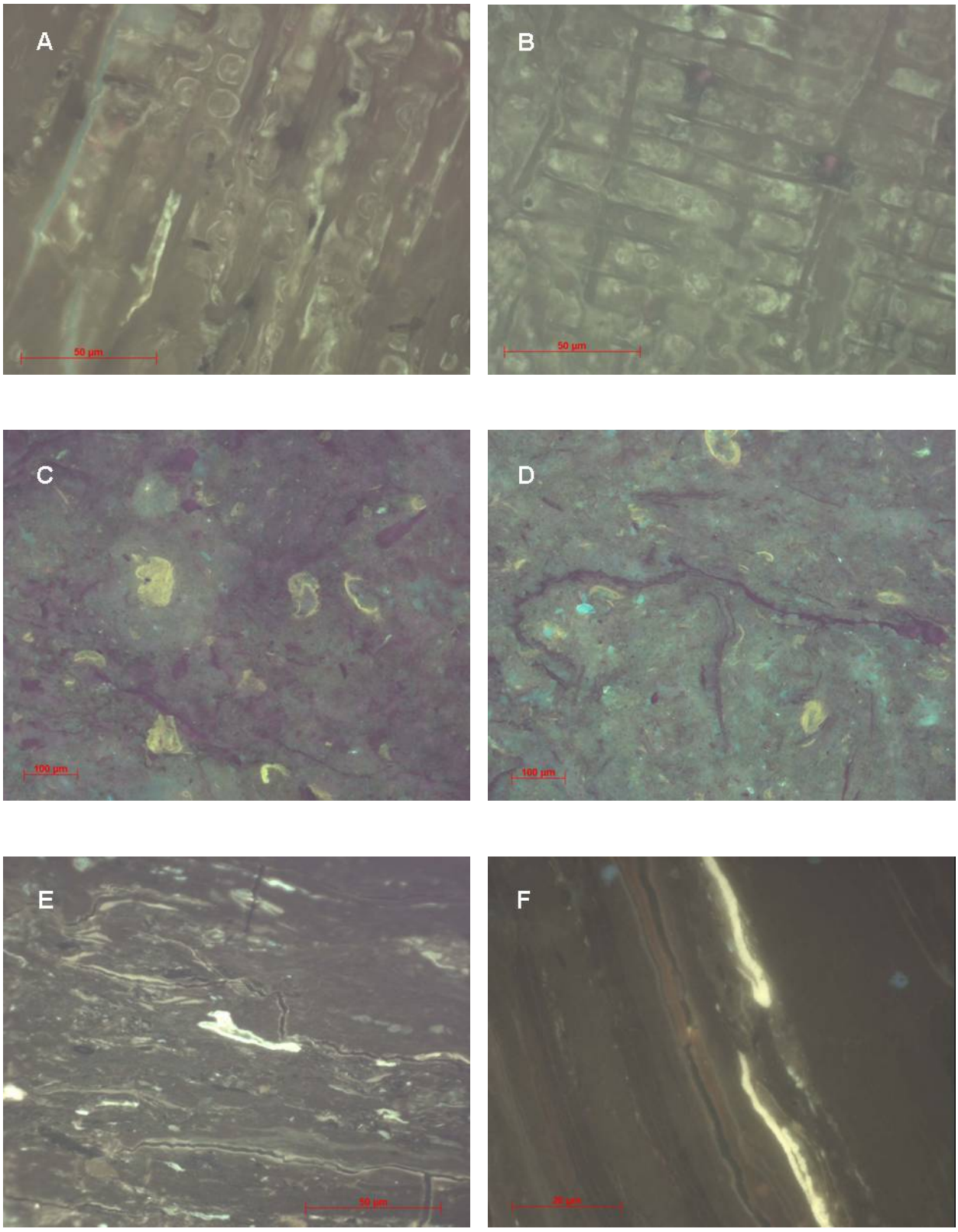

A & B: Structure of woody material of conifer in fluorescence light (CO93409); C & D: Spores (sporinite, yellow) in fluorescence light (CO104310); E & F: Sporangium (sporinite, yellow) and woody material (ulminite, brown/grey) in fluorescence (CO105353).

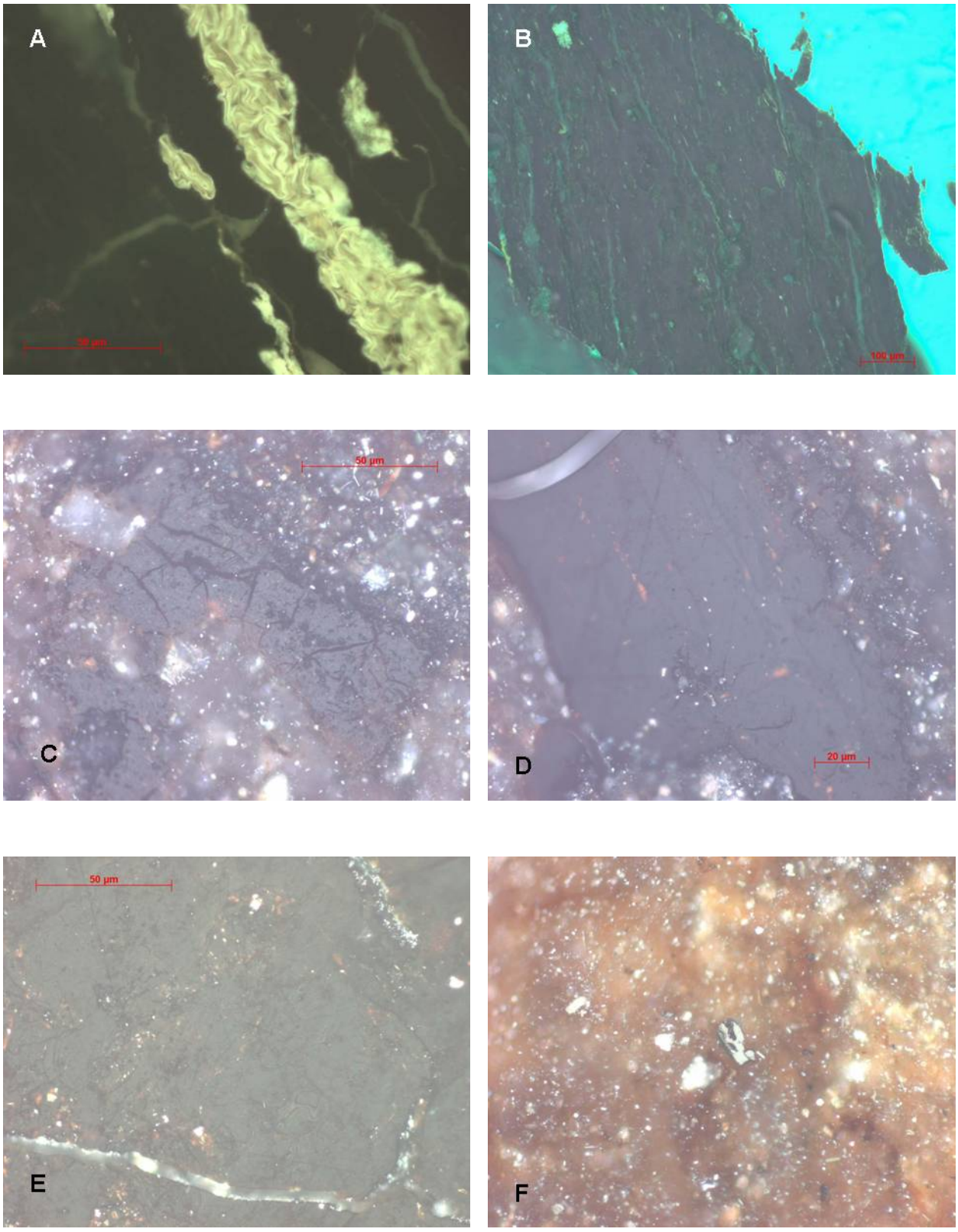

A: Sporangium (sporinite, yellow) and woody material (ulminite, brown/grey) in fluorescence (CO108138); B: Ulminite particle in fluorescence light (CO108138; blue = epoxy resin); C & D: Huminite particle in reflected white light (MB103360); E: Huminite particle in reflected white light (CO105353); F: Inertinite particle in reflected white light (CO104310).

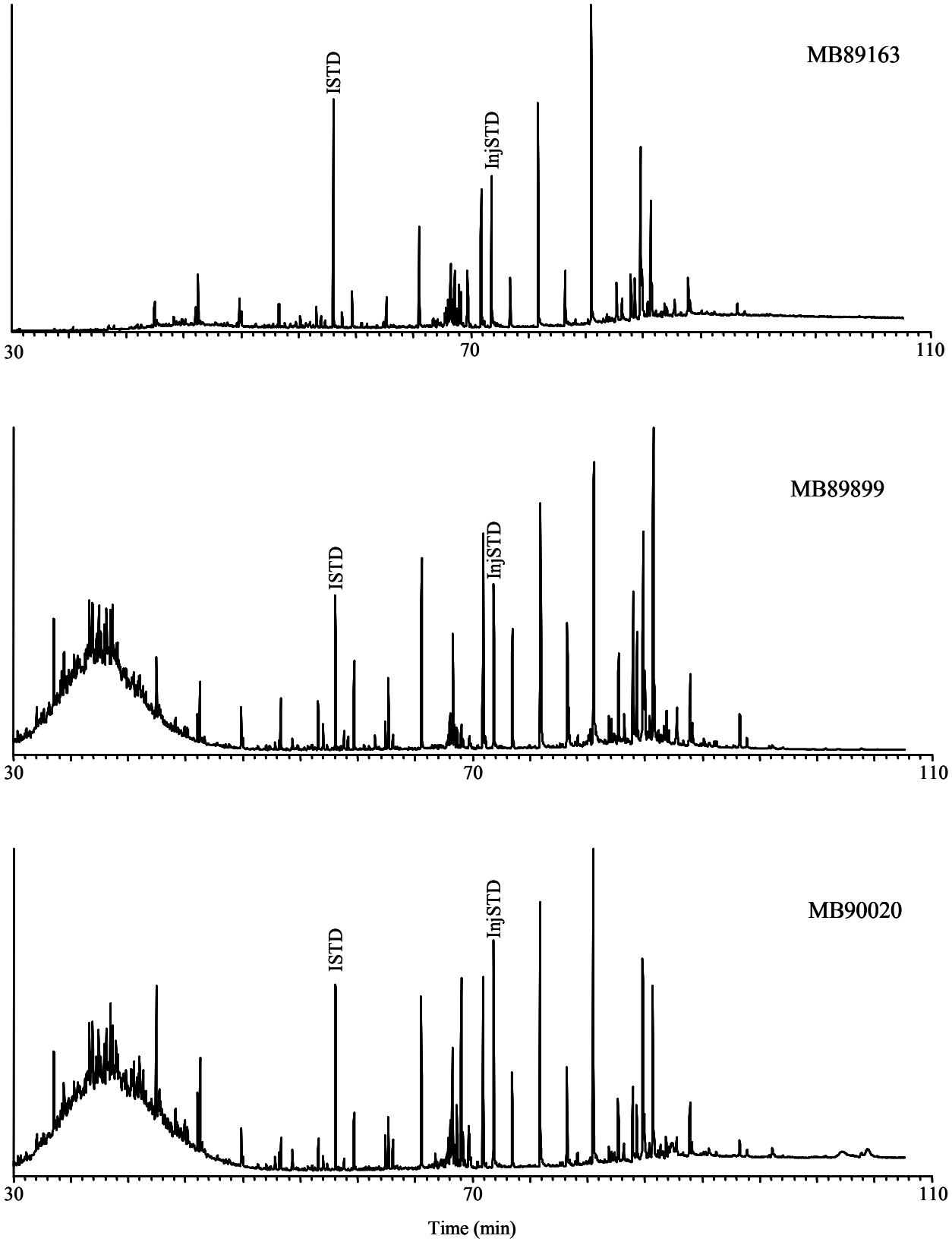
MB89163
ISTD
InjSTD
30
70
110
MB89899
ISTD
InjSTD
30
70
110
MB90020
ISTD
InjSTD
30
70
110
Time (min)

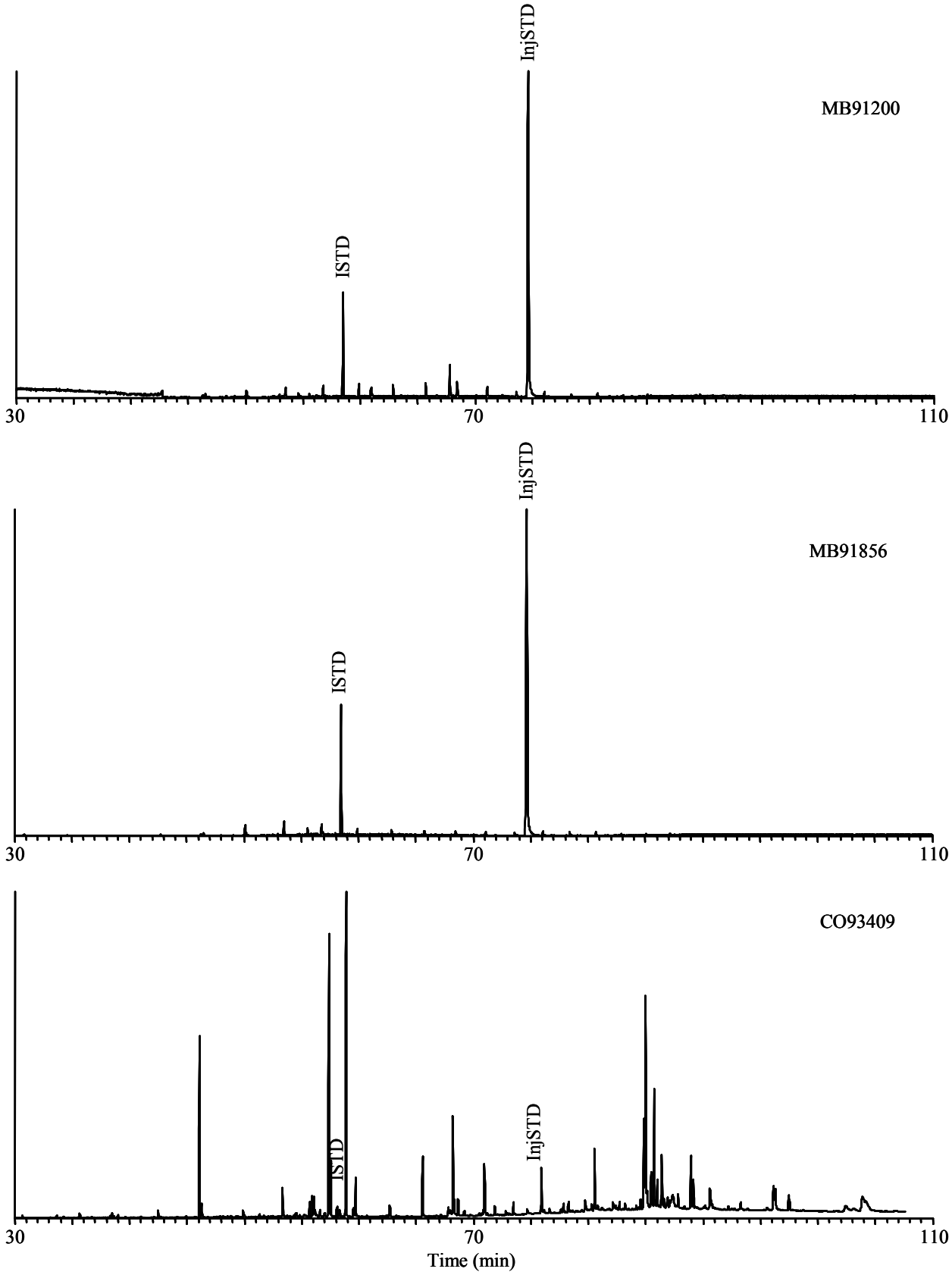
InjSTD
MB91200
ISTD
30
70
110
InjSTD
MB91856
ISTD
30
70
110
CO93409
ISTD
InjSTD
30
70
110
Time (min)

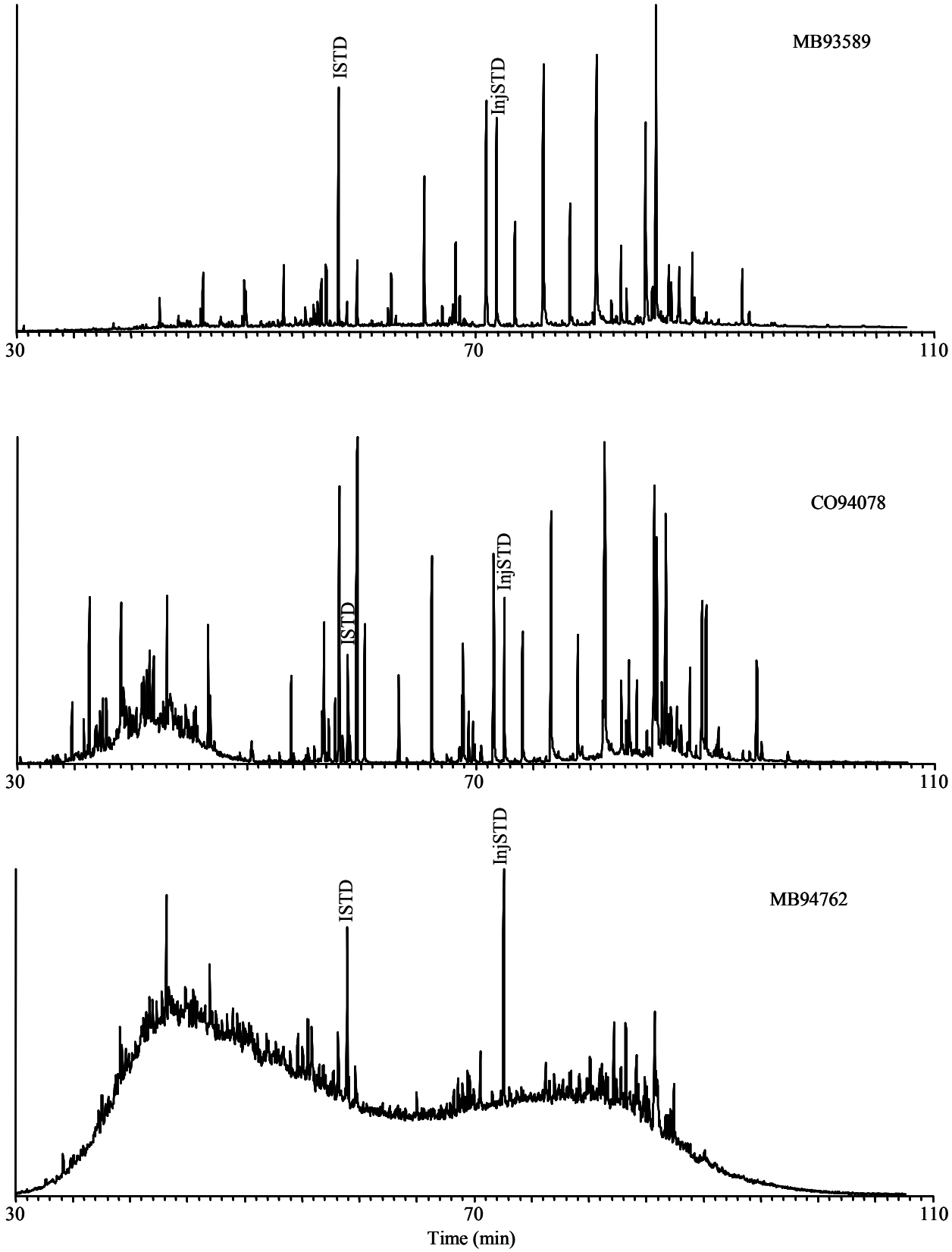
MB93589
ISTD
InjSTD
30
70
110
CO94078
ISTD
InjSTD
30
70
110
MB94762
ISTD
InjSTD
30
70
110
Time (min)

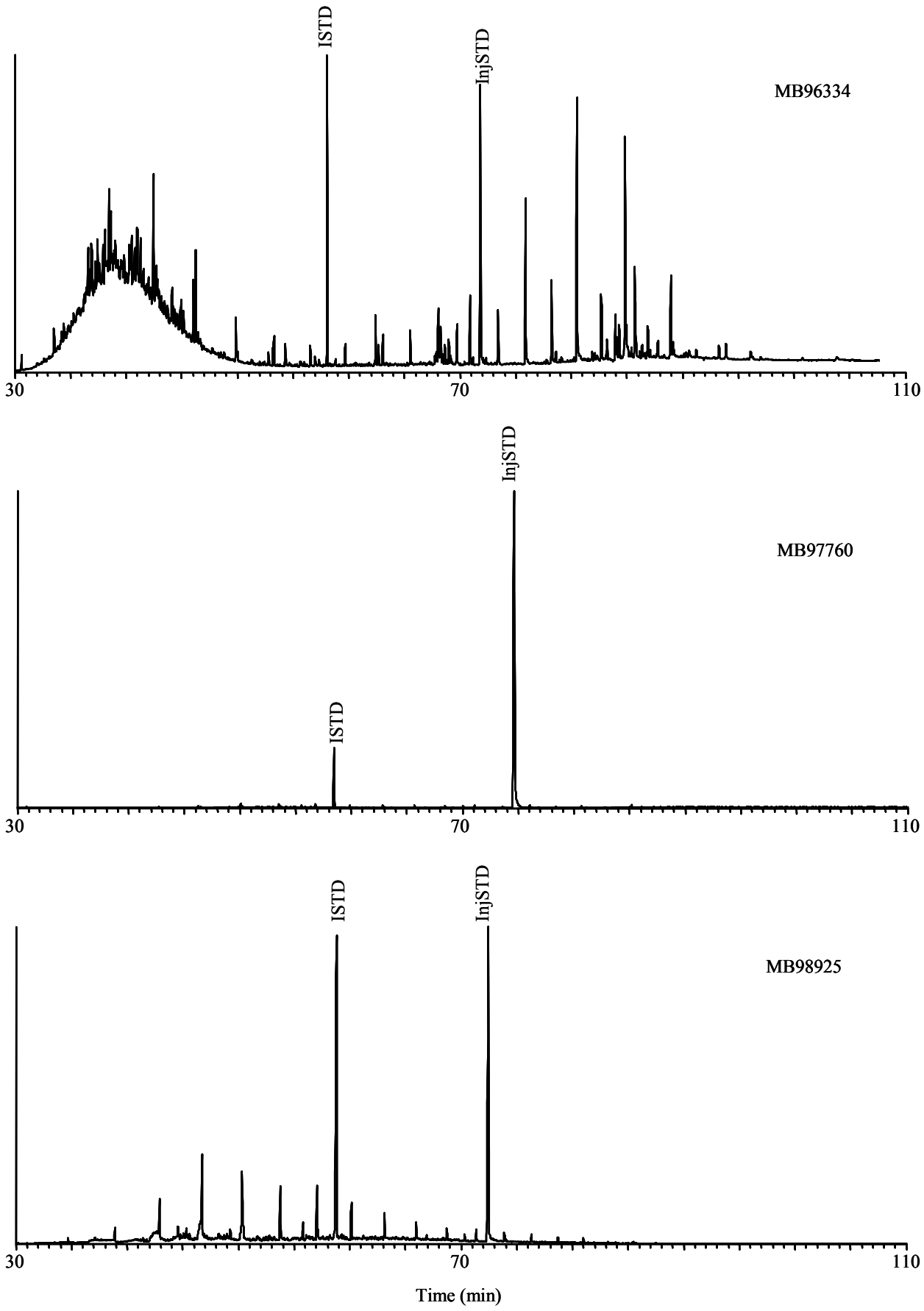
ISTD
InjSTD
MB96334
30
70
110
InjSTD
MB97760
ISTD
30
70
110
ISTD
InjSTD
MB98925
30
70
110
Time (min)

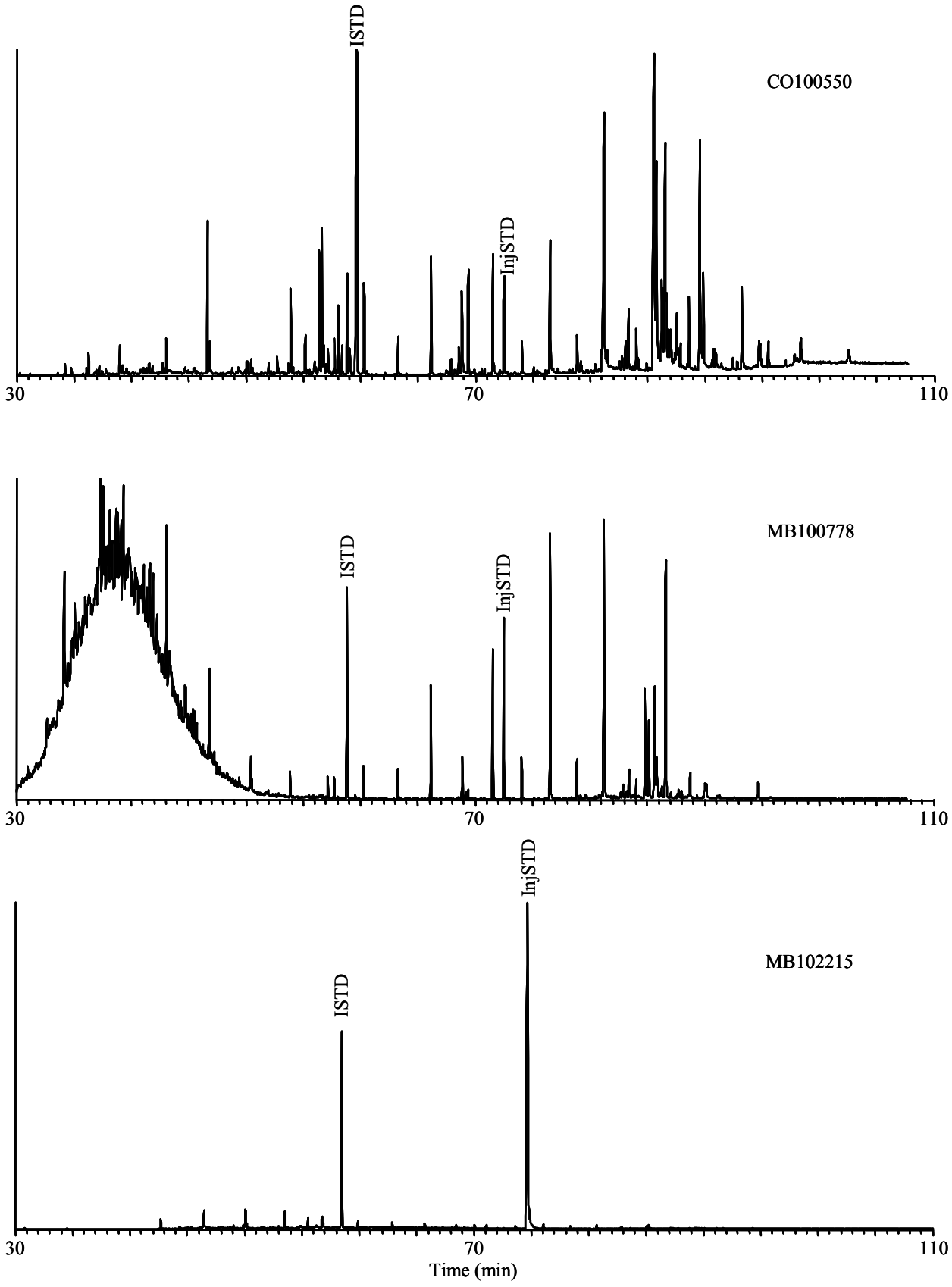
ISTD
InjSTD
CO100550
30
70
110
ISTD
InjSTD
MB100778
30
70
110
InjSTD
ISTD
MB102215
30
70
110
Time (min)

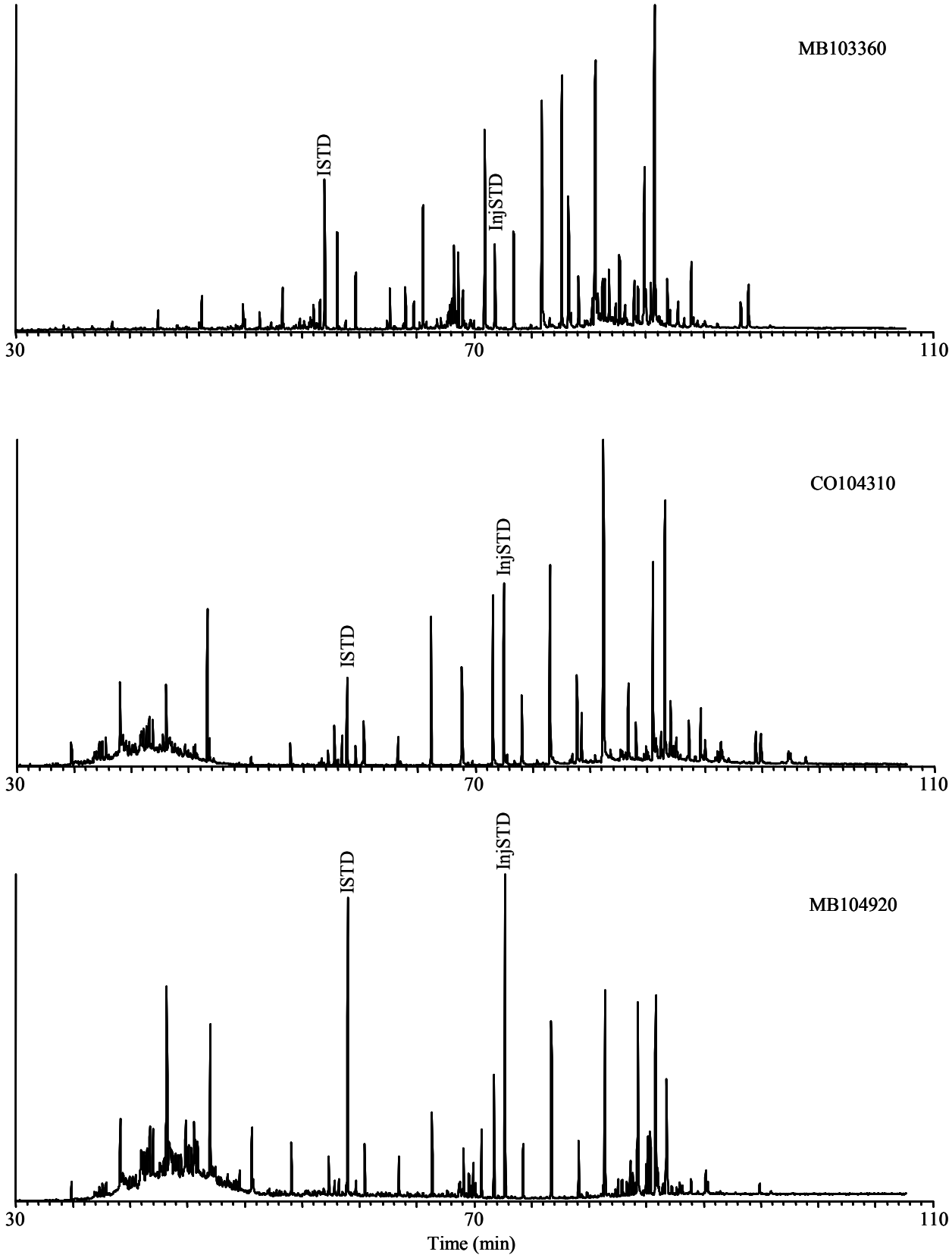
MB103360
ISTD
InjSTD
30
70
110
CO104310
ISTD
InjSTD
30
70
110
MB104920
ISTD
InjSTD
30
70
110
Time (min)

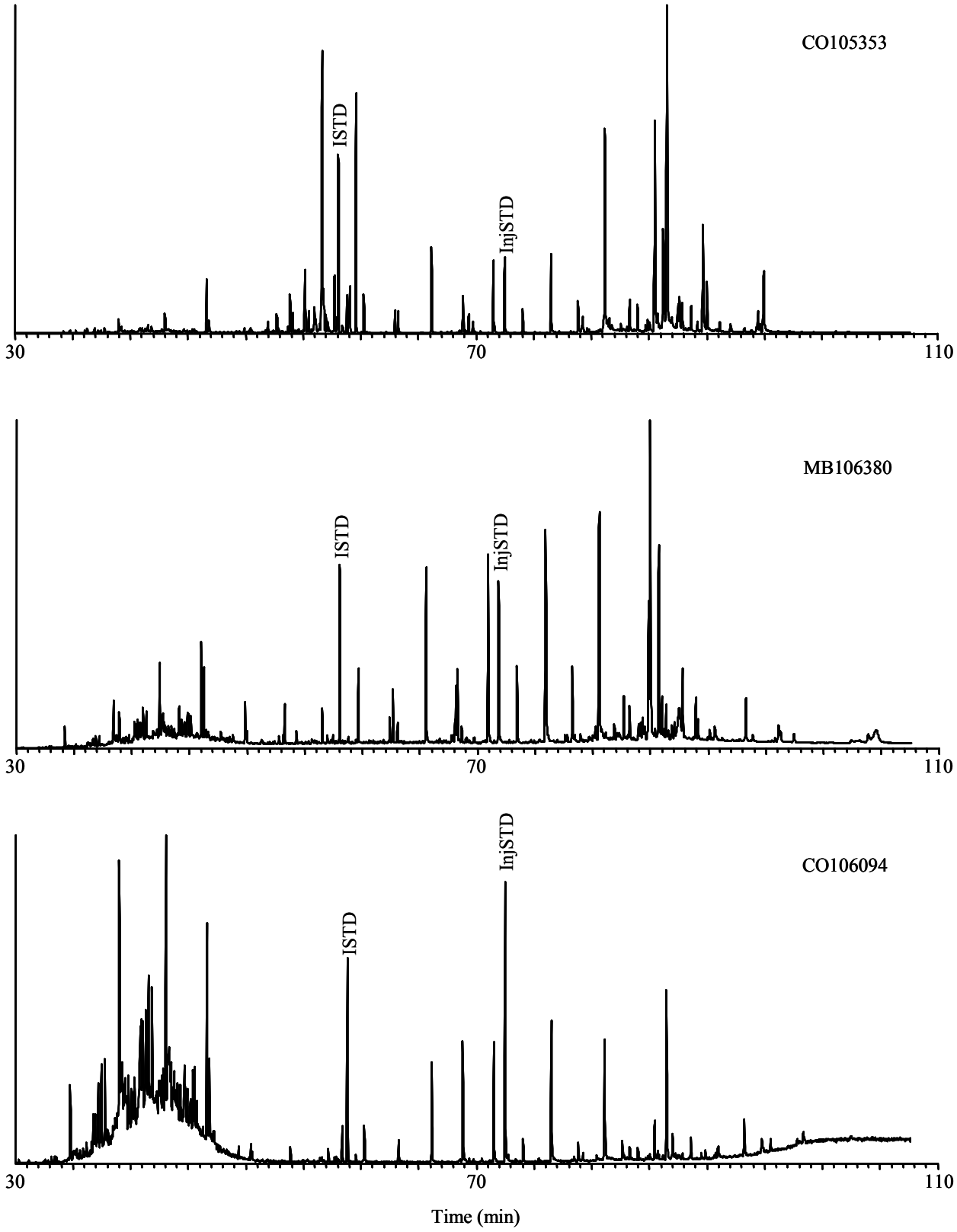
CO105353
ISTD
InjSTD
30
70
110
MB106380
ISTD
InjSTD
30
70
110
CO106094
InjSTD
ISTD
30
70
110
Time (min)

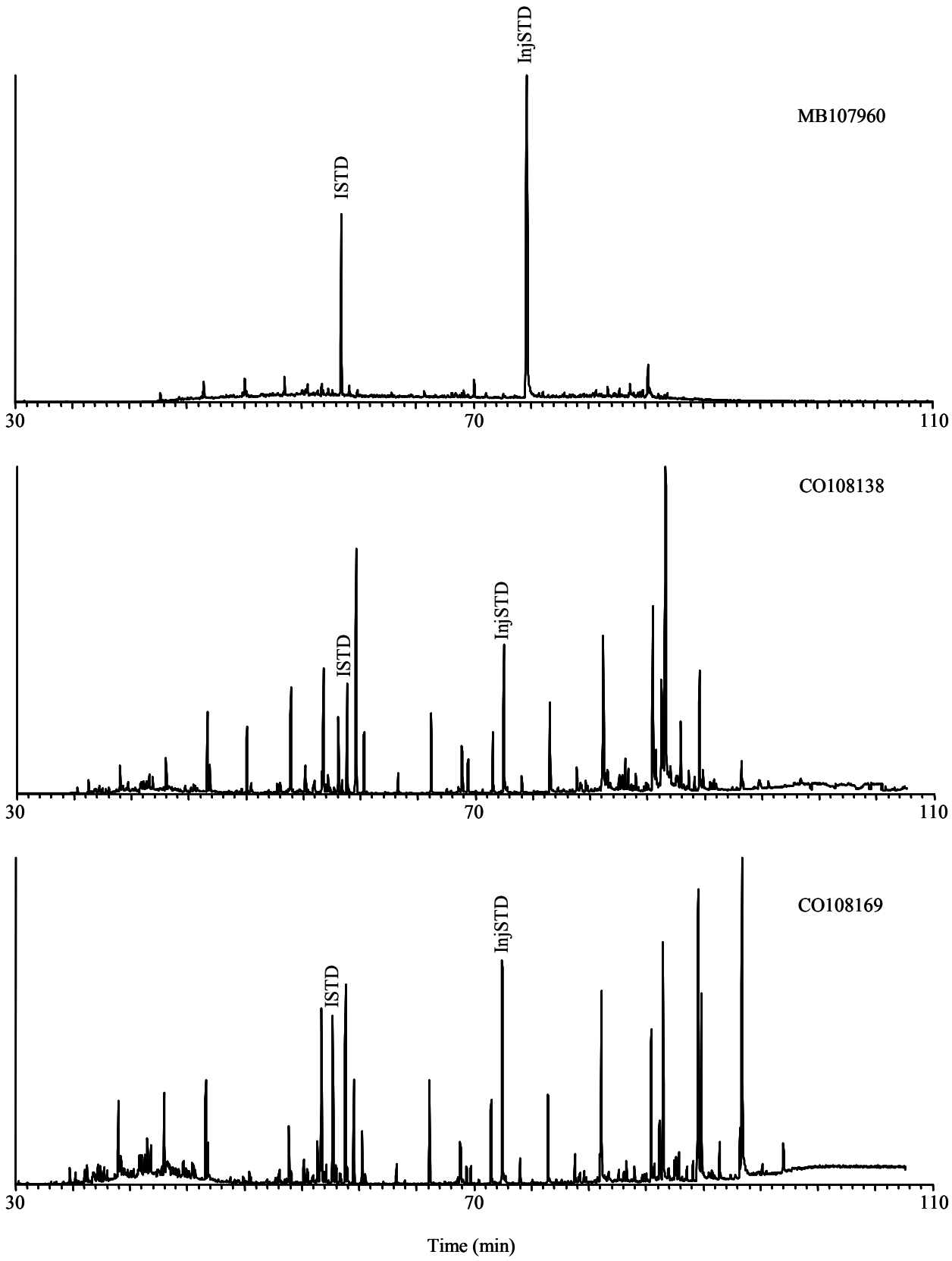
InjSTD
ISTD
MB107960
30
70
110
CO108138
ISTD
InjSTD
30
70
110
CO108169
ISTD
InjSTD
30
70
110
Time (min)

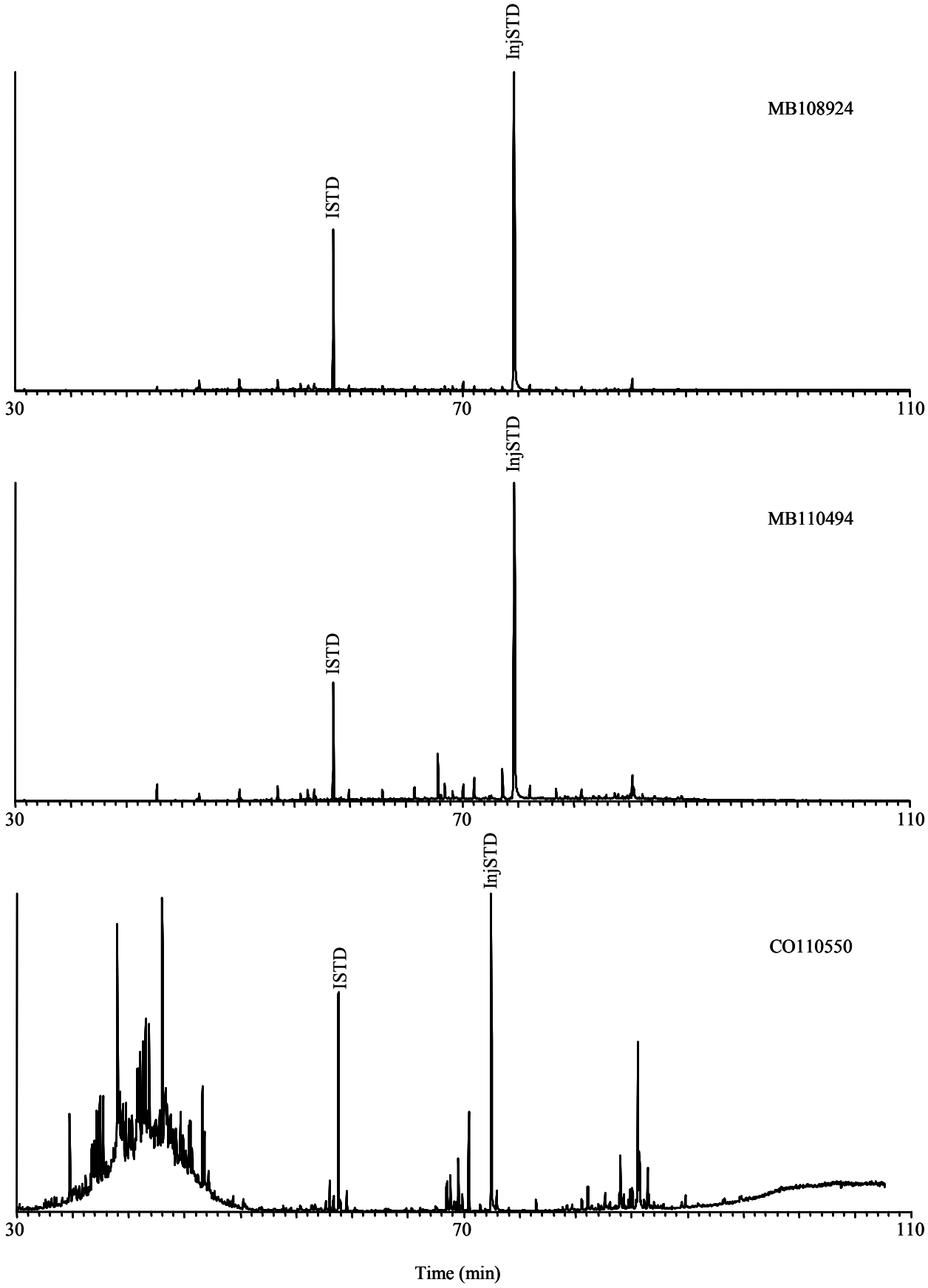
InjSTD
MB108924
ISTD
30
70
110
InjSTD
MB110494
ISTD
30
70
110
InjSTD
CO110550
ISTD
30
70
110
Time (min)

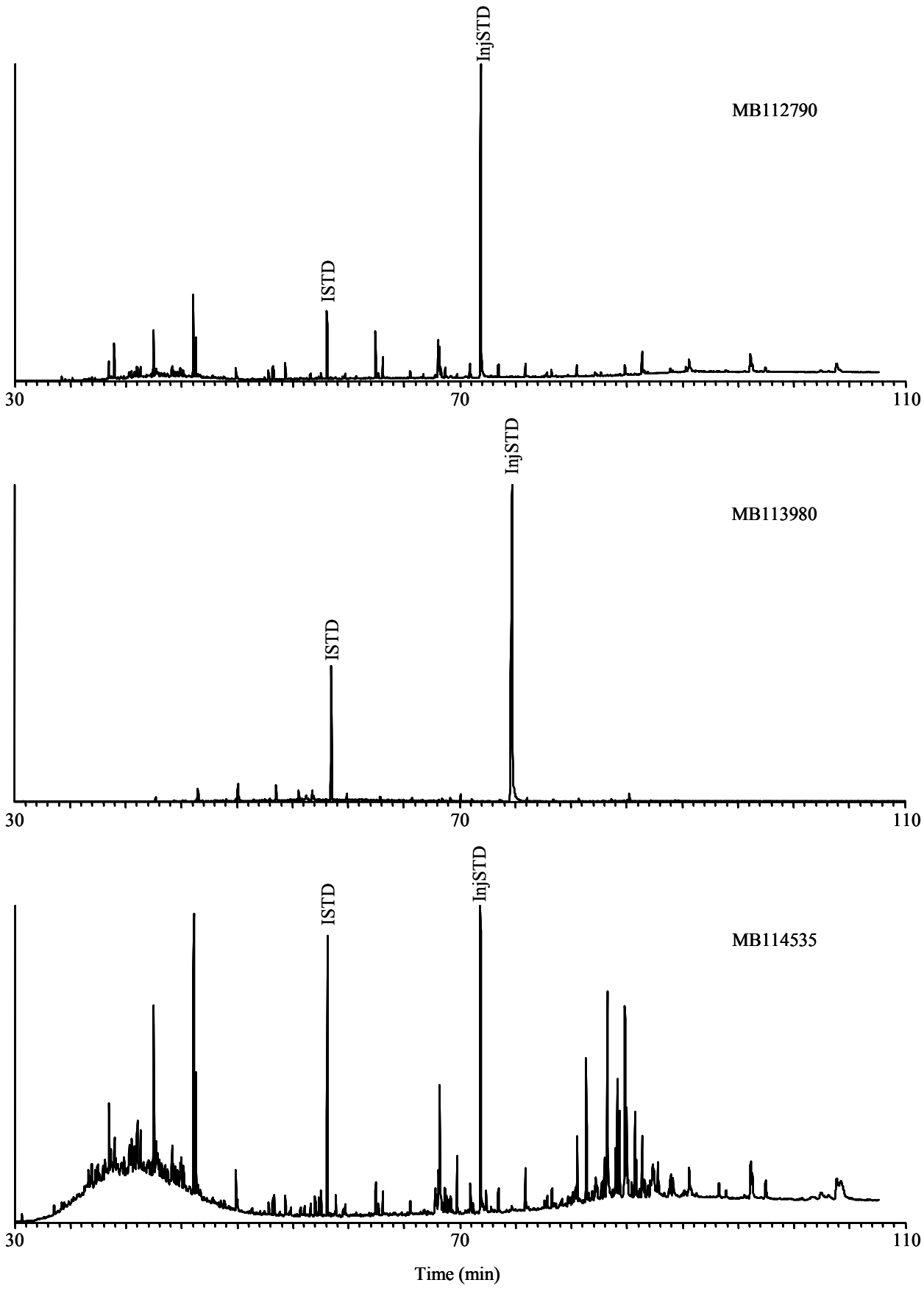
InjSTD
MB112790
ISTD
30
70
110
InjSTD
MB113980
ISTD
30
70
110
InjSTD
ISTD
MB114535
30
70
110
Time (min)

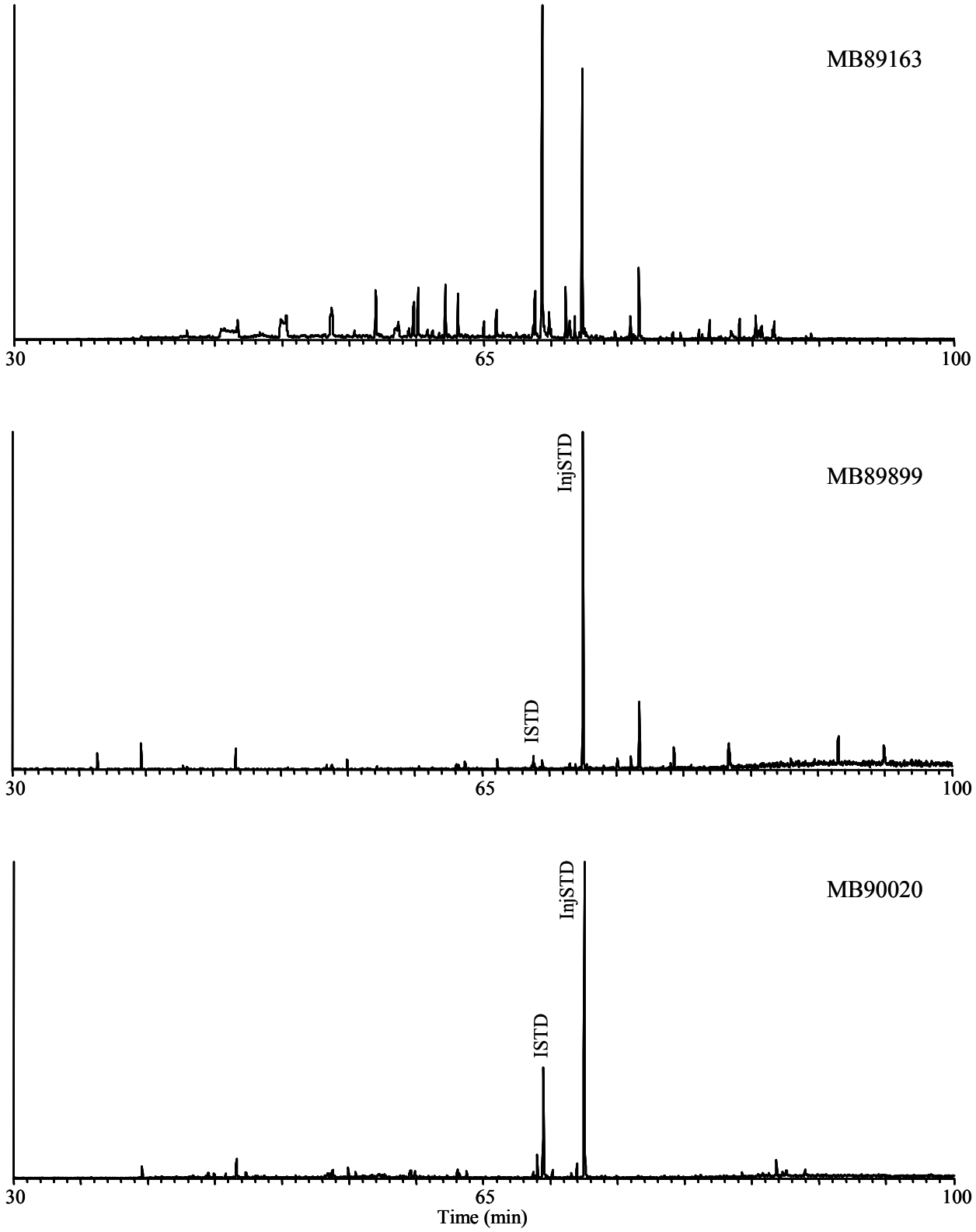
MB89163
30
65
100
InjSTD
MB89899
ISTD
30
65
100
InjSTD
MB90020
ISTD
30
65
100
Time (min)

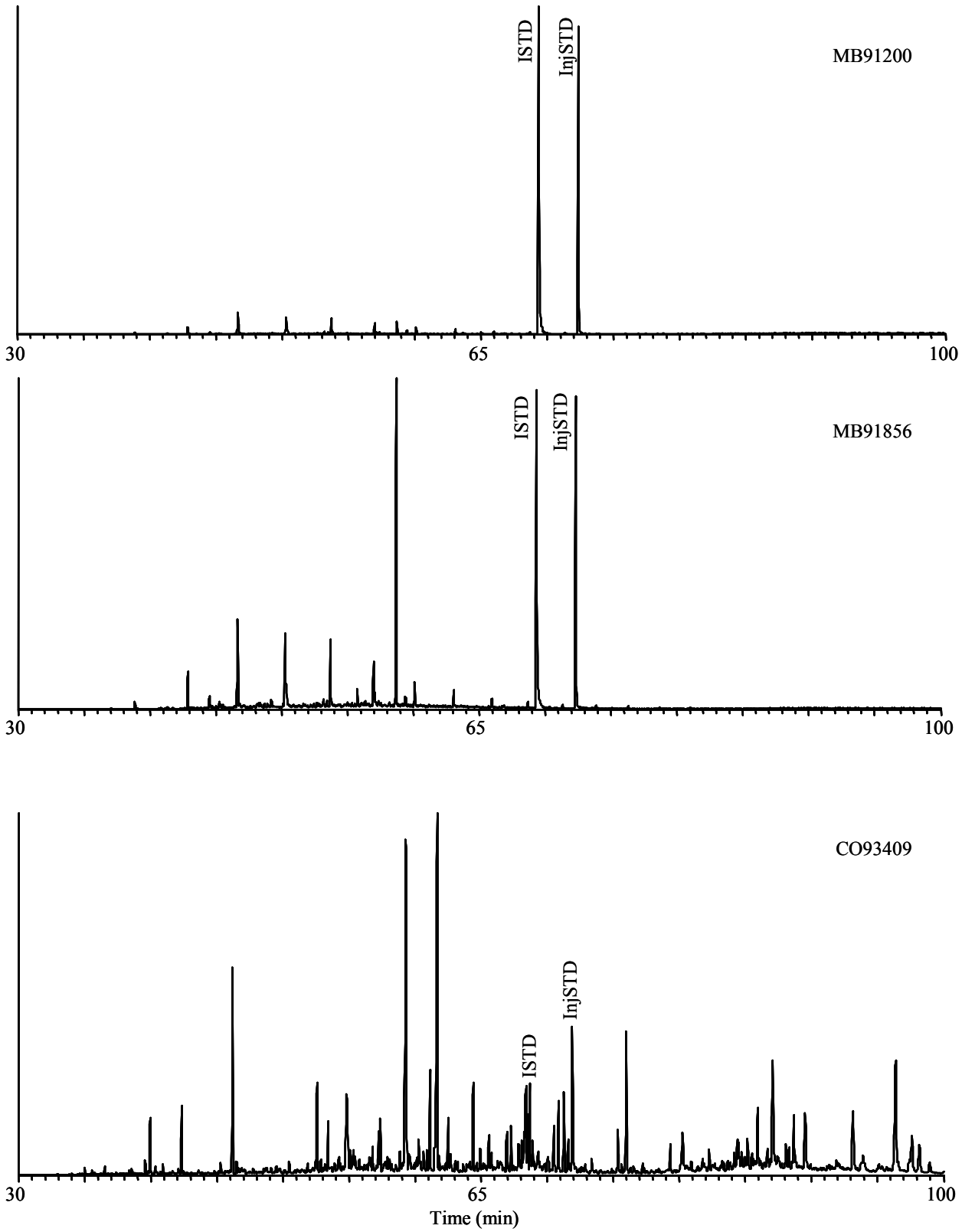
ISTD
InjSTD
MB91200
30
65
100
ISTD
InjSTD
MB91856
30
65
100
CO93409
InjSTD
ISTD
30
65
100
Time (min)

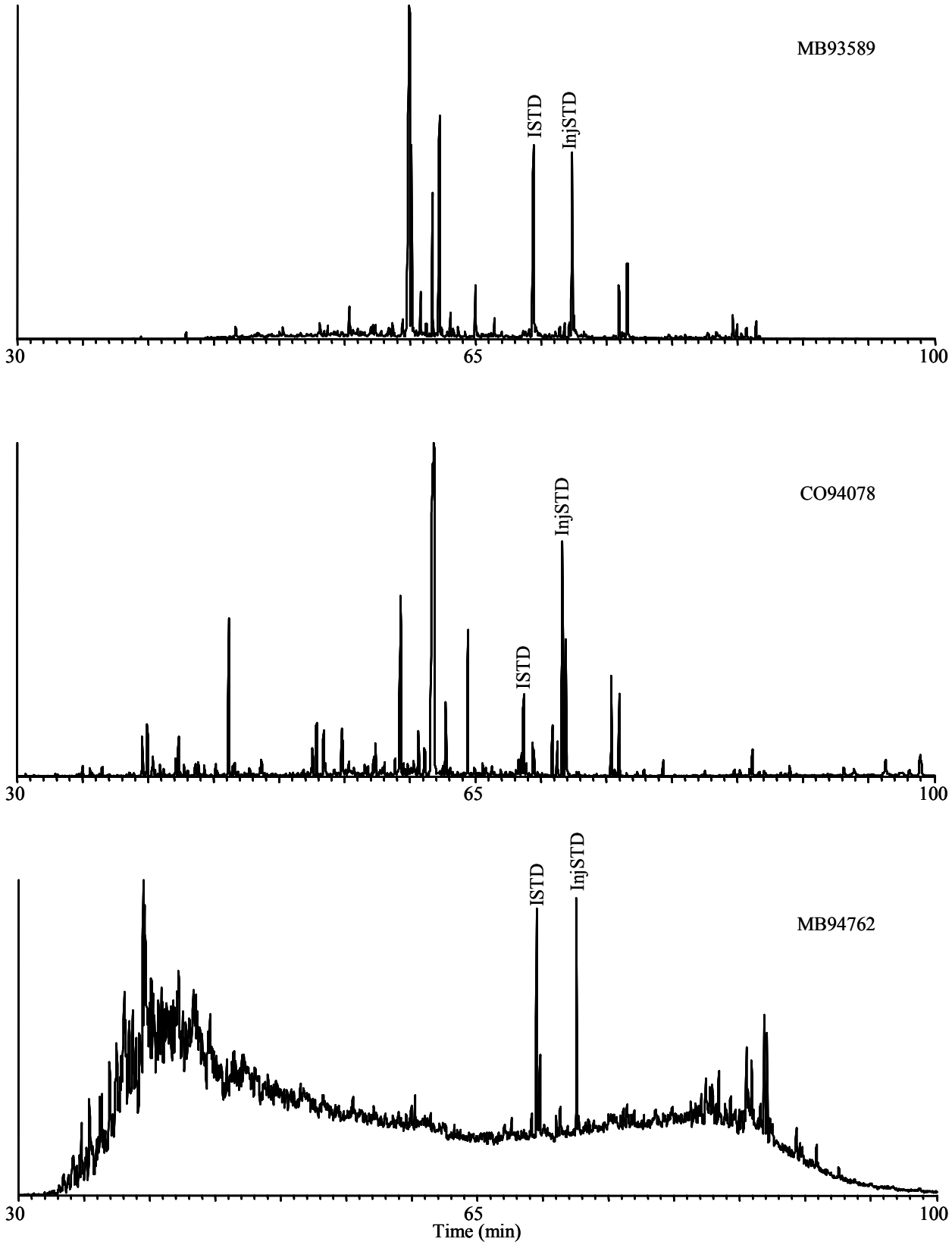
MB93589
ISTD
InjSTD
30
65
100
CO94078
ISTD
InjSTD
30
65
100
MB94762
ISTD
InjSTD
30
65
100
Time (min)

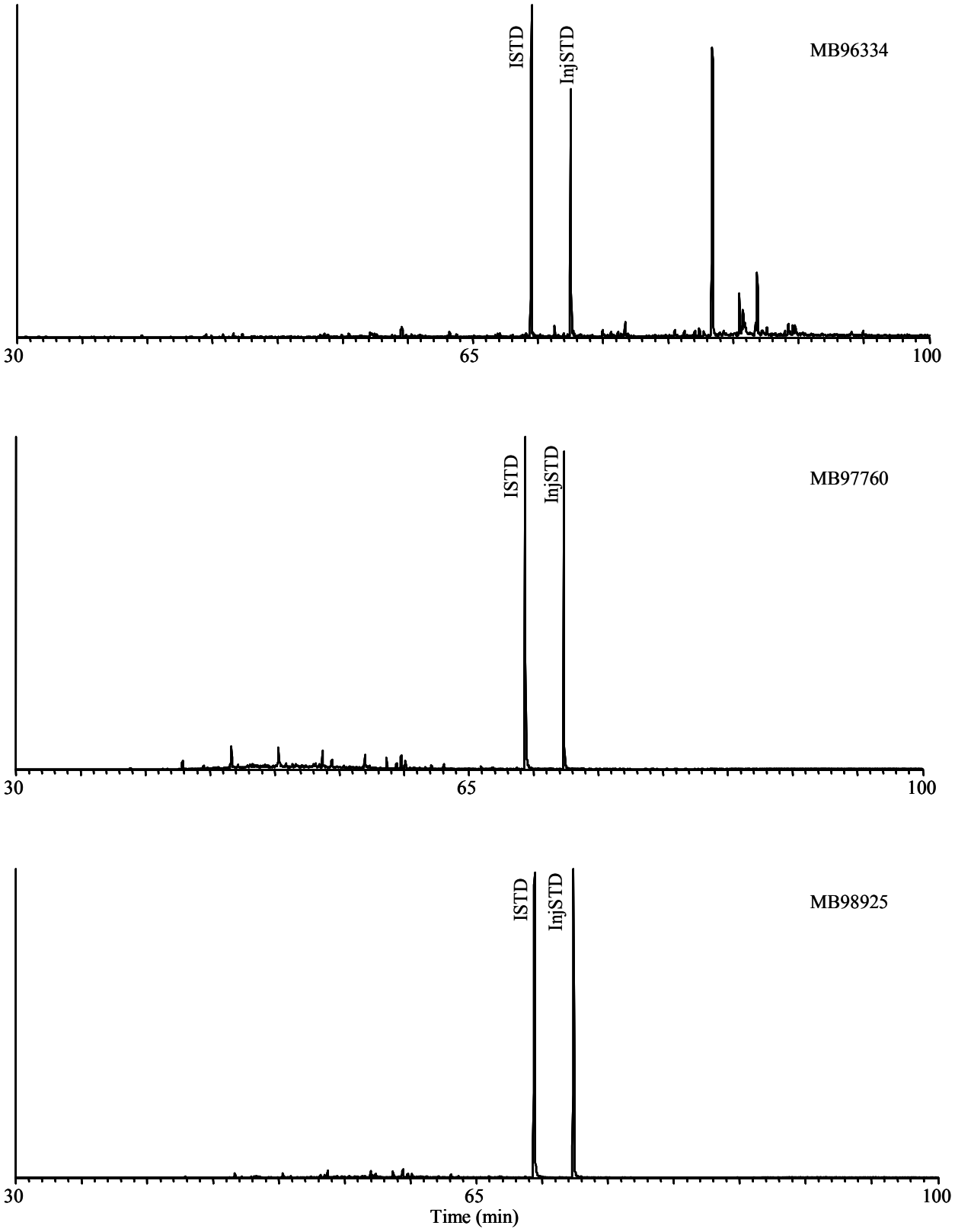
ISTD
InjSTD
MB96334
30
65
100
ISTD
InjSTD
MB97760
30
65
100
ISTD
InjSTD
MB98925
30
65
100
Time (min)

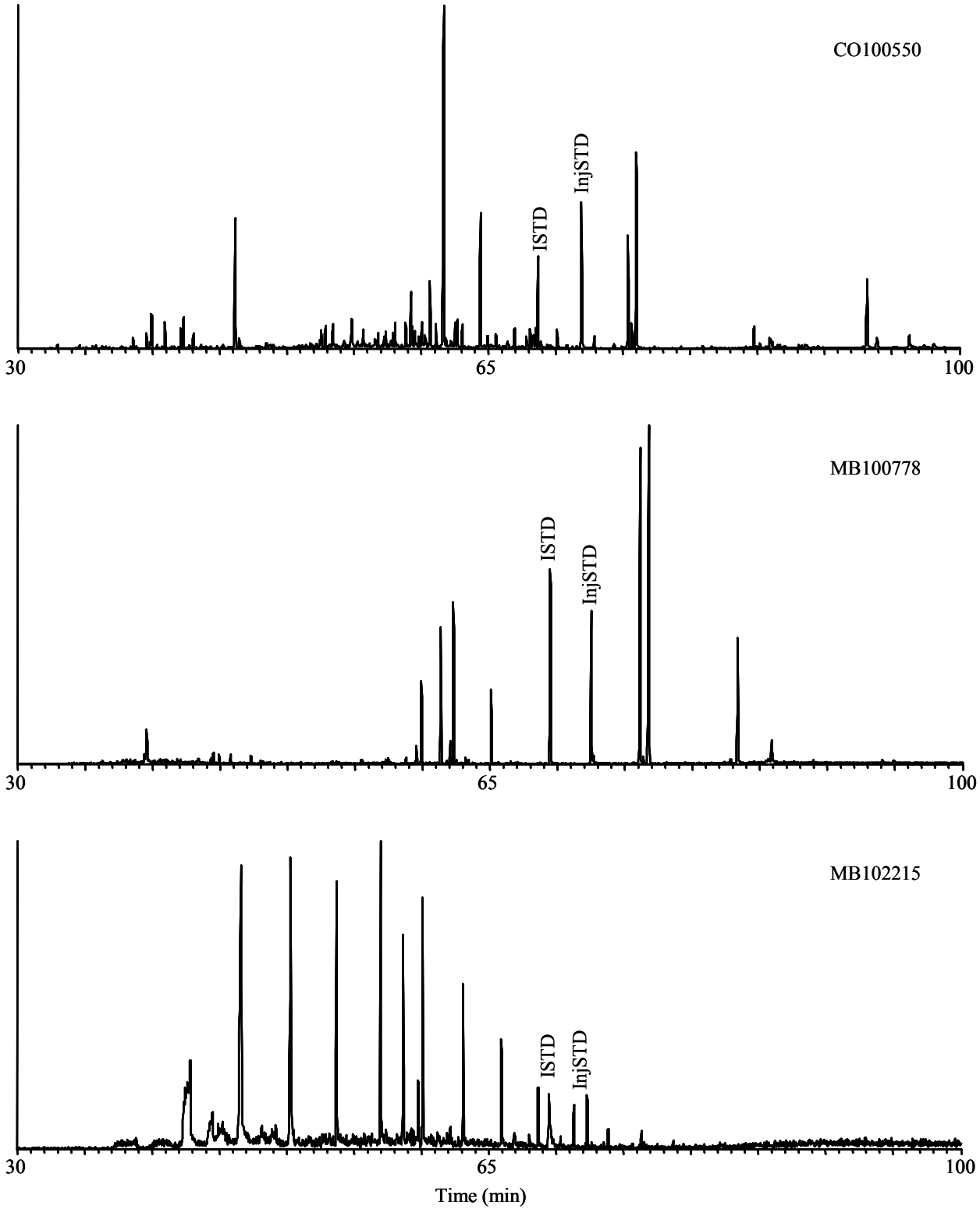
CO100550
ISTD
InjSTD
30
65
100
MB100778
ISTD
InjSTD
30
65
100
MB102215
ISTD
InjSTD
30
65
100
Time (min)

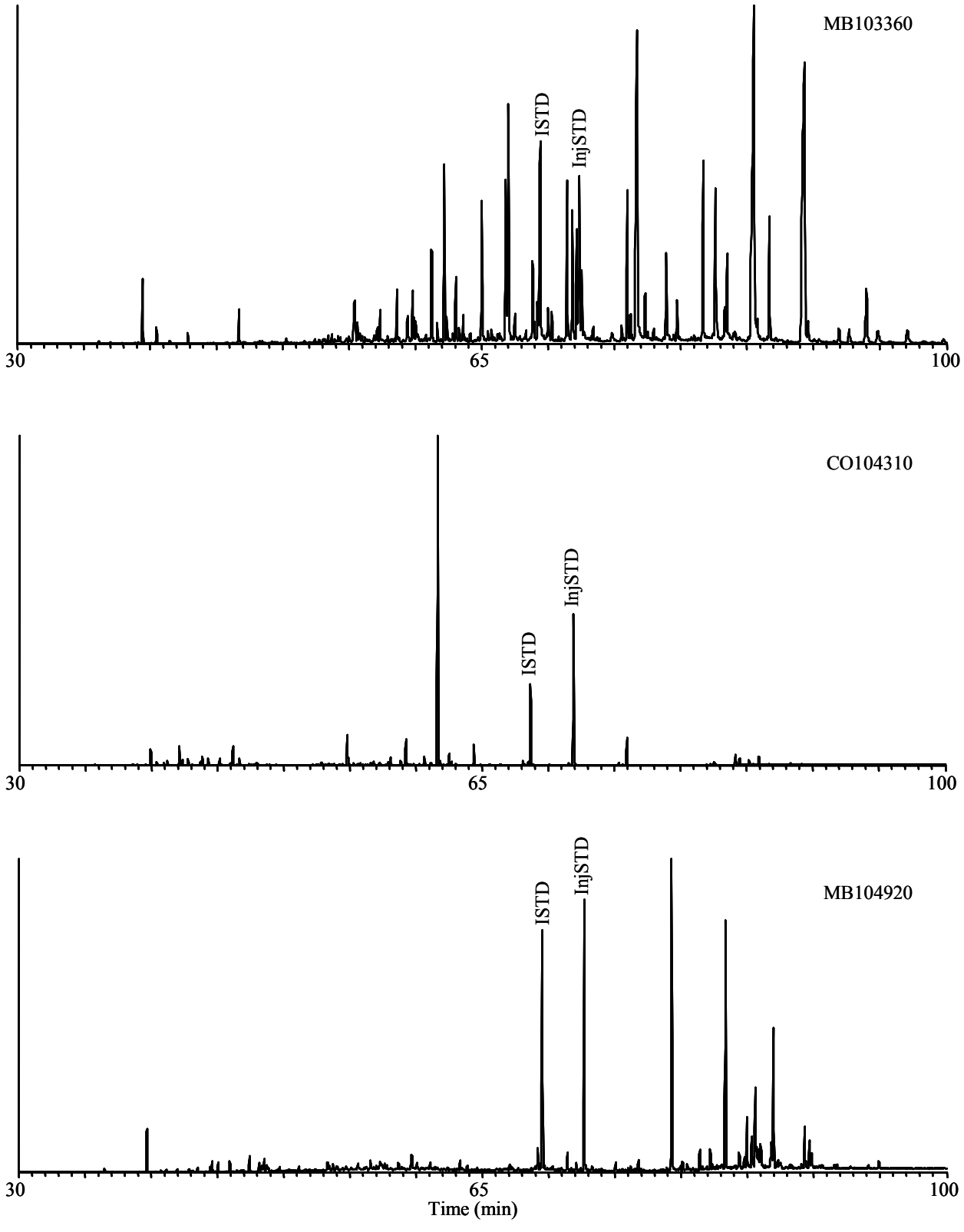
MB103360
ISTD
InjSTD
30
65
100
CO104310
ISTD
InjSTD
30
65
100
MB104920
ISTD
InjSTD
30
65
100
Time (min)

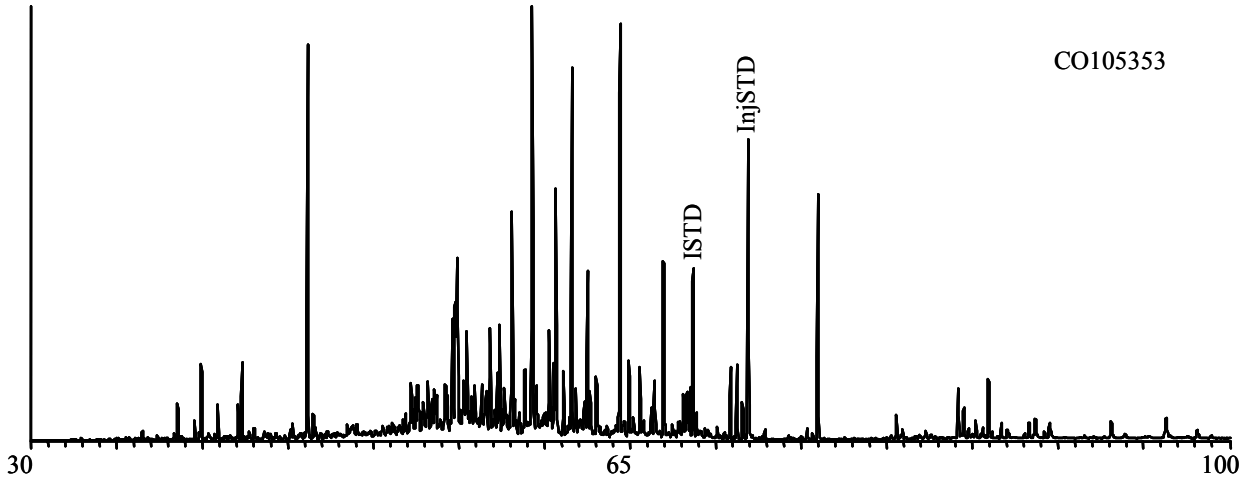
CO105353
InjSTD
ISTD
30
65
100

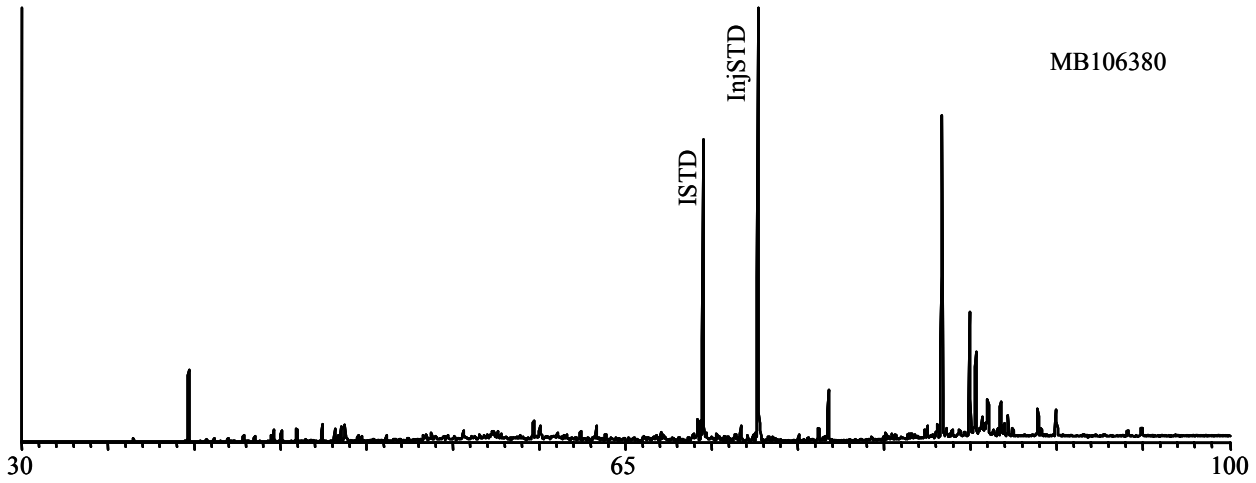
MB106380
InjSTD
ISTD
30
65
100

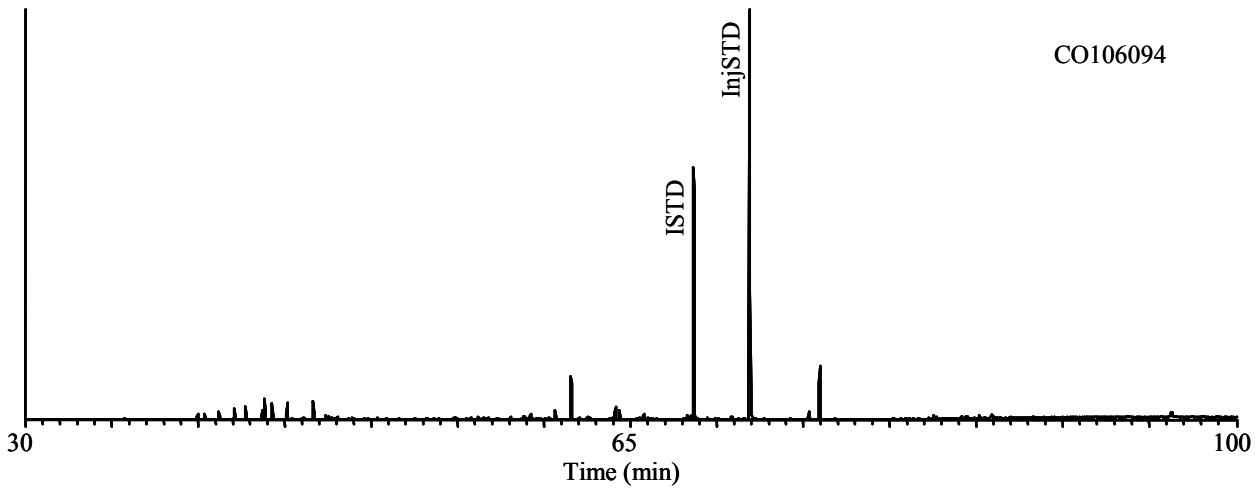
CO106094
InjSTD
ISTD
30
65
100
Time (min)

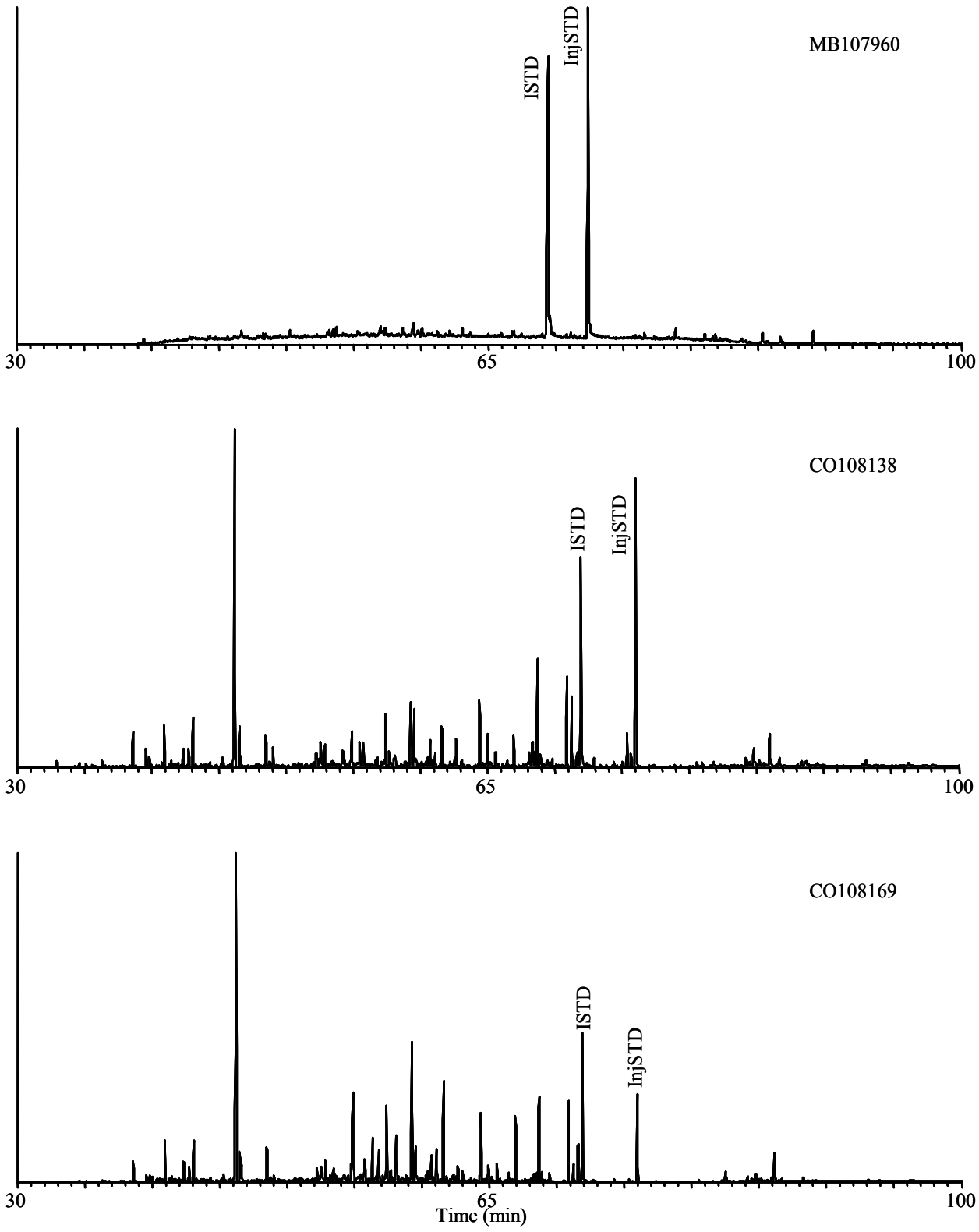
MB107960
ISTD
InjSTD
30
65
100
CO108138
ISTD
InjSTD
30
65
100
CO108169
ISTD
InjSTD
30
65
100
Time (min)

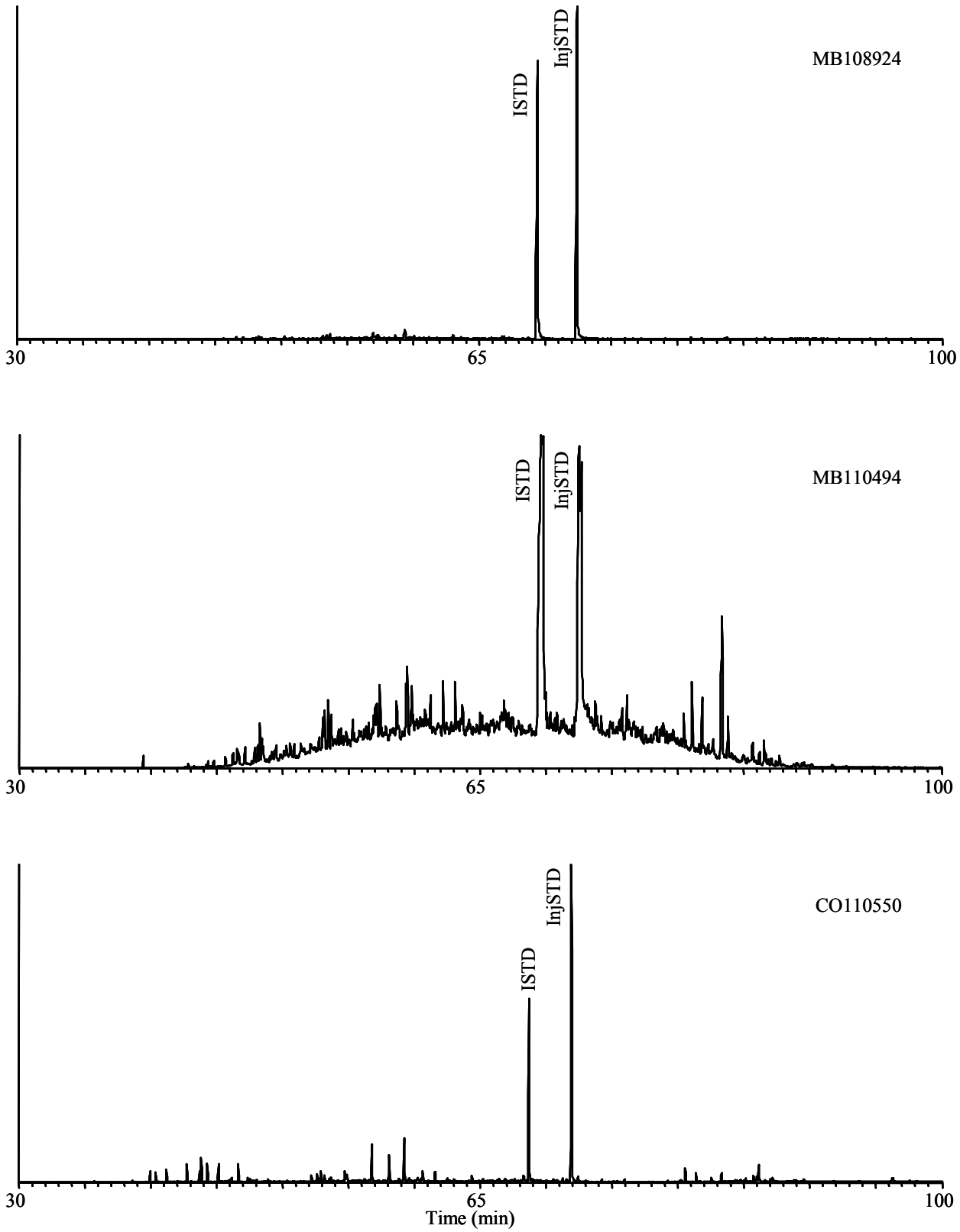
ISTD
InjSTD
MB108924
30
65
100
ISTD
InjSTD
MB110494
30
65
100
InjSTD
ISTD
CO110550
30
65
100
Time (min)

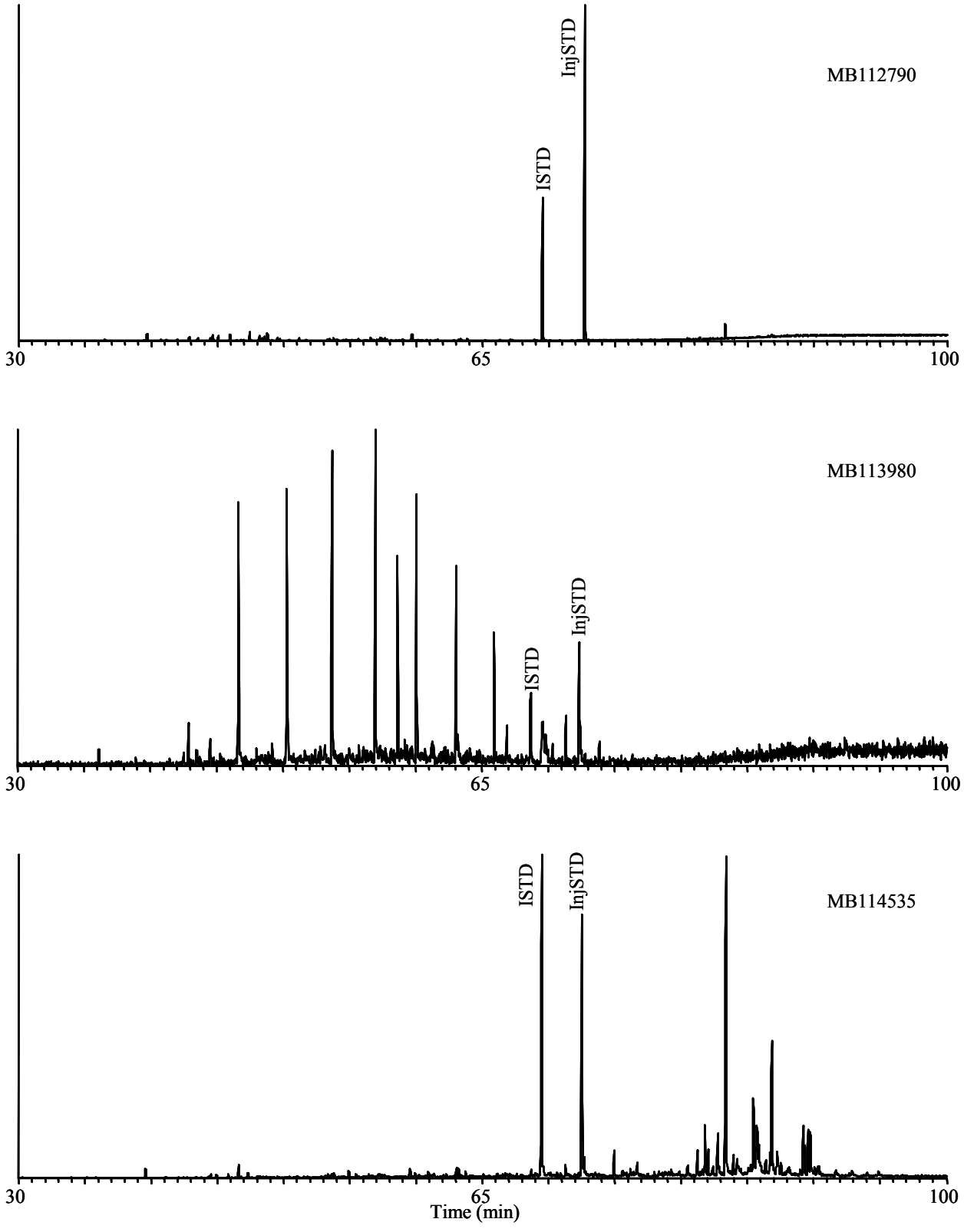
InjSTD
ISTD
MB112790
30
65
100
MB113980
ISTD
InjSTD
30
65
100
ISTD
InjSTD
MB114535
30
65
100
Time (min)